

DISS. ETH NO. – 27570

Different Perspectives of Metabolism: Gut Feelings and Love Handles

A thesis submitted to attain the degree of

DOCTOR OF SCIENCES of ETH ZURICH

(Dr. sc. ETH Zurich)

presented by

CAROLINE ANNABELLE MOSER

MSc. ETH in Health Science and Technology, ETH Zurich

born on 08.11.1990

citizen of Germany

accepted on the recommendation of

Prof. Dr. Christian Wolfrum, examiner
Prof. Dr. Katrien De Bock, co-examiner
Prof. Dr. Brice Emanuelli, co-examiner

2021

Abstract

Obesity and type 2 diabetes (T2D) are on the rise globally. As obesity is one of the major risk factors for T2D, the two diseases are irrevocably connected with each other. Two organs that play a central role in the disease etiology of obesity and T2D are the adipose tissue and the gut. Both are essential in orchestrating metabolic processes throughout our body. The adipose tissue is the safe storage place in our body for excess energy, but once we exceed its capacity a deteriorating process of metabolic complications starts. Through ectopic lipid accumulation as well as fibrotic, inflammatory adipose tissue expansion, the development of T2D is promoted. A promising target to combat metabolic diseases is a special sub-set of adipocytes, the brown adipocytes. They have the capability of uncoupling the mitochondrial membrane via Uncoupling protein 1 (Ucp1). Through this they burn glucose and lipids for heat production. The gut is the entry point of all the nutrients into the body. However, the gut does not solely digest and absorb nutrients; via enteroendocrine hormones and the gut-brain axis the gut is also in close contact with further distant metabolic organs. Through these connections, the gut plays a central role in the regulation of blood glucose levels, food intake, and satiety.

The first project of this thesis focused on the quantification of adipocytes. Transgenic mouse lines allowed us to trace and quantify Adiponectin+ and Ucp1+ cells in a manner unbiased by size or spatial location. Along with obesity, changes in the ambient temperature can remodel the adipose tissue tremendously. We used our mouse models to observe the kinetics of remodeling in response to thermoneutral and cold housing temperatures. In a thermoneutral environment, the number of Ucp1+ cells in the brown adipose tissue (BAT) decreased and the tissue developed a white adipose tissue-like morphology. However, physiologically it remained fully responsive and beta3-adrenergic stimulation could completely recover all Ucp1+ cells back to levels observed at room temperature. In response to cold housing, the number of Ucp1+ cells in the interscapular BAT (iBAT) peaked after one week. This peak was primarily derived from pre-existing adipocytes. In the inguinal white adipose tissue (ingWAT), the presence of Ucp1+ cells, named brite/beige adipocytes, plateaued only after three weeks of cold housing. Lastly, we determined the regenerative potential of the iBAT. By utilizing an Ucp1-DTR construct we could ablate all Ucp1+ cells with diphtheria toxin and study the kinetics of regeneration. One week of cold exposure could fully recover all Ucp1+ cells in the iBAT, and we were able to show that the recovery was driven mainly by precursor cells. The quantification of the adipose tissue remodeling gave us a measureable insight into its remodeling potential and the underlying processes. This knowledge

will hopefully help us to be able to use the remodeling of the adipose tissue to our advantage for the treatment of metabolic diseases.

The second project of the presented thesis centered around the gut secreted protein FAM3D and its metabolic function in the context of T2D. It is now widely recognized that gut-secreted proteins are powerful in regulating the metabolism in our body. Today, two classes of approved T2D drugs, namely GLP-1 receptor agonist and DPP4 inhibitors, are based on the function of gut-secreted proteins. FAM3D is another promising drug candidate. Upon adeno-associated virus (AAV) mediated overexpression of FAM3D in diet-induced obese mice an improvement in glucometabolic parameters, namely fasting blood glucose levels or glucose and insulin tolerance, could be observed. We identified FAM3D as insulin sensitizer, which increased glucose uptake into various tissues. Further, reduced hepatic lipid deposition and an amelioration of hepatic steatosis markers were detected, suggesting additional potential of FAM3D for the treatment of non-alcoholic fatty liver disease (NAFLD). We have first indications, that the positive metabolic phenotype of FAM3D is mediated by receptor tyrosine kinase signaling. However, the exact underlying molecular mechanism remains elusive.

In summary, this thesis provided insight into the vast remodeling potential of the adipose tissue and characterized the potential of a novel gut secreted protein for the treatment of T2D and NAFLD. This combination allowed us to examine metabolic processes from different perspectives and thus find new solution approaches to resolve obesity and T2D.

Zusammenfassung

Übergewicht und Typ 2 Diabetes (T2D) sind weltweit auf dem Vormarsch. Übergewicht ist einer der grössten Risikofaktoren für T2D und folglich sind diese zwei Krankheiten eng miteinander verbunden. In der Krankheitsätiologie von Übergewicht und T2D spielen zwei Organe eine zentrale Rolle, das Fettgewebe und der Darm. Beide Organe koordinieren metabolische Prozesse in unserem Körper. Das Fettgewebe ist ein sicherer Speicherplatz für Energie, wenn wir allerdings seine Kapazitäten überschreiten, dann startet eine Abwärtsspirale von metabolischen Komplikationen. Durch ektopische Lipidakkumulation und eine fibrotische entzündliche Expansion des Fettgewebes wird die Entstehung von T2D unterstützt. Ein vielversprechendes Ziel im Kampf gegen metabolische Krankheiten ist eine spezielle Untergruppe von Adipozyten, die braunen Adipozyten. Diese haben die Eigenschaft die Mitochondrien Membran über das Uncoupling protein 1 (Ucp1) kurzzuschliessen und so Zucker und Fett zur Generation von Wärme zu verbrennen. Der Darm ist nicht nur dafür zuständig Nahrung zu verdauen und zu absorbieren. Er steht über die enteroendokrinen Hormone und die Darm-Gehirn Achse in engem Kontakt mit weiteren metabolischen Organen. Mittels diesen Verbindungen spielt der Darm eine zentrale Rolle in der Regulation des Blutzuckers, der Nahrungsaufnahme und der Sättigung.

Der erste Teil dieser Arbeit fokussierte sich auf die Quantifizierung von Fettzellen. Dank transgener Mäuse konnten Adiponectin+ und Ucp1+ Zellen, unabhängig von ihrer räumlichen Position oder ihrer Grösse, verfolgt und quantifiziert werden. Neben Übergewicht kann vor allem die Umgebungstemperatur das Fettgewebe nachhaltig verändern. Mit den Mausmodellen haben wir die kinetische Antwort auf thermoneutrale oder kalte Umgebungstemperaturen verfolgt. In thermoneutraler Umgebung reduzierte sich die Anzahl von Ucp1+ Zellen im braunen Fettgewebe der Tiere und die Morphologie des Gewebes ähnelte der des klassischen weissen Fettgewebes. Dennoch, blieb das braune Fettgewebe auf physiologischer Ebene voll reaktionsfähig. Durch eine beta3-adrenergische Stimulation konnte das Level der Ucp1+ Zellen wieder, auf das bei Raumtemperatur beobachtete Niveau, zurückgeführt werden. Wenn die Tiere in die Kälte transferiert wurden, zeigte sich nach einer Woche der maximale Höchstwert von Ucp1+ Zellen im interscapularen Braunen Fettgewebe (iBAT). Wir konnten zeigen, dass das gefundene Maximum von Ucp1+ Zellen mehrheitlich von schon bei Raumtemperatur existierenden Adipozyten generiert wurde. Die im weissen Fettgewebe entstehenden Ucp1+ Zellen, auch genannt beige Adipozyten, benötigten im Gegensatz dazu drei Wochen in der Kälte bis sie ein Plateau erreichten. Abschliessend wurde das regenerative Potenzial des iBATs bestimmt. Dank einem Ucp1-DTR Konstrukts konnten alle Ucp1+ Zellen durch Diphtherietoxin eliminiert und so die Kinetik des

Regenerationsprozesses untersucht werden. Es zeigte sich, dass bereits nach einer Woche in der Kälte, das iBAT wieder komplett hergestellt war und darüber hinaus, dass die Regeneration primär durch Vorläuferzellen geschehen ist. Die Quantifizierung des Umbaus von Fettgewebe hat uns nicht nur einen messbaren Einblick in das Umbaupotenzial des Gewebes gegeben, sondern auch in die zugrundeliegenden Prozesse. Dieses Wissen hilft den Umbau von Fettgewebe besser zu verstehen und so zu unserem Vorteil zur Behandlung von metabolischen Krankheiten zu nutzen.

Der zweite Teil dieser Arbeit drehte sich rund um das darmsekretierte Protein FAM3D und seine metabolische Funktion im Zusammenhang mit T2D. Es ist allgemein anerkannt, dass darmsekretierte Proteine sehr wirksam sind metabolische Funktionen in unserem Körper zu regulieren. Entsprechend basieren die heutzutage zugelassenen T2D Medikamente aus der Klasse der GLP-1 Rezeptor Agonisten und der Klasse der DPP4 Inhibitoren, auf der Funktion von darmsekretierten Proteinen. FAM3D ist ein neuer vielversprechender Medikamenten Kandidat. Wir konnten zeigen, dass FAM3D überexprimiert über einen adeno- assoziierten Virus (AAV), den Glukosemetabolismus in übergewichtigen Mäusen positiv beeinflusst. Speziell die Glukose Werte im nüchternen Zustand, sowie die Glukose- und Insulin-Toleranz waren deutlich verbessert. Des Weiteren, konnten wir zeigen, dass FAM3D die Insulinsensitivität verbessert und so die Aufnahme von Glukose in unterschiedlichen Geweben stimuliert. Zudem nahmen hepatische Fett Einlagerungen ab und die Steatosis Marker der Leber waren ebenfalls verbessert. Das suggeriert für FAM3D ein zusätzliches Potenzial zur Behandlung von nicht-alkoholischer Fettleber (NAFLD). Erste Anhaltspunkte aus dieser Arbeit zeigten, dass FAM3D seinen positiven metabolischen Phänotyp über Rezeptor Tyrosine Kinase Signaling ausübt. Der exakte molekulare Wirkungsmechanismus ist allerdings noch nicht erforscht.

Am Ende bietet diese Arbeit zum einen, einen quantitativen Einblick in die Fähigkeit des Fettgewebes sich umzubauen und an klimatische Veränderungen anzupassen. Zum anderen, charakterisiert die Arbeit FAM3D, ein neuartiges darmsekretiertes Protein, mit Potential zur Behandlung von T2D und NAFLD. Die beiden Themen erlaubten es metabolische Prozesse aus unterschiedlichen Perspektiven zu betrachten und so neue Lösungsansätze für zur Behandlung von Übergewicht und T2D zu finden.

Table of Contents

Abstract	I
Zusammenfassung	III
Table of Contents	V
CHAPTER 1 General Introduction.....	1
1.1 The adipose tissue	1
1.2 The gut	3
1.3 The metabolic syndrome	5
1.4 Obesity	5
1.5 Type 2 diabetes.....	8
1.6 The adipose tissue in the context of metabolic disorders.....	12
1.7 The gut in the context of metabolic disorders.....	17
CHAPTER 2 Quantification of adipocyte numbers following adipose tissue remodeling	22
2.1 Introduction	24
2.2 Results	24
2.3 Discussion	35
2.4 STAR Methods.....	37
2.5 Supplementary Material	40
CHAPTER 3 FAM3D a novel gut secreted protein and its potential in the regulation of glucose metabolism	45
3.1 Introduction	47
3.2 Results	48
3.3 Discussion	59
3.4 Conclusion	61

3.5	Materials and Methods.....	62
3.6	Supplementary Figures.....	71
CHAPTER 4 General Discussion		74
4.1	Remodelling of adipose tissue	74
4.2	Gut secreted proteins and their potential for type 2 diabetic treatment.....	80
4.3	Summary	85
CHAPTER 5 Further publications.....		86
	Inhibition of Mevalonate Pathway Prevents Adipocyte Browning in Mice and Men by Affecting Protein Prenylation.....	87
	Antioxidants protect against diabetes by improving glucose homeostasis in mouse models of inducible insulin resistance and obesity	113
	A Genetic Model to Study the Contribution of Brown and Brite Adipocytes to Metabolism..	126
Acknowledgements.....		142
Bibliography		144
Curriculum Vitae		164

CHAPTER 1

General Introduction

1.1 The adipose tissue

For a very long time, the adipose tissue was solely seen as an organ for energy storage and insulation. This constricted view has widened over the last decade, and has resulted in people starting to appreciate the manifold physiological function as well as the variety of cell types present in adipose tissue. Besides white, brown, and brite/beige adipocytes, also immune cells, endothelial cells, fibroblasts, neurons, and stem cells are present in the adipose tissue. In terms of volume, most of the adipose organ is made up of white adipocytes, which store energy in the form of triglycerides. Triglycerides cannot cross the cell membrane and are thus hydrolyzed by circulating very low-density lipoprotein (VLDL) particles or chylomicrons through the lipoprotein lipase (LPL). The resulting free fatty acids (FFA) are absorbed by the underlying tissue and re-esterified into triglycerides inside the adipocytes. Additionally, FFA can be generated from glucose through the process of lipogenesis. If energy is needed, triglycerides are hydrolyzed by a set of lipases (adipose triglyceride lipase (ATGL), hormone sensitive lipase (HSL), monoacylglycerol lipase (MGL)) to FFA and glycerol, which are subsequently released and can be metabolized either in the adipose tissue itself or in other organs. The morphology of white adipocytes, attributable to their function as a location for energy storage, is characterized by a large lipid droplet that pushes the nucleus and the other cell organelles to the site and brings them into close contact with the plasma membrane, giving the cell a unilocular shape. In mice and men, adipose tissue is scattered throughout the whole body, but for simplicity it is often classified into just two main depots: The visceral adipose tissue, which surrounds the inner organs, and the subcutaneous adipose tissue, which is located beneath the skin [1]. In contrast to white adipocytes, brown adipocytes dissipate energy by generating heat from free fatty acids and glucose. Key for this process is the Uncoupling protein 1 (Ucp1). Ucp1 leaks the inner mitochondrial membrane, thus uncoupling the inner mitochondrial respiration from adenosine triphosphate (ATP) synthesis. The generated energy is dissipated as heat instead, therefore the process is called non-shivering thermogenesis. One of the strongest stimuli that activates this highly energy-demanding process is norepinephrine released from the sympathetic nerves in response to cold. However, other

activators are also known. For example, synthetic adrenergic agonists, cardiac natriuretic peptides, exercise, or a meal can all induce brown fat activity [2–4]. Upon the activation of brown adipose tissue, the transcription of thermogenic genes is induced, FFA are released from lipid droplets, and Ucp1 is activated [5]. Again, the highly specialized task defines the morphology. Brown adipose tissue is highly vascularized to ease the transport of substrates and heat. The high abundance of mitochondria gives the brown adipocytes a brownish appearance. Furthermore, brown adipocytes have many small multilocular lipid droplets which allow for the process of thermogenesis to be rapidly fueled [1]. In mice, the biggest depot of brown adipose tissue is found in the interscapular region. However, smaller depots can be also found in the cervical, axillary, or perirenal regions [6]. The presence of brown adipose tissue in adult humans was not discovered until 2009. Only after, brown adipose tissue was localized in the supraclavicular, neck, and perirenal regions [7–9]. If animals are either cold exposed or exposed to beta3-adrenergic receptor agonists, a subset of Ucp1 positive cells arises, especially within the subcutaneous white adipose tissue depot. These are called brite or beige adipocytes. Brite/beige adipocytes have a similar morphology to brown adipocytes; they are also rich in mitochondria that express Ucp1 and have many multilocular lipid droplets [1]. A unique feature of brite/beige adipocytes is their inducible and reversible thermogenic capacity in response to environmental stimuli. Upon stimulation, brite/beige adipocytes can either differentiate de novo from precursors [10,11] or transdifferentiate from existing white adipocytes [12,13]. Nonetheless, when the cold stimulus is removed, the brite/beige adipocytes gradually change their morphology back into unilocular, lipid droplet filled white-like adipocytes, only to become brite/beige again if exposed to a second cold stimulus [14]. Besides the three types of adipocytes, the majority of cells in the adipose tissue are other cell types, such as fibroblasts, endothelial, or immune cells. They can be found in the so-called stromal vascular fraction (SVF) of adipose tissue. They are all in close contact with the adipocytes, and together they are orchestrating the role of adipose tissue as one of the key metabolic organs in the body.

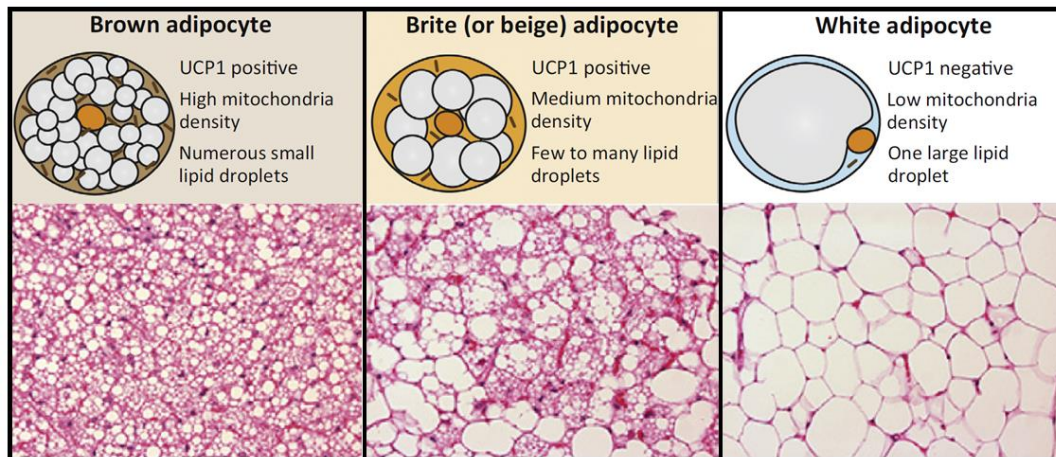


Figure 1: Characteristics and morphology of brown, brite and white adipocytes, adapted from Sanchez-Gurmaches et al., 2016 [15]

1.2 The gut

The Gastrointestinal (GI) tract plays a tremendous role in our daily life, seeing as the absorption of nutrients is a key vital function of our body. When we eat, our food travels from the pharynx into the stomach via the esophagus. From there, the journey continues through the small and large intestine before everything not yet absorbed by the body is excreted from the rectum. In the focus of this thesis are the small and large intestine, which are jointly referred to as the gut. The gut is where the majority of nutrient absorption takes place. In order to maximize absorption, the surface of the gut is characterized by a villus structure.

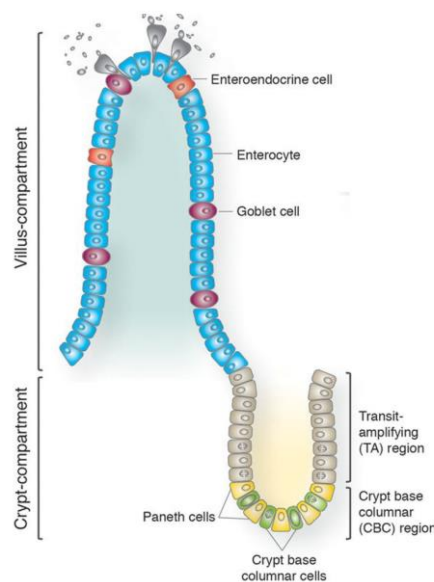


Figure 2: Cellular structure of the gut adapted from Leushacke and Barker, 2014 [16]

The villi are covered by an epithelial layer comprised of multiple different cell types. The stem cells, which give rise to new cells, are localized in the crypts, from where the cells differentiate on their way up to the villus. Also found in the crypts are the paneth cells, which, on the one hand, secrete factors that help to maintain the cellular fate of the stem cells. On the other hand, they also secrete multiple antimicrobial peptides that protect the host from pathogens [17]. Goblet cells secrete a thick mucus which not only facilitates the journey of the digested food through the gut, but also serves as the first line of defense against microbial, chemical, or physical hazards coming from digested food. Furthermore, the mucus traps the microbiome in the gut and prevents its excretion through the peristaltic [18]. The majority of the gut epithelium is made up of enterocytes. These are firmly connected by tight junctions and form an epithelial barrier which separates our body from the external environment. Enterocytes are further specialized for the absorption of nutrients. In order to fulfill this task they are highly polarized. The apical site is characterized by a brush of microvilli, which further maximizes the absorption surface of the gut. Small molecules can enter the enterocytes via transporters, while bigger macromolecules get absorbed via endocytosis. Inside of the enterocytes, the nutrients are either metabolized or further transported to the basal site of the enterocytes, where they are delivered into the systemic circulation either with or without prior absorption by the lymphatic system. Enterocytes are also antigen-presenting cells. They internalize and process antigens to present them via MHC class II molecules to CD4+ T-cells at the basolateral membrane of the enterocyte [19]. Lastly, we have the enteroendocrine cells (EEC), which are scattered throughout the epithelium and function as the chemosensors of the gut. EECs also have the apical site covered with microvilli to increase the surface for nutrient sensing by nutrient transporters and G-protein coupled receptors (GPCRs). In response to the luminal content, enteroendocrine hormones are released from the basolateral membrane of the EECs. From there, the enteroendocrine hormones can either enter the systemic bloodstream to act on distant organs or act in a paracrine manner on the neighboring cells. Alongside with the enteroendocrine hormones, EECs also release other small molecules (e.g. glutamate, ATP) at their basolateral membrane. They can activate the local endings of the afferent vagal neurons, thereby mediating information from the gut to the brain [20,21]. Thus, the enteroendocrine hormones and small molecules can act within the GI tract as well as outside of it to regulate many physiological and metabolic functions throughout the body. The bidirectional cross talk between the brain and the gut is essential in regulating homeostasis of the body. The gut sends information to the brain via vagal and spinal afferent neurons, gut hormones, immune mediators and microbiota-related signaling molecules. The reverse informative flow from the brain to the gut occurs via autonomic neurons and neuroendocrine factors [22]. As mentioned before, a last key part of the gut is the microbiome. The human gut hosts a complex assembly of

microorganisms that have a sustaining impact on nutrient uptake, metabolism, immune defense, and behavior [23].

In conclusion, the gut is not only the entry point of food into the body; it also plays a significant role in the regulation of many metabolic processes, through the EECs, through its central role in the immune system, and through its very close connection to the brain.

1.3 The metabolic syndrome

The adipose tissue and the gut are two organs that have a big impact on the metabolism of the body. Both are key in managing energy uptake, storage, and expenditure. If the tightly controlled metabolic system of the body becomes misbalanced, several diseases start to manifest. The association between obesity, type 2 diabetes (T2D) and cardio vascular diseases (CVD) has been accepted for a long time. However, the first definition of the metabolic syndrome was not made until 1998 [24]. Today, the metabolic syndrome is defined by the International Diabetes Federation as the following [25]:

Central obesity (waist circumference \geq ethnic specific values or BMI \geq 30 kg/m ²) <i>along with two of the following</i>
Raised triglycerides (\geq 50 mg/dl or specific treatment for this lipid abnormality)
Reduced HDL cholesterol ($<$ 40 mg/dl in males; $<$ 50 mg/dl in females or specific treatment for this lipid abnormality)
Raised blood pressure (systolic \geq 130 mmHg or diastolic: \geq 85 mmHg or treatment of previously diagnosed hypertension)
Raised fasting plasma glucose (\geq 100 mg/dl or previously diagnosed type 2 diabetes)

Table 1: Definition of the Metabolic Syndrome; adapted from Zimmet, 2005 [25]

The metabolic syndrome has various facets and many underlying interactions. In the context of this thesis, obesity and increased fasting plasma glucose/T2D in relation to adipose tissue and the gut will be discussed in more detail.

1.4 Obesity

What are we talking about when we talk about obesity? Obesity is defined as abnormal or excessive fat accumulation that presents a risk to health [26]. Obesity is generally measured by the body mass index (BMI), defined as $BMI = \text{weight (kg)} / (\text{height (m)})^2$. According to the World Health Organization (WHO), people with a BMI \geq 25 are overweight, and people with a BMI \geq 30 are obese [26]. Alongside the BMI, many other measurements are available, ranging from very

simple hip-to-waist ratio measurement to very sophisticated Dual Energy X-ray Absorptiometry (DEXA) [27]. None of the measurements can deny that obesity has reached the dimension of a global epidemic. In the year 2016, ~ 2 billion adults worldwide were overweight, and among them 650 million were obese. In the same year, 340 million children aged 5-19 were overweight or obese [26]. Currently, more people die globally from obesity than from undernutrition [26]. Starting off as a disease of affluence in the United States of America (USA) and Europe, many low- and middle-income countries underwent a drastic shift from undernutrition to overnutrition during the last few years. In the USA and Europe, where the global epidemic started, the continuous rise seems to have flattened a bit at a prevalence of ca. 35% [28,29]. However, in regions like Central/Latin America or China, the curves are still on the rise [30]. Thus, it is not surprising that trends are predicting that 38% of the global adult population will be overweight and 20% will be obese by 2030 [31]. This begs the question: Why are so many people gaining too much weight? At first glance, it seems to be a simple imbalance between too much energy income and too little energy expenditure, resulting in an excessive storage of energy in the body in the form of fat. However, this simple equation has many underlying traits; bodyweight regulation is a complex interaction between genetic, environmental, and socioeconomic factors.

The idea that obesity is heritable was suggested by twin studies. According to these studies, 40%-70% of the bodyweight is determined by genetic factors [32,33]. In very rare cases, monogenic mutations in central parts of the energy metabolism pathway are responsible for the development of obesity. However, a polygenic predisposition to become obese is far more common. If we look back at our ancestors, food was not always readily available, and populations tended to experience periods of feast and famine. Based on this, Neel proposed the "thrifty" gene hypothesis in 1962. Natural selection would favor carriers of the "thrifty" genes that would be able to store more energy during periods of feast and thus have better survival rates during periods of famine. Over the decades, humans subsequently acquired a set of genes which is detrimental to the modern setting, where food is constantly available [34]. Through evolving techniques, more sophisticated studies of the human genome became possible. Many groups tried to identify positively selected loci or SNPs which would favor fat accumulation; however, limited empirical evidence for the "thrifty" gene hypothesis was found [35,36]. Further, genome-wide association studies (GWAS) could identify 97 BMI-associated loci. However, they only account for roughly 20% of the BMI variation [37]. Thus, no polygenetic score can so far entirely and satisfactorily predict the risk of obesity. In conclusion, a strong gene-lifestyle interaction is proposed by the scientific society. It is hypothesized that certain sets of genes make an individual more susceptible to gain weight when exposed to an obesogenic environment [38,39].

Key factors of an obesogenic environment are eating and drinking behaviors as well as the activity profile. The first question is, do people simply eat too much or do they eat the wrong things? Both answers are actually correct, with the start of the industrialization food processing evolved, resulting in easy to access highly processed, and highly caloric meals. Fast food and highly sugary drinks became staples of many people's daily meal plan, with the portion sizes being drastically increased [40]. Additionally, industrialization changed our daily life by drastically promoting a more sedentary lifestyle where many physically demanding tasks and jobs are now performed by machines instead of humans. Due to the global popularity of televisions and computers, many people have also become less active during their leisure time [41,42]. Further, socioeconomic factors can influence obesity. It was demonstrated that, especially in developed countries, paternal education inversely correlates with childhood obesity [43]. In households with lower socioeconomic standing, both knowledge and financial constraints exacerbate the access to healthy food and physical activity [39]. Many more environmental and socioeconomic factors could be listed here. However, the next question I would like to answer is how can we get rid of the excess kilograms if we are overweight or obese?

Losing weight requires a multidisciplinary approach including strict caloric restriction, increasing energy expenditure through exercise, and modification of the patient's behavior. The diet and the exercise plan need to be adjusted to the patient's preconditions and preferences. Otherwise, the patient's compliance will be limited [44]. A lot of effort was made to find the ideal macro- and micronutrient composition for maximizing weight loss. Various dietary programs are available nowadays. However, the key to success for all of these programs is caloric restriction and not a special combination of macronutrients [45]. In obese patients, exercise without accompanied caloric restriction has only limited effects on weight loss. Even though, exercise plays a tremendous role in preventing weight regain after weight loss [46,47] and the positive effects of exercise in preventing the loss of lean body mass and improving cardiovascular fitness are undeniable [48]. Behavioral intervention aims to improve self-monitoring and stimulus control, it should give the patient clear goals, and accompany the patient on the way to reach his goals [49]. However, in many cases, lifestyle interventions are not sufficient and need support from other adjuvant therapies, such as pharmaceuticals or even surgical interventions. Currently, six anti-obesity drugs are approved by the FDA, namely Orlistat, Lorcaserin, Phentermine/Topiramate, Naltrexone/Bupropion, and Liraglutide. Most of them act on the serotonergic, dopaminergic, or noradrenergic pathways, where they regulate appetite. The exception is Orlistat, which inhibits the absorption of fat by inhibiting lipase, the key enzyme for breaking down triglycerides into FFA. All drugs often have significant side effects and many contraindications, thus the matching drug for

each patient should to be chosen wisely [50,51]. The ultimate but most effective treatment against obesity is bariatric surgery, which will be discussed later in detail.

In conclusion, the global obesity pandemic is not only challenging patients throughout the world but is also challenging our economies and health care systems. Thus, it is of great interest to understand the disease of obesity with its multiple facets more deeply in order to combat excessive weight gain and the associated comorbidities.

1.5 Type 2 diabetes

In a healthy human being, glucose is cleared from the systemic blood flow through insulin-stimulated uptake in the muscle, liver, and adipose tissue, where it is stored in the form of glycogen or triglycerides. However, if there is a constant nutritional overload, which is commonly seen during obesity, it is hypothesized that the storage cells become exhausted and start to protect themselves by becoming insulin resistant. In the first phase, the pancreatic beta cells try to counteract by expanding and producing more insulin until they can also no longer cope with the detrimentally high levels of glucose and FFA in the blood. If the beta cell function is impaired, insulin secretion is reduced, blood glucose levels rise, and the disease T2D is manifested [52]. The WHO defines the diagnosis criteria for diabetes as the following: Fasting blood glucose levels ≥ 7.0 mmol/L or a plasma glucose of ≥ 11.1 mmol/L in an oral glucose tolerance test or glycated hemoglobin (HbA1c) $\geq 6.5\%$ [53].

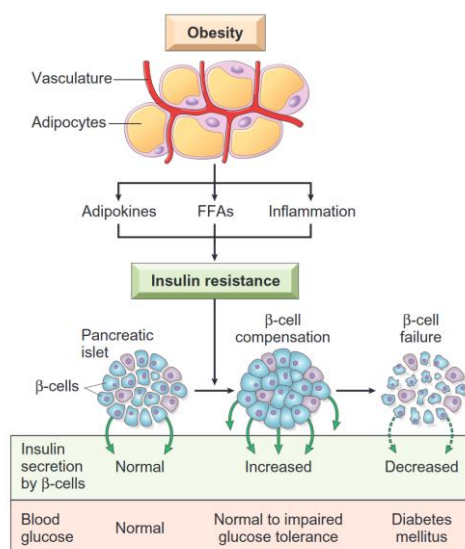


Figure 3: Development of type 2 diabetes, taken from Moini, 2019 [52]

T2D is a very silent disease and often remains undiagnosed for many years. Until then, irreversible damage resulting from the consistently high blood glucose levels might have already occurred. Primary symptoms hinting at T2D can be frequent urination and/or sweet-smelling urine, which occurs when the kidney is no longer capable of completely reabsorbing the excess glucose. The frequent urination might also cause the patients to feel thirstier. Despite the fact that there is a lot of glucose in the blood, the insulin-resistant cells might not be able to take it up. Thus, they enter into an energy deficit, which can cause fatigue or hunger [52]. However, T2D is most frequently diagnosed by secondary symptoms. Excessively high blood glucose levels are closely associated with microvascular complications, namely, retinopathy, which impairs the vision of the patient, neuropathy, which causes numbness especially in the extremities, nephropathy, or dramatically impaired wound healing. Moreover, T2D causes macrovascular complications that drastically increase the risk of cardiovascular disease or stroke [54]. Thus, it is extremely important that people who are at high risk of developing T2D are examined frequently in order to treat the disease before it is too late. The disease is still completely reversible through lifestyle modifications and pharmacological treatment, especially in the early stage of insulin resistance/pre-diabetes. However, untreated up to 70% of prediabetic patients will eventually become diabetic [55]. Overweight and obesity are the most important modifiable risk factors; a weight loss of just 7% sustainably reduces the risk of developing T2D and CVD [45]. Further risk factors for T2D are age, family history, and ethnicity. According to the American Diabetes Association (ADA) and the American Association of Clinical Endocrinologists (AACE), people above 45 years of age should be regularly screened for diabetes [56]. Having a first degree relative with T2D is associated with a ca. 2.5-fold higher risk of developing T2D. However, various studies demonstrated that the increased risk is only partly mediated through the genes, with part of the risk also stemming from non-genetic familial behaviors and norms [57,58]. Lastly, being Asian, African-American, Hispanic, Native American, or Pacific Islander increases an individual's risk of developing T2D. Again, the presence of genetic risk alleles was found to be similar across ethnicities, so it is rather an environmental and cultural component which is increasing the T2D risk for these ethnicities. All of them show a higher prevalence of obesity, a major risk factor for T2D [59]. Additionally, they often live with inferior or no health insurance, meaning that glucose monitoring and glucose control are more difficult to achieve [60].

From a global perspective, alongside the global pandemic of obesity, the numbers of T2D are also on the rise. In the year 2019, 463 million people were diabetic, or one out of every eleven people on the planet. The majority of diabetics (79%) live in low- and middle-income countries. Approximately 4.2 million adult deaths worldwide were credited to T2D and its complications in

the year 2019. In the same year, the cost of health care attributed to T2D and the concomitant complications were estimated to be 760 billion US dollars [61].

What treatment options are available to combat this disease? The most effective method is prevention. Prevent obesity and monitor people at high risk closely. Alongside with lifestyle interventions focusing on nutrition and exercise, the ADA and the AACE recommend pharmacological therapeutics to support blood glucose control. They suggest to follow a stepwise therapy plan which combines lifestyle management and up to three different pharmaceutical therapeutics based on the measured Hb1Ac levels [62]. The recommended first line of therapy is Metformin, which is the most prescribed T2D drug worldwide. Despite this fact, Metformin's mechanism of action is still not fully understood. It is suggested that it acts in a pleiotropic manner resulting in various underlying mechanisms depending on the organ of action. In the liver, Metformin inhibits the mitochondrial respiratory chain complex 1, which leads to a decrease in ATP production. This decrease in cellular energy production is sensed by the AMP-activated protein kinase (AMPK), which conversely inhibits gluconeogenesis. Additionally, independent of AMPK, Metformin also decreases hepatic glucose production via the modulation of the intracellular redox status or the inhibition of adenylate cyclase and fructose 1,6-bisphosphatase (FBP1) [63]. Besides the inhibition of hepatic glucose production, Metformin performs multiple actions in the gut. It increases the glucose utilization in enterocytes, it increases the secretion of the gut incretin hormone glucagon-like peptide 1 (GLP-1), and it modulates the composition of the gut microbiota [63]. Furthermore, Metformin was shown to ameliorate the chronic low-grade inflammation associated with obesity [63]. If Metformin and lifestyle modifications alone do not sufficiently lower Hb1Ac levels below 9%, dual or triple therapy with a second or even a third drug is endorsed. The mechanism of action and the physiological response of the most prevalent T2D drug types is summarized in the following table.

Drug class (Examples)	Mechanism of action	Physiological effects
Biguanides (Metformin)	Activate AMPK Improve cellular insulin signaling Reduce respiratory chain activity Alter gut glucose–lactate metabolism	Reduce hepatic glucose output Improve insulin sensitivity Increase GLP-1 levels
Sulfonylureas (Glipizide Glimepiride Glyburide)	Bind to SUR1 on β cells, resulting in closure of K_{ATP} channels, depolarization, and calcium influx	Increase insulin secretion
Thiazolidinediones (Pioglitazone Rosiglitazone)	PPAR- γ agonists	Increase insulin sensitivity Reduce free fatty acid release
DPP4 inhibitors (Sitagliptin Saxagliptin Linagliptin Alogliptin)	Inhibit DPP-4 activity, increase endogenous incretin levels	Glucose-dependent increase in insulin secretion and inhibition of glucagon secretion
SGLT2 inhibitors (Canagliflozin Dapagliflozin Empagliflozin)	Inhibit SGLT2 transporters in proximal renal tubules	Increase urinary glucose excretion
GLP-1 Receptor Agonist (Exenatide Liraglutide Lixisenatide Albiglutide Dulaglutide)	Activate the GLP-1 receptor	Glucose-dependent increase in insulin secretion and inhibition of glucagon secretion Reduce postprandial glucose excretion Increase satiety
Insulin Rapid, short, intermediate, and long acting	Directly activate the insulin receptor	Increase glucose disposal Reduce hepatic glucose output Decrease lipolysis

Table 2: Summary of T2D drugs. Adapted from Tahrani et al; 2016 [64] AMPK=AMP-activated protein kinase; DPP-4=dipeptidyl peptidase 4; GLP-1=glucagon-like peptide 1;PPAR- γ =peroxisome proliferator-activated receptor γ ; SGLT2=sodium/glucose cotransporter 2; SUR1=sulfonylurea receptor 1

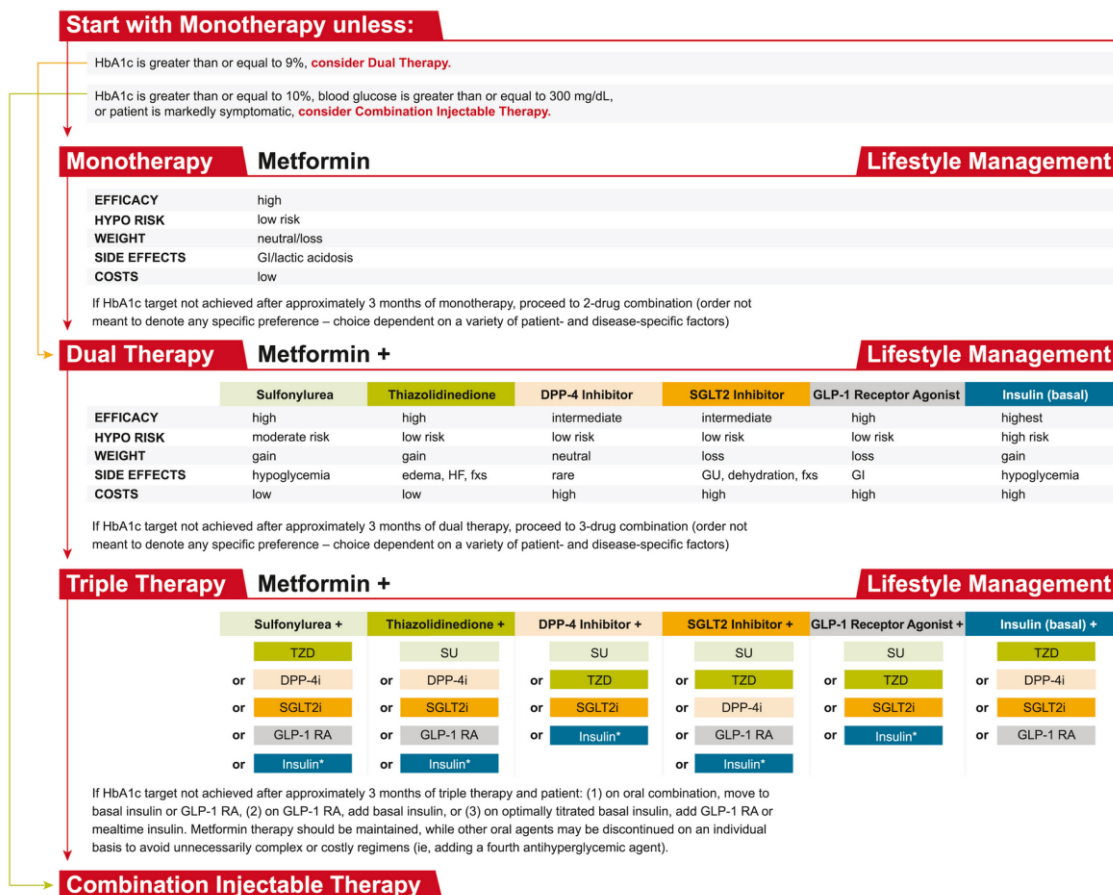


Figure 4: Stepwise therapy plan of ADA, taken from Thrasher; 2017 [62] DPP-4i = dipeptidyl peptidase-4 inhibitor; fxs = fractures; GI = gastrointestinal; GLP-1 RA = glucagon-like peptide-1 receptor agonist; GU = genitourinary; HbA1c = glycated hemoglobin; HF = heart failure; HYPO = hypoglycemia; NPH = neutral protamine Hagedorn; SGLT2i = sodium glucose cotransporter 2 inhibitor; SU = sulfonylurea; T2DM = type 2 diabetes mellitus; TZD = thiazolidinedione.

In addition to lifestyle interventions and pharmacological treatments, bariatric surgery is a powerful treatment that resolves T2D in 78 % of all patients [65]. The details of bariatric surgery will be discussed later.

In summary, insulin resistance and the concomitant failure of insulin-secreting beta cells drives the development of T2D. As the disease develops in silence, people at high risk should be screened regularly in order to treat T2D before accompanying micro- and macrovascular complications emerge. Only if blood glucose levels are monitored and regulated tightly the dwindling spiral of the disease can be stopped and global rise of the disease is stemmed.

1.6 The adipose tissue in the context of metabolic disorders

In the context of metabolic disorders, white adipose tissue is often seen as the bad guy. It is true that the adipose tissue is a starting point for obesity and the associated diseases, but only if we

overstrain the safe storage space in our body. The adipose tissue is the warehouse of our body and protects us from detrimentally high levels of glucose and fat in the blood and other organs. However, if we exceed the storage space, the declining path of metabolic disorders starts. Animals or people who have no adipose tissue or are unable to maintain adipose tissue start to ectopically accumulate lipids, especially in the liver or the muscle. This leads to insulin resistance, hypertriglyceridemia, and non-alcoholic fatty liver disease (NAFLD), resulting in an early onset death mostly due to liver failure [66]. This nicely demonstrates the importance of the adipose tissue as a safe storage space of which we should neither have too little nor too much. Upon overnutrition, the adipose tissue can drastically remodel and expand its storage capacity through either hypertrophy or hyperplasia. During hypertrophy, the size of the adipocytes increases, while during hyperplasia the number of adipocytes increases. In earlier times, it was thought that the adipocytes first expand until they reach a threshold of ca. 0.7–0.8 $\mu\text{g}/\text{cell}$ and start to proliferate after this point [67]. More recently, it was suggested that the mechanism of expansion and the temporal order is rather depot specific. In male and female mice, the visceral adipose tissue depot first undergoes hypertrophy, while in parallel precursors starts to proliferate. Upon prolonged high fat diet (HFD) feeding the precursors, mature and the visceral adipose tissues also expands through hyperplasia. In the subcutaneous adipose tissue of males, predominantly hypertrophy and only very minimal precursor proliferation was observed. In contrast, hypertrophy and de novo adipogenesis was observed in the subcutaneous depots of females [10,68,69]. This is in accordance with the sex-dependent distribution of fat. Males tend to accumulate fat predominantly in the visceral region, resulting in a rather apple shaped silhouette, in contrast to females, where the deposition of fat in the subcutaneous lower body region results in a rather pear shaped contour. This is not only due to hormonal differences; the neuronal input and genetic make-up also differ between the sexes [70]. Epidemiological and clinical studies could clearly demonstrate that the accumulation of fat in the visceral region is associated with a higher risk of metabolic diseases [71,72]. Various not mutual exclusive pathways have been proposed for this, with the first being the differential neural innervation and venous drainage. The visceral depot drains directly into the portal vein, thus sending a lot of FFA and other signaling molecules directly to the liver. Second, cell-autonomous mechanisms create depot-specific metabolic differences [73]. In general, it is thought that having many small adipocytes is metabolically healthier than having a few overstuffed large adipocytes.

If the adipose tissue expands during obesity and the adipocytes become hypertrophic, the blood supply of the tissue must also expand. The adipose tissue can promote blood vessel outgrowth by secreting pro-angiogenic factors. It was demonstrated by several groups that increased

angiogenesis can protect against pathologic adipose tissue expansion and fellow insulin resistance [74–76]. Nonetheless, hypoxia is often found in obese adipose tissue. This in turn activates the master regulator of oxygen homeostasis HIF-1. The transcription factor HIF-1 directly regulates hypoxia-associated genes like vascular endothelial growth factor A (VEGF-A), but it also initiates adipose tissue fibrosis [77]. During the expansion of adipose tissue, several adipocytes undergo necrosis or apoptosis, increasing together with the hypoxia-induced fibrosis, the infiltration of immune cells into the adipose tissue, thus generating an inflammatory response.

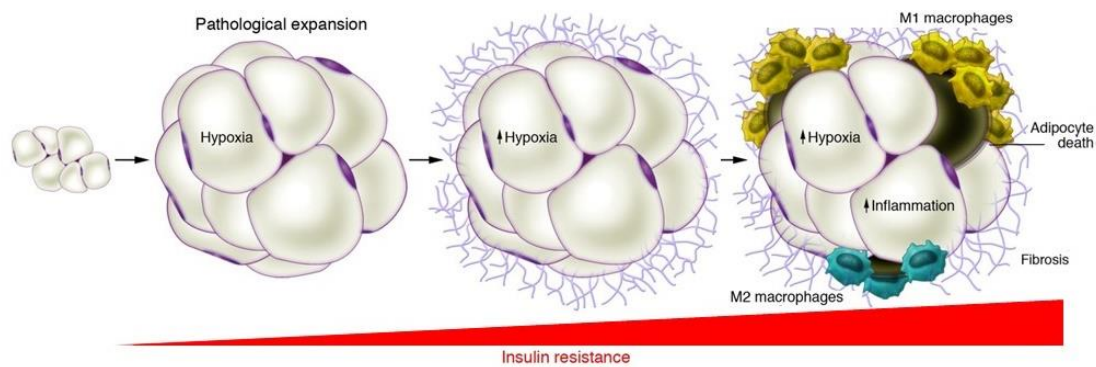


Figure 5: Pathological adipose tissue expansion, adapted from Sun et al. 2011 [78]

Around the dying adipocytes, a cluster of macrophages can be observed building so-called crown-like structures [79]. These macrophages are from the activated type M1, which is known to be pro-inflammatory and can be distinguished from the residing adipose tissue macrophages type M2, which are characterized by their anti-inflammatory and homeostatic functions. M1 macrophages express CD11c as a surface marker and secrete pro-inflammatory cytokines like TNF- α , IL-6, and IL-1 β [73]. These cytokines can either directly interfere with the insulin signaling through phosphorylation of the inhibitory serine residue of the insulin receptor substrate (IRS) or they activate other signaling pathways (c-Jun N-terminal kinase (JNK) pathway and I-kappa B kinase β (IKK β)/NF κ B pathway) that disrupt the insulin signaling [80]. Additionally, pro-inflammatory cytokines can stimulate lipolysis, thus increasing the levels of FFA in the blood, another hallmark of the metabolic syndrome [81]. Furthermore, inflammatory signals can inhibit the nuclear receptor peroxisome proliferator-activated receptor γ (PPAR γ), the master regulator of adipogenesis and adipocyte maintenance. Through this, adipocyte function is further compromised, resulting in less storage capacity [82]. Thus, the vicious cycle is established. The aforementioned residing M2 macrophages are characterized through their surface receptors CD206 and CD301 [73]. They support the adipose tissue homeostasis through the secretion of anti-inflammatory factors like IL-10, which potentiates insulin signaling [83], or arginase, which

blocks iNOS activity and the associated the profibrogenic response [84]. Upon diet induced obesity, macrophages infiltrate and residing adipose tissue macrophages undergo phenotypic switch from M2 to M1. However, not only the macrophages are involved; other immune cells like neutrophils or B- and T-lymphocytes are also attracted by the pro-inflammatory cytokines and contribute to the inflammatory response [85]. In summary, the inflammation and the affiliated pro-inflammatory cytokines significantly impair the insulin sensitivity of the adipose tissue. Unfortunately, this low-grade adipose tissue inflammation also affects further distant tissues such as the liver or muscle, establishing one major link of how obesity is associated with insulin resistance and T2D.

As illustrated in the previous section, adipocytes are not alone in the adipose tissue. Therefore, the adipocytes secrete a wide range of factors, generally named adipokines. They allow the adipocytes to communicate with other cell types present in the adipose tissue, but also allow for crosstalk with further distant organs. With the discovery of leptin in 1994 [86] and adiponectin in 1995 [87], the adipose tissue started to be appreciated as an endocrine organ and more than 600 different secretory proteins have been identified until today [88,89]. Thus, lots of hope regarding the combat against obesity and T2D lies within the adipokines. Leptin is secreted by adipocytes in proportion to the size of their triglyceride stores [90]. Its main function was initially described as regulating appetite via the leptin receptors, being expressed mainly in brain regions regulating energy metabolism. Patients with mutations in the leptin gene or the leptin receptor suffer from severe hyperphagia and decreased energy expenditure, resulting in serious obesity and metabolic disease [91]. In the context of obesity, leptin levels rise. It was demonstrated that patients become leptin resistant, probably due to fact that leptin can no longer cross the blood-brain barrier [92]. Hence, people who are already lack their satiety signal and continue eating. Albeit that the majority of leptin's function is mediated centrally, it also has various effects on the periphery. Through its pro-inflammatory properties on innate and adaptive immune cells, leptin promotes the chronic low-grade inflammation associated with T2D. In the adipose tissue, leptin is stimulating lipolysis in an autocrine manner as well as in a centrally mediated manner [93,94]. The other probably most described adipokine is adiponectin. Adiponectin receptors are expressed throughout the body, and therefore have a variety of functions. In the context of the metabolic syndrome, adiponectin can be described as insulin-sensitizing, anti-inflammatory, and antioxidant. It is abundantly but exclusively secreted by adipocytes. The positive effect of adiponectin on glucose metabolism is mostly mediated by the liver and skeletal muscle. Adiponectin sends signals via AMPK to reduce hepatic gluconeogenesis, and increase glucose uptake into the muscle. Additionally, it stimulates fatty acid oxidation in both tissues, resulting in

lower ectopic fat deposition, which in turn increases insulin sensitivity [95]. Furthermore, adiponectin promotes adipogenesis, which allows for a healthy expansion of the adipose tissue and prevents ectopic lipid accumulation [96]. Finally, adiponectin is also widely anti-inflammatory, e.g. through the inhibition of TNF- α secretion by adipocytes or through the upregulation of anti-inflammatory IL-10 from macrophages. Adiponectin expression is increased by the T2D drug class of Thiazolidinediones and it is suggested that the insulin-sensitizing effect of these drugs is mediated by the anti-inflammatory effect of adiponectin rather than by the direct insulin-sensitizing effect [97]. Many other adipokines have been identified and described. However, discussing all of them would go beyond the constraints of this thesis [98].

This leads us to the question, are the brown and brite/beige adipocytes the solution to the entire metabolic problem? Can we utilize them to cure obesity and T2D? Since the discovery of active brown fat in humans in the year 2009, more and more attention has been drawn towards the therapeutic potential of brown adipose tissue (BAT). As human brown adipose tissue is still a very recent research field, the majority of studies designed to understand brown adipose tissue function are performed in rodents. In the beginning, the main function of BAT was described as producing heat by burning glucose and fat, hence increasing energy expenditure. This was the starting point of the idea of using BAT activation to cure obesity. With the time and a better understanding of BAT function, it became more and more clear that the role of BAT goes beyond heat generation and that it plays a significant role as a "metabolic sink" for glucose and lipids in the body [99,100]. Thus, it has great potential to combat obesity and T2D, especially since it was shown that the amount of brown adipose tissue in humans inversely correlates with BMI and body fat mass [7,101]. Furthermore, the activation of human BAT improves insulin sensitivity and accelerates lipid metabolism [102,103]. However, until today, the hunt for a BAT activating drug is still ongoing, with one highly promising candidate being Mirabegron. It was shown that acute as well as chronic treatment of humans with Mirabegron stimulates BAT activity and increases BAT glucose uptake while having only minimal effects on the cardiovascular system [104,105]. Until now, Mirabegron was only tested chronically in a small group. However, based on the initial promising results, larger trials are expected. In parallel, research in the human BAT field is ongoing. The fact that BAT activity in humans is negatively regulated by age opens an evolutionary point of view from which one could try to find new treatment strategies to potentially reactivate BAT. The cross talk with other organs via BAT specific adipokines, named BATokines, might also open up new therapeutic potentials [106].

In conclusion, it is not about the amount of adipose tissue; it is about the healthiness of the adipose tissue. As soon as the white adipose tissue expands in a pathological manner, things take

their course. Fibrosis, Inflammation, and dysregulated adipokine release accelerate the progression of metabolic diseases. In rodents, the activation of brown and brite/beige adipose tissue can tackle a lot of the harmful metabolic processes. Translating this knowledge into humans is an ongoing process which will hopefully enable us to stop the pandemics of obesity and T2D in the near future.

1.7 The gut in the context of metabolic disorders

In research to combat obesity and T2D, many have focused on the effector organs like the adipose tissue, skeletal muscle, or pancreas. However, one should perhaps tackle the problem at its root. The gut is the entry point for food into the body. Gut cells sense and absorb nutrients and then they communicate and dissipate the information about the nutrients, as well as the nutrients themselves, to the body, thereby integrating them into the metabolic network.

Currently, the most effective treatment against obesity and T2D is bariatric surgery. Presently, the four most popular bariatric surgery techniques are Roux-en-Y gastric bypass (RYGB), vertical sleeve gastrectomy (VSG), adjustable gastric banding (AGB), and biliopancreatic diversion with or without duodenal switch (BPD and BPD-DS) [107]. RYGB and VSG are the most commonly performed procedures, thus they are also studied most extensively. Originally, bariatric surgery aimed to restrict food intake by reducing the stomach volume and promoting the malabsorption of nutrients by rearranging the intestines. Over the years, it became clear that bariatric surgery achieves more than this; it changes the metabolism of the gut and the signaling to many other organs. Complex changes in gut hormones, gut microbiota, afferent and efferent signaling of the enteric nervous system, and bile acid secretion mediate the positive metabolic effects of the bariatric surgery. As a result, it is also called metabolic surgery nowadays.

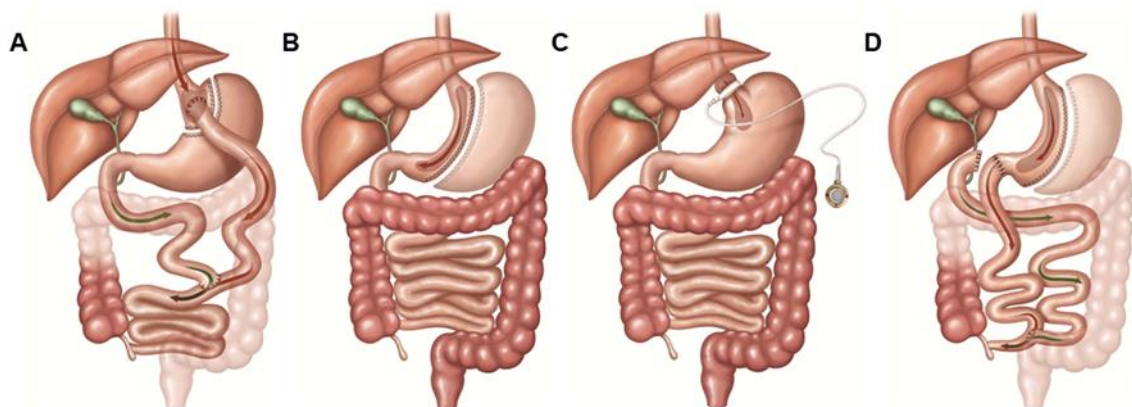


Figure 6: Bariatric surgery techniques, adapted from Neff et al., 2013 [107], *continued on the following page*

published under the creative commons licence, images are the property of Johnson and Johnson and Ethicon Endo-Surgery (Europe). **(A)** RYGB: a gastric pouch out of the upper part of the stomach is created and anastomosed to the distal part of the jejunum. The excluded biliary limb is connected back to the jejunum distal to the gastrojejunostomy. **(B)** VSG: the majority of the stomach is excised leaving a ca. 150 ml stomach pouch behind. **(C)** AGB: an inflatable band is placed around the very proximal part of the stomach. The tightness of the band can be adjusted accordingly. **(D)** BPD: a sleeve gastrectomy is performed and a biliopancreatic limb is created and anastomosed to the distal ileum.

Manipulating the gut's structure through bariatric surgery is highly efficient; patients lose 20 - 30% of their body weight and, more importantly, maintain this weight loss over the years [108,109]. Moreover, other metabolic diseases like dyslipidemia or hypertension can be improved or resolved with bariatric surgery [109]. In 87% of the patients, T2D is improved or resolved. The most effective resolution of T2D is observed in patients undergoing BPD-DS, followed by patients undergoing RYGB [65]. Interestingly, the remission of T2D can already be observed a few days after the surgery, which is before the patients even begin to lose weight. This suggests that there is also a weight-independent component of T2D remission [110]. The improvement in glucose levels immediately after the surgery is most likely due to the caloric restriction caused by the surgery itself. This stimulates the loss of ectopic fat in the liver, which dramatically improves hepatic insulin resistance [111]. Further on, the improvements in T2D are suggested to be mediated by changes in glucose absorption, gut hormones, microbiota, and ultimately weight loss. However, until today, the exact underlying mechanisms mediating the T2D resolution are not completely understood [112].

The gut-secreted hormones are another reason why the gut has great power over our metabolism. As mentioned before, they are secreted by the EECs in response to nutritional stimuli. Depending on the location and the type of EECs, different hormones are secreted. They have various physiological roles in relation to obesity and T2D. Glucagon-like peptide 1 (GLP-1) and gastric inhibitory polypeptide (GIP) mediate the incretin effect. This describes the phenomenon where, if a glucose bolus is administered orally, more insulin is secreted than if the same amount of glucose is administered intravenously [113]. They provide a gut-derived signal which augments glucose-dependent insulin secretion. GLP-1 and GIP endorse insulin secretion, islet beta cell survival, and insulin biosynthesis. Moreover, GLP-1 inhibits glucagon secretion directly and indirectly via the promotion of somatostatin. Both GLP-1 and GIP are inactivated by dipeptidyl peptidase-4 (DPP4) [114]. Besides GLP-1 and GIP, cholecystikinin (CCK) acts on the pancreas and induces the secretion of pancreatic enzymes for lipid digestion when a fat-rich meal is eaten [20]. Further gut secreted hormones play an important role in food intake control. GLP-1, GIP, CCK, and GLP1-oxintomodulin-peptide YY (PYY) all function as anorexigenic hormones and induce postprandial satiety. However, their exact mechanism of action is still under investigation. Receptors for all of them are located on the afferent vagus but also in the appetite-regulating regions of the central

nervous system, the hypothalamus, and the brainstem [20]. On the other side, there are also orexigenic hormones, namely Ghrelin and insulin-like peptide 5 (INSL5). Ghrelin is secreted from the EECs located in the stomach in anticipation of a meal, although Ghrelin secretion is suppressed as soon as food is ingested [20]. INSL5 is produced by colonic and rectal L-Cells and, surprisingly, is co-released with the anorexigenic hormones PYY and GLP-1 [115]. Nonetheless, the administration of INSL5 significantly increased food intake in mice, although the underlying physiological roles are still poorly understood [116]. Regulation of the gastric emptying is another factor that greatly influences the digestion and absorption of food. Thus, this process is tightly regulated by a set of hormones. CCK, GLP-1, GIP, and PYY regulate the food passage through the gut. Thus, they can determine the amount and frequency of nutrients getting absorbed [20].

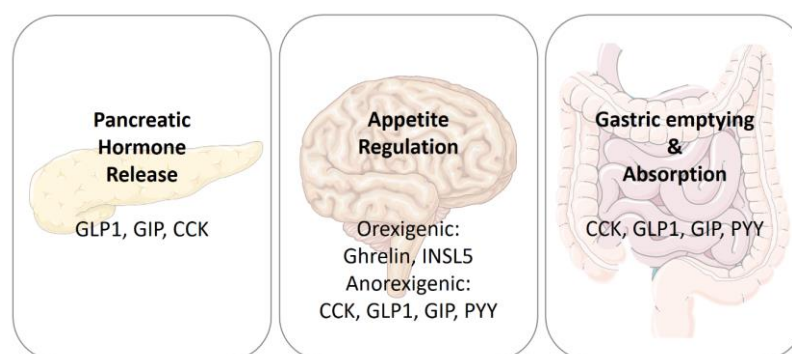


Figure 7: Gut hormones in the context of T2D and obesity, based on Gribble and Reimann, 2019 [20]. Glucagon-like peptide 1 (GLP-1); gastric inhibitory polypeptide (GIP); cholecystokinin (CCK); GLP1-oxynomodulin-peptide YY (PYY); insulin-like peptide 5 (INSL5)

The powerful action of gut hormones regarding metabolism was also recognized by the pharmaceutical companies. GLP-1 receptor agonists and DPP4 inhibitors successfully made it to the market and are becoming more and more popular for the treatment of T2D and obesity. GLP-1 receptor agonists improve blood glucose levels, induce weight loss, and further display cardio protective effects. However, dose dependent side effects like nausea, diarrhea, or vomiting limit the use of higher doses of GLP-1 receptor agonist, which would drive a greater weight loss [117,118]. DPP4 inhibitors also display great effects in the glycemic control with limited side effects. However, no effect on bodyweight was observed [119]. GIP receptor agonists alone turned out to be almost ineffective in T2D patients [120]. However, GLP-1-GIP dual agonists demonstrated great potential to treat obesity, hyperglycemia, and dyslipidemia. Thus, several companies are in phase I or phase II of clinical trials with this agonist combination [117,121,122]. Several other peptides or combinations of gut peptides are currently being investigated, but they still require further investigation [123,124].

Another aspect that needs to be highlighted in the context of the gut and metabolic diseases is the gut-brain axis. Here, the nervous vagus, which is the bidirectional communication route eliciting gut feelings, stands in the center. As aforementioned, the chemosensors in the EECs stimulate gut hormone secretion, which can signal to the afferent endings of the vagus in a paracrine manner to govern satiation and food preferences. Furthermore, tension and mechanoreceptors sense the gut luminal content. Hence, the brain can direct gastric volume and gastric motility [125]. Additionally, one must also consider the hedonic component of food. Taste sensors on the tongue as well as in the gut can sense palatable food, which results in more “food reward” than eating plain food. After bariatric surgery, a change in “food reward” can be observed in many patients. The patients spend less time thinking about food and start to prefer fruits and low-calorie foods. However, these are only observations, and a study directly testing the changes in the reward centers of the brain following bariatric surgery is missing yet [126]. At the moment, we are still far away from fully understanding the complex bidirectional interaction of the gut and the brain. Studies in this area are ongoing and will hopefully further elucidate the gut-brain axis in the future [125].

Lastly, the microbiota of the gut must be mentioned. The gut is the host for trillions of microorganisms. It was demonstrated that the microbiome of the gut can significantly influence obesity and T2D. Bäckhed et al., showed that germfree mice do not develop obesity and insulin resistance when placed on HFD. However, if these mice were reconstituted with gut microbiota from lean mice, they rapidly started to gain weight and became glucose intolerant within two weeks [127]. Similarly, when germ-free mice received gut microbiota from mice or humans that underwent RYGB, a loss in bodyweight and an increase in energy expenditure was observed [128,129]. This demonstrates the power of the gut microbiota, although the underlying mechanisms are difficult to understand and have not been completely dissected yet. Lean people and mice show an equal balance of Firmicutes to Bacteroidetes, but in obesity the balance shifts towards Firmicutes [130]. The gut microbiota of obese individuals increase the energy harvest from the digesting food, thus linking the bacteria to the development of obesity. The bacteria produce short chain fatty acids (SCFA) through the hydrolyzation and fermentation of polysaccharides. SCFAs modulate the lipid metabolism of the host by promoting lipogenesis and inhibiting the fasting-induced adipocyte factor (FIAF), which suppresses LPL. Hence, fat accumulation in adipocytes is favored [131]. Furthermore, SCFAs stimulate the expression of the Na⁺/glucose cotransporter (SGLT-1), which favors the absorption of monosaccharides [132]. Another very important consequence of an altered microbiota composition is the so-called “leaky gut” syndrome. The gut microbiota, modulated upon HFD, stimulate the intestinal epithelial cells.

As a response, they secrete pro-inflammatory cytokines. In turn, these increase the intestinal permeability, and bacterial lipopolysaccharide (LPS) can cross the intestinal barrier, resulting in low-grade intestinal inflammation. Through this, the permeability of the gut is further perturbed and the local inflammation progresses into a systemic inflammatory response, which can consequently promote the adipose tissue inflammation and concomitant insulin resistance [133].

In summary, our digestive tract offers a wide range of options to treat the metabolic syndrome. However, as the example of the bariatric surgery nicely demonstrates, there is not one single factor alone in the gut that needs to be changed in order to achieve ultimate success over the metabolic syndrome. The metabolic power of the gut is the result of a strong interplay between the gut cells, the secreted gut hormones, the crosstalk with other organs, and the hosted microbiota. All factors are tightly connected to each other. The manifold interactions and functions of the gut are still not fully elucidated; thus, the research will go on, and hopefully new powerful treatment options against the metabolic syndrome will emerge.

CHAPTER 2

Quantification of adipocyte numbers following adipose tissue remodeling ^a

Caroline Moser, Leon G. Straub, Yael Rachamin, Dianne Dapito, Elisabeth Kulenkampff, Lianggong Ding, Wenfei Sun, Salvatore Modica, Miroslav Balaz, Christian Wolfrum

Contribution:

Caroline Moser performed and analyzed part of the experiments, prepared the figures and wrote the manuscript.

^a *This article was accepted in Cell Reports. This chapter is a preprint of the prepared manuscript.*

Quantification of adipocyte numbers following adipose tissue remodeling

Caroline Moser^{1,2}, Leon G. Straub^{1,2}, Yael Rachamin¹, Dianne Dapito¹, Elisabeth Kulenkampff¹, Lianggong Ding¹, Wenfei Sun¹, Salvatore Modica¹, Miroslav Balaz¹, Christian Wolfrum^{1*}

¹ *Institute of Food Nutrition and Health, Eidgenössische Technische Hochschule Zürich (ETH), Schwerzenbach, 8603, Switzerland*

² *These authors contributed equally*

* *Correspondence: christian-wolfrum@ethz.ch*

Abstract

To analyze the capacity of white and brown adipose tissue remodeling, we developed two novel mouse lines, to label, quantitatively trace and ablate white, brown and brite/beige adipocytes, at different ambient temperatures. We show here that the brown adipocytes are recruited first and reach a peak after one week of cold stimulation followed by a decline during prolonged cold exposure. Contrary brite/beige cell numbers plateau after three weeks of cold exposure. At thermoneutrality, brown adipose tissue in spite of being masked by a white-like morphology, retains its brown-like physiology, as Ucp1+ cells can be recovered immediately upon beta3-adrenergic stimulation. We further demonstrate that the recruitment of Ucp1+ cells in response to cold is driven by existing adipocytes. In contrast, the regeneration of the interscapular brown adipose tissue following ablation of Ucp1+ cells is driven by de novo differentiation.

2.1 Introduction

White adipocytes are the storage cells of neutral lipids [134], while brown adipocytes utilize energy from glucose and fat to produce heat. Under cold stimulation, brown-like adipocyte cells, named brite or beige adipocytes, arise within the predominantly white adipose tissue depots [135,136]. Several features distinguish these cell types, including but not limited to lipid droplet morphology, mitochondrial content and the expression of Uncoupling protein 1 (Ucp1) [134]. In mice and humans, the adipose organ consists of various depots which can be distinguished by their ratio of white, brown and beige adipocytes [37,137,138]. In addition to the functional mature adipocytes, other cell types such as pre-adipocytes, fibroblasts, immune cells or endothelial cells can be found in the stromal vascular fraction of adipose tissue [10].

Upon cold stimulation, the thermogenic capacity and number of brown adipocytes is increased [139–141], while within the inguinal white adipose tissue depot (ingWAT), Ucp1 expressing multilocular brite/beige adipocytes arise from precursor cells [10,142] or interconvert from white adipocytes [12,14,143]. In contrast, under thermoneutral housing conditions, the brown adipocytes obtain a morphologically white-like appearance, while their transcriptome maintains a brown-like pattern [144,145]. Adaptation and remodeling of the adipose tissue in response to various external stimuli has been studied by different methods, such as transcriptomic and proteomic profiling, epigenomics, histology, and other imaging methods [14,137,144,146]. However, the change in the numbers of white, brown, and brite/beige adipocytes during adipose tissue remodeling remain elusive, due to the lack of quantitative methods. We report here detailed kinetics of adipose tissue remodeling, which provides new insight into the adaptive processes that take place within adipose tissue to maintain thermogenesis.

2.2 Results

2.2.1 Establishment of a quantitative recombination assay to determine adipocyte numbers

Given the heterogeneity of the adipose organ we aimed to establish an assay to quantify adipocyte numbers in whole adipose tissue depots. The Adipoq-tracer-deleter mouse line (Adipoq-CreERT2 x ROSA26-tdRFP x Ucp1-DTR-GFP) and the Ucp1-tracer-deleter mouse line (Ucp1-CreERT2 x ROSA26-tdRFP x Ucp1-DTR-GFP) were generated to genetically label all Adiponectin+ (Adipoq+) or Ucp1+ cells with an RFP label upon administration of tamoxifen. In addition, due to the *Ucp1-DTR-GFP* allele, all Ucp1+ cells are constitutively labeled by GFP and

the diphtheria toxin receptor (DTR), which is transiently expressed under the control of the Ucp1 promoter, can be used to deplete all Ucp1⁺ cells by administration of diphtheria toxin (DT) [Fig. 1A, Suppl. Fig. 1A]. Initially, we observed that one to five days of oral tamoxifen administration (2 mg/mouse/day) resulted in a constant number of recombined Adipoq⁺ cells, both in the interscapular brown adipose tissue depot (iBAT) (25.0M Adipoq⁺ cells; M = 10⁶) and in inguinal white adipose tissue (ingWAT) (18.1M Adipoq⁺ cells) [Fig. 1B; C]. No significant difference in the number of either the total, or the recombined Adipoq⁺ cells was observed between males and females [Fig. 1B; C]. The recombination of Adipoq⁺ cells was found exclusively in the adipose tissue [Fig. 1I] and no signal was observed in the iBAT and the ingWAT of wild-type mice [Fig. 1E; G], while in mice heterozygous for the Adipoq-CreERT2 allele, all adipocytes were labelled RFP positive [Fig. 1F; H]. The method works equally efficient in the epididymal white adipose tissue (eWAT), without any effects on bodyweight, while lower tamoxifen doses were not sufficient to label all adipocytes [Suppl. Fig. 1B; D; E]. The same labeling efficiency was observed in the Ucp1-tracer-depleter mouse line [Suppl. Fig. 1F-M]. Taken together, we developed a system, which can be used to accurately quantify Adipoq⁺ cells and Ucp1⁺ cells in complete adipose depots.

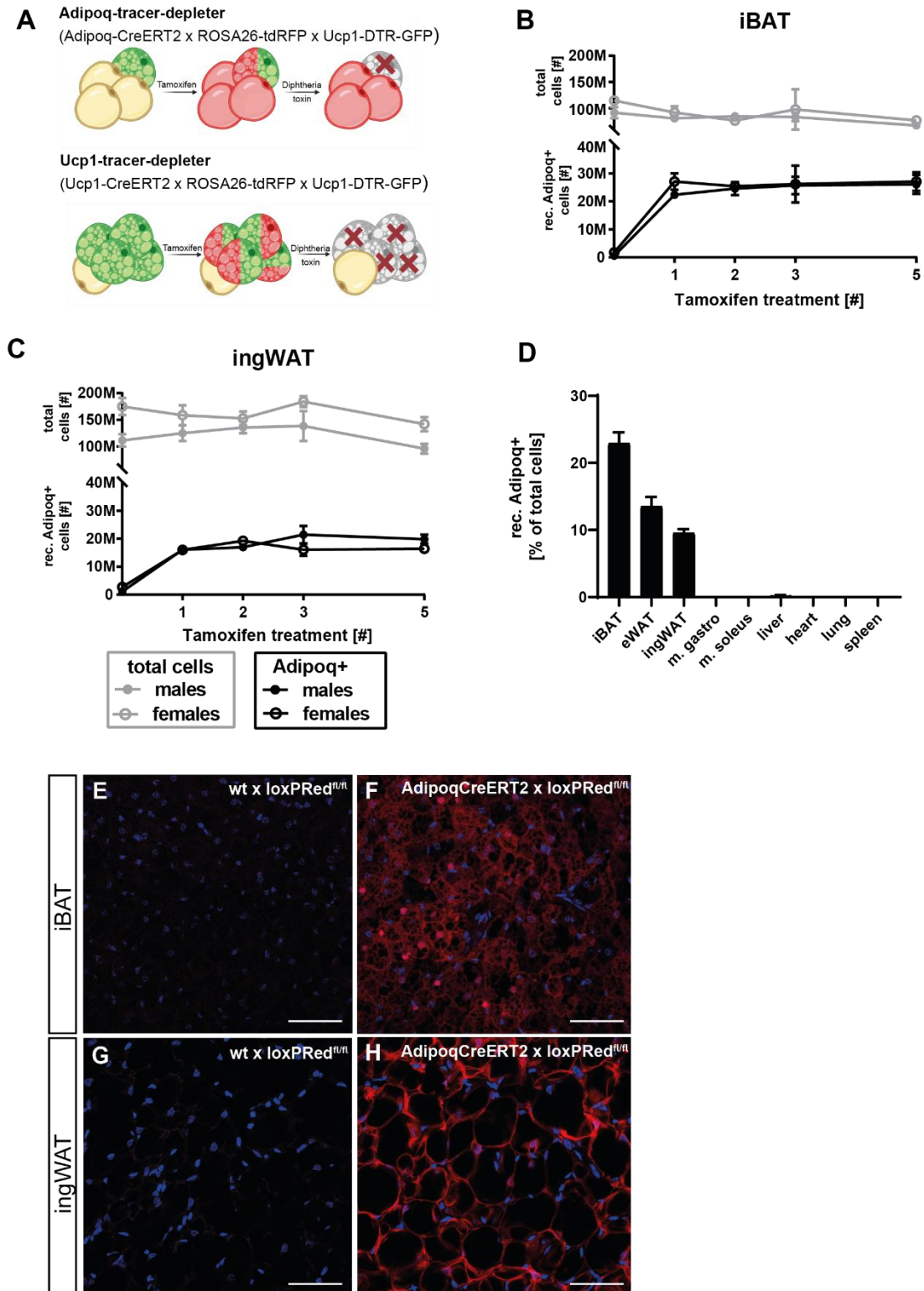


Figure 1: (A) Schematic description of the mouse models. (B-C) Effect of tamoxifen dosing on recombination: Adipoq-tracer-deleter animals received 1 to 5 treatments with tamoxifen (2mg/per animal/day, administered orally) on consecutive days. All tissues were taken on day 6 after the first tamoxifen treatment. The total as well as the Adipoq+ recombined cell number, was analyzed in **(B)** iBAT, **(C)** ingWAT, male and females were analyzed and shown individually, n=2-7. **(D) Tissue specificity of the Adipoq-tracer-deleter line:** Animals received tamoxifen (2x 2 mg/per animal/day). Multiple tissues were taken 7 days later and analyzed for percentage *continued on the following page*

of recombined Adipoq+ cells, n=8. Data are presented as mean \pm SEM, M = 10⁶, rec. = recombined **(E-H)**
Histological analysis of recombination efficiency: Samples of **(E)** iBAT wt x loxPRed^{fl/fl} **(F)** iBAT
AdipoqCreERT2 x loxPRed^{fl/fl} **(G)** ingWAT wt x loxPRed^{fl/fl} **(H)** ingWAT AdipoqCreERT2 x loxPRed^{fl/fl} were
harvested 2 days after tamoxifen treatments. DNA was stained with Hoechst 3342 (blue), and recombined
cells were stained with Anti-RFP (red). Scale bar = 50 μ m.

2.2.2 Brown adipocytes maintain responsiveness to ADRB3 under thermoneutrality

Standard animal housing conditions range from 22°C – 25°C, which is below the thermoneutral zone and thus elicits a constant cold stress in mice [147]. To mimic the thermogenic state of a human more closely, many groups have investigated the brown adipose tissue of animals housed at thermoneutrality (30°C). Most observed a white-like tissue morphology and reduced Ucp1 protein and mRNA content under these conditions [148,149]. However, there is an ongoing debate in the field, whether brown adipocytes maintain their inducibility even after acquiring a white-like cellular morphology.

When we administered tamoxifen (2x 2 mg/per animal) after five weeks of thermoneutral housing, significantly less Ucp1+ cells were recombined in iBAT, axillary BAT (aBAT) and cervical BAT (cBAT) compared to room temperature [Fig. 2A]. As expected, the cellular morphology in iBAT at thermoneutrality changed from multilocular to unilocular [Fig. 2H; I]. Albeit these changes, the amount of recombined Ucp1+ cells remained at 30-45% of those observed at room temperature, suggesting that the Ucp1 promoter retains partial activity, even after prolonged thermoneutral housing.

To further characterize the functionality of these cells, we analyzed their responsiveness to beta-adrenergic stimulation [Fig. 2B]. Upon activation by cold or by administration of the beta3-adrenergic receptor (ADRB3) agonist CL316,243 (CL), brown adipocytes react by upregulating thermogenic genes, lipolysis and energy expenditure [1]. At room temperature, ADRB3 stimulation reduced lipid droplet size in iBAT indicating an increased lipolysis and thermogenic activity [Fig. 2J], while the numbers of Ucp1+ cells in iBAT and aBAT remained unchanged [Fig. 2D]. In ingWAT the number of Ucp1+ cells increased from non-detectable levels to $1.3 \pm 0.7M$ Ucp1+ cells after CL injection [Fig. 2D]. In thermoneutral conditions, ADRB3 stimulation increased the number of Ucp1+ cells in the iBAT, aBAT, cBAT and ingWAT to similar levels observed at room temperature [Fig. 2D; E]. Nevertheless, at thermoneutrality, brown adipocytes displayed a more paucilocular phenotype following ADRB3 stimulation [Fig. 2K]. Based on these data, we conclude that, despite their unilocular appearance at thermoneutrality, brown adipocytes maintain their responsiveness to ADRB3 stimulation and the Ucp1+ cell numbers can be recovered completely

within two days of ADRB3 stimulation. This supports the notion that brown adipocytes do not convert into white adipocytes at thermoneutrality, but rather acquire a “masked” state.

To further confirm that at thermoneutrality no brown-to-white adipocyte conversion is taking place, we took advantage of the deleter properties of our mouse models. Therefore, we first labeled all Ucp1+ cells by tamoxifen at room temperature, before transferring the mice to thermoneutrality for five weeks [Fig. 2C]. If brown adipocytes would convert into white adipocytes, it would not be possible to ablate these cells with DT, as the DTR is expressed transiently under the control of the Ucp1 promoter. In accordance with our previous results, we observed also an almost complete ablation of all Ucp1+ cells in all depots even at thermoneutral housing [Fig. 2F; G], which was confirmed by histological analysis [Fig. 2L; M]. Of note is the observation that Ucp1+ cell numbers in the saline treated group at room temperature were reduced five weeks post tamoxifen administration in all three brown adipose tissue depots [Fig. 2F], compared to room temperature conditions after acute labeling [Fig. 2A]. This indicates that a certain level of cell-turnover took place. As we did not observe any difference in the remaining Ucp1+ cell numbers at either room temperature or thermoneutrality [Fig. 2F; G], we conclude that the cell turnover is similar under both housing conditions.

In summary, we show here that at thermoneutrality, brown adipocytes remain fully responsive to ADRB3 stimulation, despite being masked by a white-like adipocyte morphology.

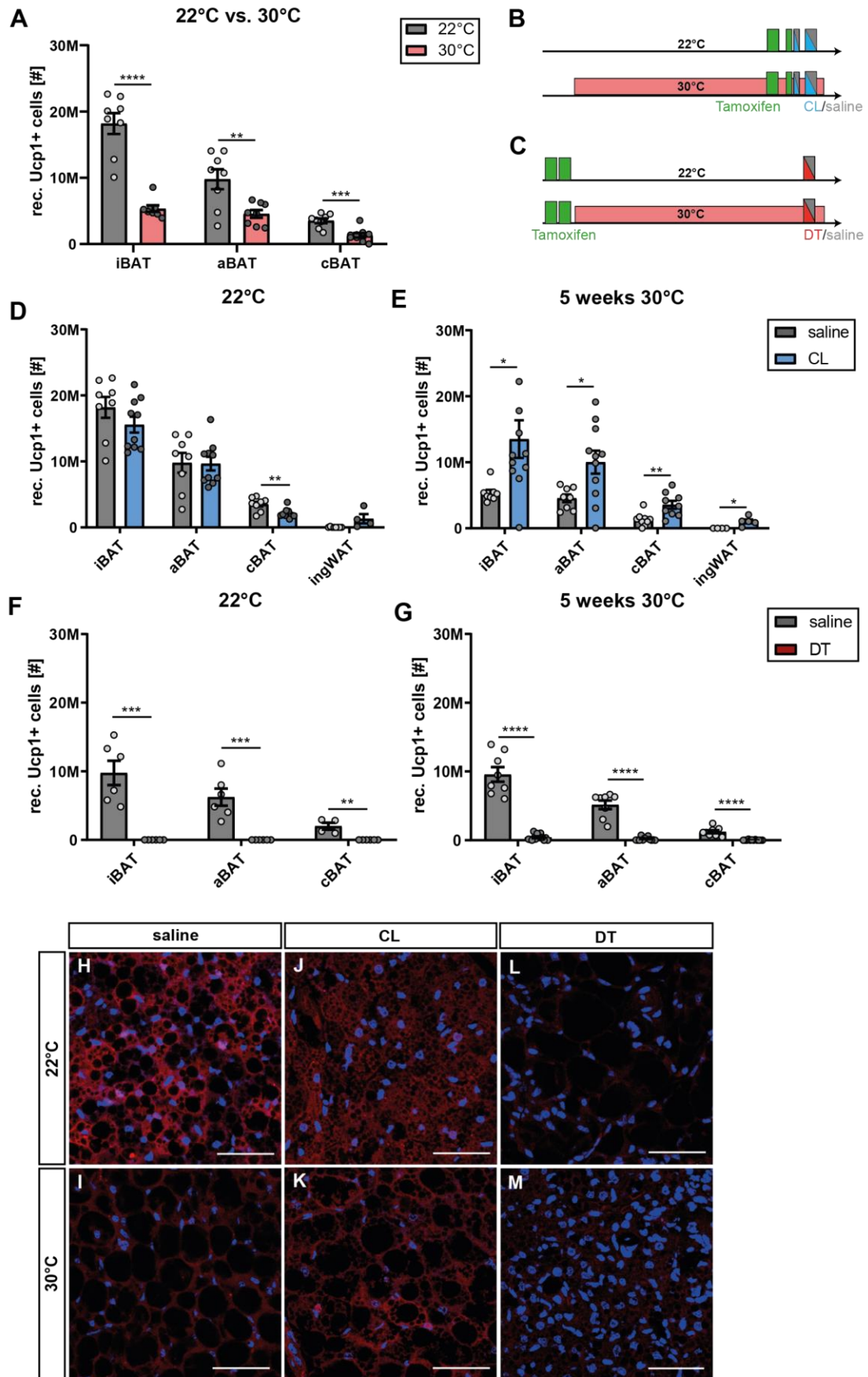


Figure 2: (A) Thermoneutrality induced plasticity of adipose tissue: *continued on the following page*

Animals of the Ucp1-tracer-deleter line were housed at thermoneutrality or at room temperature for 5 weeks. Tamoxifen was applied at the end. The number of Ucp1+ cells was analyzed in iBAT, aBAT and cBAT, n=8. **(B) Schematic description of ADRB3 stimulation:** Animals of the Ucp1-tracer-deleter line were housed at 22°C or 30°C for five weeks. At the end, they received tamoxifen followed by a second treatment with tamoxifen and ip. injection of CL the next day. A second CL injection was given the following day. Tissue samples were taken at day 2 after the last CL injection. **(C) Schematic description of ablation efficiency:** Tamoxifen was administered before start of the experiment. After 5 weeks at room temperature or thermoneutrality, DT or saline was injected. Tissues were harvested 2 days post DT injection. **(D-E) Quantification of ADRB3 stimulation:** The Ucp1-tracer-deleter animals received thermoneutrality and tamoxifen, CL/saline as depicted in the scheme under (B). The total number of Ucp1+ cells in the iBAT, aBAT and cBAT was quantified at **(D)** room temperature and **(E)** thermoneutrality, n=8-11. **(F-G) Quantification of ablation efficiency:** The Ucp1-tracer-deleter animals received tamoxifen, thermoneutrality and DT/saline as depicted in the scheme under (C). The total number of Ucp1+ cells in the iBAT, aBAT and cBAT was quantified at **(F)** room temperature and **(G)** thermoneutrality, n=6-12. **(H-M) Histological analysis of thermoneutrality induced plasticity of iBAT:** Animals were housed and treated as indicated. DNA was stained with Hoechst 3342 (blue), and recombined cells were stained with Anti-RFP (red). Scale bar = 50 μ m. **(H)** room temperature; saline **(I)** thermoneutrality; saline **(J)** room temperature; CL **(K)** thermoneutrality; CL **(L)** room temperature; DT **(M)** thermoneutrality; DT. Data presented are mean \pm SEM, M = 10^6 , rec. = recombined.

2.2.3 Different kinetics of thermogenic cell recruitment in response to chronic cold exposure

It is widely known that, upon cold stimulation, brown adipose tissue mass, as well as Ucp1 mRNA and protein levels increase [149,150], while white adipose tissue “browning” can be observed in certain depots [151]. However, the capacity and kinetics to form Ucp1+ cells in response to cold is unknown.

By employing the Ucp1-tracer-deleter line, we were able to quantify the number of Ucp1+ cells in different adipose tissue depots following short- and long-term cold exposure. In the iBAT, the number of Ucp1+ cells almost doubled within the first week of cold exposure from 28.9 ± 7.5 M to 53.2 ± 5.2 M Ucp1+ cells [Fig. 3A]. Similarly, the total number of cells increased within the first week (128.6 ± 27.6 M vs. 167.2 ± 12.4 M total cells), thus the relative number of Ucp1+ cells within the depot increased only by 50% from 21.2 ± 2.5 % to 32.6 ± 3.8 % [Fig. 3B]. In contrast, chronic cold exposure for eight weeks resulted in a decrease in Ucp1+ cells in iBAT (26.3 ± 4.7 M Ucp1+ cells; 25.7 ± 1.7 % Ucp1+ cells) to levels observed at room temperature [Fig. 3A; B]. While in the eWAT no browning was observed [Fig. 3E; F], in ingWAT the kinetics of browning were slower than in iBAT and saturated at around 4.2 ± 0.5 M Ucp1+ cells only after three weeks of cold exposure [Fig. 3C]. The total cell numbers in the ingWAT reached a maximum after one week of cold exposure (136.8 ± 24.5 M to 276.2 ± 32.0 M total cells) and after 3 weeks of cold exposure plateaued at approximately 234M cells. It should be noted that brite/beige fat cells constitute only 2% of all cells present within the ingWAT depot [Fig. 3D].

Altogether the number of Ucp1+ cells from iBAT and ingWAT amounted to 55.5M cells after one week of cold exposure, while after eight weeks numbers were reduced to 30.5M, which is similar

to the numbers observed at room temperature (29.3M Ucp1+ cells). Thus, the increase in the number of brite/beige fat cells is not compensating for the reduction in Ucp1+ cells in iBAT upon prolonged cold exposure.

To determine the browning capacity of the ingWAT, the ratio of Ucp1+ and Ucp1- adipocytes is important. To quantify these numbers, we stimulated brown and brite/beige adipocyte formation by CL administration and then depleted Ucp1+ cells from the adipose tissue by DT injection. In the ingWAT a 16% reduction of Adipoq+ cells was observed upon DT mediated ablation of Ucp1+ cells ($20.2 \pm 1.0M$ vs. $17.0 \pm 2.0M$ Adipoq+ cells) which equals 3.2M brite/beige fat cells [Fig. 3G].

In summary, we provide here kinetics of adipose tissue plasticity upon cold exposure. Our data suggest that iBAT is the early responder to cold, while in the ingWAT maximal browning is observed after three weeks of stimulation. Interestingly, our data suggest that the total numbers of Ucp1+ cells in iBAT and ingWAT upon long term cold exposure are similar to numbers observed at room temperature. This suggests that either the individual Ucp1+ cells increase their thermogenic activity or the presence of alternate strategies to maintain thermogenesis.

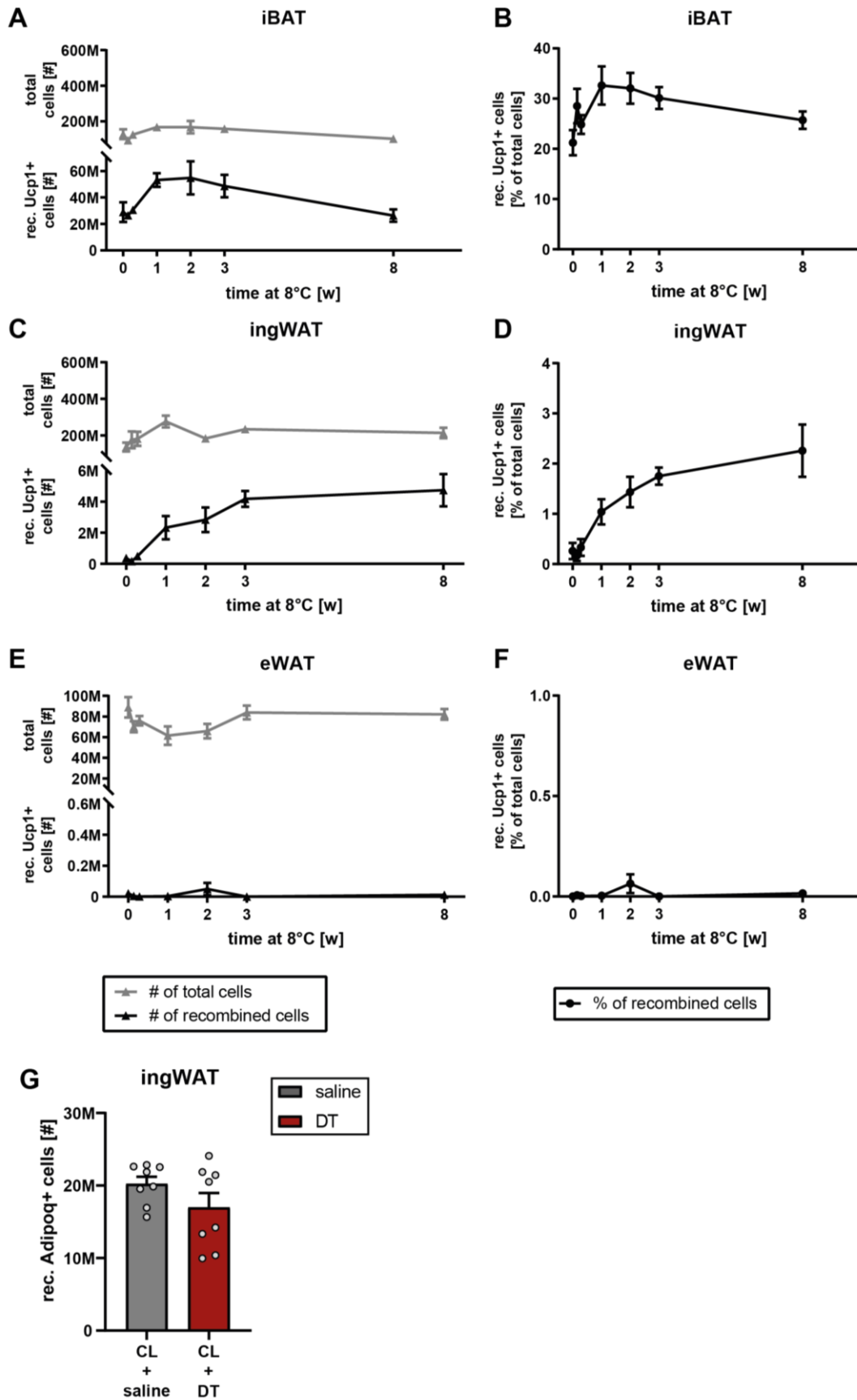


Figure 3: (A-F) Cold induced plasticity of adipose tissue: *continued on the following page*

Animals of the Ucp1-tracer-deleter line were cold exposed at 8°C. Tissue samples were taken before cold exposure and after 1 day, 2 days, 1 week, 2 weeks, 3 weeks, and 8 weeks of cold exposure. Tamoxifen was administered every week. The number of Ucp1+ cells and the total cell number as well as the % of Ucp1+ cells with respect to total cell number was analyzed in **(A)&(B)** iBAT; **(C)&(D)** ingWAT; **(E)&(F)** eWAT, n=5-9. **(G) Number of Ucp1+ cells ablated from the pool of Adipoq+ cells:** The animals of the Adipoq-tracer-deleter line received 2 tamoxifen treatments. 1 week later the animals were injected with DT or saline. The consecutive 3 days all animals received CL & DT/saline. Tissues were harvested one day after the last injection. The number of Adipoq+ cells was quantified in **(G)** ingWAT, n=8. Data presented are mean \pm SEM, M = 10^6 , rec. = recombined.

2.2.4 The iBAT depot has a high remodelling capacity

In humans the presence and activity of brown adipose tissue reduces with age [7–9,101] suggesting that, the mechanism of regeneration and recruitment of brown adipose tissue is important to maintain organ function.

To study the regeneration of brown adipose tissue, all Ucp1+ cells were depleted by DT administration. Subsequently, animals were cold exposed for one week to stimulate re-growth and treated with tamoxifen at the end of the cold exposure to quantify the full regrowth potential of iBAT [Fig. 4A]. From baseline (1.7 ± 0.6 M Ucp1+ cells), the iBAT showed the capacity to regrow 22.4 ± 2.8 M Ucp1+ cells [Fig 4B], which constitutes approximately 92% of the Ucp1+ cells observed at room temperature (28.9 ± 7.5 M Ucp1+ cells) [Fig 3A]. In absolute numbers this amounts to an increase of 20.7M Ucp1+ cells [Fig 4B], which is comparable to the increase in Ucp1+ cells in iBAT after one week of cold exposure (24.3 M Ucp1+ cells) [Fig 3A].

The increase in Ucp1+ cells after cold exposure (recruitment) or after ablation (regeneration) can be due to differentiation or proliferation of adipogenic precursors, or due to interconversion of Ucp1- adipocytes into Ucp1+ adipocytes [12,152]. We used the Adipoq-tracer-deleter mice to first determine the origin of regenerating cells in the iBAT after ablation. Therefore, we initially labeled all Adipoq+ cells by administration of tamoxifen, followed by a three-week washout period [Suppl. Fig. 2A–C]. Subsequently, all Ucp1+ cells were ablated by DT and afterwards, the animals were transferred into cold for one week to stimulate the re-growth [Fig. 4C]. Adipocytes positive for the recombined Adiponectin label would under these conditions be derived from pre-existing Ucp1- adipocytes, while cells negative for the Adiponectin label would have originated from precursor cells. Only a very small amount of 2.1 ± 0.5 M Adipoq+ cells were detected [Fig. 4E] in our experimental paradigm, suggesting that during the regeneration of iBAT, only a minority of adipocytes originated from pre-existing adipocytes, and that the majority was derived from precursor cells. By administering tamoxifen at the end of the cold exposure we could calculate a re-growth of 21.4 ± 3.7 M Adipoq+ cells [Fig. 4E], which is equal to the numbers detected upon iBAT ablation [Fig. 4B], confirming the observed regeneration potential.

To determine the origin of the cold recruited cells in the iBAT, we labeled all Adipoq⁺ cells by tamoxifen, followed by a three-week washout period [Suppl. Fig. 2A–C], before we stimulated the recruitment of brown adipocytes by one week of cold exposure [Fig. 4D]. If the numbers of Adipoq⁺ cells with and without tamoxifen re-administration would be similar, the cold induced recruitment of brown adipocytes would be driven by pre-existing adipocytes, while if there was a difference, the recruitment would be driven by the differentiation of precursors, which were not labeled at room temperature. When comparing the amount of Adipoq⁺ cells in the iBAT of both groups, we did not observe any significant difference in cell numbers ($53.7 \pm 5.2\text{M}$ Adipoq⁺ cells vs. $58.1 \pm 3.2\text{M}$ Adipoq⁺ cells) [Fig. 4F]. Thus, we conclude that contrary to the regeneration, the recruitment of brown adipocytes in cold is driven by conversion of pre-existing adipocytes. We observe an increase of 20M-30M Adipoq⁺ in both the regeneration and the recruitment paradigm, which suggests that both the interconversion and the *de novo* formation are equally potent mechanisms to increase the number of brown adipocytes.

In conclusion, we show that the iBAT displays a high capacity of remodeling upon cold exposure. Interestingly, the origin of recruited vs. regenerated brown adipocytes differs. During BAT regeneration, the increase in cells is mainly due to the differentiation from precursors cells, while newly recruited brown adipocytes in BAT are formed mainly from pre-existing adipocytes.

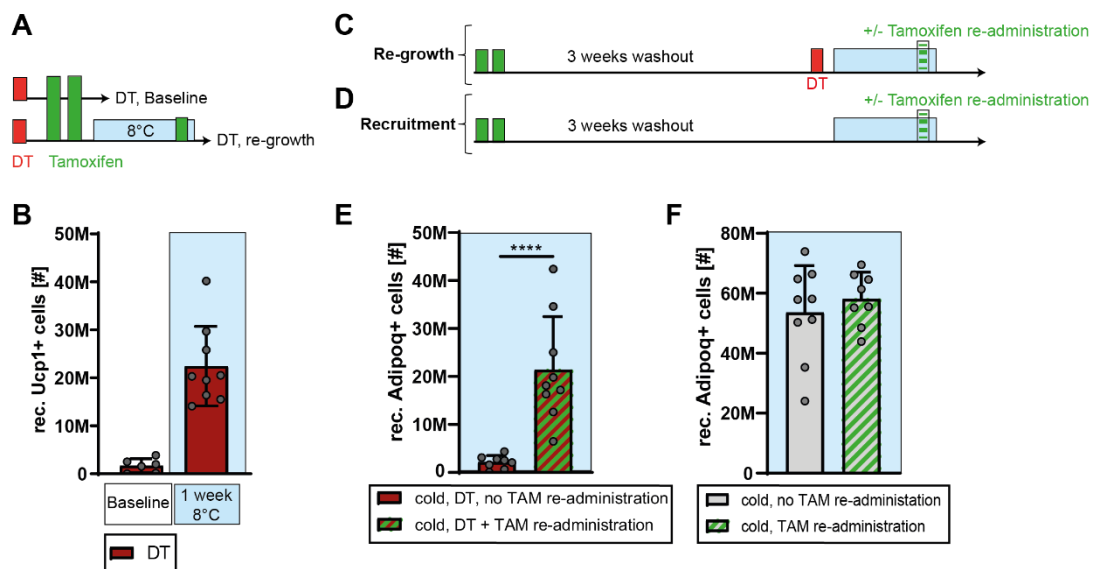


Figure 4: (A) Schematic description of the re-growth experiment: In the baseline group first all Ucp1⁺ cells were ablated by DT, followed by the administration of tamoxifen 2- and 3-days post DT injection. Tissues were harvested 4 days post DT injection. In the re-growth group, all Ucp1⁺ cells were ablated by DT, followed by 2 administrations of tamoxifen and 1 week of cold exposure with a re-administration of tamoxifen at the end. **(B) Ablation and re-growth quantification:** The Ucp1-tracer-depleter animals received DT, tamoxifen, and cold exposure, as depicted in the scheme under (A). The total number of Ucp1⁺ cells in the iBAT was analyzed, n=6-9. **(C) Schematic description origin of the re-growing brown adipocytes:** The Adipoq-tracer-depleter line received tamoxifen followed by a 3-week washout period. At the end of the washout period, DT was applied, *continued on the following page*

and the animals were cold exposed for 1 week. Part of the animals received a tamoxifen re-administration at the end of the cold exposure. **(D) Schematic description origin of the recruited brown adipocytes:** The Adipoq-tracer-depleter line received tamoxifen followed by a 3-week washout period. At the end of the washout period, the animals were cold exposed for 1 week. Part of the animals received a tamoxifen re-administration at the end of the cold exposure. **(E) Re-growth quantification:** The Adipoq-tracer-depleter animals received tamoxifen, DT/saline, and cold exposure, as depicted in the scheme under (F). The total number of Adipoq+ cells in the iBAT was quantified, n=8-9. **(F) Recruitment quantification:** The Adipoq-tracer-depleter animals received tamoxifen and cold exposure as depicted in the scheme under (G). The total number of Adipoq+ cells in the iBAT was quantified, n=8-9. Data presented are mean \pm SEM, M = 10^6 , rec. = recombined.

2.3 Discussion

The plasticity of the adipose tissue is extensive, it can adapt to environmental and metabolic cues with a wide dynamic range. Most commonly, the adaptations are investigated by analysis of the cellular morphology [137], protein and gene expression profiles [149], by epigenomic approaches [153] or even single cell transcriptomics [154]. However, none of these methods allow for the quantification of all adipocytes within a complete adipose depot in an unbiased manner. Here, we describe such a method and utilize this assay to answer several important questions in the field of adipose tissue biology.

When thermal stress is absent, brown adipocytes downregulate their thermogenic program and develop a morphology similar to that of white adipocytes [148]. However, it is not clear whether acquisition of a white adipocyte-like phenotype affects the inducibility of these cells. Brown adipose tissue in rodents was shown to maintain its epigenetic signature on a chromatin level after prolonged exposure to thermoneutrality [145] while on a transcriptional level, the “whitened” brown adipose tissue resembles classical white and mildly activated brown adipose tissue [144]. We were able to show here that, despite being masked, brown adipocytes maintain responsiveness to ADRB3 stimulation, and that they also remain fully responsive to DT mediated depletion, even under thermoneutral conditions.

In contrast, cold exposure promotes the formation of new thermogenic fat cells in both brown and white fat depots. Within the first week of cold exposure, we observed a burst of proliferation and a peak in the number of Ucp1+ cells and total cell numbers in the iBAT [12,140], which occurred most likely due to extensive angiogenesis to secure sufficient nutrient supply and heat distribution [12,155]. Accordingly, other groups observed an increase in iBAT mass and in total iBAT protein content upon cold exposure [149,156]. Upon prolonged cold exposure, the number of Ucp1+ cells in the iBAT returned to numbers which were observed at room temperature. In contrast, in ingWAT Ucp1+ cell numbers continuously increased during cold exposure until they ranged between 1.3 – 4.2M Ucp1+ cells. This means that 16% of all adipocytes were brite/beige cells, which is in accordance with the thermogenic capacity of the ingWAT determined by others

[144,149,156]. Others determined the number of brite/beige cells based on histology [12,137,157,158]. Their numbers are however difficult to compare due to differences in methods, classification of the depots and mouse strains. Our quantitative insight into the kinetics of Ucp1+ cells upon cold exposure demonstrated that, despite the continuous increase in brite/beige cells in ingWAT, this could not compensate the reduction in Ucp1+ cells in the iBAT [159]. This suggests that upon prolonged cold exposure the animals gradually adapt by adjusting other metabolic pathways [160] and/or their behavior and physiology [161,162]. As demonstrated previously, Ucp1 per se is not vital for the adaptation to long-term cold exposure [163,164], seeing as muscle shivering or Ucp1 independent thermogenic futile cycles are alternative strategies to generate heat [165–167].

Short term cold exposure could also stimulate the complete re-growth of an ablated depot within one week. In other models, studying the regeneration of the adipose tissue, the re-growth of brown adipose tissue took substantially longer. However, in those models the whole adipose tissue was ablated, which induces a prominent metabolic phenotype [168,169].

We could demonstrate that, during the regeneration of the iBAT, the newly formed cells are derived from precursor cells. In contrast, newly formed brown adipocytes in iBAT upon acute cold exposure originate primarily from pre-existing adipocytes. Song and colleagues observed the same phenomenon, despite differences in the labeling of Adipoq+ cells [170]. Others also observed the contribution of precursor cell proliferation to the increase in the iBAT mass upon cold exposure [12,150]. One possible explanation could be the use of different tracer lines, which are not 100% specific for adipocyte precursors. Surprisingly, the increase in Ucp1+ cells upon cold exposure with and without previous ablation was very similar (20M-30M Ucp1+ cells), indicating that this process occurs naturally in response to a cold environment in order to maintain temperature homeostasis. Furthermore, our data suggests that two pools exist within the iBAT which can be utilized to expand the tissue, namely precursor cells, which are capable to fully regenerate iBAT after tissue ablation, as well as cold inducible adipocytes, which are recruited upon cold exposure. With the emerging advances in single cell sequencing, it has become evident that different adipocyte subpopulations exist within the adipose tissue, which are involved in regulation of proliferation, differentiation as well as paracrine crosstalk [154,171,172]. Future studies will be needed to characterize the properties of the two proposed brown adipocyte pools.

Acknowledgements

The authors would like to thank Manuel Klug for his great support with the animal experiments and Ian Mitchell for his help editing the manuscript. All microscopy work was carried out at the

Scientific Center for Optical and Electron Microscopy (ScopeM) at ETH Zurich. The work was supported by the Swiss National Science Foundation

Author Contributions

C.M., L.S. and C.W conceived and designed the study. C.M., L.S. and Y.R. performed the experiments and did the analysis of the samples. D.D., E.K., W.S., S.M and M.B. helped with the harvest of the tissue samples. Y.R. and L.D performed the confocal imaging. C.M., L.S., M.B. and C.W. wrote the manuscript and generated the figures, with the help of feedback from all other authors. C.W. supervised the study.

Declaration of Interest

The authors declare no competing interests

2.4 STAR Methods

LEAD CONTACT

Further information and requests for resources and reagents should be directed to and will be fulfilled by the Lead Contact, Christian Wolfrum (christian-wolfrum@ethz.ch)

MATERIALS AVAILABILITY

Plasmids and animal lines are available from the corresponding author upon request.

DATA AND CODE AVAILABILITY

This study did not generate/analyze datasets or codes

2.4.1 Experimental model and subject details

Transgenic Mouse Strains

The Ucp1-tracer-deleter mouse line is a crossing of the three mouse strains which were previously described: Ucp1–CreERT2 [14], ROSA26–tdRFP [173] and Ucp1–RTR–GFP [14,174]. The Adipoq–CreERT2 strain, was created using bacterial artificial chromosome (BAC) cloning as described previously [175]. We used the Adiponectin gene containing BAC RP24–69M4 (BACPAC Resources Center). Cloning primer sequences are provided upon request. Transgenic mice were generated by pronuclear injection into C57BL/6N oocytes according to standard procedures [176].

The Adipoq-tracer-deleter mouse line was generated by crossing the Adipoq-CreERT2 strain with ROSA26-tdRFP strains [173] and the Ucp1-DTR-GFP line [14]. All mice were kept on a C57BL/6N background. Unless otherwise indicated, adult male and female mice at the age of 13 weeks were housed at room temperature (20-22°C) on an inverted light-cycle (7 pm - 7 am light on). Standard chow (Kliba-Nafag purified diet #2222; 18% protein, 7% fat, 58% carbohydrate by mass) and water were provided ad libitum. All animal experiments were approved by the Cantonal Veterinary Office of Zurich. All animal experiments complied with the ARRIVE guidelines and were carried out in accordance with local guidelines.

Experimental Animal Procedures

CreERT2 activity was induced by oral gavage with 2 mg (80 mg/kg) of tamoxifen (Sigma-Aldrich) in 100 µl sunflower oil per day for two consecutive days (total dose 160 mg/kg). Diphtheria toxin (Sigma-Aldrich) was injected subcutaneously in the neck region of the animal, 3x each 100 ng in saline, every six hours to ablate Ucp1+ cells. Beta3-adrenergic agonist CL316,243 (CL) (Sigma-Aldrich) was injected intraperitoneally (0.1mg in saline/kg/day). For cold exposure, the animals were housed at 8°C. For thermoneutral housing, animals were kept at 30°C.

2.4.2 Method details

Sample Harvest

Animals were euthanized by carbon dioxide asphyxiation. The fat depot nomenclature ascribed by de Jong et al [6] was utilized. One lobe of each depot was used for the quantification of recombination, while the other lobe was used for histological analysis. Popliteal lymph nodes were carefully removed from the ingWAT depot.

Quantification of Cre recombination in tissues

Genomic DNA (gDNA) was prepared by lysing the tissue in 1 ml of 50 mM NaOH (Sigma-Aldrich) with one to two metal beads at 50 s⁻¹ for 6-12 minutes with the TissueLyser LT (Qiagen). Subsequently, the tissues were shaken (1000 rpm) at 92 °C for 1 h. Thereafter, 250 µl of 1 M TrisHCl (Sigma-Aldrich) was added to neutralize the pH. The samples were centrifuged two times at 12000 rpm for 5 minutes and the aqueous phase was carefully transferred to a fresh tube. The fat free aqueous DNA solution was diluted 1:30 in pure H₂O.

In order to assess the number of labeled adipocytes, primers [Tab. 1] were designed to identify the number of recombined loxP site loci in genomic DNA, reflecting the amount of Ucp1+ (for the Ucp1-tracer-deleter) or Adipoq+ (for Adipoq-tracer-deleter) cells. The apolipoprotein B

gene (*ApoB*) was used as an internal control, indicating total cell numbers [Tab. 1]. Schematic description of the quantitative recombination analysis is depicted in [Suppl. Fig. 1A]. Absolute quantification of the number of recombined *ROSA26-tdRFP* transgene and *ApoB* genomic loci was performed by Fast SYBER green (Life Science Technology) quantitative real-time polymerase chain reaction (qPCR) of genomic DNA. The number or molecules of recombined *LoxPRed* sites or *ApoB* can be quantified using a standard curve generated from a synthesized plasmid pUC57recloxPRed-ApoB [Tab. 1]. The dilution curve of the plasmid can be found in Table 2 [Tab. 2]. The concentration was calculated based on the molar weight of the plasmid. On the plasmid only one recombined *loxPRed* site is present, thus the cycle threshold (Ct) values of each sample needed to be adjusted according to the animal's genotype (divide by two if the animal is homozygous). Similarly, *ApoB* Ct values had to be reduced by factor two in order to calculate the number of non-recombined cells.

Recombined ^{fl}stop^{fl}tdRFP, or rec13 (product length: 197 bp)	
FW	GCGCATGAACTCTTTGATGAC
RV	TCGCGGTTGAGGACAACTC
ApoB (product length: 85 bp)	
FW	GTCCAGGTTGAATCACGGGT
RV	AGGATCCTGCAAGGTCAAGC
Plasmid (485 bp)	
CTTGAAGCGCATGAACTCTTTGATGACGTCCTCGGAGGAGGCCAGCATGGATCCAGCGCTAGCTTG GCTGGACGTAACTCCTCTTCAGACCTAATAACTTCGTATAGCATAATTATACGAAGTTATGCGGC CGACCGTAAGCTTATCGATACCGTCGATCCCCACTGGAAAGACCGCGAAGAGTTTGTCTCAACC GCGAGCTGTGGAGGTGGGGTCCAGGTTGAATCACGGGTTCTTCAGCACAATGCACAGTTCTCCAAT GACCAAGAAGAAATACGGCTTGACCTTGACAGATCCTTAGACGGAGCCGGAGAACCCTGCGTGCAA TCCATCTTGTTCAATGGCCGATCCCATGGCGGCACAGATGAATTCTTAATAACTTCGTATAGCATA ATTATACGAAGTTATGCGGCCGACCGGTAAGCTTATCGATACCGTCGATCCCCACTGGAAAGACCG CGAAGAGTTTGTCTCAACCGC	

Table 1: Primer for recombination analysis and sequence of the pUC57recloxPRed-ApoB plasmid

Concentration (ug/ul)	1x 10 ⁶	5x 10 ⁷	2.5x 10 ⁷	1x 10 ⁷	5x 10 ⁸	2.5x 10 ⁸	1x 10 ⁸	5x 10 ⁹	2.5x 10 ⁹	1x 10 ⁹	5x 10 ¹⁰
------------------------------	-----------------------	-----------------------	-------------------------	-----------------------	-----------------------	-------------------------	-----------------------	-----------------------	-------------------------	-----------------------	------------------------

Table 2: Dilution curve of the pUC57recloxPRed-ApoB plasmid

Histological Analysis

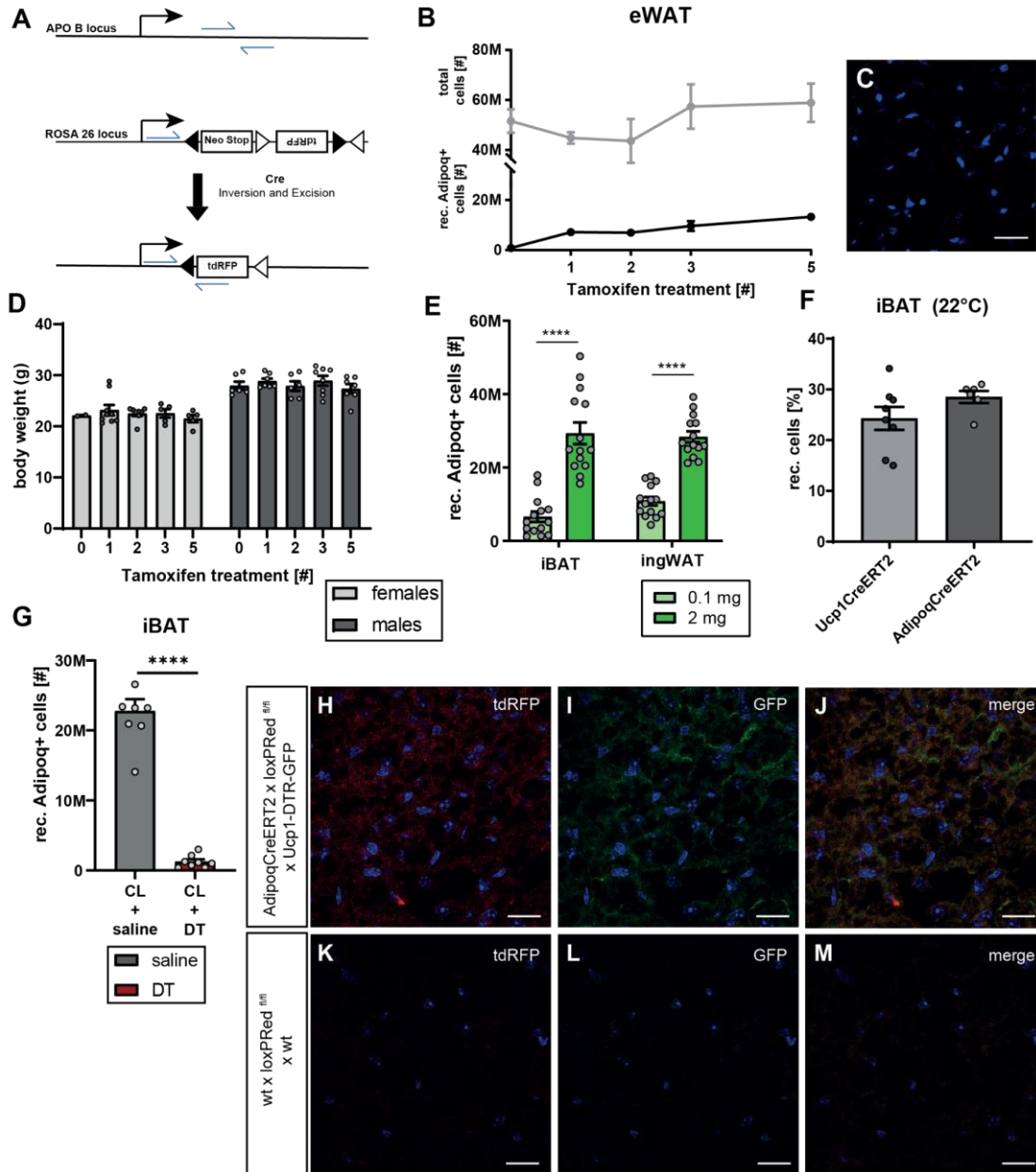
Adipose tissue depots were incubated in phosphate-buffered saline (PBS) (Thermo Scientific) containing 4% paraformaldehyde (PFA) (Sigma-Aldrich) for 24 hours. After a wash in PBS, the tissue was dehydrated for five days in 30 % sucrose (Sigma-Aldrich). Subsequently, they were

embedded in Shandon Cryomatrix (Thermo Scientific™) flash frozen on dry ice, and stored at -20°C. Tissues were cut at -30°C on Cryostar NX70 (Thermo Scientific) at 25-50 µm thickness and mounted to Superfrost slides (Thermo Scientific). For RFP staining, the sections were washed with PBS containing 0.05% Tween™ (PBS-T) (Sigma-Aldrich) and incubated with 10% donkey serum (Sigma-Aldrich) for 1h, followed by overnight incubation at 4 °C with primary antibody against RFP (Rockland, 1:100 in 10% donkey serum). As secondary antibody, anti-rabbit Alexa Fluor® 568 antibody (Thermo Scientific™, 1:200 in 10% donkey serum) was used. Nuclei were stained with Hoechst 33342 (Invitrogen, 1:10'000 in PBS). Slides were mounted with ProLong™ Diamond Antifade Mountant (Invitrogen) and visualized by confocal microscope Leica SP8-AOBS. If no antibody for RFP was used, the tissues were only fixed for 1h in 4% PFA. Continuously, only the nuclei were stained with Hoechst 33342 (Invitrogen, 1:10'000 in PBS) and the Slides were mounted with ProLong™ Diamond Antifade Mountant (Invitrogen).

2.4.3 Quantification and statistical analysis

Unless otherwise indicated, all results are expressed as mean ± standard error of the mean (SEM). All graphs and statistical analyses were performed using Graphpad Prism (Version 9) We used a two-tailed, unpaired student's t-test (significance cut off: $p < 0.05$) to assess statistical significance. * = $p \leq 0.05$; ** = $p \leq 0.01$; *** = $p \leq 0.001$; **** = $p \leq 0.0001$.

2.5 Supplementary Material



Supplementary Figure 1: Establishment of the Quantification Method (A) Quantitative recombination analysis: Schematic description of the quantitative recombination analysis. The first primer pair (upper part) is specific for the *ApoB* locus, an internal control to quantify total number of cells in a depot. The second primer pair (lower part) is specific for the recombined transgene at the *ROSA26* locus. The primer pair only produces a PCR product, when ^{fl}stop^{fl}-cassette is genetically deleted by the Cre recombinase. **(B) Effect of tamoxifen dosing on recombination:** Adipoq-tracer-depleter animals received 1 to 5 treatments with tamoxifen (2mg/per animal/day, administered orally) on consecutive days. The tissues were taken on day 6 after the first tamoxifen treatment. The total as well as the Adipoq+ recombined cell number, was analyzed in the eWAT n=2-7. **(C) Secondary Antibody control:** iBAT AdipoqCreERT2 x loxPRed^{fl/fl} were harvested 2 days after tamoxifen administration (2 mg/per animal). 25 μ m cryosections were prepared, DNA was stained with Hoechst 3342 (blue) and secondary anti-rabbit Alexa Fluor® 568 antibody. Scale bar = 50 μ m **(D) Bodyweight:** Adiponectin-tracer-depleter animals received 1 to 5 treatments with tamoxifen (2 mg/ per animal/day) on consecutive days. Bodyweight was measured on day 6 after the final treatment. **(E) Dose dependency of recombination:** Animals received 0.1 mg or 2 mg tamoxifen as indicated. Tissues were taken 2 days later. The number of Adipoq+ recombined cells was analyzed in iBAT and ingWAT, n=14. **(F) Comparison of the Ucp1-tracer-depleter vs. the Adipoq-tracer-depleter line:** Animals of the Ucp1-tracer-depleter line and the Adipoq-tracer-depleter line received tamoxifen (2x 2 mg/per animal/day) continued on the following page

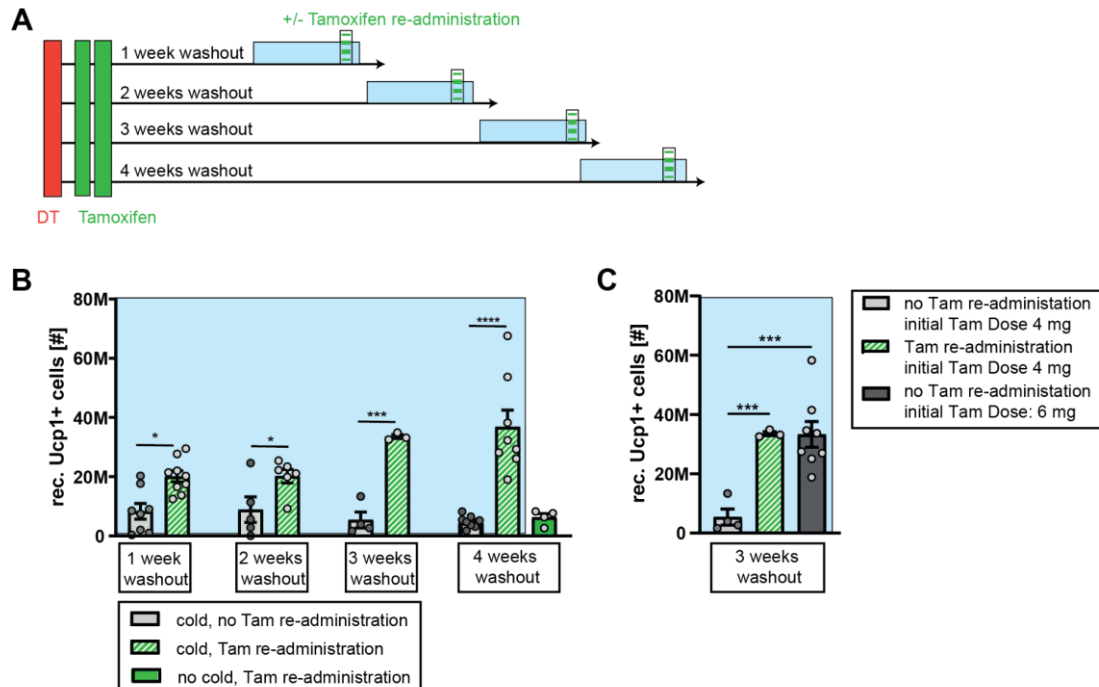
on 2 consecutive days. 2 days later the tissues were taken. The percentage of recombined Ucp1+ cells and Adipoq+ cells, respectively, were analyzed with respect to total cell numbers, n=6-8. **(G) Number of Ucp1+ cells ablated from the pool of Adipoq+ cells:** The animals of the Adipoq-tracer-deleter line received 2 tamoxifen treatments. 1 week later the animals were injected with DT or saline. The consecutive 3 days all animals received CL & DT/saline. Tissues were harvested one day after the last injection. The number of Adipoq+ cells was quantified in iBAT, n=8. **(H-M) Overlay of Adipoq+ and Ucp1+ cells in iBAT:** Adipoq-tracer-deleter animals and wt animals received 2x 2mg of tamoxifen. The tdRFP and GFP signal was visualized without antibody staining; DNA was stained with Hoechst 3342 (blue). Scale bar = 50 μ m. Data presented are mean \pm SEM, M = 10^6 , rec = recombined

To quantify the number of Adipoq+ or Ucp1+ cells, genomic DNA from a whole adipose tissue depot was isolated and the number of recombined *ROSA26-tdRFP* alleles (*loxPRed*) and non-recombined *ApoB* alleles was quantified by qPCR [Suppl. Fig. 1A]. The number of recombined Adipoq+ or Ucp1+ cells was calculated based on a standard curve, generated from a plasmid harboring the recombined *loxPRed* and the *ApoB* sequence. Further details can be found in the methods section.

Working with the tamoxifen inducible CreERT2-loxP system allows tissue specific and temporal controlled recombination of DNA. If multiple tamoxifen treatments were applied, then the number of Adipoq+ cells remained constant in the epididymal white adipose tissue (eWAT) from one to two tamoxifen treatments ($7.2 \pm 1.2M$ Adipoq+ cells). Further administration increased the Adipoq+ cell number ($13.3 \pm 1.1M$ Adipoq+ cells) [Suppl. Fig. 1B]. This might be explained by the use of oil as a solvent for tamoxifen which increases adipocyte formation in the eWAT, as reported previously [10,68,177]. However, in accordance with the Adipoq+ cell numbers observed in the iBAT and ingWAT [Fig. 1A; B] we decided to continue with a tamoxifen treatment regimen of 2 mg/animal on two consecutive days.

Toxic effects of tamoxifen at higher doses on the adipose tissue [178] have been reported due to the lipophilic nature of the compound. With a dose of 2 mg/animal on two consecutive days, we administer 30% - 80% tamoxifen compared to others, and the constant numbers of recombined Adipoq+ cells suggest that there is no induced cell death due to tamoxifen [Fig 1B, C; Suppl. Fig. 1B] [12,178,179]. Additionally, we did not observe any effects of tamoxifen administration on bodyweight, which was reported for higher doses [Suppl. Fig. 1D]. We found that 2 mg of tamoxifen per mouse were sufficient to label all adipocytes, while a dose of 0.1 mg per mouse led to incomplete labeling [Suppl. Fig. 1E]. Next, we compared the number of recombined Adipoq+ cells to the number of Ucp1+ cells in the iBAT under standard housing conditions. The same percentage of recombined cells was found [Suppl. Fig. 1F], demonstrating that both the Adipoq- and the Ucp1-tracer-deleter line are equally efficient in labeling brown adipocytes. This was supported by the finding that the vast majority of the Adipoq+ cells in the iBAT were depleted following DT mediated ablation of all Ucp1+ cells ($22.8 \pm 1.7M$ vs. $1.3 \pm 0.3M$ Adipoq+ cells) [Suppl. Fig. 1G]. Further, in the iBAT of the Adipoq-tracer-deleter mice, RFP expression

overlapped entirely with GFP expressed under the control of the Ucp1 promotor [Suppl. Fig. 1 H-M]. In general, the observed cell numbers in either mouse line were consistent between the experiments, supporting the quantitative strength of the method employed.



Supplementary Figure 2: Washout of Tamoxifen (A) Schematic description washout experiment: In order to study the washout period of tamoxifen all Ucp1+ cells were ablated with DT to create an even baseline. On day 2 and day 3 after ablation, tamoxifen was applied. Different time periods for tamoxifen washout periods were given, before the animals were cold exposed for 1 week to initiate re-growth of the brown adipose tissue. Half of the animals, which served as a control group, received a tamoxifen re-administration at the end of the cold exposure. **(B) Washout quantification:** The Ucp1-tracer-depletor animals received DT, tamoxifen and cold exposure as depicted in (A). The total number of Ucp1+ cells in the iBAT was quantified n=3-9. **(C) Washout of higher tamoxifen doses:** The Ucp1-tracer-depletor animals received DT and cold exposure as depicted in the scheme under (A). While two groups received 2x 2 mg of tamoxifen, a third group received 3x 2 mg of tamoxifen. Following 3 weeks of washout, the total number of Ucp1+ cells in the iBAT was quantified. When the initial dose of tamoxifen was increased to 6 mg/mouse, a washout period of 3 weeks was not sufficient, seeing as no difference between the re-administration group and the washout group n=3-8. Data presented are mean \pm SEM, M = 10^6 , rec. = recombined.

As Tamoxifen accumulates in adipose tissues due to its lipophilicity [178], we aimed to determine the washout period of tamoxifen. After the ablation of all Ucp1+ cells through DT and administration of tamoxifen, one to four weeks of washout were allowed before stimulating the re-growth via cold exposure [Suppl. Fig. 2A]. The total number of Ucp1+ cells that re-grew after depletion was quantified in a control group of mice, which were re-administered with tamoxifen at the end of cold exposure [Suppl. Fig. 2A]. Already after one week of washout, a significant difference in Ucp1+ cells could be observed between the non-re-administered washout group and the re-administered group [Suppl. Fig. 2B]. A significant difference between the washout group and the re-administered group was also observed for two, respectively three weeks of

washout. After four weeks of washout, the strongest difference was observed ($4.9 \pm 0.7M$ vs. $36.8 \pm 5.7M$ Ucp1+ cells) [Suppl. Fig. 2B]. Furthermore, when the animals were not cold exposed at the end of the washout period the iBAT did not regrow [Suppl. Fig. 2B], and when the initial dose of tamoxifen was increased to 6 mg/mouse, a washout period of three weeks was not sufficient, seeing as no difference was observed between the re-administration group and the washout group [Suppl. Fig. 2C]. Taken together, we show here that, at the lowest effective dose ($2x$ 2mg/animal/day), the tamoxifen washout period in brown adipose tissue is three to four weeks. A drawback of this method is the minor proportion of Ucp1+ cells ($5M - 8M$ Ucp1+ cells, equals 3-6%) which was detected in the washout groups, and could be due to an incomplete tamoxifen washout. However, it is similarly possible that this small proportion is due to de novo formed adipocytes at room temperature within the first week after the ablation, when tamoxifen is still present. In line with this hypothesis is the fact that the number of labeled cells in the washout group remains constant, independent of the duration of the washout period, and that the cell number after four weeks at room temperature is the same as in the cold-stimulated washout group.

CHAPTER 3

FAM3D a novel gut secreted protein and its potential in the regulation of glucose metabolism^b

Caroline Moser, Katherine Rollins, Miroslav Balaz, Lucia Balazova, Carla Horváth, Leon Straub, Susanne Wolfrum, Katarzyna Maria Okreglicka, Fengqi Li, Manfred Kopf, Matthias Blüher, Birgit Stierstorfer, Thorsten Lamla, Bradford Hamilton, Heike Neubauer, Christian Wolfrum

Contribution:

Caroline Moser designed the study, performed most of the experiments, prepared the figures and wrote the manuscript.

^b*This article is in preparation for the submission to Molecular Metabolism. This chapter is a preprint of the prepared manuscript.*

FAM3D a novel gut secreted protein and its potential in the regulation of glucose metabolism

Caroline Moser¹, Katherine Rollins¹, Miroslav Balaz¹, Lucia Balazova¹, Carla Horvath¹, Leon Straub¹, Susanne Wolfrum¹, Katarzyna Maria Okreglicka², Fengqi Li², Manfred Kopf², Matthias Blüher³, Birgit Stierstorfer⁴, Thorsten Lamla⁴, Bradford Hamilton⁴, Heike Neubauer⁴, Christian Wolfrum^{1*}

¹ *Institute of Food, Nutrition and Health, Swiss Federal Institute of Technology (ETH) Zurich, 8603 Schwerzenbach, Switzerland*

² *Institute of Molecular Health Sciences, Swiss Federal Institute of Technology (ETH) Zurich, 8093 Zurich, Switzerland*

³ *Department of Medicine, University of Leipzig, Leipzig, Germany*

⁴ *Cardiometabolic Diseases Research Department, Boehringer Ingelheim Pharma GmbH and Co. KG, Biberach/Riss, Germany*

*Correspondence: christian-wolfrum@ethz.ch

Abstract

Objective: The numbers of diabetic patients are rising globally and concomitantly so do the diabetes associated complications. A substantial number of diabetes medications are based gut secreted peptides. However, as for most pharmaceuticals there are downsides regarding side effects or efficacy. The gut is secreting a variety of proteins to control blood glucose levels and/or food intake, thus other peptides which have yet been unexplored might be better tolerated or have better activities. Our aim was to characterize the potential of a novel gut secreted protein, FAM3D, for the treatment of type 2 diabetes.

Methods: FAM3D was overexpressed in diet induced obese mice via an adeno-associated virus (AAV). Glucose metabolism was assessed by glucose and insulin tolerance tests, as well as hyperinsulinemic euglycemic clamps. Liver lipid deposition and morphology was investigated to determine the hepatic metabolic phenotype. For the investigation of the underlying molecular mechanism of FAM3D a kinase activity screen was performed *in vivo* and signaling patterns were analyzed *in vitro* in immortalized adipocytes.

Results: The AAV-mediated overexpression of FAM3D resulted in a significant improvement fasting blood glucose levels, glucose tolerance and insulin sensitivity. The hyperinsulinemic clamp data indicated that FAM3D is a global insulin sensitizer, which is increasing the glucose uptake

into various tissues. First indications propose that the positive metabolic phenotype of FAM3D is mediated by receptor tyrosine kinase signaling however, to identify to exact signaling mechanism further ligand-receptor interaction studies are needed

Conclusions: The current study demonstrated great potential for the novel gut secreted protein FAM3D as an insulin sensitizing peptide for blood glucose control.

3.1 Introduction

The global burden of diabetes is tremendous, currently being one of the leading causes of death in the world. According to the latest estimation of the International Diabetes Federation from 2019, approximately 463 million adults were living with diabetes and 374 million people are at increased risk of developing type 2 diabetes (T2D) [61]. The diabetes-associated aberrant high blood glucose levels can lead to severe complications, including cardiovascular complications, stroke, vision loss, nerve damage or kidney failure [180]. These complications pose a significant burden to the patients, but also to our health care system. Thus, it is essential to lower and control the blood glucose levels in diabetic patients before the concomitant complications of diabetes manifest. In the case of T2D, from which the majority of diabetic patients suffer, various treatment options are available. As lifestyle interventions are often not sufficient, pharmaceutical therapies with different classes of drugs are commonly prescribed. Besides, biguanides, sulfonylureas, thiazolidinediones, sodium-glucose co-transporter-2 (SGLT2) inhibitors and insulin, stable analogues of the gut secreted protein glucagon-like peptide 1 (GLP-1) or Dipeptidyl peptidase-4 (DPP4) inhibitors to prevent the rapid degradation of gut peptides are currently very successful diabetes medications [117,181]. Even though several treatment options exist, there is nevertheless an unmet need for the development of alternative treatments. The gut is secreting a wide variety of proteins which are able to control gastric motility, satiety and blood glucose levels [21]. Hence, based on the previous success of GLP-1 analogues and DPP4-inhibitors, other novel gut secreted peptides might be equally or even more potent in the treatment of diabetes.

The FAM3 family is a cytokine like family containing four members. FAM3A, FAM3B (PANDER), FAM3C and FAM3D. The first three members of the family are fairly well characterized and described to be involved in pathophysiology of diabetes [182–185]. While the physiological role of the fourth member, FAM3D remains mostly unknown. FAM3D is primarily expressed in the digestive system [186]. The intestinal expression of FAM3D is induced by ingestion of fats and reduced by fasting in mice [187]. In humans FAM3D plasma levels are increased following a high fat meal [187]. FAM3D is discussed as chemotactic agonist for the G-protein coupled receptors,

formyl peptide receptors 1 & 2 (FRP1 & FRP2), which are primarily expressed on neutrophils and monocytes, suggesting rather pro-inflammatory properties of FAM3D [188]. In contrast, the data of the FAM3D knock out mouse model, rather suggest its essential role in the maintenance of the colon homeostasis. It protects against inflammation associated cancer and supports a normal microbiota composition [186]. Despite all these findings, the role of FAM3D in regulation of metabolism and pathophysiology of diabetes remains unknown.

In the presented study we identified FAM3D as a gut secreted protein, of which circulating levels increase in patients after bariatric surgery. By using an adeno associated virus (AAV) approach to overexpress FAM3D in diet induced obese mice, we investigated the role of FAM3D in glucose metabolism and elucidated its potential as a novel gut secreted protein for T2D treatment. FAM3D not only displayed great insulin sensitizing potential, it also ameliorated symptoms of non-alcoholic fatty liver disease (NAFLD). We could identify receptor tyrosine kinase signaling as a potential molecular mechanism mediating the positive metabolic phenotype.

3.2 Results

3.2.1 FAM3D is a gut secreted protein associated with the beneficial metabolic effects of bariatric surgery

As we were interested in the identification of novel gut secreted proteins for diabetic treatment, the targets identified in our previous study, in which we characterized the transcriptome of mouse ileal and colonic L- and epithelial cells following high fat diet (HFD) and bariatric surgery were further analyzed [189]. The identified targets were filtered for secreted proteins and ranked based on their differential expression upon HFD or vertical sleeve gastrectomy (VSG). Following, the targets were filtered for novelty and screened for first evidence to be involved in metabolic functions. Based on this analysis, we identified several candidates and selected FAM3D for further analysis.

The expression of FAM3D is significantly higher in the colon compared to the small intestine (SI) in both, the L-Cells and the enterocytes. Given the expression profile, FAM3D is not a classical gut peptide per se, as it is expressed in the enteroendocrine L-cells, as well as in the surrounding enterocytes [Fig. 1A]. After bariatric surgery an increased secretion of well described gut hormones eg. GLP-1 or GLP1-oxynomodulin-peptide YY (PYY) can be observed. They are being discussed to mediate at least partly the positive metabolic effects of the surgery [110,190]. Thus, we investigated FAM3D serum levels in human patients before and after bariatric surgery and

detected a significant increase 12 months post-surgery compared to pre-surgery baseline levels [Fig. 1B]. This led us to the hypothesis that FAM3D is a gut secreted protein which might be involved in the regulation of energy metabolism and eventually contributing to the beneficial effects of bariatric surgery.

3.2.2 The overexpression of FAM3D evokes a positive glucometabolic phenotype

Based on our findings, we decided to further assess the anti-diabetic potential of FAM3D in an obese and diabetic mouse model. For the overexpression of FAM3D, an adeno-associated virus (AAV) expressing FAM3D under the LP1 promoter was injected intravenously. This resulted in a distinct and long-lasting hepatic overexpression and increase of FAM3D in the plasma, while no endogenous FAM3D could be detected [Suppl. Fig. 1A; B]. The overexpression of FAM3D resulted in a significant improvement of the glucometabolic phenotype in HFD fed mice. Fasting and random fed blood glucose levels [Fig. 1C; F], as well as glucose and insulin tolerance [Fig. 1D; E] were significantly improved upon FAM3D overexpression. The analysis of plasma from fasted animals demonstrated a significant reduction of triglycerides [Fig. 1G], while free fatty acids, insulin and glucagon levels were unchanged [Fig 1H - J]. Other hormones which are known to improve blood glucose levels, such as Leptin, Adiponectin, Thyroxine (T4) were unchanged in both fasted and fed state [Suppl. Fig. 1C - E]. Also, random fed vascular endothelial growth factor A (VEGF-A) and free fatty acids did not differ between the groups [Suppl. Fig. 1F; G]. Additionally, no increased glucose excretion via the urine could be observed [Suppl. Fig 1H]. The fact that that FAM3D is a very potent peptide to improve the glucometabolic phenotype is further supported by the fact that reduced fasting blood glucose levels [Suppl. Fig. 1J] and improved glucose tolerance [Suppl. Fig. 1I] upon FAM3D overexpression were observed in lean chow fed mice. All these effects were independent of bodyweight [Fig. 1K], lean or fat mass [Fig. 1L]. Accordingly, in response to FAM3D overexpression energy expenditure, as well as respiratory quotient, food/water intake and activity were unchanged [Suppl. Fig. 1K - O]. Since FAM3D was reported to be a chemotactic agonist for neutrophils and monocytes [188], we investigated liver and peritoneum after FAM3D overexpression for the presence of inflammatory markers. No increased infiltration of macrophages or neutrophils was observed upon overexpression of FAM3D [Suppl. Fig. 2A; B]. Further, the alanine transferase (ALT) activity in plasma did not differ between the two groups suggesting, that the AAV mediated overexpression is not eliciting liver damage [Suppl. Fig. 2C]. In contrast to the FAM3D overexpression model, the inducible global FAM3D knockout mouse (Rosa26-creERT2 x FAM3D fl/fl) [Suppl. Fig. 2D] did not displayed any metabolic phenotype following tamoxifen induced knockout of FAM3D under obesogenic conditions. Neither, the

fasting blood glucose levels, nor the glucose tolerance (ip. and oral), nor the body weight was changed upon FAM3D knockout [Suppl. Fig. 2E - H].

In summary, we identified FAM3D as a secreted peptide which when expressed at supraphysiological levels leads to improved glucose metabolism in obese/diabetic mice. The presented overexpression model suggests, that FAM3D improves the insulin sensitivity, without eliciting any adverse inflammatory effects.

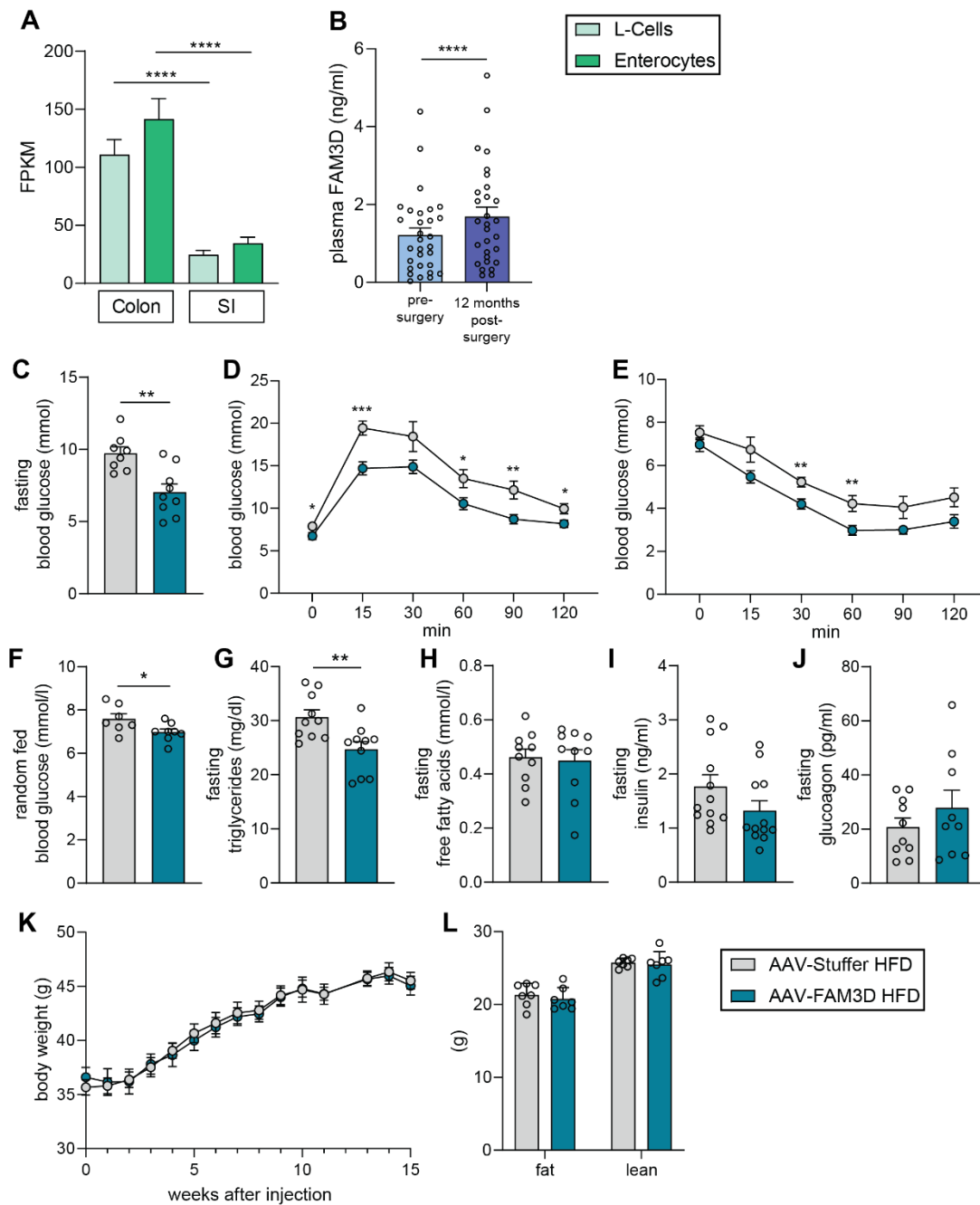


Figure 1: (A) Transcriptomics of L-cells and enterocytes from colon and small intestine (SI). Fragments per kilobase of transcript per million mapped reads (fpkm) of are presented (n = 7). *continued on the following page*

(B) FAM3D levels in human plasma samples sampled pre- and 12 months post-surgery. (n = 30). (C) Fasting blood glucose was measured two weeks post virus injection (n = 8-9). (D) Intraperitoneal glucose tolerance test (ipGTT) was performed three weeks post virus injection (n = 8-9). (E) Insulin tolerance test (ITT) was performed five weeks post virus injection (n = 8-9). (F) Random fed blood glucose was measured three weeks post virus injection (n = 8). (G) Fasting triglycerides and (H) Fasting free fatty acids were measured in plasma sampled two weeks post virus injection (n = 10). (I) Fasting insulin levels were measured in plasma sampled two weeks post virus injection (n = 12). (J) Fasting glucagon levels were measured in plasma sampled two weeks post virus injection (n = 10). (K) Bodyweight was monitored weekly after virus injection (n = 7). (L) Lean and fat mass was determined 16 weeks post virus injection (n = 7). All data presented are mean \pm SEM, Statistical analysis was performed by ordinary one-way ANOVA and multiple comparison testing (A), by paired Student's t-test (B) and by unpaired Student's t test (C-L), Significance is indicated as * p < 0.05, ** p < 0.01 and *** p < 0.001.

3.2.3 FAM3D ameliorates hepatic lipid deposition and steatosis

Since the FAM3 family is discussed as target for the treatment of NAFLD and T2D [182], we next studied the effect of FAM3D on liver steatosis. We observed a significant reduction in the deposition of liver triglycerides following AAV-mediated overexpression of FAM3D [Fig. 2A], which can be also observed at the histological level [Fig 2D; E]. In line, a trend towards a reduction in liver steatosis area (p = 0.0597) and a significant reduction of the liver micro steatosis area was observed upon FAM3D overexpression in mice on HFD [Fig. 2B; C]. Similar to the ipGTT and the ITT [Fig 1E; F], FAM3D overexpressing animals performed significantly better [Fig 2F] in a sodium pyruvate tolerance test, suggesting reduced gluconeogenesis in liver, possibly due to improved insulin sensitivity. Contrary, liver glycogen levels, which are primarily regulated by insulin, were unchanged [Fig. 2G] In contrast to FAM3A and FAM3C, which are both activating the AKT signaling pathway in liver, FAM3D did not increase AKT and pAKT^{Ser437} levels in liver [Fig 2H - J] [183,184].

In conclusion FAM3D overexpression leads to reduced hepatic lipid deposition and steatosis. Unlike the other family members FAM3A and FAM3C, FAM3D does not affect the AKT signaling cascade in the liver.

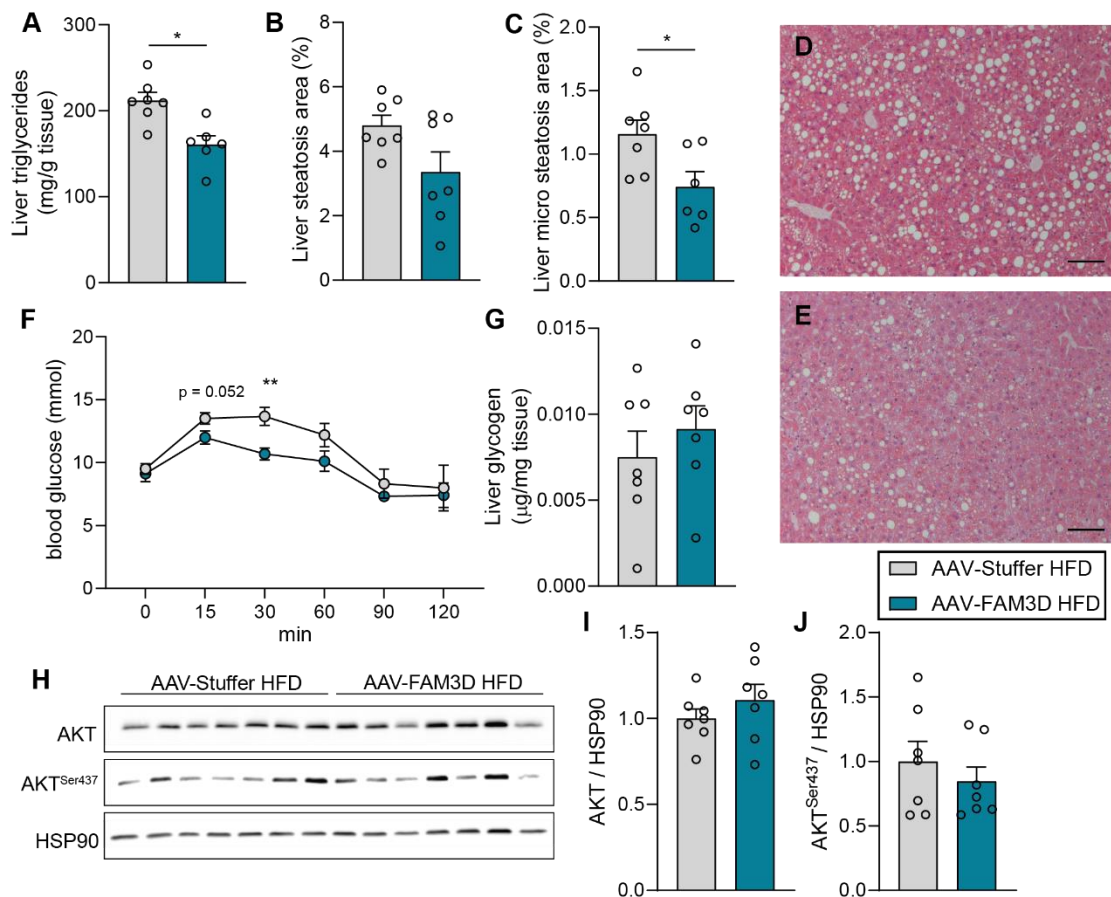


Figure 2: (A) Liver triglycerides isolated from random fed animals 10 weeks post virus injection (n = 6-7) **(B)** Liver steatosis area and **(C)** Liver micro steatosis area analyzed from random fed animals 10 weeks post virus injection (n = 7). Representative picture of **(D)** AAV-Stuffer HFD animal liver and **(E)** AAV-FAM3D HFD animal liver, Scale bar = 100 μm **(F)** Pyruvate tolerance test three weeks post virus injection with a dose of 2.0 g/kg sodium pyruvate (n = 7-8) **(G)** Liver glycogen isolated from random fed animals 10 weeks post virus injection (n = 7) **(H)** Westernblots of liver lysates from animals euthanized 8 weeks post virus injection in fasted state. Quantification of **(I)** AKT levels and **(J)** pAKT^{Ser437} normalized to HSP90 of the westernblot displayed in (H), (n = 7). All data presented are mean ± SEM, possible outliers were removed if they differed more than the standard deviation multiplied times two from the mean. Statistical analysis was performed by unpaired Student's t test. Significance is indicated as * p < 0.05, ** p < 0.01 and *** p < 0.001.

3.2.4 FAM3D acts as a systemic insulin sensitizer

Hyperinsulinemic euglycemic clamps are widely considered as the gold standard to assess the action of insulin *in vivo* [191,192]. Therefore, we performed hyperinsulinemic euglycemic clamps [Fig. 3A] to investigate the improvement in systemic insulin sensitivity, following FAM3D overexpression and to determine which organs contribute to the improved glucose uptake. In agreement with the metabolic data, FAM3D overexpressing mice required a significantly higher glucose infusion rate (GIR) to maintain euglycemia [Fig. 3B]. While the glucose turnover at basal conditions was unchanged, it was significantly improved in AAV-FAM3D HFD animals under insulin stimulated conditions [Fig. 3C]. The endogenous glucose production (EGP) was unchanged

at basal and at insulin stimulated conditions [Fig. 3D]. When determining the glucose uptake into the individual organs, a significant increase in glucose uptake was observed in the interscapular brown adipose tissue (iBAT), inguinal white adipose tissue (ingWAT), liver, heart, soleus muscle and in the tibialis anterior muscle [Fig 3E – J]. Only in the gastrocnemius muscle and the extensor digitorum longus (EDL) muscle did not show any increase in glucose uptake [Fig 3K; L].

In summary, the hyperinsulinemic euglycemic clamp confirmed that FAM3D is a systemic insulin sensitizer. The increased glucose uptake into various tissues supports this notion and demonstrates that FAM3D has a global effect and the positive metabolic phenotype is not mediated by a single organ.

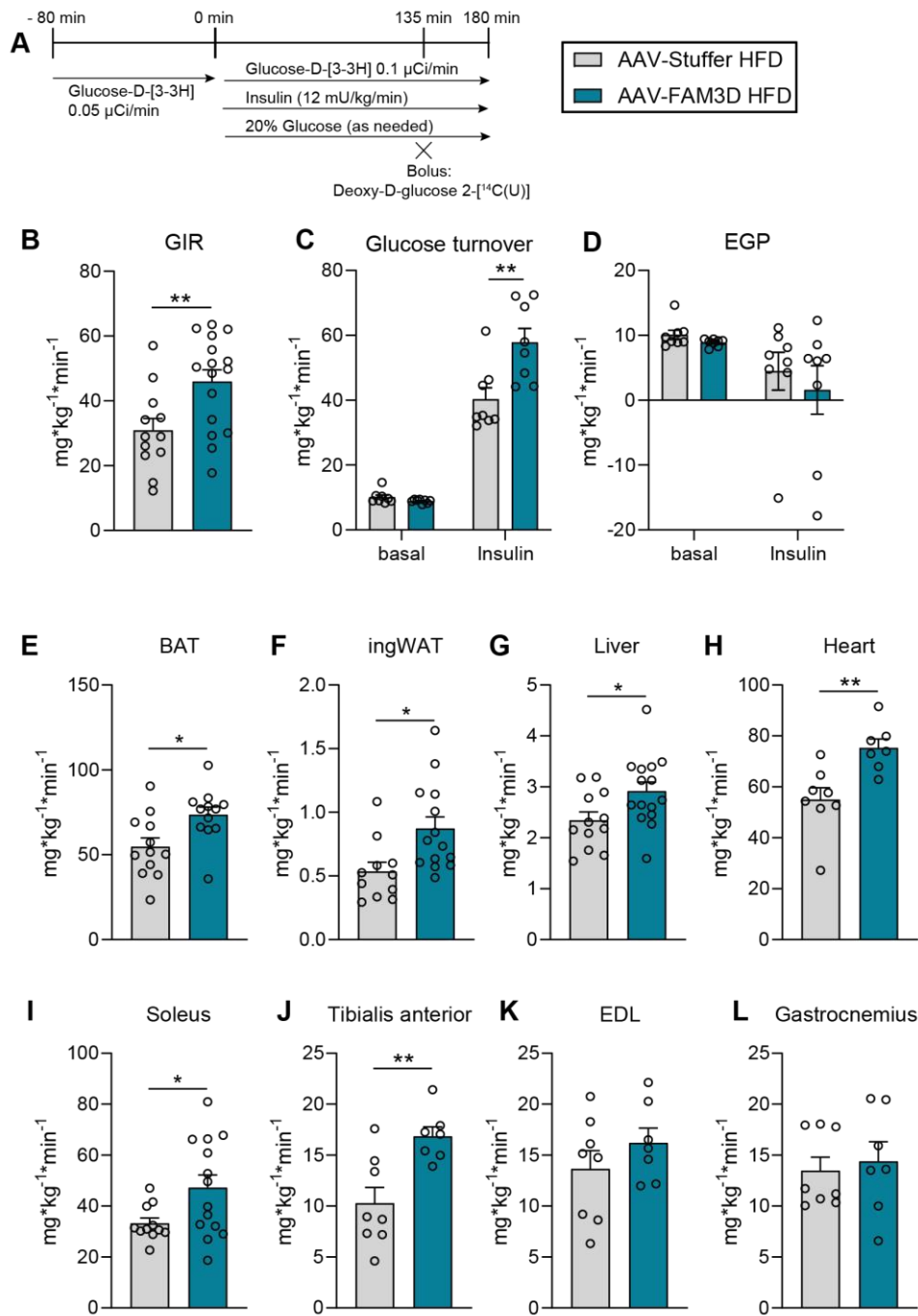


Figure 3: (A) Schematic description of the experimental set-up for the hyperinsulinemic euglycemic clamps (B) Glucose infusion rate (GIR) at the steady state at a level of 6 mmol/l blood glucose, data of the two clamp studies were pooled ($n = 12 - 16$) (C) Glucose turnover at basal and insulin stimulated levels ($n = 8$) (D) Endogenous glucose production (EGP) at basal and insulin stimulated levels ($n = 8$). Tissue specific glucose uptake in (E) Brown adipose tissue (BAT), data of the two clamp studies were pooled ($n = 12$), (F) inguinal white adipose tissue (ingWAT), data of the two clamp studies were pooled ($n = 11-14$), (G) Liver, data of the two clamp studies were pooled ($n = 12-15$), (H) Heart, ($n = 7-8$), (I) Soleus muscle, data of the two clamp studies were pooled ($n = 11-14$), (J) Tibialis anterior muscle ($n = 7-8$), (K) Extensor digitorum longous muscle (EDL), ($n = 7-8$). (L) Gastrocnemius muscle, ($n = 7-8$). Two rounds on hyperinsulinemic clamps were performed and where possible the data were pooled. All data presented are mean \pm SEM, possible outliers were removed if they differed more than the standard deviation multiplied times two from the mean. Statistical analysis was performed by unpaired Student's t test. Significance is indicated as * $p < 0.05$, ** $p < 0.01$ and *** $p < 0.001$.

3.2.5 Effects of FAM3D are mediated by receptor tyrosine kinase signaling

Despite the global insulin sensitizing effect, for the further analysis of the molecular mechanism we aimed to determine the main target tissue of FAM3D. To do so, we investigated the accumulation of recombinant Fc-tagged FAM3D protein in various tissues. A single intravenous injection of recombinant FAM3D in HFD fed animals, resulted in a significant improvement in glucose tolerance four hours post injection, suggesting that the recombinant protein is functional [Fig. 4A; B]. For the determination of the target tissue/s, recombinant FAM3D was injected intravenously, four hours later the animals were perfused thoroughly and the accumulation of FAM3D was determined by high throughput western blotting. An accumulation of FAM3D was observed especially in the inguinal and epididymal white adipose tissue (ingWAT and epiWAT) [Fig. 4C]. As the FAM3D protein does not display, besides a small transmembrane region, any lipophilic structures, it is very likely that this accumulation of FAM3D in the white adipose tissue is protein function specific [193]. Further, accumulation of FAM3D could be also observed in the heart [Fig. 4C]. Since white adipose tissue was identified as the major target tissue of FAM3D, this allowed us to proceed with the investigation of the molecular mechanism.

To elucidate the molecular mode of action a kinase activity screen of the inguinal white adipose tissue was performed. An overall reduction in peptide phosphorylation was observed upon long-term AAV mediated overexpression of FAM3D [Suppl. Fig. 3B; C]. A majority of the top kinases, which were identified based on the peptide phosphorylation at the tyrosine residue (PTK) belong to the group of receptor tyrosine kinases [Fig. 4D] [194]. Whereas, variety of kinases predicted based on the changes in phosphorylation of peptides at serine and threonine residues (STK) in response to FAM3D were involved in cell cycle regulation [Fig. 4E] [195,196]. The data of the kinase screen were validated for ERK 1/2 [Fig. 4F; G] and Janus kinase 1 (JAK1) ($p = 0.0959$) [Fig. 4F; H], targets which were amongst the top five regulated kinases predicted by the PTK or STK chip.

In summary, we could identify the white adipose tissue as the main target of FAM3D. Moreover, we identified changes in receptor tyrosine kinase signaling upon chronic overexpression of FAM3D.

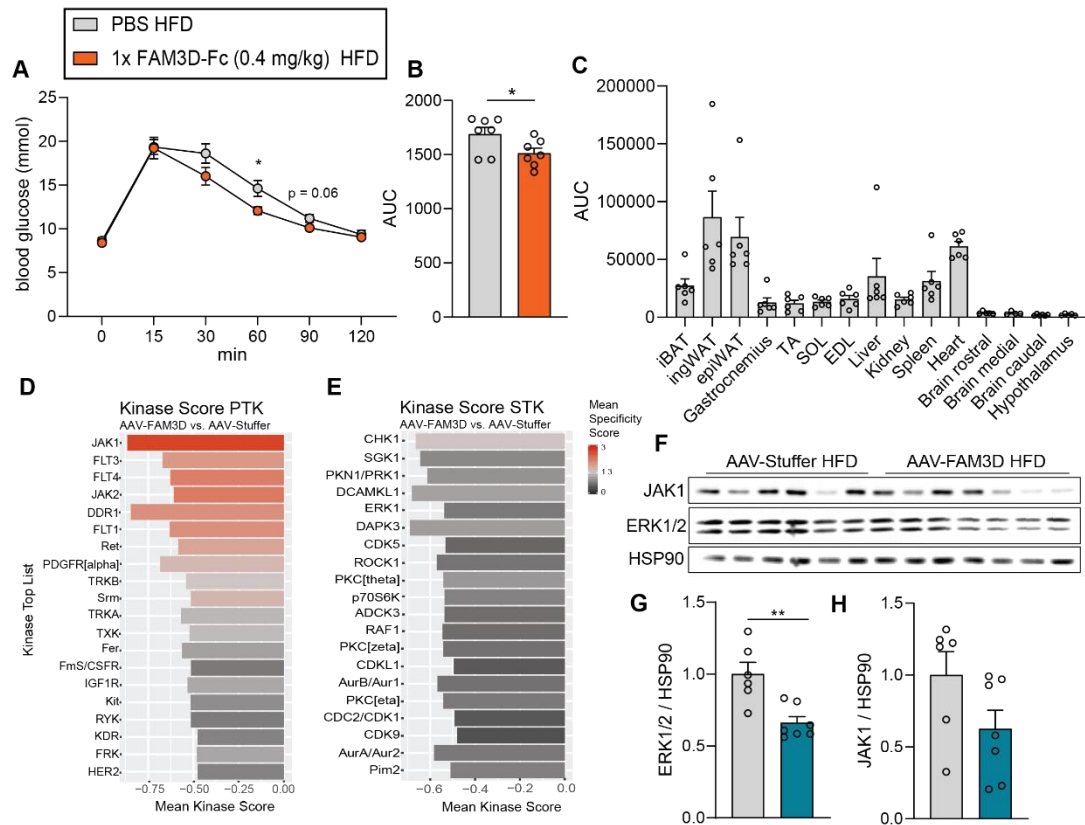


Figure 4: (A) Intraperitoneal glucose tolerance test (ipGTT) 4h after the injection of recombinant FAM3D protein (0.4 mg/kg), (n = 9) **(B)** Area under the curve (AUC) of the ipGTT displayed under (A), (n = 9) **(C)** Accumulation of recombinant FAM3D in tissues, 0.4 mg/kg recombinant FAM3D was injected iv. 4h later the animals were perfused. Various tissues analyzed by the automated Westernblotsystem Sally Sue, the area under the curve (AUC) was calculated (n = 6) **(D)** List of the top ranked regulated Kinases predicted by the phosphorylation pattern on the phosphotyrosine kinases chip (PTK), scored by the mean kinase score and the mean specificity score (n = 10) **(E)** List of the top ranked regulated Kinases predicted by the phosphorylation pattern on the serine-threonine kinases chip (STK), scored by the mean kinase score and the mean specificity score (n = 10) **(F)** Westernblots of ingWAT lysates of the kinase activity screen, animals were euthanized fasted two weeks post virus injections. Quantification of **(G)** ERK1/2 and **(H)** JAK1 levels normalized to HSP90 of the westernblots displayed in (F), (n = 6-7). All data presented are mean \pm SEM. Statistical analysis was performed by unpaired Student's t test (A; B; G; H). Significance is indicated as * p < 0.05, ** p < 0.01 and *** p < 0.001.

3.2.6 *In vitro* signaling data support the notion that FAM3D is involved in receptor tyrosine kinase signaling

For the further investigation of the molecular mechanism mediating the action of FAM3D, we utilized *in vitro* systems, which allowed us to study the acute signaling of FAM3D without any compensatory effects resulting from long-term overexpression of the protein.

First, we investigated the signaling in ingWAT derived explants upon the treatment with FAM3D and observed a significant increase in pAKT^{Ser437} and pERK1/2^{Thr202/Tyr204} after 10 min [Fig. 5A-C]. AKT and ERK1/2 are both central hubs downstream of many receptor tyrosine kinases [194,197], hence this observation further confirms the results of the kinase activity screen.

In accordance with the data obtained on ingWAT explants, in immortalized white adipocytes we could also observe a significant increase in phosphorylation of pAKT^{Ser437} and pERK1/2^{Thr202/Tyr204} following an acute treatment with FAM3D [Fig. 5D; E; G]. Additionally, AKT was also more phosphorylated at the Thr308 phosphosite [Fig. 5D; F]. SHP2, which is involved in downstream signaling of many receptor tyrosine kinases [194], was significantly more phosphorylated at Tyr 580 phosphosite and a strong trend was observed at the Tyr543 phosphosite ($p = 0.0518$) [Fig. 5D; H; I]. P38 MAPK and P70S6, which are also both downstream signal integrators of receptor tyrosine kinase signaling [198,199], displayed an increased phosphorylation as well [Fig. 5D; J-L]. This further strengthens our hypothesis, that FAM3D is involved in receptor tyrosine kinase signaling. His-tagged recombinant FAM3D protein dose dependently increased the phosphorylation of AKT and ERK1/2, excluding that the previously observed effects were elicited by the Fc-tag of the recombinant protein [Fig. 5M - O]. Lastly, also immortalized brown adipocytes demonstrated an increase in pAKT^{Ser437} and pERK1/2^{Thr202/Tyr204} upon treatment with recombinant FAM3D [Fig. 5P - R], underlining further the effect of FAM3D on the phosphorylation of AKT and ERK1/2.

In conclusion the acute signaling data of the explants and the immortalized white and brown adipocytes supports the notion that an acute short-term treatment with FAM3D is stimulating receptor tyrosine kinase signaling.

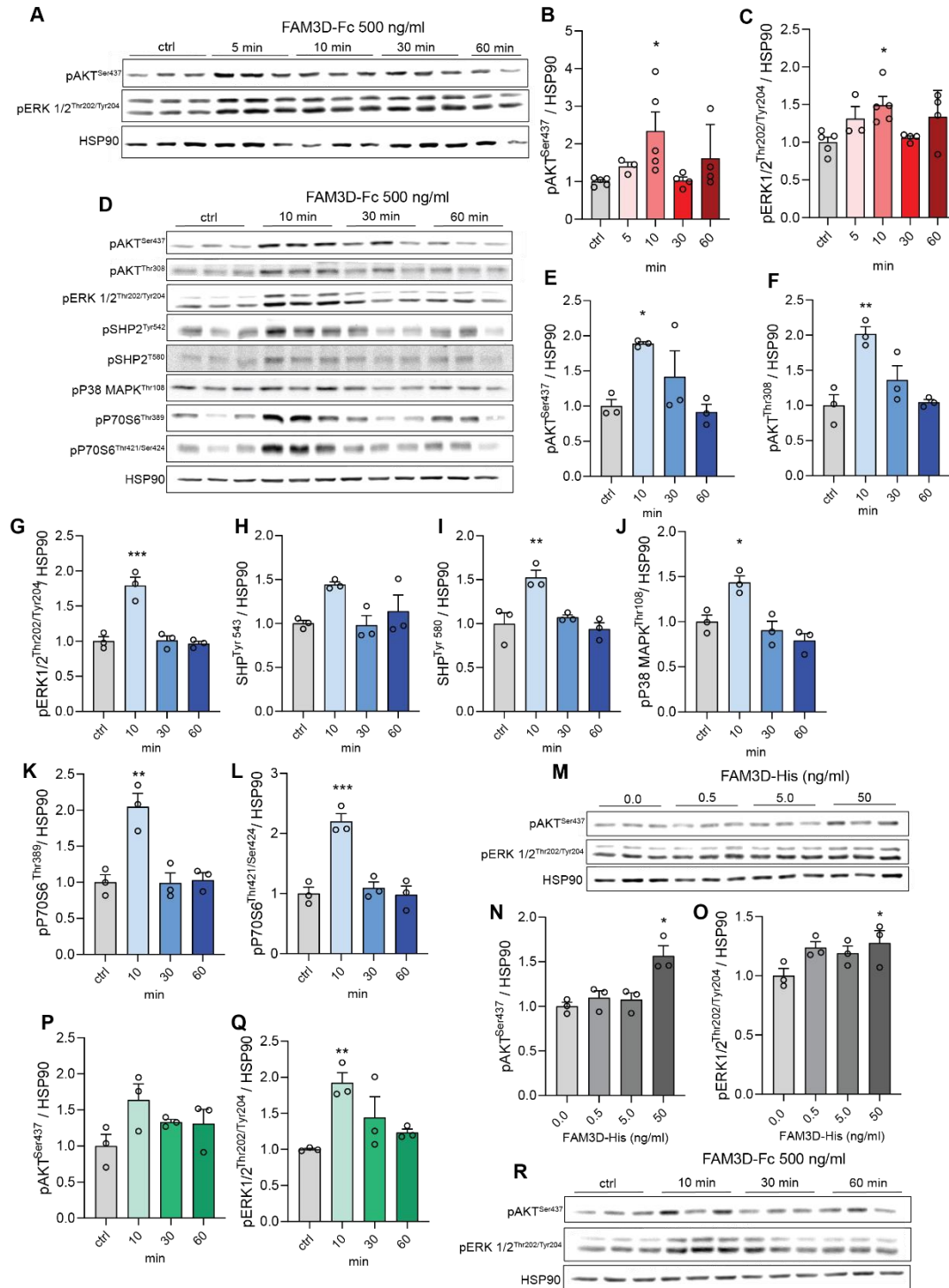


Figure 5: (A) Westernblots of explants from ingWAT treated with recombinant Fc tagged FAM3D (500 ng/ml) for the indicated times. Quantification of (B) pAKT^{Ser437} (C) pERK1/2^{Thr202/Tyr204} normalized to HSP90 of the westernblots displayed in (A) (n = 3-5). (D) Westernblots of immortalized white adipocytes treated with recombinant Fc tagged FAM3D (500 ng/ml) for the indicated times. Quantification of (E) pAKT^{Ser437} (F) pAKT^{Thr308} (G) pERK1/2^{Thr202/Tyr204} (H) pSHP2^{Tyr542} (I) pSHP2^{Tyr580} (J) pP38 MAPK^{Thr108} (K) pP70S6^{Thr389} (L) pP70S6^{Thr421/Ser424} normalized to HSP90 of the westernblots displayed in (D) (n = 3) (M) Westernblots of immortalized white adipocytes treated with recombinant His tagged FAM3D for 10 min at indicated concentrations. *continued on the following page*

Quantification of **(N)** pAKT^{S437} **(O)** pERK1/2^{Thr202/Tyr204} normalized to HSP90 of the westernblots displayed in (M) (n = 3). Quantification of **(P)** pAKT^{S437} **(Q)** pERK1/2^{Thr202/Tyr204} normalized to HSP90 of the westernblots displayed in (R) (n = 3) **(R)** Westernblots of immortalized brown adipocytes treated with recombinant Fc tagged FAM3D (500 ng/ml) for the indicated times. All data presented are mean ± SEM. Statistical analysis was performed by ordinary one-way ANOVA and multiple comparison testing. Significance is indicated as * p < 0.05, ** p < 0.01 and *** p < 0.001.

3.3 Discussion

The potential of gut secreted peptides for diabetic treatment is well known. GLP-1 synthetic peptide agonists which pose a longer-half live compared to the naïve protein or DPP4-inhibitors which stop the rapid degradation of peptides aim for the increase of gut peptide levels in the blood and thus, take advantage of their positive metabolic actions [117]. Hence, they are part of the standard care for many diabetic patients [200]. However, they often only have a very narrow therapeutic window and can cause severe side effects. Thus, there is an unmet need to develop novel anti-diabetic agents. Here, we identified FAM3D as a novel gut secreted protein with great potential for diabetic treatment. The AAV-mediated overexpression of FAM3D significantly improved the glucose tolerance and insulin sensitivity in diet induced obese mice. The global insulin sensitizing effect of FAM3D caused a significant increase in glucose uptake into various organs and ameliorated hepatic lipid deposition and steatosis. In addition, we provide evidence that the effects of FAM3D are mediated by the action of receptor tyrosine kinases.

The potential of the FAM3 family as a powerful target for the treatment NAFLD and T2D was previously reported [182]. While FAM3A and FAM3C levels are decreased in livers of diabetic mice and humans, levels of FAM3B (PANDER) in serum, pancreatic islets and liver are increased. This differential regulation of the individual FAM3 family members in a diabetic state is discussed to result in a reduction of AKT- and AMPK-activity, which leads to increased hepatic gluconeogenesis and lipogenesis and ultimately to NAFLD [182]. If FAM3A or FAM3C are overexpressed in obese and diabetic mice an attenuation of hepatic lipid deposition and an improvement of global insulin sensitivity can be observed [183,184]. Both peptides, activate the AKT-pathway in the liver independent of insulin and contribute via this to a healthier metabolic phenotype [183,184]. Based on our data, we can conclude that FAM3D induces a very similar positive metabolic phenotype as the other two family members FAM3A and FAM3C, despite the fact that no effect on AKT-signaling in the liver could be observed upon FAM3D overexpression.

We did not observe any bodyweight or glucose phenotype upon FAM3D knockout. However, in light of the existing data on other gut peptides, this finding is not surprising as the knockout of gut peptides rarely shows any effects on glucose metabolism. For instance, the disruption of the glucagon or the GIP gene (Gcg^{Gfp/Gfp} and GIP^{Gfp/Gfp}) led in both cases to reduced bodyweight gain

on HFD, improved insulin tolerance, as well as increased glucose stimulated insulin release. However, both models displayed only a mild a mild phenotype on glucose tolerance [201–203]. Further, with the technical progress in omics techniques [204], it has become clearer that there is a wide variety of gut secreted hormones hence, it is well possible that the ablation of a single gut peptide can be compensated by others and therefore the ablation of FAM3D is not causing any distortion of the systemic metabolism. Similarly, the knockout of a single incretin receptor, eg. GLP-1R $-/-$ or GIPR $-/-$, leads to only a mild phenotype, while a double incretin receptor knockout (DIRKO) displays a much stronger phenotype [205]. Genetic ablation of the corresponding receptor is an often-applied strategy to study the role of a peptide. Thus, it would be very interesting to identify the receptor of FAM3D and study the role of the ligand-receptor pair in regulation of energy metabolism. Peng et al., identified FAM3D as a chemotactic agonist for the formyl peptide receptors FPR1 and FPR2, primarily expressed on monocytes and neutrophils [188]. However, based on our data we could not observe any attraction of immune cells upon FAM3D overexpression. Further, as T2D is characterized by a low grad inflammation, a pro-inflammatory protein would rather worsen the diabetic phenotype, which contradicts the improved glucose metabolism we observed [206]. Additionally, FPR1 and FPR2 were not expressed in immortalized white adipocytes, where we could observe a clear signaling response upon FAM3D treatment. Hence, we propose the existence of an alternative receptor mediating the positive metabolic phenotype of FAM3D. However, future studies are needed to identify novel FAM3D receptor/s.

We identified receptor tyrosine kinase signaling as a possible molecular mode of action for FAM3D. Receptor tyrosine kinases are a family of transmembrane receptors containing 19 different subfamilies. All display a classical structure of an N-terminal extracellular domain, a single transmembrane domain and an intracellular kinase domain. While the kinase domain is highly conserved among most receptor tyrosine kinases, the extracellular domain differs greatly between the different receptor subfamilies. Receptor tyrosine kinases play an essential role in the regulation of cell survival and metabolism, proliferation and differentiation, as well as cell migration and cell cycle control [207]. Thus, the observed reduction in receptor tyrosine kinase signaling is in accordance with the observed reduction in activity of cell cycle regulating kinases. That the general kinase activity was downregulated can be explained by our model. Upon ligand binding many receptor tyrosine kinases undergo endocytosis. From the endosomes the receptors are then either recycled to the cell surface or they are degraded by lysosomes [208]. With our long-term chronic overexpression model, it is likely, that we did established a constantly active negative feedback loop resulting in a downregulation of kinase activity. In contrast, a short and acute treatment with FAM3D *in vitro* resulted in an increase in phosphorylation of known downstream targets of

receptor tyrosine kinases further supporting the notion that FAM3D is involved in receptor tyrosine kinase signaling. Receptor tyrosine kinases are involved in several cancer types and various receptor tyrosine kinase inhibitors are approved for malignant therapy. In the context of these therapies, it became evident that tyrosine kinase inhibitors likewise have a positive effect on T2D and even type 1 diabetes (T1D). Several patient reports, *in vivo*, and *in vitro* experiments, which are reviewed here [209–211] displayed great potential of tyrosine kinase inhibitors in the improvement of glucose metabolism. This is in accordance with the observed downregulation of receptor tyrosine kinase signaling upon chronic FAM3D overexpression and the observed positive glucometabolic phenotype. As potential underlying molecular mediators are discussed amongst others the platelet derived growth factor receptor (PDGFR) family and vascular endothelial growth factor receptor (VEGFR) family. Both appeared within the top regulated kinases after FAM3D overexpression. Upon the inhibition of PDGFR an increase in insulin sensitizing adiponectin can be observed [212] while, through the inhibition of VEGFR the reduced vascular remodeling is causing an amelioration of the with T2D associated inflammation [213]. However, neither adiponectin, nor VEGF-A levels were changed upon FAM3D overexpression, suggesting a different mechanism of action for FAM3D. Another possible mediator of the glucometabolic phenotype might be the MAPK/ERK pathway. ERK1/2, was significantly regulated upon chronic and acute FAM3D treatment and MEK inhibitors greatly improve insulin sensitivity in diet induced obese mice [214,215]. As possible molecular mechanisms mediating this effect are discussed, beside others, a reduction in the ERK-mediated negative feedback loop to the insulin receptor substrate 1 (IRS1) [216]. Alternatively, the inhibition of MAPK/ERK was described to reduce lipolysis in the adipose tissue, ameliorating the release of insulin resistance driving free fatty acids [217]. Though, no evidence for either of the options could be observed upon FAM3D overexpression. Nonetheless, various other options are discussed as underlying mechanism for the anti-diabetic effects of tyrosine kinase inhibitors, but further studies are needed to further elucidate the molecular mechanism of them. Also further studies about the potential receptor and the underlying signaling mechanism of FAM3D are needed. Once these are identified the positive metabolic phenotype of FAM3D will be hopefully explained better.

3.4 Conclusion

In summary FAM3D was identified as novel gut secreted protein which improves glucose metabolism in diet induced obese mice. Upon the overexpression of FAM3D a global insulin sensitizing effect could be observed. This resulted not only in improved fasting blood glucose levels, glucose tolerance and insulin tolerance, but also in an increased glucose uptake into various

tissues during hyperinsulinemic euglycemic clamps. Further, an amelioration of hepatic lipid deposition and steatosis was observed. Thus, FAM3D is a potential candidate for the treatment of T2D and NAFLD. While we could identify a downregulation of RTK-signaling as a possible underlying molecular mechanism, further studies are needed to fully elucidate the pathway and receptor mediating the positive metabolic effects of FAM3D.

Acknowledgments

We would like to acknowledge Manuel Klug for his great support in all the animal experiments. Further acknowledgment goes to Myrtha Arnold for performing the surgery for the hyperinsulinemic clamps, and Elke Kiehlmann for preparing the liver histological slides. Our acknowledgement also goes to Gommaar D'Hulst and Evi Masschelein for demonstrating us the harvesting of various skeletal muscles.

Author Contributions

C.M., B.H., H.N., S.W. and C.W. designed the study; C.M., M.B., C.H., L.B., L.S. performed the experiments; K.M.O., F.L., M.K. supported the flow cytometry experiments and their analysis, M.B. provided the human plasma samples, B.S. did the liver steatosis analysis, T.L. produced the AAV and the recombinant protein, C.M., M.B. and C.W. wrote the manuscript. All authors reviewed and edited the manuscript

3.5 Materials and Methods

3.5.1 Materials

All chemicals were purchased from Sigma Aldrich unless otherwise specified.

3.5.2 Human FAM3D plasma levels

FAM3D levels were measured in serum of patients who underwent open abdominal surgery for Roux-en-Y bypass or sleeve gastrectomy. All investigations have been approved by the ethics committee of the University of Leipzig (363-10-13122010 and 017-12-230112) and were carried out in accordance with the Declaration of Helsinki, and all study participants provided witnessed written informed consent before entering the study. The human FAM3D levels were analyzed by the Ab-Match ASSEMBLY Human FAM3D kit (Labforce).

3.5.3 *In vivo* experimental procedures

All animal experiment were approved by the Veterinary office of the Canton Zürich. Animals were housed in individually ventilated cages at standard housing conditions (22°C, 12 h reversed light/dark cycle, dark phase starting at 7am). The animals had access to food and water *ad libitum*. Chow diet contained 18 % proteins, 4.5 % fibers, 4.5 % fat, 6.3 % ashes (Provimi Kliba SA). Dietary intervention with HFD was started in eight week old animals (23.9 % proteins, 4.9 % fibers, 35 % fat, 5.0 % ashes (Provimi Kliba SA)).

3.5.4 Global inducible FAM3D knockout mouse

The FAM3D fl/fl mice were generated by ETH Phenomics Center Zurich (epic.ethz.ch). LoxP sites flanking the exon six of FAM3D were introduced using the newly developed technique of EASI-CRISPR. Here, specific CRISPR/Cas9 complexes for the insertion sites of the loxP sites were injected directly into mouse oocytes together with a single-stranded template for homologous recombination that contains 150 base long homology arms and the two loxP-sites flanking exon 6. Following the embryos were transferred into foster mothers. The offspring's where the insertion of the loxP sites was successful, were once backcrossed to C57BL6/N mice. Following the animals were mated to Rosa26-creERT2 animals (Taconic). At eight weeks of age recombination of the floxed allele was induced by oral tamoxifen gavage (2x 2mg/mouse in sunflower oil) and the animals were changed to HFD. To sustain the knock-out tamoxifen was reapplied every four weeks. Following eight weeks of HFD the metabolic phenotyping was started. Male and female mice were carefully phenotyped.

3.5.5 Injection of AAV

Male C57BL/6 animals received HFD for 10 weeks before AAV injection and were maintained on HFD throughout the experiment. Animals were assignment to the experimental groups based on bodyweight and fasting blood glucose levels. 1×10^{11} Virus genomes per mouse were diluted in PBS (Gibco) to a volume of 50 ul and injected intravenously. Two weeks post virus injection the metabolic phenotyping was started.

3.5.6 Assessment of metabolic parameters

Fasting blood glucose:

For the measurement of fasting blood glucose food was withdrawn for six hours during the dark phase. Blood was collected from a little incision at the tail vein. Blood glucose levels were determined using a standard glucometer (ACCU-CHEK Aviva, Roche).

Intraperitoneal glucose tolerance test (ipGTT):

The bodyweight of the animals was determined before fasting the animals for six hours during the dark phase. Following, fasting blood glucose levels were determined and D-glucose in saline (Braun) was injected intraperitoneal at dose 1 g/kg body weight. Blood glucose levels were measured 15 min, 30 min, 60 min, 90 min and 120 min post glucose injection using a standard glucometer (ACCU-CHEK Aviva, Roche).

Insulin tolerance test (ITT):

For the ITT the same procedure as for the ipGTT was applied. Insulin (Actrapid, Novo Nordisk) was injected at a dose of 0.75 U/kg bodyweight.

Pyruvate tolerance test:

For the Pyruvate tolerance test the same procedure as for the ipGTT and the ITT was applied. Pyruvate was dissolved in saline (Braun) and injected at a dose of 2.0 g/kg.

Blood collection for the determination of plasma parameters:

Blood was collected submandibular in EDTA coated tubes from either random fed or fasted animals. Immediately after blood collection 3 ul of Aprotinin (25000 KIU/ml) (Roth) were added. To obtain the plasma the whole blood was centrifuged at 2000 g for 20 min at 4°.

Urine collection:

The animals were placed over a collection tube and urination as facilitated by light strokes over the abdomen of the animals.

Body composition:

The body composition was determined by magnetic resonance imaging (EchoMRI 130, Echo Medical Systems). Fat and lean mass were analyzed using Echo MRI 14 software.

Indirect calorimetry:

Indirect calorimetry measurements were performed in the Phenomaster (TSE Systems) according to the manufacturer's guidelines. O₂ and CO₂ levels were measured for 60s every 13 minutes

continuously. Energy expenditure was determined according to the manufacturer's guidelines. The respiratory quotient was calculated by the ratio of CO₂ production to O₂ consumption. Activity, food and water intake were monitored continuously.

Tissue harvest:

For tissue harvest the animals were euthanized by carbon dioxide asphyxiation. The tissues were carefully dissected and snap frozen in liquid Nitrogen. From the ingWAT the popliteal lymph node was removed.

3.5.7 Hyperinsulinemic euglycemic clamps

Two weeks post virus injection the animals underwent surgery and a catheter was implanted into the vena jugularis. After 5-7 days of recovery, hyperinsulinemic euglycemic clamps were performed only on animals which regained more than 90% of their preoperative weight. For the clamps the animal were fasted for 6h, in the last 80 min of the fasting period Glucose-D-[3-3H] (0.05 μ Ci/min) (Perkin Elmer) was infused to determine the basal glucose uptake and glucose production. Blood was sampled at the end of the 80 min basal Glucose-D-[3-3H] infusion. Following Glucose-D-[3-3H] (0.1 μ Ci/ml), Insulin (12 mU/kg/min) (Actrapid, Novo Nordisk) and 20% glucose (Braun) as needed was infused until the animal reached a steady state at 6 mmol/l blood glucose. When in steady state a bolus of Deoxy-D-glucose 2-[14C(U)] (10 μ Ci) (Perkin Elmer) was administered to determine the glucose uptake into the individual organs. Blood was sampled at steady state and 2 min, 15 min, 25 min, 35 min after the Deoxy-D-glucose 2-[14C] bolus. Subsequently, the animals were euthanized and tissues were harvested. For the analysis the plasma samples were deproteinized with Ba(OH)₂ and ZnSO₄ as described in Kim et al, 2009 [192]. Tissues were homogenized, boiled and the phosphorylated Deoxy-D-glucose 2-[14C] was separated from the non-phosphorylated Deoxy-D-glucose 2-[14C] by ion exchange columns (chloride form) (BioRad). The glucose turnover is calculated through the division of the rate of Glucose-D-[3-3H] infusion by the Glucose-D-[3-3H] specific activity in the plasma [192]. The endogenous glucose production was determined through the subtraction of the glucose infusion rate from the glucose disposal rate [192]. The insulin stimulated glucose disposal rate is determined by subtracting the basal glucose disposal rate from the glucose disposal rate during the clamp [192]. The organ specific glucose uptake was calculated by determining the organ specific accumulation of phosphorylated Deoxy-D-glucose 2-[14C] and the decay of Deoxy-D-glucose 2-[14C] in the plasma. Two rounds on hyperinsulinemic clamps were performed and where possible the data were pooled.

3.5.8 Recombinant protein injection

Recombinant protein was diluted in saline (Braun) and injected intravenously into the tail vein at a dose of 0.4 mg/kg bodyweight. Thereafter the animals were fasted and 4,5 h later they either underwent a glucose tolerance test or they were thoroughly perfused with ice cold PBS (Gibco) and tissues for further analysis were harvested.

3.5.9 *In vitro* experimental procedures

Adipose tissue explants

The animals were starved for 4h during the dark phase before euthanization. Adipose tissue depots were excised and cut in ca. 20-25 mg pieces. The explants were starved in glucose free DMEM (Gibco), 0.5% BSA for 2h and subsequently treated with 500 ng/ml recombinant FAM3D-Fc. At the end of the incubation time the explants were washed in ice cold PBS (Gibco), briefly dried and snap frozen.

Cell culture

All cells were cultured in a cell culture incubator (humidified, 5% CO₂, 37°C). Standard culture medium was DMEM high glucose media (4,5 mg/ml D-Glucose) containing 10% FBS and 1% PenStrep (all Gibco), media was changed every other day.

Immortalized white adipocytes:

Immortalized white adipocytes were plated on collagen-coated plates. One day post confluence they were induced for 48h with Insulin (650 nM), IBMX (500 µM), rosiglitazone (1 µM) and dexamethasone (1 µM). Afterwards, the cells were cultured in maintenance media with Insulin (650 nM). At day four post induction the differentiating adipocytes were trypsinized and replated on collagen-coated multi-well plates in a density of 145 000 cells/cm². All assays were performed on day eight post induction.

Immortalized brown adipocytes:

Immortalized brown adipocytes were plated on collagen-coated plates. Upon confluence they were induced for 48h with Insulin (20 nM), IBMX (500 µM), rosiglitazone (1 µM), dexamethasone (1 µM) and T3 (1 nM). Afterwards, the cells were cultured in maintenance media with Insulin (20 nM) and T3 (1 nM). At day four post induction the differentiating adipocytes were trypsinized and replated on collagen-coated multi-well plates in a density of 145 000 cells/cm². All assays were performed on day eight post induction.

Recombinant FAM3D treatment:

For the treatment with recombinant FAM3D protein the cells were starved for 3h in low glucose DMEM (1 mg/ml D-Glucose), before recombinant protein was added at a dose of 500 ng/ml.

3.5.10 Transcriptomics of L-cells and enterocytes

Preparation and processing of the samples is described in Rollins et al, 2019 [189]. The sequencing data are available under:

<https://www.sciencedirect.com/science/article/pii/S0196978119300014?via%3Dihub#sec0125>

3.5.11 Immune cell characterization in liver and peritoneum

Cell suspension preparation:

For the collection of peritoneal immune cells the animals were euthanized and the abdomen was washed twice with with PBS (Gibco) containing 2 mM EDTA through a syringe inserted into the peritoneal space. Cells were collected by centrifugation. The livers were minced and digested in IMDM (Gibco) with 3% FBS (Gibco), 2 mg/ml of type IV collagenase and 0.125 mg/ml Dnase and passed to a 40 µ filter. The liver cells were first centrifuged for 5 min at 20g and following separated by density centrifugation with 30% Percoll at 2000 rpm, 20 min, low acceleration and no brake. The pellet in the bottom was collected for further analysis. Erythrocytes were lysed by ACK buffer.

Flow cytometry analysis:

Cell suspensions were incubated with fluorochrome-conjugated or biotinylated monoclonal antibodies specific to mouse in FACS buffer (PBS containing 2% FBS and 2 mM EDTA) and then washed twice before detection. Unless otherwise stated antibodies were purchase from BioLegend: CD45 (30-F11), CD11b (M1/70), CD11c (N418), CD64 (X54-5/7.1), F4/80 (BM8), MHCII (M5/114.15.2, eBioscience), Ly6C (HK1.4), Ly6G (1A8, BD Biosciences). eFluor780 (eBioscience) was used as live/dead marker for dead cell exclusion. LSR Fortessa (BD) was used for multiparameter analysis and the data were analyzed with FlowJo software (TreeStar).

3.5.12 Analysis of metabolic parameters in plasma and urine

Triglycerides in plasma were determined COBAS TRIGB kit (Roche/Hitachi). Free fatty acids were determined by NEFA-HR(2) assay (Wako Chemicals). Glucose in urine was determined by using

colorimetric glucose-assay-kit. Insulin, Glucagon, Leptin and Adiponectin levels were all measured by mouse ELISA kits (Crystal Chem). VEGF A levels were determined by Mouse VEGF Quantikine ELISA Kit (R&D). ALT activity was determined by kinetic colorimetric assay and T4 was determined by Thyroxine (T₄) competitive ELISA kit (Invitrogen). All assays were performed according to manufacturer's instructions.

3.5.13 Liver histology and liver triglycerides and glycogen

One lobe of the liver was fixed for 24h in 4% PFA and then processed by STP120 Spin Tissue Processor (ThermoScientific) according to standard protocol. Subsequently, the samples were paraffin embedded and cut to 5 µm sections. Staining with hematoxylin eosin was performed. The tissues sections were imaged by light microscopy using AxioPhot microscope equipped with AxioCam MR (Zeiss). Liver steatosis was analyzed as described in [218], for the analysis of liver micro steatosis the pipeline presented in [218] was modified and trained for micro steatosis recognition. The other lobes of the liver were snap frozen in liquid nitrogen for further analysis. Liver triglycerides were extracted using chloroform: methanol (2:1) mixture and normalized to tissue weight. Liver glycogen was extracted by homogenization of the tissue in ice cold water. For enzyme inactivation the samples were boiled for 10 min and cleared by centrifugation. The supernatant was analyzed by colorimetric based Glycogen Assay kit (Biovision) according to the manufacturer's instructions.

3.5.14 FAM3D tissue accumulation

To determine the accumulation of FAM3D in tissues, tissues were lysed in RIPA buffer (Cellsignaling) supplemented with protease inhibitor cocktail (Complete, Roche). Protein concentration was determined by Pierce™ BCA Protein Assay Kit (ThermoFisher) and the lysate was diluted to 0.04 mg/ml total protein. The presence of FAM3D in the tissues was analyzed using the high throughput western blot system Sally Sue (ProteinSimple) according to the manufacturer's instructions. Mouse FAM3D primary antibody (RD systems) was used 1:50 diluted.

3.5.15 Kinase activity screen

To determine the kinase activity profile in white adipose tissue, the frozen tissues were grinded by a handheld mortar and lysed in MPER buffer (ThermoFisher) supplemented with Halt protease and phosphatase inhibitor cocktail (ThermoFisher) for 20 min at 4°C on a rotor. Then lysates were cleared by two to three centrifugation steps (12 000 rpm, 4°C) and aliquots were prepared and

snap frozen for further analysis. For the whole process all tubes were always pre-chilled on ice. The protein concentration was determined by Pierce™ BCA Protein Assay Kit (ThermoFisher).

With the PAMGene technology the kinase activity profile in the lysates was analyzed. Therefore, 1µg of protein was loaded onto phosphotyrosine kinase (PTK) and phosphoserine/threonine kinase (STK) chip arrays. Each array contained peptides (196 PTK and 144 STK) with tyrosine or serine/threonine phosphorylation sites. Upon phosphorylation FITC-labelled anti-phosphotyrosine or antiphosphoserine/threonine antibodies were used to monitor peptide phosphorylation. The kinetics of phosphorylation were recorded by a charge coupled device (CCD) camera in combination with the Evolve software v1.2 (PamGene). The PAMGene experiments were performed by the Functional Genomics Center Zürich. For the analysis AAV-FAM3D animals were compared with AAV-Stuffer animals. The Bionavigator software v. 6.2 (PamGene) was used for data analysis und upstream kinase activity prediction. The Analysis was performed by PamGene.

3.5.16 Protein extraction and western blot

Tissues, explants and *in vitro* cultured cells were lysed in RIPA buffer (50mM Tris-HCl pH 7.4, 150mM NaCl, 2mM EDTA, 0.5% sodium deoxycholate, 1.0% Triton X100, 10% glycerol) supplemented with protease inhibitor cocktail (Complete, Roche) and Halt phosphatase inhibitor cocktail (ThermoFisher). Tissues and explants were homogenized in RIPA buffer by metal beads in the TissueLyser LT (Qiagen). The lysates were centrifuged for 5-10 min at 12 000 rpm and the cleared supernatant was collected. Protein concentration was determined by Pierce™ BCA Protein Assay Kit (Thermo Fisher) and equal amounts of protein (10µg – 30µ) were loaded onto SDS-Polyacrylamide gels for size separation. The proteins were transferred to nitrocellulose membranes, which were blocked for 1h at RT in 5% BSA or 5% milk before incubation with primary antibody at 4°C overnight. Unless otherwise stated antibodies were purchase from Cellsignaling and diluted 1:1000: AKT (9272S), pAKT^{Ser437} (4060S), pAKT^{Thr308} (13038S), ERK 1/2 (4695S), pERK^{Thr202/Tyr204} (4370S), SHP2 (3397S), pSHP2^{Tyr542} (3751S), pSHP2^{Tyr580} (3703S), P38 MAPK (8690S), pP38 MAPK^{Thr108/Tyr 182} (9211S), P70S6 (9202), pP70S6^{Thr389} (9205S), pP70S6^{Thr421/Ser424} (9204S), HSP90 (4877S), FAM3D (AF3027, RD systems). Rabbit secondary HRP-conjugated antibody (1:10 000, Merck) and goat secondary HRP-conjugated antibody were used to detect the signal with the Image Quant system (GE Healthcare Life Sciences).

3.5.17 Virus production

Murine FAM3D/Oit1 (UniProt P97805) was codon optimized for the expression in mice and cloned into a pFB vector under a LP1 promoter⁵⁸ to allow liver-specific protein expression. A pFB-Stuffer vector⁵⁹ was used as control. AAV8 was produced by transfection of human embryonic kidney (HEK)-293T cells with the expression plasmids (pFB_LP1-mFAM3D or pFB_Stuffer) plus the plasmids pDP8 (Plasmid Factory) and the pHelper plasmid (ThermoFisher). The purification and titration was performed as described previously [219].

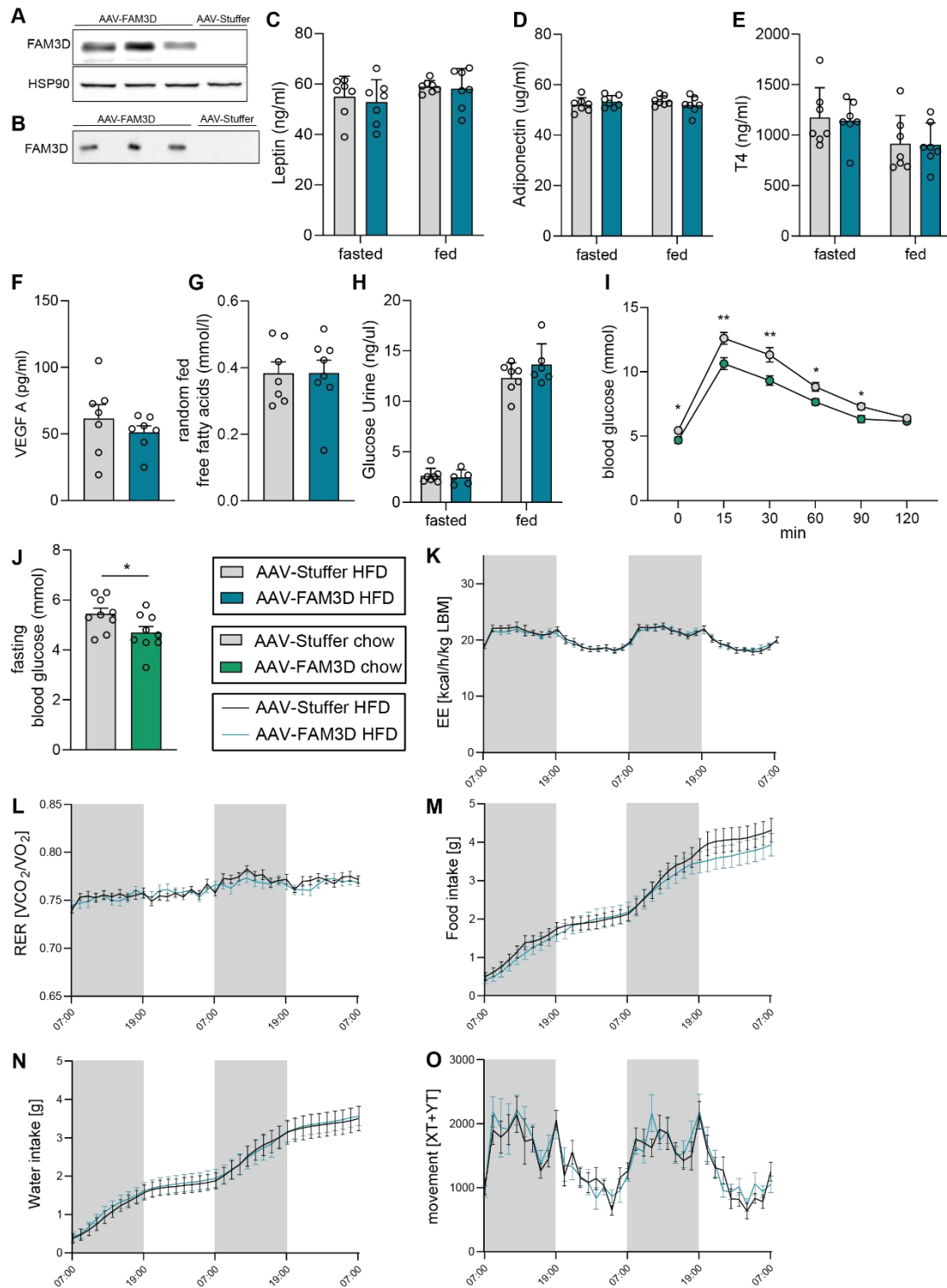
3.5.18 Recombinant mouse FAM3D-Fc production

Recombinant FAM3D was produced in HEK 293-E6 suspension cells cultured in F17 + 0,1% Pluronic F68 + L-Glutamin/Glutamax + 25µg/mL G418 (all ThermoFisher). For transfection plasmids harboring mFAM3D-Fc under the CMV promoter were diluted in Opti MEM I mixed 1:1 with in Opti MEM I diluted 293fectin (both ThermoFisher). 24h after transfection Tryptone N1 at an end concentration of 0,5% were added. At day five post transfection the cell suspension was cleared by centrifugation. The supernatant was mixed with Mab-Select beads (GE Healthcare) and incubated overnight. Protein purification was performed in Econo-Pac® Chromatography Columns (Biorad) where the beads were collected, washed and ultimately the protein was eluted.

3.5.19 Quantification and statistical analysis

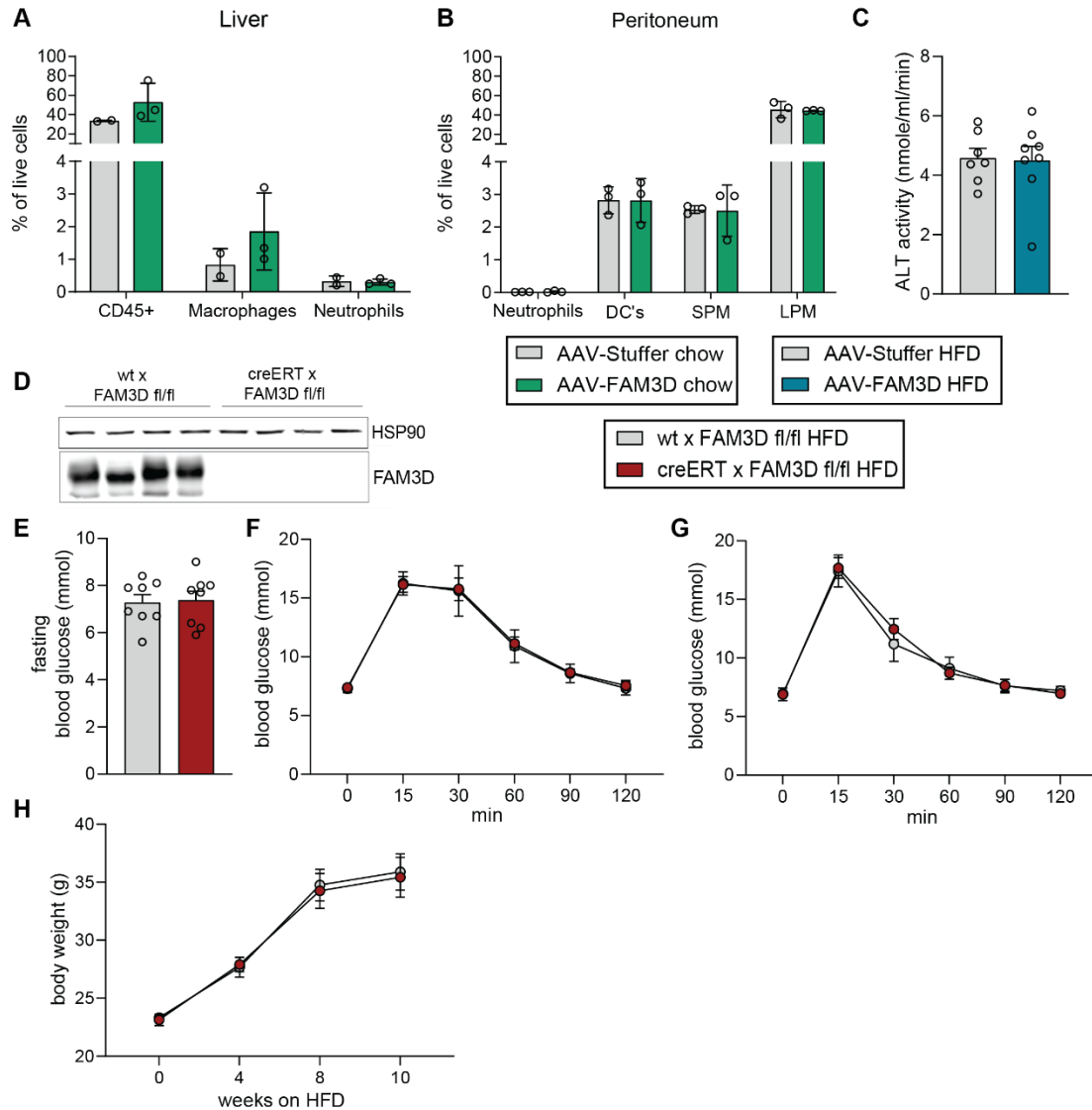
For *in vivo* studies, littermates were used for all experiments. All *in vitro* studies were performed with 3 technical replicates and the experiments were reproduced 2-3 times independently. Unless otherwise indicated, all results are expressed as mean ± standard error of the mean (SEM). Outliers were identified by ROUT with a Q = 1%. When two groups were compared a two-tailed, unpaired student's t-test (significance cut off: $p < 0.05$) was used to assess statistical significance. If more than two groups were compared a two-way ANOVA with Turkey multiple comparison testing was applied to test for statistical significance. Paired Student's t test was used to analyze the differences in paired samples. Possible outlier were removed if they differed more than the standard deviation multiplied times two from the mean. All graphs and statistical analyses were performed using Graphpad Prism (Version 8). Statistical significance is indicated as following: * = $p \leq 0.05$; ** = $p \leq 0.01$; *** = $p \leq 0.001$; **** = $p \leq 0.0001$.

3.6 Supplementary Figures

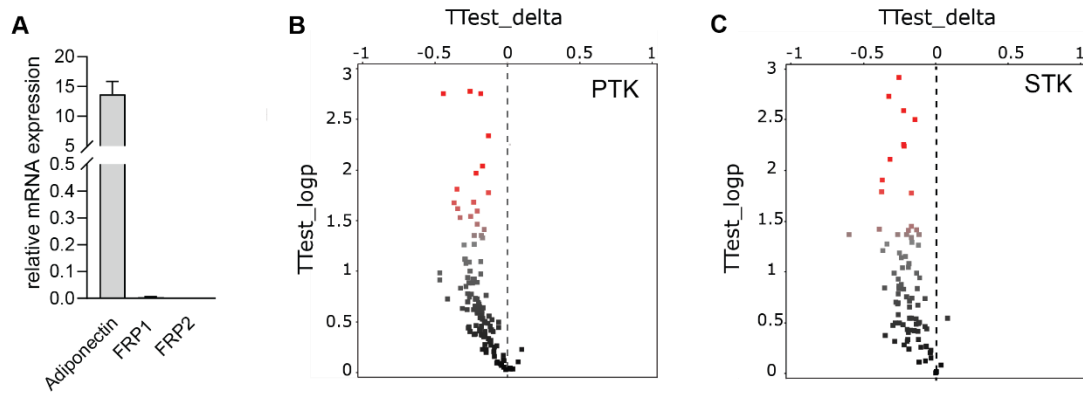


Supplementary Figure 1: (A) Westernblot of FAM3D in liver lysates from animals euthanized 2 weeks post virus injection, HSP90 is displayed as loading control (B) Westernblots of FAM3D in plasma taken from animals 2 weeks post virus injection, only every second lane was loaded. (C) Leptin levels (D) Adiponectin levels and (E) Thyroxin (T4) levels sampled in fasted state 3 weeks post virus injection and sampled in fed state 4 weeks post virus injection (n = 7). (F) VEGF A in plasma sampled 3 weeks post virus injection in random fed mice (n = 7). *continued on the following page*

(G) Free fatty acids in plasma sampled 3 weeks post virus injection in random fed mice (n = 8). **(H)** Glucose levels in the urine, sampled 3 weeks post virus injection in fed state and sampled 4 weeks post virus injection in fasted state (n = 5-7). **(I)** Intraperitoneal glucose tolerance test in chow was performed two weeks post virus injection (n = 9). **(J)** Fasting blood glucose levels in chow mice, two weeks post virus injection (n = 9). **(K)** Energy expenditure (EE) **(L)** Respiratory exchange ratio (RER) **(M)** Food intake **(N)** Water intake **(O)** Activity measured during two days in the Phenomaster system (TSE) two weeks post virus injection (n = 12). All data presented are mean \pm SEM. Statistical analysis was performed by unpaired Student's t test (B-N). Significance is indicated as * p < 0.05, ** p < 0.01 and *** p < 0.001.



Supplementary Figure 2: (A) % of CD45+ cell, macrophages and neutrophils of total live cells in the liver of chow mice two weeks post virus injection (n=2-3). **(B)** % neutrophils, dendritic cells (DC's), small peritoneal macrophages (SPM) and large peritoneal macrophages (LPM) of total live cells in the peritoneum of chow mice two weeks post virus injection (n=3). **(C)** Alanine transferase (ALT) activity in the serum 10 weeks post virus injection (n=7-8). **(D)** FAM3D protein levels in colon from wild type (wt x FAM3D fl/fl) animals and global inducible FAM3D KO animals (Rosa26-creERT x FAM3D fl/fl) one week after tamoxifen treatment. HSP90 is shown as loading control **(E)** Fasting blood glucose levels and **(F)** Intraperitoneal glucose tolerance test in wild type and global inducible FAM3D KO male animals after eight weeks of HFD and eight weeks post induction of the KO (n = 8) **(G)** Oral glucose tolerance test in wild type and global inducible FAM3D KO male animals after 10 weeks of HFD and 10 weeks post induction of the KO (n = 8) **(H)** Bodyweight of wild type and global inducible FAM3D KO male animals following the induction of the KO and HFD treatment (n = 8). All data presented are mean \pm SEM. Statistical analysis was performed by unpaired Student's t test (B-N). Significance is indicated as * p < 0.05, ** p < 0.01 and *** p < 0.001.



Suppl. Figure 3 (A) Gene expression analysis in differentiated immortalized white adipocytes. TBP was used as a reference gene, $2^{-\Delta CT}$ is presented. Data presented are SEM \pm mean, (n = 4) **(B)** Vulcano Blot PTK chip. Log-fold-change (x-axis, TTest_delta) versus significance (y-axis, $-\log_{10}(\text{pvalue})$). Red spots are peptides that show significant difference compared to control ($p < 0.05$) **(C)** Vulcano Blot PTK chip. Log-fold-change (x-axis, TTest_delta) versus significance (y-axis, $-\log_{10}(\text{pvalue})$). Red spots are peptides that show significant difference compared to control ($p < 0.05$)

CHAPTER 4

General Discussion

4.1 Remodelling of adipose tissue

*“Love handles: fat on the sides of a man or woman held onto during copulation” -
Richard Spears: Slang and Euphemism (1981)*

Obesity is possibly the most commonly occurring cause of adipose tissue remodeling, in the best case generating only “love handles”, but far more often manifesting in morbid obesity. In addition to the expansion of adipose tissue in response to an excess of nutrients, the adipose tissue displays great remodeling capacity in response to changes in ambient temperature. Understanding the underlying mechanisms of the remodeling processes can be helpful to block, activate, or, reverse them. Finding a way to expand the adipose tissue in a healthy manner without concomitant tissue fibrosis and inflammatory responses as well as activating the brown adipose tissue as a metabolic sink for glucose and lipids can be useful strategies to prevent the global rise of obesity and metabolic diseases.

In chapter 1 of this thesis, an introduction to the adipose tissue in the context of metabolic disorders was given. Chapter 2 of this thesis focuses on adipose tissue remodeling in response to thermoneutrality and cold exposure. With the help of the Adiponectin- and Ucp1-tracer-depleter mouse lines, we could quantify the remodeling potential of adipose tissue and study the kinetics of the remodeling process. This part of the thesis will return to the discussion of chapter 2 to bring the results into a wider scientific context and deepen the discussion beyond the scope covered chapter 2.

Thermoneutral housing of animal's plays an important role, seeing as us humans live either at or close to a state of thermoneutrality. We usually comfort ourselves with heating and warm clothes so that we do not feel cold [220]. Thus, to improve the translation potential of brown adipose tissue research from mice to humans, it is getting more relevant to perform the experiments in the thermoneutral zone of the animals. The general tenor is that thermoneutral zone for mice is somewhere between 28°C – 32°C. However, the exact thermoneutral point remains highly discussed in the field [221–223]. When animals are transferred into thermoneutrality, the brown

adipose tissue obtains a white-like morphology characterized by adipocytes filled with larger lipid droplets, with classical multilocular brown adipocytes being only sporadically observed [148,224]. One reason for this morphological change is the reduction in lipolysis due to a reduced sympathetic innervation, resulting in more filled lipid droplets. Secondly, a recent study identified *de novo* lipogenesis controlled by the carbohydrate response element-binding protein (ChREBP) as the mediating mechanism in thermoneutrality that fills the adipocytes with lipids [148,225]. In addition, the color of the tissue becomes more whitish as the number of mitochondria responsible for the brownish appearance of brown adipose tissue is reduced [226]. The loss of the mitochondria upon thermoneutral housing is mediated by the transcription factor EB (TFEB), which controls the autophagosomal and lysosomal processes for the clearance of the mitochondria from the tissue [226,227]. The remarkably different morphology of brown adipose tissue at thermoneutrality becomes even more pronounced when the animals are fed a high fat and/or energy rich diet [144,148]. This led to the question regarding the existence of a brown-to-white interconversion. This discussion is especially important in the context of the humans living at thermoneutrality subsisting on a rather energy rich diet.

In chapter 2, we could demonstrate with our Ucp1-tracer-ablater mouse model that the “classical” brown adipocyte characteristics were maintained despite a morphological whitening. We could fully recover Ucp1+ cell numbers following a beta3-adrenergic stimulus and fully ablated all Ucp1+ cells with diphtheria toxin in thermoneutrality. This observation is in accordance with the publication from Roh et al., 2018, which was briefly mentioned in the discussion of chapter 2. However, I would like to discuss it a little further at this time. Roh and colleagues housed mice in a cold for one week to induce beigeing in the ingWAT, followed by four weeks of thermoneutral housing. With their mouse model of the NuTRAP mouse, they were able to mark and isolate nuclei for epigenomic and ribosomes for transcriptomic profiling in parallel [228]. On both epigenomic and transcriptomic levels, they could demonstrate that the brown adipocytes undergo only a minor change in their epigenomic and transcriptomic identity upon thermoneutral housing. In contrast, the brite/ beige adipocytes undergo a profound change in their cellular identity, indicating a real transdifferentiation of cells [145]. One very plausible reason explaining the maintenance of the cellular identity of brown adipose tissue is the sympathetic innervation, which is much higher in the interscapular region when compared to the inguinal fat depot. However, even when denervated, the brown adipose tissue maintained its identity upon thermoneutral housing [145]. This suggests that the classical brown adipocyte identity is profoundly anchored, meaning that no brown-to-white interconversion takes place upon thermoneutral housing, even when the morphology displays a rather white-like phenotype [145]. In distinction, the brite/beige

adipocytes are much more versatile. They are capable of transforming back and forth between white and brite/beige on morphological, transcriptional, and epigenomic levels [14,145].

This poses the question: is the main brown adipose tissue depot in humans, which lays under the clavicular, most accurately resembled by rodents "classical brown" or by rodents "brite/beige" adipocytes? When immortalized brown or brite/beige adipocytes are cultured *in vitro*, the gene expression signature of brite/beige cells closely resembles the signature of human brown adipose tissue [136,229]. However, culturing adipocytes *in vitro* drastically changes their transcriptomic profile [171]. Hence, *in vivo* data pose a higher relevance to the question raised above. Various studies aimed to compare human brown adipose tissue with murine classical brown or brite/beige adipose tissue [230,231]. The challenge here is the heterogeneity of the adipose tissue. A human biopsy is never purely made up of adipocytes and will always contain various other cell types. Two important factors in determining the classification of the biopsy are the location from where the biopsy was taken and the chosen reference genes [230,231]. In addition, the mouse model to which we compare the human biopsy is highly relevant. De Jong et al., 2019 proposed the use of humanized mice [144]. They reason that we cannot compare a juvenile, chow diet-eating mouse housed at a temperature below thermoneutrality to a middle-aged human eating a western diet, wearing clothes, and living in heated rooms. Thus, they suggest that mice should be housed at thermoneutrality for six to eight months while being fed an energy rich diet [144]. Indeed, the interscapular brown adipose tissue (iBAT) depot of these humanized mice accurately resembled human supraclavicular brown adipose tissue on a morphological level as well as in the transcriptomic signature [144,232]. In contrast, when the mice were not humanized, then the human brown adipose tissue clustered much closer to the brite/beige adipocytes of mice on a transcriptomic level [232]. Thus, concluding if the human brown adipose tissue is either brown or brite/beige heavily depends on what is used as a reference for comparison. The answer is not necessarily mutually exclusive; we might not even be able to compare it at all. Further, with the emergence of evolving tools and techniques in the field of bioinformatics and single cell sequencing, the current classical definitions of white, brown, and brite/beige adipocytes are already being challenged. Currently, new populations of adipocytes are identified, posing new thermoregulatory properties [154,233].

Arguably, the most important question in this field is: How can we expand and activate the brown adipose tissue? In general, there are two construction sites available; either the brown adipose tissue can be made browner or the white adipose tissue can be made more brite/beige. In chapter 2, we could quantify the number of brown cells in the iBAT and the number of brite/beige in the ingWAT arising upon cold exposure. In the iBAT, we observed a peak of Ucp1+ cells within the

first week of cold exposure, followed by a continuous decline in Ucp1+ cells upon prolonged cold exposure until they were back at levels observed at room temperature. In the ingWAT, the Ucp1+ cells only reached a plateau after three weeks of cold exposure. This plateau was maintained upon prolonged cold housing.

From a functional perspective, both brown and brite/beige adipocytes pose the same function: the production of heat through Ucp1. Both cell types respond to the same activators, especially norepinephrine released from the sympathetic nerve ends in response to cold or synthetic beta-agonists [234]. Few other mutually exclusive activators are available (listed in Figure 1) [5]. Both cell types rely on a common transcriptional cascade for adipogenesis, involving the peroxisome proliferator-activated receptor γ (PPAR γ) and CCAAT/enhancer-binding proteins (C/EBPs) [235]. Several other key transcription factors are shared between the two types of thermogenic active adipocytes, namely the PR domain-containing protein-16 (PRDM16) [236,237] or the peroxisome proliferator-activated receptor-coactivator-1 α (PGC-1 α) [238,239]. Despite sharing many similarities, brown and brite cells develop from two different lineages. Originally, the majority of brown adipocytes were described to be derived from the Myf5+/Pax3+ lineage, originating from the central dermomyotome, whereas the brite/beige adipocytes are primarily derived from the Myf5- lineage [240]. However, with the development in mice models for tracing, it became clear that nearly all brown adipocytes in the iBAT were derived from the Myf5 lineage. In contrast, only half of the cells in the cervical BAT (cBAT) were found to be from the Myf5 lineage. Other markers, like Pax3 or Pax7, were subsequently tested for tracing. All these markers suggest that the different lineages are not mutually exclusive to just one adipose tissue depot. Rather, the origin of the brown/brite/beige adipocytes depends on their location along the dorsoventral axis of the dermomyotome [241]. In conclusion, there is great heterogeneity in adipocyte development, and the adipocytes in the different adipose tissue depots are most likely derived from different embryonic origins [242]. Tracing the developmental origin of human brown and brite/beige adipocytes is difficult due to technical and ethical limitations. In order to overcome these limitations, a recent report successfully differentiated human pluripotent stem cells (hPSCs) into brown adipocytes *in vitro* by mimicking the developmental steps of murine iBAT *in vivo*. This gives first indications of some similarity in the developmental process of human- and mouse-derived brown adipose tissue [243].

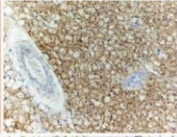
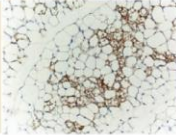
	Immunohistochemistry with anti-Ucp1	Location in humans	Location in mice	Developmental origin in mice	Enriched markers	Key transcription factors	Activators
Brown		Neck Interscapular (newborns) (Perirenal?)	Interscapular Cervical Axillary Perirenal (Endocardial?)	Myf5 ⁺ cells (dermomyotome)	<i>Zic1</i> <i>Lhx8</i> <i>Eva1</i> <i>Pdk4</i> <i>Epst1</i> <i>miR-206, miR-133b</i>	<i>C/ebpβ</i> <i>Prdm16</i> <i>Pgc-1α</i> <i>Ppar-α</i> <i>Ebf2</i> TR	Cold Thiazolidinediones Natriuretic peptides Thyroid hormone Fgf21, Bmp7, Bmp8b Orexin
Beige		Supraclavicular (Paraspinal?)	Interspersed within WAT subcutaneous fat > visceral fat	Myf5 ⁻ cells Pdgfr-α ⁺ (perigonadal)	<i>Cd137</i> <i>Tbx1</i> <i>Tmem26</i> <i>Cited1</i> <i>Shox2</i>	<i>C/ebpβ</i> <i>Prdm16</i> <i>Pgc-1α</i> (<i>Ppar-α</i> ?)	Cold Thiazolidinediones Natriuretic peptides (Thyroid hormone?) Fgf21 Irisin

Figure 1: Similarities and differences between brown and brite/beige adipocytes. Taken from Harms and Seale, 2013 [5]

When we look at the kinetics of recruitment of Ucp1⁺ cells, the iBAT was clearly recognized to be the first responder to cold, with the brite/beige only following afterwards. As the classical brown adipocytes are specialized for their heat generating task, this was not too surprising. At room temperature, they already display high Ucp1 protein levels, high sympathetic innervation, and a high vascularization to supply the tissue with energy substrates and dissipate the heat [244]. However, we were a bit surprised by the fact that the majority of Ucp1⁺ cells arising upon cold exposure were derived from pre-existing adipocytes and not from precursors. Although, we did not go further into the underlying mechanism during chapter 2, I would like to take the chance to briefly speculate about possible scenarios. One option that would enable the rapid transformation of pre-existing adipocytes into Ucp1⁺ adipocytes cells could be epigenetics. Epigenetics include DNA methylation, histone modifications, and noncoding RNAs [245]. The silencing and enhancing of promotor regions through epigenetic modifications allow the cells to respond on a transcriptional level to environmental challenges [246]. One could imagine that there are several pre-brown adipocytes in the iBAT where the Ucp1 promotor region is silenced by an epigenetic modification to save energy. Upon a cold stimulus, these pre-brown adipocytes can be quickly “switched-on” through the removal of the epigenetic break at the promotor. Most epigenetic studies in adipocytes to date have been performed *in vitro* [247–249]. Shore and colleagues demonstrated that the Ucp1 expression is regulated via the demethylation of CpG dinucleotides of cyclic AMP response elements in the Ucp1 promotor region [250]. Roh et al. have demonstrated profound changes *in vivo* in the epigenom in response to changes in housing temperature [145]. A recent publication from our laboratory could show on a single cell level that there are several cells in the iBAT which are Adipoq⁺ but Ucp1⁻ at room temperature. They could potentially represent these pre-brown adipocytes, which can be switched on if needed [154]. However, the fact that we label the same amount of Adipoq⁺ cells and Ucp1⁺ cells at room temperature as well as upon cold exposure, does not support this hypothesis. Thus, the scenario, where the pre-

existing adipocytes at room temperature proliferate upon cold exposure, is more likely [170]. To ultimately prove this hypothesis with our method, we would require two independent genomic labels, driven by either the Adipoq- or the Ucp1-promotor. Alternatively, 5-Bromo-2'-deoxy-uridine (BrdU) could be applied to label the proliferative cells. However, this would require analysis by histology or flow cytometry. Both methods require tissue processing and thus do not allow for the unbiased quantification of the adipocytes regarding localization and size. The brite/beige cells arising within the inguinal white adipose tissue depot responded to the cold stimulus much more slowly when compared to the brown adipocytes. In the literature, both the transdifferentiation from white to brite/beige [12,14,251] and the proliferation of precursors [10,142] are described as the driving mechanisms behind this process.

Nonetheless, I would like to return to our initial question on the activation of brown and brite/beige cells. When translated into the human setting, it has already been pointed out that activating either brown or brite/beige cells is most likely impossible. Furthermore, it is currently unknown if the thermogenic adipose tissue in humans is brown or brite/beige. However, what is known is that it is no longer necessary to search for a beta3-adrenergic receptor agonist. Mature brown and brite/beige adipocytes in rodents express beta3-adrenergic receptors. Hence, a lot of effort was put into identifying beta3-receptor agonists, which pose only minimal off-target effects in humans [104,105]. However, the recent discovery that brown adipocytes in humans primarily express beta2-adrenergic receptors caused the birth of a new perspective in the field [252]. I am persuaded that, through this observation, the search for activating agents in the brown/brite/beige adipose tissue of humans will be massively accelerated and novel treatment options will be found soon.

Lastly, I would like to briefly mention the astonishing regeneration potential of the iBAT. We observed that, upon a complete ablation of all Ucp1+ cells by diphtheria toxin, the iBAT completely recovered within one week of cold exposure. This regeneration was driven by precursor differentiation, suggesting that, at least in rodents, the precursors are potent enough to recover the entire adipose tissue depot. One experiment not yet performed, but which would be highly interesting, would consist of ablating the regenerated Ucp1+ cells again and seeing if the precursors are capable to recover the adipose tissue a second time. In the visceral adipose tissue, we have a pool of precursors that differentiate upon a short term HFD stimulus of three days. This pool is finite and a second short-term HFD stimulus does not elicit a second burst of proliferation [177]. It would be interesting to see if the pool of precursors replenishing the iBAT following a complete ablation is finite or infinite. When translated into the human setting, this pool of precursors capable of regenerating a whole adipose tissue depot would serve as a

powerful tool to increase the brown adipose tissue in humans. It is currently unclear if such a pool exists in humans, as is the existence of a suitable stimulus. One other approach to increase brown adipose tissue currently being tested in rodent models is the transplantation of brown adipose tissue or brown differentiated mesenchymal stem cells [253,254]. While both approaches display great potential in mice, with significant improvements of metabolic parameters, the potential for translation into humans should be approached with caution.

In conclusion, we investigated the capacity of the adipose tissue to remodel and to regenerate. The versatility of the adipose tissue is astonishing. By characterizing the remodeling potential in rodents, we could deepen our understanding about the kinetics and the underlying mechanisms. In the future, these insights will hopefully help us to better understand the remodeling in human adipose tissue.

4.2 Gut secreted proteins and their potential for type 2 diabetic treatment

“Gut feeling - An instinct or intuition; an immediate or basic feeling or reaction without a logical rationale” – Wiktionary.com

Gut secreted hormones are powerful messengers which can elicit feelings in humans that go beyond our logical or rational intellect. This powerful connection between the gut and our brain was recognized early on. It is not for nothing that we have sayings in many languages along the lines of: “having butterflies in the stomach” or “the way to a man’s heart is through his stomach.” Our feelings are not the only thing that is heavily influenced by the gut; it also regulates many other essential functions in our body. The role of the gut in the context of metabolic diseases was described in detail in chapter 1, the introduction of this thesis. Chapter 3 of this thesis focused on FAM3D, a novel gut secreted protein, and its potential for diabetic treatment. In this part of the discussion, I would like to give an outlook about what necessary next steps are needed in the FAM3D project in order to bring FAM3D from the bench to the bedside.

We discovered that FAM3D metabolically acts as an insulin sensitizer. The root of T2D is insulin resistance. Thus, the restoration of insulin sensitivity poses an effective strategy for the prevention or treatment of T2D. Hence, a lot of effort was put into finding insulin sensitizing agents early on. Today, the biguanide Metformin, and the two thiazolidinediones (TZDs) Rosiglitazone and Pioglitazone, are successfully used in patients as insulin sensitizing agents. While Metformin primarily acts via the activation of AMPK, Rosiglitazone and Pioglitazone elicit their metabolic function over PPAR γ agonism. We have primary indications that FAM3D acts via receptor tyrosine

kinase signaling. However, the exact molecular mechanism via which FAM3D provokes its insulin sensitizing effects remains elusive to us.

One approach to dissect the molecular mechanism of FAM3D would be to identify the receptor mediating the positive metabolic phenotype. The formyl peptide receptors 1&2 (FRP1 & FRP2), which are primarily expressed on monocytes and neutrophils, were proposed as possible receptors for FAM3D [188]. As already outlined in chapter 3, we suggest an alternative receptor-ligand interaction, since, we did not observe any immune cell infiltration in either the liver or the peritoneum upon overexpression of FAM3D. Possible methods for receptor identification are the TriCEPS method or an APEX2 construct. The centerpiece of the TriCEPS method is a chemoproteomic reagent containing three moieties. One part binds to the amino groups of the ligand, one part binds to the glycosylated parts of receptors, and a third part contains a biotin tag for the purification of the receptor peptides for later investigation by mass spectrometry [255,256]. One significant advantage of this method is that the labeling can be performed in live cells that are fully attached to the plate, under physiological conditions, ensuring that the expression pattern of the surface receptors is not changed [255,256]. This method was successfully applied for the identification of various ligand-receptor pairs, including insulin and the insulin receptor, as well as Erb2 and the epidermal growth factor receptor, both of which belong to the class of receptor tyrosine kinases. Especially promising is the fact that the insulin and insulin receptor-ligand pair were identified in differentiated immortalized white adipocytes (similarly to our study), suggesting that the lipids of the differentiated adipocytes are not interfering with the assay [255]. Further, with the development of this method towards flow-TriCEPS, where the biotin at the third moiety of the TriCEPS linker was replaced by a fluorophore, the validation of the identified receptors became significantly faster. Using flow-TriCEPS in combination with a siRNA mediated knockdown of one or multiple identified receptors results in a clearly distinguishable shift of the fluorescent signal [257]. Another possible method to identify the receptor of FAM3D would be an APEX2 construct. APEX2 is the second generation of an engineered ascorbate peroxidase. APEX2 can generate a very short-lived biotin-phenoxyl radical by catalyzing the oxidation of biotin-phenol. This reaction tags proteins in close proximity to APEX2 [258,259]. Thus, by linking APEX2 to FAM3D, binding partners can be tagged and identified with mass spectrometry. Again, similarly to the TriCEPS method, the labeling can be performed under physiological conditions [259]. Zhen et al., 2018 successfully identified interaction partners for the secreted protein FGF1 via this method [260]. Compared to the TriCEPS method, the APEX2 method is more unspecific, seeing as everything in ca. 20 nm radius gets biotinylated. Thus, the validation of the identified receptors should not only include the validation of interaction (for example, via immunoprecipitation or co-

localization) but should also perform the validation for functional relevance, for example via the investigation of the downstream signaling responses [261]. In conclusion, both methods pose great potential. Thus, we are currently working on the setting up both methods to hopefully identify the receptor mediating the metabolic phenotype of FAM3D.

In parallel to the receptor hunting, we should also investigate more pharmacologically relevant administration routes of FAM3D to examine whether FAM3D is still a potent insulin sensitizer, even when not supraphysiologically overexpressed by an AAV. To achieve this, one could inject mice with a daily dose of recombinant FAM3D protein. The fact that we observed an improvement in glucose tolerance following a single injection with 0.4 mg/kg recombinant FAM3D is already very promising. However, further studies to determine the pharmacokinetics, including the estimation of the half-life, as well as the bioavailability of FAM3D *in vivo*, are needed. Additionally, the minimal effective dose of FAM3D should be analyzed. Limiting factors, which have hindered us from performing these experiments to date, were the limited availability of the recombinant protein as well as the lack of a working mouse FAM3D ELISA. Nevertheless, based on the demonstrated potential of FAM3D, these are two hurdles which are possible to overcome, and which will be tackled in future. Once the half-life and the effective dose of FAM3D *in vivo* are determined, one could also implant an osmotic mini pump constantly releasing FAM3D at a low dose. This would allow for the investigation of the metabolic effects of chronic FAM3D administration with a defined dose. Osmotic minipumps have been used in rodent research for many years, and many metabolic active peptides have been successfully applied [262–265]. For GLP-1 receptor agonists, even an osmotic minipump for humans is now in the process of phase III clinical trials [266]. Nonetheless, during the aforementioned experiments, we must maintain our hypothesis that the chronic overexpression of FAM3D reduces the RTK activity and thereby elicits the positive metabolic phenotype in mind. It might well be that we do not need a receptor agonist; perhaps we should rather look for a receptor antagonist. However, if the pharmacologically relevant administration of FAM3D successfully improves glucose metabolism another important step towards the use of FAM3D as an insulin sensitizer in T2D patients will have been made.

Additionally, we should characterize A) the endogenous secretion pattern and B) the endogenous degradation pattern of FAM3D. By knowing the endogenous secretory pattern, the medication can be tailored more effectively to physiologically relevant needs. Elevated FAM3D levels were described to increase in human serum upon the ingestion of a high-fat milk shake [187]. Therefore, we have a first indication that a high fat meal could stimulate the secretion of FAM3D. To determine the secretory pattern of FAM3D in mice, we currently lack the tool of a commercially available mouse FAM3D ELISA. However, as mentioned before, this is a technical hurdle which can

be overcome, especially now that the FAM3D knockout mouse is available, which allows for a solid validation of an in-house developed ELISA. However, the identification of the degradation of the FAM3D pattern is probably more important for the road from the bench to the bedside. This was a reason why early injections of GLP-1 were disappointingly unsuccessful [267]. Only with the development of DPP4 resistant GLP-1 analogues the successful journey of GLP-1 as an antidiabetic drug started [268]. Therefore, it is likely that, to bring FAM3D to the market, stable analogues or small peptides mimicking the effect of the full length FAM3D must be developed.

Another hurdle for new medications is that they must be superior to what is already on the market in order to get approved. Thus, a substance purely treating T2D will probably have difficulties becoming permitted. FAM3D displayed ameliorating effects on NAFLD. Even though we currently are far away from understanding the underlying mechanisms responsible for the observed positive liver phenotype, this massively improves the chances of FAM3D making it to the market. The fact that the other family members of the FAM3 family display great potential to treat both T2D and NAFLD supports the potential of FAM3D [182]. Even though direct effects on the AKT signaling cascade in the liver, as observed with FAM3A or FAM3C, this was not detected upon FAM3D overexpression [183,184]. Based on our current knowledge, we hypothesize that the reduced lipid deposition and the ameliorated steatosis were instead secondary effects resulting from the insulin sensitization that occurs upon FAM3D overexpression. Obesity, T2D, and the development of NAFLD are tightly connected. When there is an excess of nutrients, the lipid metabolism of the liver is overwhelmed and the liver starts to accumulate triglycerides instead of secreting them via very low-density lipoproteins (VLDL) [269]. Further, in cases of insulin resistance, the lipolysis in the adipose tissue is no longer restricted and an increased flux of FFA from the adipose tissue to the liver can be observed [269,270]. Additionally, the de novo lipogenesis machinery of the liver can contribute to the increased lipid deposition in the liver. This causes lipotoxicity and inflammation, and may ultimately lead to fibrosis in the liver [271]. This inflammation is further boosted by low-grade inflammation present in insulin resistant adipose tissue [272]. Conversely, the insulin resistance in the liver drives the development of T2D due to increased gluconeogenesis [273]. Thus, once the metabolic balance is lost, the dwindling spiral of metabolic disease is very difficult to stop.

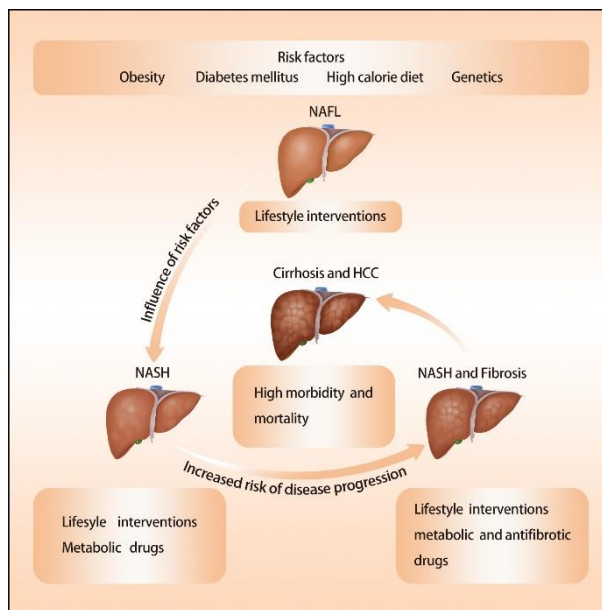


Figure 2: The progression of NAFLD to NASH and cirrhosis. Taken from Lv et al., 2020 [274]

So far, no pharmacological treatment for NAFLD is licensed, and the current standard therapy focuses mainly on weight loss and lifestyle modifications. Due to the tight connection between T2D and NAFLD, many T2D medications are currently evaluated for their potential to treat NAFLD [275,276]. Multiple clinical trials provide evidence that the GLP-1 receptor agonist does improve NAFLD. However, to evaluate the effect on NASH, fibrosis, or even cirrhosis, further randomized control trials are needed [274]. Similarly, DPP4 inhibitors, TZDs, and SGLT2 inhibitors are currently under evaluation for the treatment of NAFLD, all displaying promising results [277–279]. In the case of Metformin, the standard first line T2D therapy, results from rodent studies proved encouraging. However, the human data regarding the effect of Metformin on NAFLD are not completely convincing [280]. Nonetheless, the rising numbers of NAFLD patients calls for the development of a pharmaceutical treatment. Thus, it will be a mere matter of time until existing T2D drugs will also be approved for NAFLD therapy. In summary, the treatment of NAFLD is an urgent topic. Hence, the amelioration of hepatic steatosis upon FAM3D overexpression may increase the interest of pharmaceutical companies to further investigate the function of FAM3D.

In conclusion, the road from FAM3D to the patient is still a very long one. Many more aspects about the molecular function, the receptor, the physiological secretion, and the degradation pattern need to be investigated to enhance the understanding of the entire function of FAM3D. Translating these investigations from rodent models into humans will eventually pose another hurdle down the road. Nevertheless, the initial characterization of the metabolic function of FAM3D was highly promising, and we believe therefore that it will be worth the effort to continue the studies on FAM3D.

4.3 Summary

-Gut Feelings and Love Handles-

The adipose tissue and the gut as well as their different perspectives on our body's metabolism were covered in the context of this thesis. Chapter 1 gave an introduction to the adipose tissue and the gut in the context of the metabolic diseases obesity and T2D. In chapter 2, the astonishing versatility of the adipose tissue was investigated with the use of a novel approach where adipocytes were unbiasedly quantified based on a genomic label. Through this, the number of adipocytes was determined in response to various environmental influences. This quantification shed light on the numbers as well as the kinetics of brown and brite/beige adipose tissue. This special subset of adipocytes poses promising features for the fight against globally rising metabolic diseases. Therefore, we could contribute to the characterization of this subset of adipocytes by providing a quantitative insight into the brown/brite/beige adipose tissue remodeling dynamics. Chapter 3 of this thesis focused on the metabolic function of the gut-secreted protein FAM3D. The overexpression of FAM3D resulted in an improvement of the glucose metabolism as well as of the amelioration hepatic symptoms associated with NAFLD. On a physiological level, FAM3D displayed great potential for the treatment of the metabolic diseases T2D or NAFLD. While the mediating molecular mechanism currently remains elusive to us, further studies will hopefully elucidate this part. This thesis demonstrates that the metabolism in our body is manifold and that metabolic diseases can be tackled by various organs and mechanisms. The adipose tissue and the gut are two major players in the game of metabolic diseases, but we should appreciate that one player alone cannot win the game. Only if the whole team works together, hand in hand, we can win the fight against the deteriorating spiral of unhealthy metabolism.

CHAPTER 5

Further publications

Inhibition of Mevalonate Pathway Prevents Adipocyte Browning in Mice and Men by Affecting Protein Prenylation

Miroslav Balaz, Anton S. Becker, Lucia Balazova, Leon Straub, Julian Müller, Gani Gashi, Claudia Irene Maushart, Wenfei Sun, Hua Dong, Caroline Moser, Carla Horvath, Vissarion Efthymiou, Yael Rachamin, Salvatore Modica, Caroline Zellweger, Sara Bacanovic, Patrik Stefanicka, Lukas Varga, Barbara Ukropcova, Milan Profant, Lennart Opitz, Ez-Zoubir Amri, Murali K. Akula, Martin Bergo, Jozef Ukropec, Christian Falk, Nicola Zamboni, Matthias Johannes Betz, Irene A. Burger, and Christian Wolfrum

Published in Cell Metabolism, 2019

Contribution:

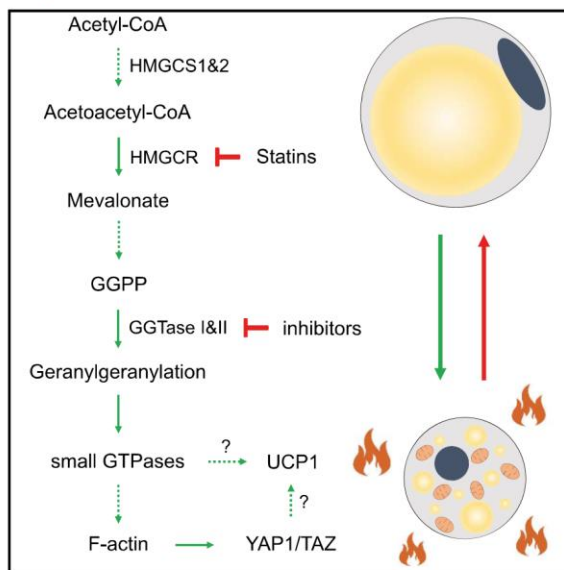
Caroline Moser performed the experiment to quantify the number of Ucp1+ cells *in vivo* upon statin treatment

This article is a reprint of the original published article with kind permission of the publisher, Elsevier GmbH. Supplementary material is available online under:
<https://doi.org/10.1016/j.cmet.2018.11.017>

Cell Metabolism

Inhibition of Mevalonate Pathway Prevents Adipocyte Browning in Mice and Men by Affecting Protein Prenylation

Graphical Abstract



Authors

Miroslav Balaz, Anton S. Becker,
Lucia Balazova, ...,
Matthias Johannes Betz,
Irene A. Burger, Christian Wolfrum

Correspondence

matthias.betz@usb.ch (M.J.B.),
irene.burger@usz.ch (I.A.B.),
christian-wolfrum@ethz.ch (C.W.)

In Brief

Through genetic and pharmacological *in vivo* and *in vitro* approaches, Balaz et al. show that the mevalonate pathway is important for adipocyte browning. The importance of this pathway is supported by a retrospective clinical study and a small volunteer trial with fluvastatin. The authors identify geranylgeranyl pyrophosphate as the key mevalonate intermediate driving adipocyte browning.

Highlights

- The mevalonate pathway is important for adipose tissue browning in mouse and human
- Statin use is inversely correlated with brown fat activity in humans
- Geranylgeranylation of small GTP-binding proteins promotes adipocyte browning
- Small GTP-binding proteins regulate F-actin formation and YAP1/TAZ stability



Balaz et al., 2019, Cell Metabolism 29, 901–916
April 2, 2019 © 2018 Elsevier Inc.
<https://doi.org/10.1016/j.cmet.2018.11.017>

CellPress

Inhibition of Mevalonate Pathway Prevents Adipocyte Browning in Mice and Men by Affecting Protein Prenylation

Miroslav Balaz,^{1,14} Anton S. Becker,^{1,2,3,14} Lucia Balazova,¹ Leon Straub,¹ Julian Müller,³ Gani Gashi,⁴ Claudia Irene Maushart,⁴ Wenfei Sun,¹ Hua Dong,¹ Caroline Moser,¹ Carla Horvath,¹ Vissarion Efthymiou,¹ Yael Rachamin,¹ Salvatore Modica,¹ Caroline Zellweger,³ Sara Bacanovic,³ Patrik Stefanicka,⁵ Lukas Varga,^{5,6} Barbara Ukropcova,^{6,7} Milan Profant,⁵ Lennart Opitz,⁸ Ez-Zoubir Amri,⁹ Murali K. Akula,¹⁰ Martin Bergo,^{10,11} Jozef Ukropec,⁶ Christian Falk,¹² Nicola Zamboni,¹³ Matthias Johannes Betz,^{4,*} Irene A. Burger,^{3,*} and Christian Wolfrum^{1,15,*}

¹Institute of Food, Nutrition, and Health, ETH Zürich, Schorenstrasse 16, Schwerzenbach 8603, Switzerland

²Institute of Diagnostic and Interventional Radiology, University Hospital of Zürich, Zürich, Switzerland

³Department of Nuclear Medicine, University Hospital of Zürich, Rämistrasse 100, Zürich 8091, Switzerland

⁴Department of Endocrinology, Diabetology, and Metabolism, University Hospital of Basel, Petersgraben 4, Basel 4031, Switzerland

⁵Department of Otorhinolaryngology – Head and Neck Surgery, Faculty of Medicine and University Hospital, Comenius University, Bratislava, Slovakia

⁶Institute of Experimental Endocrinology, Biomedical Research Center at the Slovak Academy of Sciences, Bratislava, Slovakia

⁷Institute of Pathological Physiology, Faculty of Medicine, Comenius University, Bratislava, Slovakia

⁸Functional Genomics Center Zürich, ETH Zürich/University of Zürich, Zürich, Switzerland

⁹Université Côte d'Azur, CNRS, Inserm, iBV, Nice, France

¹⁰Sahlgrenska Cancer Center, Department of Medicine, University of Gothenburg, Gothenburg, Sweden

¹¹Department of Biosciences and Nutrition, Karolinska Institute, Huddinge, Sweden

¹²Department of Medical Data Management, University Hospital of Zürich, Zürich, Switzerland

¹³Department of Biology, Institute of Molecular Systems Biology, ETH Zürich, Zürich, Switzerland

¹⁴These authors contributed equally

¹⁵Lead Contact

*Correspondence: matthias.betz@usb.ch (M.J.B.), irene.burger@usz.ch (I.A.B.), christian-wolfrum@ethz.ch (C.W.)

<https://doi.org/10.1016/j.cmet.2018.11.017>

SUMMARY

Recent research focusing on brown adipose tissue (BAT) function emphasizes its importance in systemic metabolic homeostasis. We show here that genetic and pharmacological inhibition of the mevalonate pathway leads to reduced human and mouse brown adipocyte function *in vitro* and impaired adipose tissue browning *in vivo*. A retrospective analysis of a large patient cohort suggests an inverse correlation between statin use and active BAT in humans, while we show in a prospective clinical trial that fluvastatin reduces thermogenic gene expression in human BAT. We identify geranylgeranyl pyrophosphate as the key mevalonate pathway intermediate driving adipocyte browning *in vitro* and *in vivo*, whose effects are mediated by geranylgeranyltransferases (GGTases), enzymes catalyzing geranylgeranylation of small GTP-binding proteins, thereby regulating YAP1/TAZ signaling through F-actin modulation. Conversely, adipocyte-specific ablation of GGTase I leads to impaired adipocyte browning, reduced energy expenditure, and glucose intolerance under obesogenic conditions, highlighting the importance of this pathway in modu-

lating brown adipocyte functionality and systemic metabolism.

INTRODUCTION

Brown adipose tissue (BAT) is considered the main thermogenic organ in newborn mammals and hibernating rodents due to its capacity to dissipate chemical energy in the form of heat (Cannon and Nedergaard, 2004). Apart from the classical interscapular BAT (iBAT), brown adipocytes are also present within specific white adipose tissues (WATs) (Frontini et al., 2013). These cells, morphologically resembling brown adipocytes, are referred to as brite or beige adipocytes, and their formation can be induced by certain environmental, hormonal, and pharmacological stimuli (Frontini et al., 2013; Rosenwald et al., 2013; Shi and Collins, 2017). Under specific conditions, physiologically relevant amounts of BAT can be found also in adult humans (Cypess et al., 2009; Nedergaard et al., 2007; van Marken Lichtenbelt et al., 2009). BAT can be activated in healthy lean subjects and its activity can be measured by indirect calorimetry or by [¹⁸F]fluorodeoxyglucose (FDG)-positron emission tomography (PET)/computed tomography (CT) (Cypess et al., 2015). BAT is dependent on glucose and free fatty acids (FFAs) as substrates for thermogenesis, suggesting a potential role for BAT in systemic glucose and lipid homeostasis (Bartelt et al., 2011; Chondronikola et al., 2014; Orava et al., 2011; Ouellet et al.,



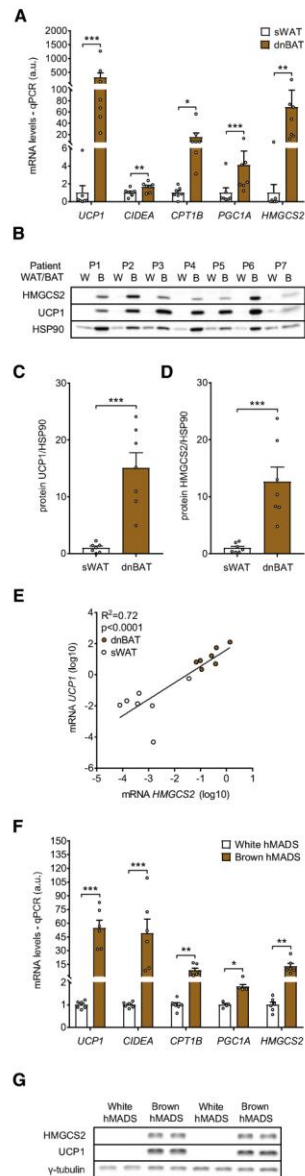


Figure 1. HMGCS2 Is Enriched in Human BAT
(A) Expression of brown adipocyte markers in human deep neck BAT (dnBAT) and subcutaneous WAT (sWAT) biopsies (n = 7).

(2012). The relevance of human BAT in energy homeostasis is further supported by the association of its presence and activity with higher energy expenditure, lower adiposity, and reduced risk of insulin resistance (Chondronikola et al., 2014; Cypess et al., 2015; Iwen et al., 2017). BAT activation is therefore considered a promising strategy to increase energy expenditure and improve metabolic control. Unfortunately, the metabolic response of BAT to cold is blunted in obesity, and long-term administration of β_3 -adrenoreceptor (β_3 -AR) agonists might be associated with adverse side effects (Cypess et al., 2015; Orava et al., 2013). Hence, the identification of mechanisms driving brown adipocyte development and activity has been the focus of recent research. Here we show that protein geranylgeranylation plays an important role in the regulation of adipocyte browning, by modulating the activity of small GTPases. Our mouse and cell culture data are complemented by a retrospective clinical study and a small prospective trial supporting the physiological relevance of this regulation in humans.

RESULTS

HMGCS2 Is Enriched in Human BAT

To identify mechanisms regulating brown adipocyte function, we analyzed the transcriptome of human deep neck BAT and subcutaneous WAT biopsies. As expected, we found that uncoupling protein 1 (*UCP1*), along with other brown adipocyte marker genes, is highly enriched in BAT compared with WAT (Figures 1A and S1A). *UCP1* was also enriched in human BAT at the protein level (Figures 1B and 1C). Interestingly, hydroxymethylglutaryl-coenzyme A (HMG-CoA) synthase 2 (*HMGCS2*) was one of the most highly enriched transcripts in human BAT (Figures 1A and S1A), in line with protein levels (Figures 1B and 1D). Furthermore, *HMGCS2* strongly correlated with *UCP1* expression (Figure 1E). These data could be confirmed in brown human multipotent adipose-derived stem (hMADS) cells, which exhibit an enrichment in *HMGCS2*, on both mRNA and protein levels (Figures 1F and 1G), along with an increase in expression of brown adipocyte marker genes (Figures 1F and S1B). Based on our data, we hypothesized that *HMGCS2* might contribute to cellular HMG-CoA levels, which in turn could alter BAT activity.

Inhibition of HMG-CoA Synthesis Suppresses Brown Adipocyte Thermogenic Function

To study the role of HMG-CoA in the regulation of brown adipocyte function, we silenced both HMG-CoA synthase isoforms (Figure S1C). Knockdown of mitochondrial *Hmgcs2* in murine immortalized brown adipocytes (iBAs) and hMADS

(B–D) (B) Representative western blot (WB) and quantification of (C) *UCP1* and (D) *HMGCS2* in deep neck BAT and subcutaneous WAT (n = 7).

(E) Correlation between *UCP1* and *HMGCS2* mRNA in deep neck BAT and subcutaneous WAT (n = 7).

(F) Expression of brown adipocyte markers in hMADS cells (n = 4–6).

(G) Representative WB showing *UCP1* and *HMGCS2* levels in hMADS cells (n = 4).

Statistical significance was calculated using Student's t test. For association of *HMGCS2* with *UCP1*, Pearson's correlation coefficient was calculated. Statistical differences are indicated as *p < 0.05, **p < 0.01, ***p < 0.001.



cells led to a marked reduction of UCP1 mRNA and protein levels (Figures 2A, 2B, S2A, and S2B), along with a significant reduction of basal uncoupled and stimulated uncoupled mitochondrial respiration (Figures 2C and 2D). A similar inhibitory effect on UCP1 levels and uncoupled mitochondrial respiration was achieved by knockdown of the cytosolic *HMGCS1* (Figures 2A–2D, S2A, and S2B). Our results indicate that both HMG-CoA synthase isoforms are important for proper thermogenic brown adipocyte function. Interestingly, ketone body levels were not changed intracellularly nor in the supernatant between brown and white hMADS cells, and neither did we observe any effect of *HMGCS2* knockdown (Figure S2C), suggesting that the regulation of UCP1 upon knockdown of *HMGCS2* is independent of ketone body synthesis, but rather dependent on mevalonate. This is supported by the finding that mevalonate levels are higher in iBAT than in inguinal WAT (iWAT) of C57BL/6 mice (Figure S2D), suggesting the importance of the mevalonate pathway in brown adipocyte functionality.

Statins Inhibit Thermogenic Function of Adipocytes *In Vitro*

To confirm the significance of mevalonate in brown adipocyte physiology, we inhibited the mevalonate pathway using statins. At 1 μ M concentration, only simvastatin and fluvastatin reduced UCP1 levels in iBAs (Figure 2E). However, all tested statins lowered UCP1 levels at 10 μ M concentration (Figure 2F). Simvastatin showed an inhibitory effect already after 24 hr (Figure S2E). Unlike other statins, cerivastatin caused cell toxicity already at 1 μ M concentration (Figure S2F). Interestingly, all tested statins inhibited preadipocyte proliferation without affecting brown adipocyte maturation (Figures S2G and S2H). Based on these results, we decided to use simvastatin in subsequent *in vitro* experiments, as it was shown to be more potent in inhibiting the mevalonate pathway in extrahepatic tissues than other statins (Olsson et al., 2002) and shows no toxic effect on mature adipocytes. Simvastatin dose dependently reduced UCP1 levels, as well as isoproterenol-stimulated uncoupled respiration in iBAs (Figures 2G, 2H, and S2I), which could be at least partially explained by reduced *Ucp1* promoter activity (Figure S2J). Importantly, also in hMADS cells, cerivastatin, simvastatin, and fluvastatin were more potent in reducing UCP1 levels than atorvastatin or rosuvastatin, without any signs of toxicity (Figures 2I and 2J). Interestingly, when mature white hMADS cells were exposed to rosiglitazone, to elicit the development of a brown phenotype (Elabd et al., 2009) in combination with simvastatin, a strong dose-dependent inhibitory effect of simvastatin on UCP1 was observed (Figures 2K and 2L). In addition, all tested statins inhibited phosphorylation of hormone-sensitive lipase (HSL) (Figures 2K and S2K). Altogether, these data indicate that the mevalonate pathway is important for the thermogenic function of brown and the browning of white adipocytes, *in vitro*.

Statins Inhibit iWAT Browning *In Vivo*

Next, we aimed to prove the importance of the mevalonate pathway in BAT function *in vivo*. Therefore, simvastatin and fluvastatin were administered to 12-week-old C57BL/6 mice by oral gavage at a dose of 10 mg/kg, which is equivalent to the

dose used to treat hypercholesterolemia in patients (Nair and Jacob, 2016). Mice were exposed to statins for 2 days at 22°C to achieve inhibition of the mevalonate pathway, followed by 4 days of cold exposure, to induce thermogenesis (Figure 3A). Only fluvastatin reduced mevalonate levels in iBAT. However, both simvastatin and fluvastatin suppressed mevalonate production in iWAT (Figure S3A). Furthermore, geranyl pyrophosphate levels were decreased by both statins in iBAT and a trend toward reduction was observed also in iWAT, indicating that the mevalonate pathway was efficiently inhibited in both tissues (Figure S3B). We also quantified hydroxymethylglutaryl-coenzyme A reductase (HMGCR); however, statin administration had no effect on HMGCR expression in neither iBAT nor iWAT (Figures S3C–S3E). Similarly, HMGCR levels were not altered by statin treatment in hMADS cells, indicating that brown adipocytes do not respond to statins by HMGCR upregulation (Figure S3F). Interestingly, both statins inhibited browning of iWAT, without affecting UCP1 levels in iBAT (Figures 3B–3D). The inhibitory effect of statins on adipocyte browning was associated with higher iWAT and epididymal white adipose tissue (eWAT), but not iBAT mass (Figures 3E, 3F, and S3G). Fluvastatin had no effect on whole-body energy expenditure, metabolic rate, or food or water intake (Figures S3H–S3M). Based on these observations, we conclude that statins inhibit iWAT browning either directly by acting in mature adipocytes and/or precursor cells, or indirectly by affecting sympathetic nervous system (SNS) activity. Since brown adipocytes are activated already at room temperature (Kalinovich et al., 2017), we investigated the effect of statins in mice housed at thermoneutrality, to study whether the inhibitory effect of statins is mediated by reduced activity of the SNS. Therefore, 14-week-old C57BL/6 mice housed at 30°C were pretreated with fluvastatin for 2 days at a dose of 10 mg/kg, followed by 2 days of fluvastatin gavage combined with administration of CL-316.243 (0.1 mg/kg), a selective β_3 -AR agonist to induce non-shivering thermogenesis (Figure 3G). Also in this experiment, fluvastatin reduced UCP1 levels in iWAT, despite a significant increase in CREB phosphorylation (Figures 3H and 3I). Similarly, brown adipocyte marker genes were significantly reduced in iWAT (Figure 3J), indicating suppression of adipocyte browning by fluvastatin. Brown adipocyte markers, UCP1 levels, and CREB phosphorylation were not affected by fluvastatin administration in iBAT (Figures S4A–S4C), suggesting that maximal activation of BAT might be able to overcome the inhibitory effect of statins. Fluvastatin-treated mice showed 2.1-fold higher iWAT mass (Figure 3K), indicating reduced lipid mobilization in response to the β_3 -AR agonist. Importantly, by combining thermoneutrality with CL-316.243, we could show that the inhibitory effect of statins on iWAT browning is not mediated by reduced SNS activity, but rather is due to cell-autonomous effects.

Next, we employed *Ucp1*-CreERT2 \times *LoxP*-Red mice, in which the number of recombined *LoxP*-Red sites reflects the amount of UCP1⁺ cells within a given depot. Using this model (Figure S4D), we could show that fluvastatin treatment significantly reduced the number of UCP1⁺ cells in iWAT, but not in iBAT (Figure 3L). Taken together, our results indicate that inhibition of the mevalonate pathway prevents adipocyte browning in mice *in vivo*.

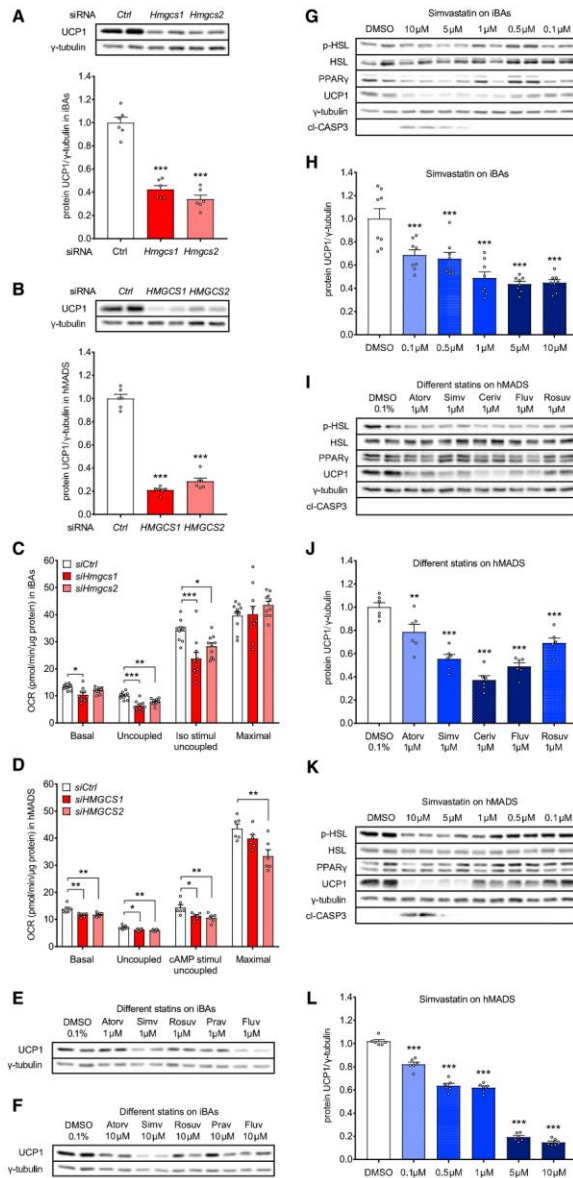


Figure 2. Inhibition of Mevalonate Pathway Suppresses Brown Adipocyte Thermogenic Function *In Vitro*

(A–D) Effect of *Hmgcs1* and *Hmgcs2* knockdown on UCP1 in (A) iBAs and (B) hMADS cells (n = 6). Effect of *Hmgcs1* and *Hmgcs2* knockdown on mitochondrial respiration in (C) iBAs (n = 10) and (D) hMADS cells (n = 6). (E and F) Representative western blot (WB) showing effect of statin treatment (48 hr) on UCP1 in iBAs at (E) 1 μ M and (F) 10 μ M concentration (2 repeats). (G and H) (G) Representative WB and (H) UCP1 quantification in iBAs treated (48 hr) with simvastatin (n = 8). (I and J) (I) Representative WB and (J) UCP1 quantification in hMADS cells treated (48 hr) with different statins (n = 6). (K and L) (K) Representative WB and (L) UCP1 quantification in hMADS cells treated (96 hr) with simvastatin (n = 6). Results are reported as mean \pm SEM. Statistical significance was calculated using ANOVA. Statistical differences are indicated as *p < 0.05, **p < 0.01, ***p < 0.001.

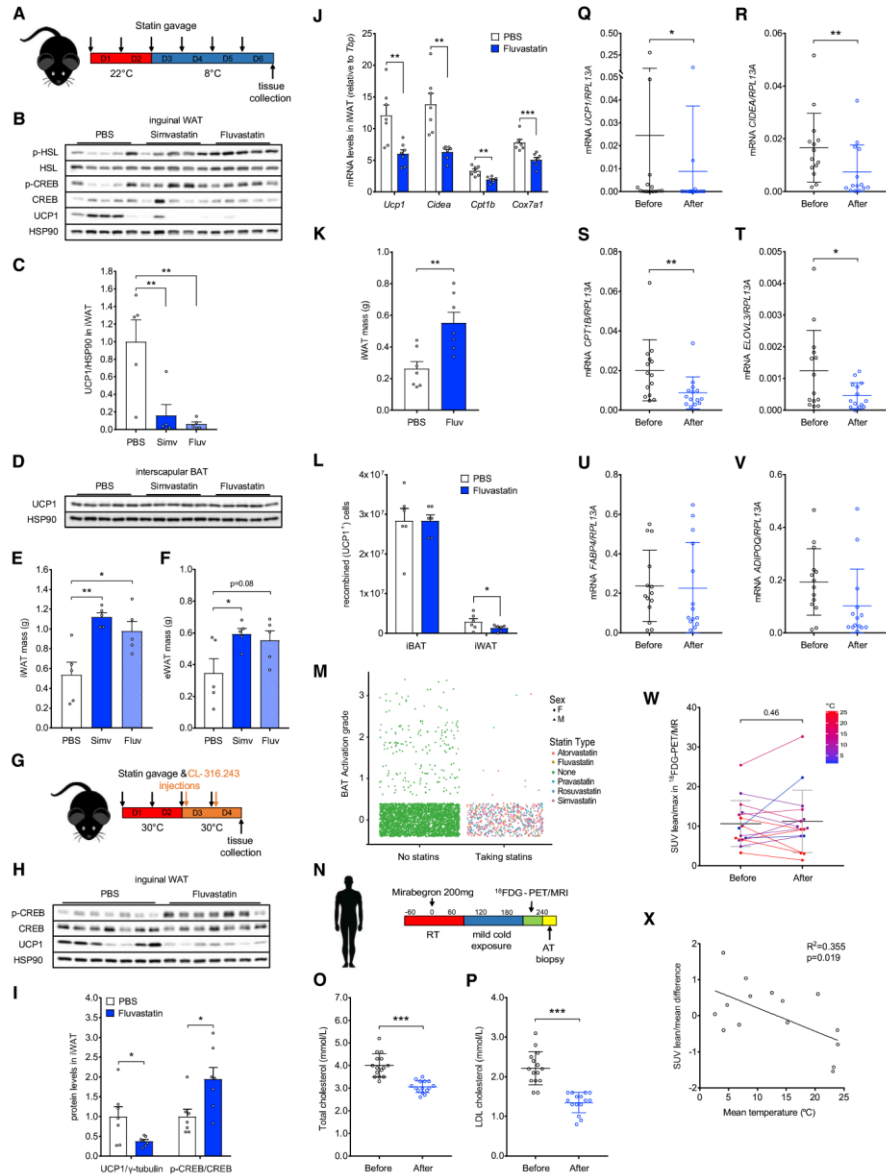


Figure 3. Statins Inhibit Adipose Tissue Browning in Mice and Men

(A) Schematic illustration of the *in vivo* statin treatment experiment.

(B–F) (B) Representative western blot (WB) and (C) UCP1 quantification in IWAT and (D) iBAT (n = 5). Effect of statins on (E) IWAT and (F) eWAT mass (n = 5).

(legend continued on next page)

Cell Metabolism 29, 901–916, April 2, 2019 905



Statin Use in Patients Is Inversely Associated with Active BAT

To investigate the effect of statins on BAT activity in humans, we conducted a retrospective study of all patients undergoing FDG-PET/CT at University Hospital of Zürich between November 2009 and February 2015. From a total of 8,409 patients, we identified 2,789 patients who had been hospitalized within 12 months prior to the PET/CT examination, for which we quantified BAT glucose uptake and analyzed statin use during the preceding hospitalization. From patients with multiple examinations ($n = 738$), the one with the strongest BAT activation was selected. Interestingly, we observed a significantly higher statin use among patients without active BAT (2,148 not on statins, 510 taking statins [19.2%]) compared with those with activated BAT (124 not on statins, 7 taking statins [5.3%]) (Figure 3M). Using a stepwise general linear regression with forward and backward feature selection, we found that statin use remained significantly associated with BAT inactivity after accounting for age, sex, and BMI (Table S1).

Statins Reduce Thermogenic Gene Expression in Human BAT

Next, we analyzed the effect of statins on activation of BAT in a prospective clinical trial. We performed the clinical trial with fluvastatin, which was more potent in inhibition of iWAT browning in our mouse experiments and shows higher systemic bioavailability and less interaction potential than other statins (Gazzerro et al., 2012). Furthermore, fluvastatin was the only statin in our retrospective study for which we did not identify any patient with active BAT (Figure 3M). We recruited 16 healthy young male lean volunteers with detectable BAT under stimulated conditions (Figure 3N). All participants underwent FDG-PET/MRI to confirm presence of active BAT, both before and after 14 days of fluvastatin treatment (80 mg/day). Two participants were excluded from the analysis due to non-compliance or failure of tissue sampling. In the 14 analyzed subjects, we could see a significant drop in total cholesterol and low-density lipoprotein (LDL) levels (Figures 3O and 3P). We could detect a significant reduction in expression of brown adipocyte markers *UCP1*, *CIDEA*, *CPT1B*, and *ELOVL3* (Figures 3Q–3T; Table S2), whereas general adipocyte markers such as *FABP4* and *ADIPOQ* were not changed by short-term fluvastatin therapy (Figures 3U and 3V). We did not detect any significant difference in expression of inflammatory markers (Figures S4E–S4G), with the exception of *TNFA*, which was slightly increased (Figure S4H). Expression of the glucose transporter *GLUT1* was not changed, whereas insulin-responsive *GLUT4* was significantly reduced following short-

term fluvastatin treatment (Figures S4I and S4J). The inhibitory effect of statins on *GLUT4* expression has already been described in different cell types and tissues (Jiang et al., 2016; Li et al., 2016; Nakata et al., 2006). Short-term fluvastatin therapy had no effect on FDG uptake in the supraclavicular BAT depot (Figure 3W). Since the clinical trial spanned over 8 months, we included outside temperature, a known factor determining BAT activity, in the analysis (Cypess et al., 2009; Senn et al., 2018). Analysis of the data in relation to the outside temperature revealed a negative correlation between average temperature during the intervention and statin-induced changes in the average standardized uptake value normalized to lean body mass (SUVlean/mean) (Figure 3X), indicating that the effect of short-term fluvastatin therapy on glucose uptake might be temperature dependent or significantly smaller than the short-term effect of temperature alone. Furthermore, these data indicate that statins alter thermogenic gene expression in human BAT.

The Effects of Statins on UCP1 Are Mediated through Protein Prenylation

Next, we tested whether the negative effect of statins on UCP1 can be rescued by one of the downstream mevalonate intermediates. Interestingly, we could rescue the inhibitory effect of statin on *Ucp1* expression with mevalonate, farnesyl pyrophosphate (FPP), and geranylgeranyl pyrophosphate (GGPP), but not with squalene or coenzyme Q9 (Figure 4A). The rescue experiment was performed in the presence of exogenous cholesterol (10% fetal bovine serum [FBS]), suggesting that the effect of statins is not mediated by inhibition of cholesterol synthesis. The inhibitory effect of simvastatin on UCP1 levels could be observed also in FBS-free medium (Figures 2I–2L and S4K). In addition, the inhibitory effect of simvastatin could be completely rescued by geranylgeraniol (GGOH), the donor of a geranylgeranyl group (Figures 4B and 4C), but not by farnesol (FOH; Figures 4B and 4C), the donor of a farnesyl group, which unlike FPP does not serve as a direct precursor for GGPP synthesis. Similarly, we could also prevent the inhibitory effect of *Hmgcs1* knockdown on UCP1 levels in iBAs by GGPP (Figures S4L and S4M). Our data indicate that inhibition of the mevalonate pathway impairs UCP1 expression by blocking synthesis of FPP and GGPP, the substrates for protein prenylation. The inhibitory effect of statins on UCP1 expression and uncoupled mitochondrial respiration could be mimicked by GGTI-298 (Figures 4D–4F and S4N), a specific inhibitor of geranylgeranyltransferase I (GGTase I; Figure S1C), as well as by knockdown of the genes encoding the PGGT1B subunit of GGTase I and RABGGTB subunit of GGTase

(G) Schematic illustration of the *in vivo* fluvastatin treatment experiment.

(H and I) (H) Representative WB and (I) quantification of UCP1 and CREB phosphorylation (Ser133) in iWAT ($n = 7$).

(J and K) Effect of fluvastatin on (J) expression of brown adipocyte markers in iWAT and (K) iWAT mass ($n = 7$).

(L) Quantification of UCP1⁺ cells in iBAT and iWAT of *Ucp1*-CreERT2 × *LoxP*-Red mice treated with fluvastatin ($n = 6$).

(M) Retrospective analysis of BAT activation grade in 2,789 patients shows a significantly higher number (chi-square test, $p = 0.0001$) of statin takers among patients without active BAT (19.2%) compared with patients with activated BAT (5.3%).

(N–W) (N) Schematic illustration of the clinical fluvastatin trial. Effect of fluvastatin therapy on (O) total cholesterol and (P) LDL levels ($n = 15$). Effect of short-term fluvastatin therapy on (Q) *UCP1*, (R) *CIDEA*, (S) *CPT1B*, (T) *ELOVL3*, (U) *FABP4*, and (V) *ADIPOQ* expression ($n = 14$) and (W) FDG uptake in supraclavicular BAT ($n = 15$). Different colors indicate average temperature during the fluvastatin intervention.

(X) Association of mean temperature during the fluvastatin intervention with change in SUVlean/mean in FDG-PET/magnetic resonance imaging ($n = 15$). Results are reported as mean ± SEM for mouse experiments and mean ± SD for the clinical study. Statistical significance was calculated using ANOVA (B–F), Student's *t* test (H–P), and non-parametric Wilcoxon test (Q–W). Chi-square test was performed with R (m). For association of temperature and SUVlean/mean change, Pearson's correlation coefficient was calculated. Statistical differences are indicated as * $p < 0.05$, ** $p < 0.01$, *** $p < 0.001$.

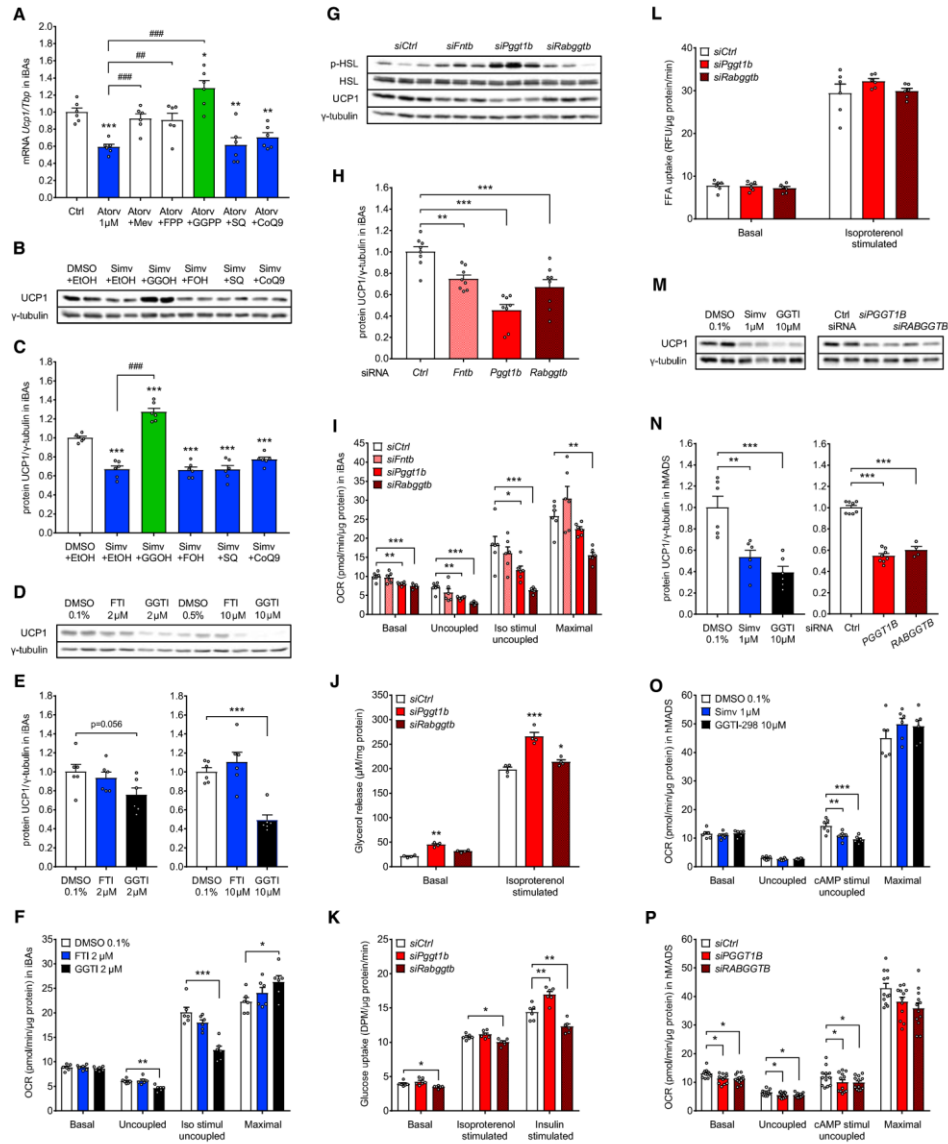


Figure 4. The Inhibitory Effect of Statins Can Be Rescued by GGPP

(A) The inhibitory effect of atorvastatin treatment (48 hr) on *Ucp1* expression in IBAs can be rescued by mevalonate (Mev; 500 μ M), farnesyl pyrophosphate (FPP; 2 μ M), and geranylgeranyl pyrophosphate (GGPP; 2 μ M), but not by squalene (SQ; 10 μ M) or coenzyme Q9 (CoQ9; 10 μ M) (n = 6). (B and C) (B) Representative WB and (C) quantification of the inhibitory effect of 1 μ M simvastatin on UCP1 in IBAs, which can be rescued by GGOH (10 μ M), but not by FOH (10 μ M), SQ (10 μ M), or CoQ9 (10 μ M) (n = 6).

(legend continued on next page)
Cell Metabolism 29, 901–916, April 2, 2019 907



II (Figures 4G–4I and S4O) in iBAs. In contrast, the farnesyltransferase (FNTase) inhibitor FTI-277 as well as knockdown of the FNTB subunit of FNTase showed no effect on UCP1 levels and mitochondrial respiration (Figures 4D–4I, S4N, and S4O). Even the toxic effect of cerivastatin on mature iBAs could be prevented by FPP and GGPP (Figure S4P), but not by squalene or CoQ9. Knockdown of *Pggt1b* increased basal and isoproterenol-stimulated lipolysis but showed no effect on basal and isoproterenol-stimulated glucose and FFA uptake in iBAs (Figures 4J–4L). In contrast, knockdown of *Rabggtb* showed no or very little effect on lipolysis and FFA uptake, but significantly reduced glucose uptake in iBAs (Figures 4J–4L). To test the contribution of other mevalonate intermediates, we silenced the expression of key branching enzymes of this pathway. Knockdown of GGPP synthase (GGPS1), the enzyme providing substrate for protein geranylgeranylation, lowered UCP1 levels in iBAs (Figures S4Q and S4R). In contrast, knockdown of genes encoding the key enzymes of cholesterol and ubiquinone synthesis had no effect on UCP1 levels (Figures S4Q and S4R). Importantly, also in hMADS cells, GGTI-298 or knockdown of *PGGT1B* and *RABGGTB* reduced UCP1 levels and cAMP-stimulated uncoupled respiration (Figures 4M–4P). Altogether, our results indicate that the negative effect of mevalonate pathway inhibition on brown adipocyte activity and white adipocyte browning mainly results from depletion of GGPP.

GGTase I Regulates Adipocyte Browning In Vivo

Next, we tested whether the inhibitory effect of statin administration on browning of iWAT *in vivo* is mediated by inhibition of protein geranylgeranylation. Therefore, GGTI-298 was administered to 14-week-old male C57BL/6 mice by intraperitoneal injection at a dose of 1 mg/kg. The mice were kept for 2 days at 22°C to achieve inhibition of GGTase I, followed by acute cold exposure to induce thermogenesis (Figure S5A). GGTI-298 reduced UCP1 levels in iWAT (Figures 5A and 5B), confirming the important role of protein geranylgeranylation in the regulation of adipocyte browning. Next, we generated an inducible adipocyte-specific GGTase I (*Pggt1b^{fl/fl} × Adip-CreERT2*) knockout mouse. Genetic deletion of GGTase I in mature adipocytes had no effect on UCP1 levels in iBAT (Figure S5B). However, UCP1 was significantly reduced in iWAT (Figures 5C and 5D), indicating suppression of adipocyte browning in response to β_3 -AR agonist. Importantly, *Pggt1b* knockdown in mature adipocytes led to a slight decrease in energy expenditure, without affecting substrate preference, food and water intake, or ambulatory activity (Figures 5E and S5C–S5G). Injection of CL-316.243 increased the maximal energy expenditure and abrogated the effect of GGTase I deletion (Figure 5E). In addition, we found that GGTase

I knockout mice, compared with the control littermates, gained more weight and developed impaired glucose tolerance when exposed to high-fat diet (Figures 5F–5H). Importantly, the effect on body weight and glucose tolerance could not be observed at thermoneutrality (Figures S5H–S5J), indicating that it results from reduction of non-shivering thermogenesis. Altogether, our data indicate that GGTase I activity is required for browning of iWAT *in vivo*.

GGPP Promotes Adipocyte Browning

Next, we tested whether protein prenylation can promote brown adipocyte activity. Treatment of mature iBAs with GGOH dose dependently increased UCP1 and mitochondrial respiration (Figures 5I–5K), whereas FOH had no effect on the thermogenic potential of iBAs (Figures S5K–S5M). Importantly, this effect of GGOH could be partially prevented by knockdown of *Pggt1b* and *Rabggtb* (Figures 5L and 5M). Interestingly, knockdown of both GGTases in parallel strongly reduced UCP1 levels in iBAs and completely blocked the stimulatory effect of GGOH (Figures 5N and 5O), indicating that the positive effect of GGOH on brown adipocyte activity is mediated by both GGTases. GGPP significantly increased UCP1 levels also in white hMADS cells (Figures 5P and 5Q), indicating that protein geranylgeranylation promotes adipocyte browning. This effect became apparent already after 48 hr (Figure S5N). Next, we tested the ability of GGOH to stimulate adipocyte browning *in vivo*. We treated 10-week-old C57BL/6 mice with GGOH at a dose of 50 mg/kg for 4 consecutive days. Even though GGOH had no significant effect on energy expenditure and UCP1 levels in iBAT (Figures S5O–S5Q), we observed a 3.5-fold induction of UCP1 in iWAT (Figures 5R and 5S), demonstrating that GGOH promotes adipocyte browning *in vivo*. In addition, the dose-dependent stimulatory effect of GGOH on UCP1 levels in iBAs was observed even upon knockdown of *Lxr α* , *Lxr β* , and *Ppar γ* (Figure S5R), suggesting that the positive effect of GGOH is independent of functional LXR and PPAR γ signaling.

GGPP Is Required for the Prenylation of Small GTPases

To identify proteins undergoing geranylgeranylation, mature iBAs were first pretreated with simvastatin to block endogenous GGPP production and supplemented for 24 hr with regular or the azide form of GGOH. Proteins incorporating the GGOH-azide group were labeled using click chemistry. We detected a band of approximately 20 kDa, corresponding to the size of small GTPases, in both iBAs and hMADS cells (Figures 6A and 6B). Whereas in control cells small GTPases were predominantly located at the plasma membrane, inhibition of the mevalonate pathway led to a reduction of their membrane-bound levels

(D and E) (D) Representative western blot (WB) and (E) UCP1 quantification in iBAs treated for 48 hr with FTI-277 and GGTI-298 (n = 6).

(F) Effect of FTI-277 and GGTI-298 on mitochondrial respiration in iBAs (n = 6).

(G and H) (G) Representative WB and (H) UCP1 quantification in iBAs transfected with small interfering RNA (siRNA) pools targeting *Fntb*, *Pggt1b*, and *Rabggtb* (n = 8).

(I–L) (I) Effect of prenyl-transferase knockdown on mitochondrial respiration in iBAs (n = 6). Effect of GGTase knockdown on (J) glycerol release (n = 4), (K) glucose (n = 6), and (L) free fatty acid uptake (n = 6) in iBAs.

(M and N) (M) Representative WB and (N) UCP1 quantification in hMADS cells treated with simvastatin or GGTI-298 (n = 6) or transfected with the siRNA pools targeting *PGGT1B* (n = 8) or *RABGGTB* (n = 4).

(O and P) (O) Effects of GGTI-298 and simvastatin (n = 6) and (P) *PGGT1B* and *RABGGTB* knockdown on mitochondrial respiration in hMADS cells (n = 12).

Results are reported as mean \pm SEM. Statistical significance was calculated using ANOVA and Student's t test. Statistical differences are indicated as *p < 0.05, **p < 0.01, ***p < 0.001; and ****p < 0.001.

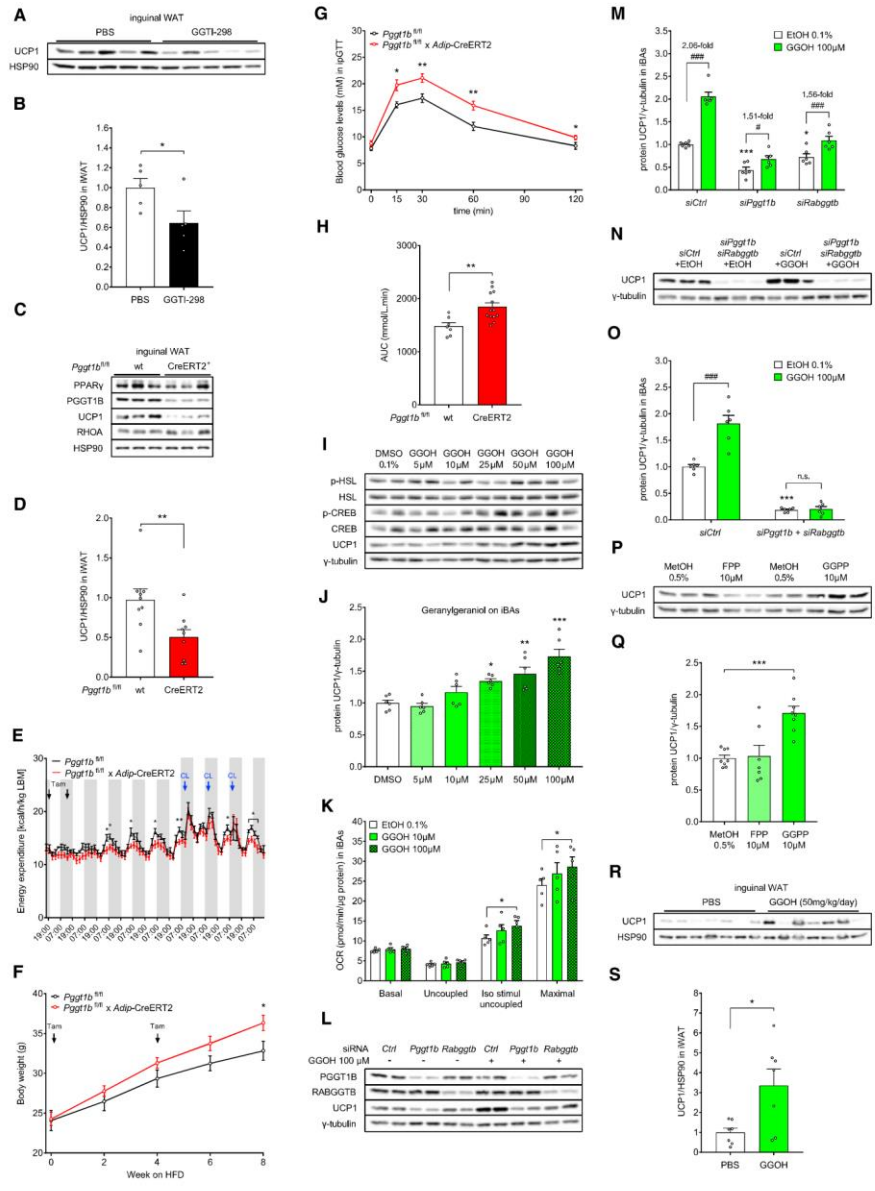


Figure 5. GGOH Promotes Adipocyte Browning In Vitro as well as In Vivo
 (A and B) (A) Representative western blot (WB) and (B) UCP1 quantification in iWAT of C57BL/6 mice treated with PBS and GGTI-298 for 6 days (1 mg/kg; n = 5).
 (C and D) (C) Representative WB and (D) UCP1 quantification in iWAT of control (*Pggt1b*^{fl/fl}) and *Pggt1b*^{fl/fl} x *Adip-CreERT2* mice (n = 9).

(legend continued on next page)
 Cell Metabolism 29, 901–916, April 2, 2019 909



and an increase of their cytosolic levels (Figures 6C–6F), indicating impairment of small GTPase geranylgeranylation. A similar shift in subcellular distribution was achieved by GGTI-298 and fluvastatin (Figures 6C–6F, S6A, and S6B). This effect of statins could be completely prevented by GGOH (Figure S6C). Cellular RHOA levels increased in response to statins, in both iBAs and hMADS cells (Figures 6G–6I and S6D), which could be a compensation for reduced RHO signaling. The effect of statins could be completely rescued by GGOH, but not by FOH, squalene, or CoQ9 (Figure 6G). Interestingly, Gallein, a specific inhibitor of the γ subunit of G protein, had no effect on UCP1 and RHOA levels in iBAs or browning of hMADS cells (Figures S6E–S6G), suggesting that the inhibitory effect of statins most likely does not result from impaired G-protein prenylation. In contrast, inhibition of RHO family members with the aid of RhoGin reduced UCP1 and cAMP-stimulated uncoupled respiration in hMADS cells (Figures 6J–6L), indicating that small GTPases might be important for adipocyte browning.

Small GTP-Binding Proteins Are Important for Adipocyte Browning

Next, we silenced the five most common small GTPases, which are abundantly expressed in adipocytes and require the C-terminal geranylgeranyl group for proper function. Knockdown of *Rhoa*, *Rheb*, *Cdc42*, *Rap1a*, and *Rap1b* affected UCP1 levels in iBAs, as well as UCP1 levels and mitochondrial respiration in hMADS cells (Figures 7A–7E). Moreover, the stimulatory effect of GGOH on UCP1 in iBAs could be partially suppressed by knockdown of individual small GTPases (Figures 7F and 7G). Several small GTP-binding proteins were shown to participate in the regulation of the cellular cytoskeleton. In agreement with our hypothesis, simvastatin dose dependently reduced F-actin levels in iBAs (Figure 7H). Importantly, this effect of simvastatin could also be prevented by GGOH in both cell lines (Figure 7I), indicating that the effect of mevalonate pathway inhibitors might be, at least partially, explained by regulation of the actin cytoskeleton. In many different cell types, it was shown that cellular F-actin levels determine the activity of the transcriptional co-regulators YAP1 and TAZ (Aragona et al., 2013). In line with our previous observations, levels of YAP1 and TAZ in iBAs were strongly reduced following simvastatin treatment (Figures 7J and 7K) and also this effect could be prevented by GGOH, which strongly increased the levels of these transcriptional co-regulators (Figure 7K). Similarly, knockdown of *PGGT1B*, but not *RABGGTB*, significantly reduced levels of YAP1 and TAZ in hMADS cells (Figures 7L and 7M). Furthermore, knockdown of YAP1 and

TAZ led to a significant reduction of UCP1 and uncoupled mitochondrial respiration in hMADS cells (Figures 7N–7P), indicating that these transcriptional co-regulators are important for adipocyte browning. Taken together, our data indicate that small GTPases play an important role in regulation of the thermogenic function of brown adipocytes and white adipocyte browning, and their activity requires the availability of GGPP, the substrate for protein geranylgeranylation.

DISCUSSION

Several studies in recent years have shown that activation of BAT can promote energy expenditure and thus protect from the development of metabolic disease (Hanssen et al., 2015). We and others (Svensson et al., 2011) have identified *HMGCS2* as one of the most highly enriched transcripts in human BAT. *HMGCS2* has been implicated in the synthesis of ketone bodies, and recent work has suggested that ketone bodies can regulate adipocyte browning (Carriere et al., 2014); however, based on our data, it seems that the negative effect of *HMGCS2* knockdown on thermogenic function and adipocyte browning is not mediated through ketone bodies. We therefore speculate that *HMGCS2* might rather contribute to cellular HMG-CoA levels and thereby provide substrate for mevalonate synthesis. Indeed, it was shown that transfection of *Hmgcs2* cDNA was able to restore cholesterol synthesis in *HMGCS1*-deficient CHO-K1 cells (Ortiz et al., 1994). The role of the mevalonate pathway in regulation of BAT function is further supported by studies showing cold-induced increase in *Hmgcs1* expression in both iWAT and iBAT (Forner et al., 2009; Shore et al., 2013). In line with these observations, we could show that mevalonate levels are higher in iBAT than in iWAT. We believe that the flux through the mevalonate pathway is determined mainly by the availability of HMG-CoA, the substrate for mevalonate synthesis.

We show here that inhibition of the mevalonate pathway affects uncoupling in mature human and murine brown adipocytes, and in line with these findings we observed a reduced uncoupled mitochondrial respiration *in vitro*. Pharmacological inhibition of the mevalonate pathway using statins showed no significant effect on UCP1 levels in iBAT, whereas browning of the iWAT was significantly reduced. Statins did not change the energy expenditure, possibly because the maximal capacity for iBAT activation was not affected, while it primarily affected the activity of brite cells in iWAT. This is in line with the recent findings demonstrating that the main thermogenic capacity in mice is present in brown and not in brite adipocytes (Kalinovich et al., 2017), and fits with

(E) Effect of *Pggt1b* deletion on energy expenditure (wild-type $n = 4$; CreERT2 $n = 7$).

(F–H) (F) Body weight gain and (G and H) glucose tolerance in *Pggt1b*^{fl/fl} \times *Adip*-CreERT2 mice ($n = 13$) and control littermates ($n = 7$) after 8 weeks on high-fat diet.

(I–K) (I) Representative WB, (J) UCP1 quantification ($n = 6$), and (K) mitochondrial respiration ($n = 5$) in iBAs treated for 48 hr with GGOH.

(L and M) (L) Representative WB and (M) UCP1 quantification in iBAs transfected with small interfering RNA (siRNA) pools targeting individual geranylgeranyltransferases in combination with GGOH treatment (48 hr; $n = 6$).

(N and O) (N) Representative WB and (O) UCP1 quantification in iBAs transfected with siRNA pools targeting both GGTases in combination with GGOH treatment (48 hr; $n = 6$).

(P and Q) (P) Representative WB and (Q) UCP1 quantification in white hMADS cells treated (96 hr) with FPP, GGPP, or methanol (control; 0.5%) ($n = 8$).

(R and S) (R) Representative WB and (S) UCP1 quantification in iWAT of C57BL/6 mice treated with PBS or GGOH for 4 consecutive days ($n = 7$). Tam, tamoxifen administration.

Results are reported as mean \pm SEM. Statistical significance was calculated using ANOVA and Student's *t* test. Statistical differences are indicated as * $p < 0.05$, ** $p < 0.01$, *** $p < 0.001$; and * $p < 0.05$, *** $p < 0.001$.

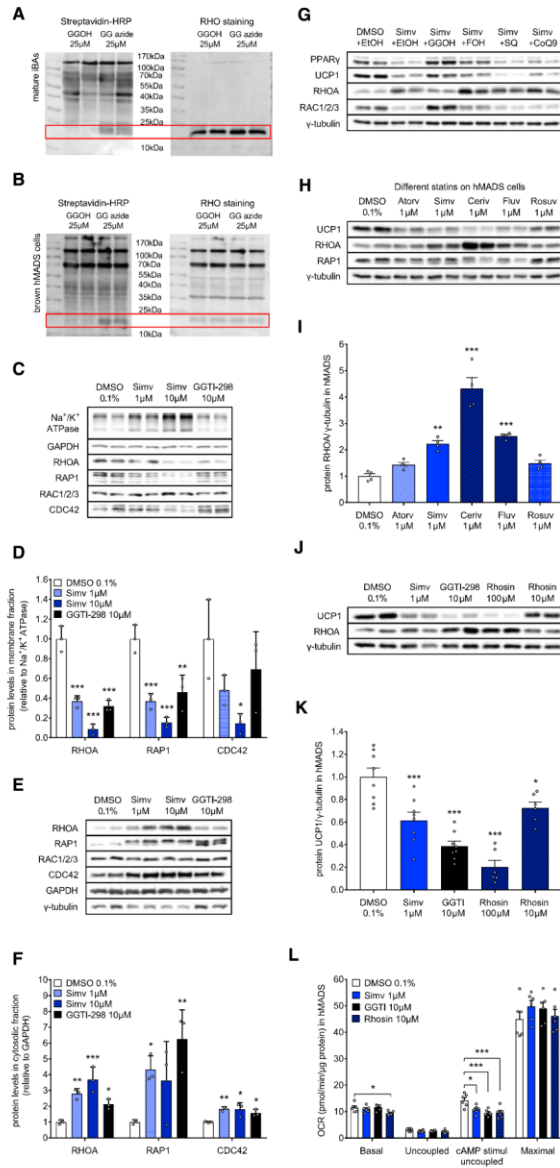


Figure 6. Inhibition of the Mevalonate Pathway Impairs Geranylgeranylation of Small GTP-Binding Proteins

(A–F) Representative western blot (WB) showing incorporation of GGOH azide (A) in iBAs and (B) in hMADS cells (n = 2; 3 repeats). Representative WB and quantification, respectively, of RHOA, RAP1, RAC1/2/3, and CDC42 in (C and D) membrane and (E and F) cytosolic fraction of iBAs treated with simvastatin or GGTI-298 for 48 hr (n = 3; 3 repeats). (G–K) (G) Representative WB showing increase of RHOA in iBAs in response to simvastatin treatment (48 hr), which could be prevented by GGOH (100 μ M), but not by FOH (100 μ M), SQ (10 μ M), or CoQ9 (10 μ M) (2 repeats). Representative WB and quantification, respectively, of UCP1 and RHOA in hMADS cells treated with (H and I) different statins (n = 4) or (J and K) GGTI-298 and Rhosin for 96 hr (n = 6–8). (L) Effect of simvastatin, GGTI-298, and Rhosin treatment (96 hr) on mitochondrial oxygen consumption rate (OCR) in hMADS cells (n = 6). Results are reported as mean \pm SEM. Statistical significance was calculated using ANOVA and Student's t test. Statistical differences are indicated as *p < 0.05, **p < 0.01, ***p < 0.001.

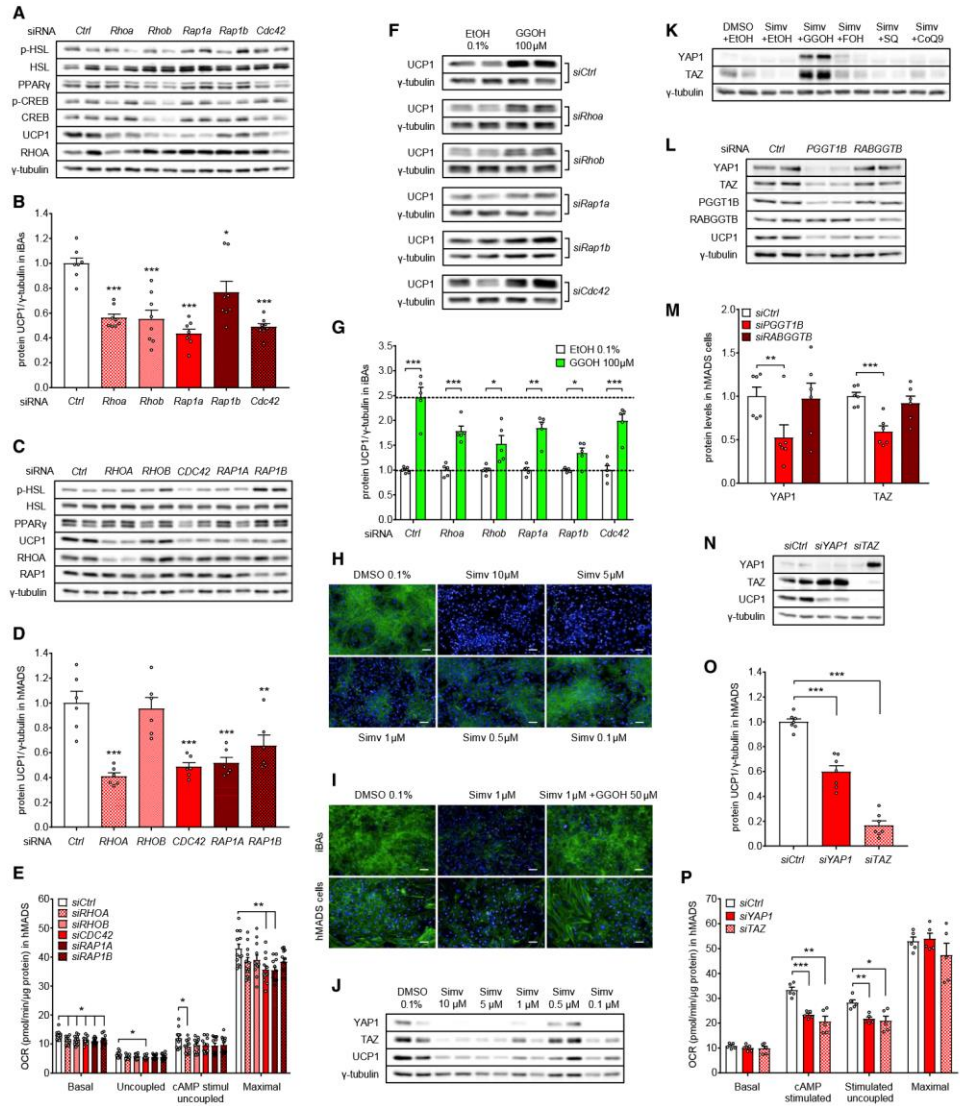


Figure 7. Small GTP-Binding Proteins Are Important for Adipocyte Thermogenic Function
(A and B) (A) Representative western blot (WB) and (B) UCP1 quantification in IBAs transfected with siRNA pools targeting individual small GTPases (n = 7–8). (C and D) (C) Representative WB and (D) UCP1 quantification in hMADS cells transfected with siRNA pools targeting individual small GTPases (n = 6). (E) Effect of individual small GTPase knockdown on mitochondrial respiration in hMADS cells (n = 12). (F and G) (F) Representative WB and (G) UCP1 quantification in IBAs transfected with siRNA pools targeting individual small GTPases in combination with GGOH treatment (48 hr; n = 5). (H) Effect of simvastatin treatment (48 hr) on F-actin levels in IBAs (F-actin in green, nuclei in blue). Scale bar, 50 μm.

(legend continued on next page)

findings of several studies, which did not observe changes in energy expenditure upon statin treatment (Chung et al., 2008; Panayiotou et al., 2013). It is important, however, to point out that we used statins as a pharmacological tool to achieve short-term inhibition of the mevalonate pathway. Statins are normally taken over several decades and long-term changes in brite adipocyte content might have a significant impact on whole-body metabolism. In addition, it should be noted that statins have many positive effects in different tissues, which makes it very complicated to dissect the impact of beige fat inhibition on whole-body metabolism in such a model. Therefore, we used the much more defined inducible adipocyte-specific ablation of GGTase I, which led to inhibition of iWAT browning, development of obesity, and impaired glucose tolerance after 8 weeks on a high-fat diet. Moreover, this negative metabolic phenotype did not develop at thermoneutrality, demonstrating that it results from impaired adipose tissue thermogenesis. This is in line with multiple reports indicating that regulating brite adipocyte formation is sufficient to elicit a metabolic phenotype (Cohen et al., 2014; Kazak et al., 2015; Qiang et al., 2012; Shinoda et al., 2015).

In adult humans, BAT depots seem to contain both classical and inducible brown adipocytes (Jespersen et al., 2013; Lidell et al., 2013). Interestingly, we found an inverse correlation of statin use with active BAT in a retrospective study. In the prospective clinical trial, we found that fluvastatin could reduce expression of brown adipocyte markers in supraclavicular BAT; however, no significant effect on FDG uptake was observed. Based on the current literature, FDG-PET is the most widely used technique to measure BAT presence in humans because of difficulties in tissue sampling and/or the measurement of whole-body energy expenditure using indirect calorimetry. As several groups have shown that *Ucp1*-knockout mice exhibit the same levels of radiolabeled glucose uptake in BAT as wild-type mice (Hankir et al., 2017; Olsen et al., 2017), it is difficult to assess whether FDG is the ideal measure for BAT activity given the wide substrate use of this tissue. Interestingly, the changes in BAT glucose uptake induced by fluvastatin treatment seem to be temperature dependent, suggesting that thermogenesis and glucose uptake are coupled only under partially stimulated conditions. Further studies will be needed to expand these results.

Several papers have reported that atorvastatin treatment inhibits preadipocyte proliferation and adipogenic differentiation, without affecting adipocyte maturation (Li et al., 2003). This is in line with reports showing that statins reduce PPAR γ , C/EBP α , and C/EBP β levels (Mauser et al., 2007; Nakata et al., 2006). We exclusively investigated here the role of the mevalonate pathway in mature brown adipocytes and in the conversion of white into brown adipocytes, and we could show that statins reduce thermogenic function and PPAR γ levels, without affecting the number of differentiated cells. We have recently shown that

PPAR γ is required to maintain the thermogenic capacity of mature brown adipocytes (Lasar et al., 2018); thus it is possible that statins inhibit BAT function through regulation of this factor.

The inhibitory effect of statins on UCP1 levels in brown adipocytes *in vitro* could be rescued by GGPP, FPP, and GGOH, but not by FOH. Metabolic labeling experiments have provided evidence that mammalian cells can use free GGOH for protein geranylgeranylation and free FOH for sterol biosynthesis and protein farnesylation (Crick et al., 1994; Fiesler and Keller, 1995). However, there is very little evidence for the conversion of FOH back to FPP and GGPP and it is mostly based on studies from plants (Thai et al., 1999). Another point of evidence against the conversion of FOH to FPP is based on multiple studies investigating the inhibitory effect of statins on the proliferation of smooth muscle, NIH 3T3, and C6 glioma cells, which could be rescued by GGPP or GGOH, but not by FOH (Crick et al., 1998; Vigano et al., 1995; Vogt et al., 1996). On the other hand, one study showed increased FPP production in rat liver lysates following FOH supplementation (Bentinger et al., 1998). The authors of this study suggest that an enzyme phosphorylating FOH into farnesyl monophosphate, as well as an enzymatic mechanism catalyzing the phosphorylation of farnesyl-P to farnesyl-PP, exists. However, these enzymes have not been identified as of yet.

Based on our data we conclude that the development and thermogenic function of brite but not of classical brown adipocytes are affected by inhibition of the mevalonate pathway and prenylation of small GTPases. We quantified not only the expression of thermogenic markers, but also the number of UCP1 $^{+}$ cells, which are significantly reduced by statins in the iWAT. Therefore, we believe that the mevalonate pathway and particularly protein prenylation are important for iWAT browning, but do not affect the thermogenic potential of fully active BAT. Nevertheless, we cannot rule out that the effect of the mevalonate pathway and GGTase I inhibition on adipocyte browning in mice is in part due to changes in brite adipocyte formation from precursors (Wang and Scherer, 2014). An argument against such a contribution stems from our genetic model, as we could show that ablation of GGTase I exclusively in mature adipocytes led to a similar effect observed in statin- and GGT1-298-treated mice. These data indicate that the effect occurs at the level of maturation or interconversion, rather than through changes in adipogenesis. Another support for this argument is the fact that mature adipocytes do not de-differentiate upon statin treatment or inhibition of protein geranylgeranylation.

We propose that the activity of the mevalonate pathway regulates adipocyte browning by affecting geranylgeranylation of small GTP-binding proteins. It has been shown recently that expression of constitutively active G α_q protein reduces brown adipogenesis in mice via modulation of RHOA/ROCK signaling (Klepac et al., 2016). In addition, the pro-adipogenic effect of

(I) Effect of simvastatin treatment on F-actin levels in iBAs and hMADS cells (F-actin in green, nuclei in blue) can be rescued with GGOH. Scale bar, 50 μ m. (J and K) Representative WB showing dose-dependent inhibitory effect of simvastatin treatment (48 hr) on YAP1 and TAZ levels in iBAs, which (K) could be rescued with GGOH (100 μ M). (L and M) Representative WB and (M) YAP1 and TAZ quantification in hMADS cells transfected with siRNA pools targeting *PGGT1B* and *RABGGTB* (n = 6). (N and O) Representative WB and (O) UCP1 quantification in hMADS cells transfected with siRNA pools targeting *YAP1* and *TAZ* (n = 7). (P) Effect of *YAP1* and *TAZ* knockdown on mitochondrial respiration in hMADS cells (n = 5). Results are reported as mean \pm SEM. Statistical significance was calculated using ANOVA and Student's t test. Statistical differences are indicated as *p < 0.05, **p < 0.01, ***p < 0.001.



BMP7 is mediated by suppression of ROCK activity; however, ROCK inhibition does not alter BMP7-induced UCP1 expression in C3H/10T1/2 mesenchymal stem cells differentiated into brown adipocytes (McDonald et al., 2015). In a proof-of-principle experiment, knockdown of the five most common GTPases resulted in a significant reduction of UCP1 levels, indicating that members of this protein class are important for function and/or formation of thermogenic adipocytes. Based on our data it seems that small GTPases have overlapping functions in the regulation of UCP1, and the effect of protein geranylgeranylation is most likely mediated by multiple pathways and not by a single target. We believe that, similar to GGTase I inhibition, GGTase II knockdown also affects many cellular processes, including vesicular transport, in which RAB proteins play a crucial role. One of the mechanisms for how impaired geranylgeranylation of small GTP-binding proteins might affect thermogenic function and adipocyte browning is impairment of F-actin formation and transcriptional activity of YAP1 and TAZ. This is supported by a recent study showing the importance of actomyosin tension and the mechanosensitive transcriptional co-activators YAP1 and TAZ for induction of oxidative metabolism and uncoupled respiration in thermogenic fat cells (Tharp et al., 2018).

In conclusion, we show that the mevalonate pathway regulates adipocyte browning. Our mouse and cell culture data are supported in part by a retrospective and a small prospective volunteer study, supporting the physiological relevance of this regulation in humans. Further clinical studies are warranted to substantiate these results and to determine whether protein geranylgeranylation or individual small GTPases might be used for therapeutic strategies to promote thermogenic activity of fat cells and thereby increase whole-body energy expenditure.

Limitations of Study

Retrospective data presented in our study should be interpreted with caution, as retrospective studies suffer from numerous weaknesses, most notably a selection bias. This may be particularly true in our cohort of mostly cancer patients, which are probably not representative of the general population. Our small prospective volunteer study shows that short-term fluvastatin treatment reduces expression of brown adipocyte markers without affecting FDG uptake in supraclavicular BAT. Further studies will be needed to test the effect of other statins on BAT activity in large patient cohorts. We provide a possible explanation for reduced UCP1 levels, namely impaired geranylgeranylation of small GTPases, which then leads to reduced F-actin levels and YAP1/TAZ inactivity. However, it is important to mention that small GTPases are involved in the regulation of a large variety of processes, and the inhibitory effect on adipocyte browning can, most likely, not be explained solely by dysregulation of YAP1 and TAZ. Further studies will be needed to completely dissect the mechanism downstream of GGTases.

STAR★METHODS

Detailed methods are provided in the online version of this paper and include the following:

- KEY RESOURCES TABLE
- CONTACT FOR REAGENT AND RESOURCE SHARING

914 Cell Metabolism 29, 901–916, April 2, 2019

● EXPERIMENTAL MODEL AND SUBJECT DETAILS

- Clinical Transcriptome Study
- Retrospective ¹⁸F-DG-PET/CT Cohort Study
- Clinical Fluvastatin Study
- Mouse Experiments
- Cell Culture – hMADS Cells
- Cell Culture – Immortalized Murine Brown Adipocytes

● METHOD DETAILS

- Intraperitoneal Glucose Tolerance Test
- Body Composition Measurement
- Indirect Calorimetry
- Tissue Harvest
- Analysis of Preadipocyte Proliferation and Adipocyte Differentiation
- Cellular Respiration
- Fatty Acid Uptake
- Lipolysis
- Glucose Uptake
- Ketone Bodies Measurement
- *Ucp1* Promoter Activity
- RNA Extraction, cDNA Synthesis, Quantitative RT-PCR
- Protein Extraction and Western Blot
- Click Chemistry
- Subcellular Fractionation
- F-actin Staining
- RNA Sequencing, Mapping and Analysis
- Quantification of Cre Recombination in Mouse Tissues
- Metabolomic Analysis

● QUANTIFICATION AND STATISTICAL ANALYSIS

● DATA AND SOFTWARE AVAILABILITY

SUPPLEMENTAL INFORMATION

Supplemental Information includes seven figures and four tables and can be found with this article online at <https://doi.org/10.1016/j.cmet.2018.11.017>.

ACKNOWLEDGMENTS

The work was supported by the International Starr Foundation, the Vontobel-Stiftung, the Swiss National Science Foundation, and the Grant Agency of the Slovak Academy of Sciences (VEGA 2/0096/17).

AUTHOR CONTRIBUTIONS

M. Balaz and C.W. designed the study; M. Balaz, I.A.B., M.J.B., L.V., and C.W. supervised the experiments; M. Balaz, L.B., L.S., W.S., H.D., C.M., C.H., Y.R., S.M., and V.E. performed the experiments; M. Balaz, J.U., L.V., P.S., B.U., and M.P. performed the clinical transcriptome study; L.O. analyzed RNA sequencing data; A.S.B., S.B., C.Z., and C.F. performed the retrospective clinical study; A.S.B., J.M., G.G., C.I.M., I.A.B., and M.J.B. performed the clinical trial; N.Z. performed the metabolome analysis; M. Bergho, M.K.A., and E.-Z.A. provided resources; M. Balaz, A.S.B., and C.W. wrote the paper; all authors reviewed and edited the manuscript.

DECLARATION OF INTERESTS

The authors declare no competing interests.

Received: August 14, 2018
Revised: October 15, 2018
Accepted: November 27, 2018
Published: December 20, 2018



REFERENCES

- Aragona, M., Panciera, T., Manfrin, A., Giullitti, S., Michielin, F., Elvassore, N., Dupont, S., and Piccolo, S. (2013). A mechanical checkpoint controls multicellular growth through YAP/TAZ regulation by actin-processing factors. *Cell* 154, 1047–1059.
- Bartelt, A., Bruns, O.T., Reimer, R., Hohenberg, H., Ittrich, H., Peldschus, K., Kaul, M.G., Tromsdorf, U.I., Weller, H., Waurisch, C., et al. (2011). Brown adipose tissue activity controls triglyceride clearance. *Nat. Med.* 17, 200–205.
- Becker, A.S., Nagel, H.W., Wolfrum, C., and Burger, I.A. (2016). Anatomical grading for metabolic activity of brown adipose tissue. *PLoS One* 11, e0149456.
- Bentinger, M., Grunler, J., Peterson, E., Swiezewska, E., and Dallner, G. (1998). Phosphorylation of farnesol in rat liver microsomes: properties of farnesol kinase and farnesyl phosphate kinase. *Arch. Biochem. Biophys.* 353, 191–198.
- Cannon, B., and Nedergaard, J. (2004). Brown adipose tissue: function and physiological significance. *Physiol. Rev.* 84, 277–359.
- Carriere, A., Jeanson, Y., Berger-Muller, S., Andre, M., Chenouard, V., Arnaud, E., Barreau, C., Walther, R., Galinier, A., Wdziekonski, B., et al. (2014). Browning of white adipose cells by intermediate metabolites: an adaptive mechanism to alleviate redox pressure. *Diabetes* 63, 3253–3265.
- Chondronikola, M., Volpi, E., Borsheim, E., Porter, C., Annamalai, P., Enerback, S., Lidell, M.E., Saraf, M.K., Labbe, S.M., Hurren, N.M., et al. (2014). Brown adipose tissue improves whole-body glucose homeostasis and insulin sensitivity in humans. *Diabetes* 63, 4089–4099.
- Chung, J., Brass, E.P., Ulrich, R.G., and Hiatt, W.R. (2008). Effect of atorvastatin on energy expenditure and skeletal muscle oxidative metabolism at rest and during exercise. *Clin. Pharmacol. Ther.* 83, 243–250.
- Cohen, P., Levy, J.D., Zhang, Y., Frontini, A., Kolodin, D.P., Svensson, K.J., Lo, J.C., Zeng, X., Ye, L., Khandekar, M.J., et al. (2014). Ablation of PRDM16 and beige adipose causes metabolic dysfunction and a subcutaneous to visceral fat switch. *Cell* 156, 304–316.
- Crick, D.C., Andres, D.A., Danesi, R., Macchia, M., and Waechter, C.J. (1998). Geranylgeraniol overcomes the block of cell proliferation by lovastatin in C6 glioma cells. *J. Neurochem.* 70, 2397–2405.
- Crick, D.C., Waechter, C.J., and Andres, D.A. (1994). Utilization of geranylgeraniol for protein isoprenylation in C6 glial cells. *Biochem. Biophys. Res. Commun.* 205, 955–961.
- Cypess, A.M., Lehman, S., Williams, G., Tal, I., Rodman, D., Goldfine, A.B., Kuo, F.C., Palmer, E.L., Tseng, Y.H., Doria, A., et al. (2009). Identification and importance of brown adipose tissue in adult humans. *N. Engl. J. Med.* 360, 1509–1517.
- Cypess, A.M., Weiner, L.S., Roberts-Toler, C., Franquet Elia, E., Kessler, S.H., Kahn, P.A., English, J., Chatman, K., Trauger, S.A., Doria, A., et al. (2015). Activation of human brown adipose tissue by a beta3-adrenergic receptor agonist. *Cell Metab.* 21, 33–38.
- Elabd, C., Chiellini, C., Carmona, M., Galitzky, J., Cochet, O., Petersen, R., Penicaud, L., Kristiansen, K., Bouloumie, A., Casteilla, L., et al. (2009). Human multipotent adipose-derived stem cells differentiate into functional brown adipocytes. *Stem Cells* 27, 2753–2760.
- Fliesler, S.J., and Keller, R.K. (1995). Metabolism of [3H]farnesol to cholesterol and cholesterologenic intermediates in the living rat eye. *Biochem. Biophys. Res. Commun.* 210, 695–702.
- Former, F., Kumar, C., Lubner, C.A., Fromme, T., Klingenspor, M., and Mann, M. (2009). Proteome differences between brown and white fat mitochondria reveal specialized metabolic functions. *Cell Metab.* 10, 324–335.
- Frontini, A., Vitali, A., Perugini, J., Murano, I., Romiti, C., Ricquier, D., Guerrieri, M., and Cinti, S. (2013). White-to-brown transdifferentiation of omental adipocytes in patients affected by pheochromocytoma. *Biochim. Biophys. Acta* 1831, 950–959.
- Fuhrer, T., Heer, D., Begemann, B., and Zamboni, N. (2011). High-throughput, accurate mass metabolome profiling of cellular extracts by flow injection-time-of-flight mass spectrometry. *Anal. Chem.* 83, 7074–7080.
- Gazzerro, P., Proto, M.C., Gangemi, G., Malfitano, A.M., Ciaglia, E., Pisanti, S., Santoro, A., Laezza, C., and Bifulco, M. (2012). Pharmacological actions of statins: a critical appraisal in the management of cancer. *Pharmacol. Rev.* 64, 102–146.
- Hankir, M.K., Kranz, M., Keipert, S., Weiner, J., Andreasen, S.G., Kern, M., Patt, M., Klotting, N., Heiker, J.T., Brust, P., et al. (2017). Dissociation between brown adipose tissue (18)F-FDG uptake and thermogenesis in uncoupling protein 1-deficient mice. *J. Nucl. Med.* 58, 1100–1103.
- Hanssen, M.J., Hoeks, J., Brans, B., van der Lans, A.A., Schaart, G., van den Driessche, J.J., Jorgensen, J.A., Boekschoten, M.V., Hesselink, M.K., Havekes, B., et al. (2015). Short-term cold acclimation improves insulin sensitivity in patients with type 2 diabetes mellitus. *Nat. Med.* 21, 863–865.
- Iwen, K.A., Backhaus, J., Cassens, M., Watt, M., Hedesan, O.C., Merkel, M., Heeren, J., Sina, C., Rademacher, L., Windjager, A., et al. (2017). Cold-induced brown adipose tissue activity alters plasma fatty acids and improves glucose metabolism in men. *J. Clin. Endocrinol. Metab.* 102, 4226–4234.
- Janmahasatian, S., Duffull, S.B., Ash, S., Ward, L.C., Byrne, N.M., and Green, B. (2005). Quantification of lean bodyweight. *Clin. Pharmacokinet.* 44, 1051–1065.
- Jespersen, N.Z., Larsen, T.J., Peijs, L., Daugaard, S., Homoe, P., Loft, A., de Jong, J., Mathur, N., Cannon, B., Nedergaard, J., et al. (2013). A classical brown adipose tissue mRNA signature partly overlaps with brite in the supraclavicular region of adult humans. *Cell Metab.* 17, 798–805.
- Jiang, Z., Yu, B., and Li, Y. (2016). Effect of three statins on glucose uptake of cardiomyocytes and its mechanism. *Med. Sci. Monit.* 22, 2825–2830.
- Kalinovich, A.V., de Jong, J.M., Cannon, B., and Nedergaard, J. (2017). UCP1 in adipose tissues: two steps to full browning. *Biochimie* 134, 127–137.
- Kazak, L., Chouchani, E.T., Jedrychowski, M.P., Erickson, B.K., Shinoda, K., Cohen, P., Vetrivelan, R., Lu, G.Z., Laznik-Bogoslavski, D., Hasenfuss, S.C., et al. (2015). A creatine-driven substrate cycle enhances energy expenditure and thermogenesis in beige fat. *Cell* 163, 643–655.
- Klein, J., Fasshauer, M., Klein, H.H., Benito, M., and Kahn, C.R. (2002). Novel adipocyte lines from brown fat: a model system for the study of differentiation, energy metabolism, and insulin action. *Bioessays* 24, 382–388.
- Klepak, K., Kilic, A., Gnad, T., Brown, L.M., Herrmann, B., Wilderman, A., Balkow, A., Glode, A., Simon, K., Lidell, M.E., et al. (2016). The Gq signalling pathway inhibits brown and beige adipose tissue. *Nat. Commun.* 7, 10895.
- Lasar, D., Rosenwald, M., Kiehlmann, E., Balaz, M., Tall, B., Opitz, L., Lidell, M.E., Zamboni, N., Krznar, P., Sun, W., et al. (2018). Peroxisome proliferator activated receptor gamma controls mature brown adipocyte inducibility through glycerol kinase. *Cell Rep.* 22, 760–773.
- Li, W., Liang, X., Zeng, Z., Yu, K., Zhan, S., Su, Q., Yan, Y., Mansai, H., Qiao, W., Yang, Q., et al. (2016). Simvastatin inhibits glucose uptake activity and GLUT4 translocation through suppression of the IR/IRS-1/Akt signaling in C2C12 myotubes. *Biomed. Pharmacother.* 83, 194–200.
- Li, X., Cui, Q., Kao, C., Wang, G.J., and Balian, G. (2003). Lovastatin inhibits adipogenic and stimulates osteogenic differentiation by suppressing PPARgamma2 and increasing Cbfa1/Runx2 expression in bone marrow mesenchymal cell cultures. *Bone* 33, 652–659.
- Lidell, M.E., Betz, M.J., Dahlqvist Leinhard, O., Heglund, M., Elander, L., Slawik, M., Mussack, T., Nilsson, D., Romu, T., Nuutila, P., et al. (2013). Evidence for two types of brown adipose tissue in humans. *Nat. Med.* 19, 631–634.
- Mausser, W., Perwitz, N., Meier, B., Fasshauer, M., and Klein, J. (2007). Direct adipotropic actions of atorvastatin: differentiation state-dependent induction of apoptosis, modulation of endocrine function, and inhibition of glucose uptake. *Eur. J. Pharmacol.* 564, 37–46.
- McDonald, M.E., Li, C., Bian, H., Smith, B.D., Layne, M.D., and Farmer, S.R. (2015). Myocardin-related transcription factor A regulates conversion of progenitors to beige adipocytes. *Cell* 160, 105–118.
- Nair, A.B., and Jacob, S. (2016). A simple practice guide for dose conversion between animals and human. *J. Basic Clin. Pharm.* 7, 27–31.
- Nakata, M., Nagasaka, S., Kusaka, I., Matsuoka, H., Ishibashi, S., and Yada, T. (2006). Effects of statins on the adipocyte maturation and expression of glucose



- transporter 4 (SLC2A4): implications in glycaemic control. *Diabetologia* 49, 1881–1892.
- Nedergaard, J., Bengtsson, T., and Cannon, B. (2007). Unexpected evidence for active brown adipose tissue in adult humans. *Am. J. Physiol. Endocrinol. Metab.* 293, E444–E452.
- Olsen, J.M., Csikasz, R.I., Dehvari, N., Lu, L., Sandstrom, A., Oberg, A.I., Nedergaard, J., Stone-Elander, S., and Bengtsson, T. (2017). beta3-Adrenergically induced glucose uptake in brown adipose tissue is independent of UCP1 presence or activity: mediation through the mTOR pathway. *Mol. Metab.* 6, 611–619.
- Olsson, A.G., McTaggart, F., and Raza, A. (2002). Rosuvastatin: a highly effective new HMG-CoA reductase inhibitor. *Cardiovasc. Drug Rev.* 20, 303–328.
- Orava, J., Nuutila, P., Lidell, M.E., Oikonen, V., Noponen, T., Viljanen, T., Scheinin, M., Taittonen, M., Niemi, T., Enerback, S., et al. (2011). Different metabolic responses of human brown adipose tissue to activation by cold and insulin. *Cell Metab.* 14, 272–279.
- Orava, J., Nuutila, P., Noponen, T., Parkkola, R., Viljanen, T., Enerback, S., Rissanen, A., Pietilainen, K.H., and Virtanen, K.A. (2013). Blunted metabolic responses to cold and insulin stimulation in brown adipose tissue of obese humans. *Obesity (Silver Spring)* 21, 2279–2287.
- Ortiz, J.A., Gil-Gomez, G., Casaroli-Marano, R.P., Vilaro, S., Hegardt, F.G., and Haro, D. (1994). Transfection of the ketogenic mitochondrial 3-hydroxy-3-methylglutaryl-coenzyme A synthase cDNA into Mev-1 cells corrects their auxotrophy for mevalonate. *J. Biol. Chem.* 269, 28523–28526.
- Ouellet, V., Labbe, S.M., Blondin, D.P., Phoenix, S., Guerin, B., Haman, F., Turcotte, E.E., Richard, D., and Carpentier, A.C. (2012). Brown adipose tissue oxidative metabolism contributes to energy expenditure during acute cold exposure in humans. *J. Clin. Invest.* 122, 545–552.
- Panayiotou, G., Paschalis, V., Nikolaidis, M.G., Theodorou, A.A., Deli, C.K., Fotopoulou, N., Fatouros, I.G., Koutedakis, Y., Sampanis, M., and Jamurtas, A.Z. (2013). No adverse effects of statins on muscle function and health-related parameters in the elderly: an exercise study. *Scand. J. Med. Sci. Sports* 23, 556–567.
- Perdikari, A., Leparo, G.G., Balaz, M., Pires, N.D., Lidell, M.E., Sun, W., Fernandez-Albert, F., Muller, S., Akchiche, N., Dong, H., et al. (2018). BATLAS: deconvoluting brown adipose tissue. *Cell Rep.* 25, 784–797.e4.
- Qiang, L., Wang, L., Kon, N., Zhao, W., Lee, S., Zhang, Y., Rosenbaum, M., Zhao, Y., Gu, W., Farmer, S.R., et al. (2012). Brown remodeling of white adipose tissue by SirT1-dependent deacetylation of Ppargamma. *Cell* 150, 620–632.
- Rosenwald, M., Perdikari, A., Rulicke, T., and Wolfrum, C. (2013). Bi-directional interconversion of brite and white adipocytes. *Nat. Cell Biol.* 15, 659–667.
- Senn, J.R., Maushart, C.I., Gashi, G., Michel, R., Lalive d'Epinay, M., Vogt, R., Becker, A.S., Muller, J., Balaz, M., Wolfrum, C., et al. (2018). Outdoor temperature influences cold induced thermogenesis in humans. *Front. Physiol.* 9, 1184.
- Shi, F., and Collins, S. (2017). Second messenger signaling mechanisms of the brown adipocyte thermogenic program: an integrative perspective. *Horm. Mol. Biol. Clin. Investig.* 31, <https://doi.org/10.1515/hmbci-2017-0062>.
- Shinoda, K., Ohyama, K., Hasegawa, Y., Chang, H.Y., Ogura, M., Sato, A., Hong, H., Hosono, T., Sharp, L.Z., Scheel, D.W., et al. (2015). Phosphoproteomics identifies CK2 as a negative regulator of beige adipocyte thermogenesis and energy expenditure. *Cell Metab.* 22, 997–1008.
- Shore, A.M., Karamitri, A., Kemp, P., Speakman, J.R., Graham, N.S., and Lomax, M.A. (2013). Cold-induced changes in gene expression in brown adipose tissue, white adipose tissue and liver. *PLoS One* 8, e68933.
- Sjogren, A.K., Andersson, K.M., Liu, M., Cutts, B.A., Karlsson, C., Wahlstrom, A.M., Dalin, M., Weinbaum, C., Casey, P.J., Tarkowski, A., et al. (2007). GGTase-I deficiency reduces tumor formation and improves survival in mice with K-RAS-induced lung cancer. *J. Clin. Invest.* 117, 1294–1304.
- Svensson, P.A., Jemas, M., Sjolholm, K., Hoffmann, J.M., Nilsson, B.E., Hansson, M., and Carlsson, L.M. (2011). Gene expression in human brown adipose tissue. *Int. J. Mol. Med.* 27, 227–232.
- Thai, L., Rush, J.S., Maul, J.E., Devarenne, T., Rodgers, D.L., Chappell, J., and Waechter, C.J. (1999). Farnesol is utilized for isoprenoid biosynthesis in plant cells via farnesyl pyrophosphate formed by successive monophosphorylation reactions. *Proc. Natl. Acad. Sci. U S A* 96, 13080–13085.
- Tharp, K.M., Kang, M.S., Timblin, G.A., Dempersmier, J., Dempsey, G.E., Zushin, P.H., Benavides, J., Choi, C., Li, C.X., Jha, A.K., et al. (2018). Actomyosin-mediated tension orchestrates uncoupled respiration in adipose tissues. *Cell Metab.* 27, 602–615.e4.
- van Marken Lichtenbelt, W.D., Vanhommerig, J.W., Smulders, N.M., Drossaerts, J.M., Kemerink, G.J., Bouvy, N.D., Schrauwen, P., and Teule, G.J. (2009). Cold-activated brown adipose tissue in healthy men. *N. Engl. J. Med.* 360, 1500–1508.
- Vigano, T., Hernandez, A., Corsini, A., Granata, A., Belloni, P., Fumagalli, R., Paoletti, R., and Folco, G. (1995). Mevalonate pathway and isoprenoids regulate human bronchial myocyte proliferation. *Eur. J. Pharmacol.* 291, 201–203.
- Vogt, A., Qian, Y., McGuire, T.F., Hamilton, A.D., and Sebti, S.M. (1996). Protein geranylgeranylation, not farnesylation, is required for the G1 to S phase transition in mouse fibroblasts. *Oncogene* 13, 1991–1999.
- Wang, Q.A., and Scherer, P.E. (2014). The AdipoChaser mouse: a model tracking adipogenesis in vivo. *Adipocyte* 3, 146–150.



STAR★METHODS

KEY RESOURCES TABLE

REAGENT or RESOURCE	SOURCE	IDENTIFIER
Antibodies		
UCP1	Thermo Fisher	Cat# PA1-24894; RRID: AB_2241459
HSP90	Cell Signaling	Cat# 4877; RRID: AB_2233307
γ-TUBULIN	Sigma-Aldrich	Cat# T-5326; RRID: AB_532292
HSL	Cell Signaling	Cat# 4107; RRID: AB_2296900
phospho-HSL (Ser660)	Cell Signaling	Cat# 4126; RRID: AB_490997
AKT	Cell Signaling	Cat# 9272; RRID: AB_329827
phospho-AKT (Thr308)	Cell Signaling	Cat# 13038; RRID: AB_2629447
CREB	Cell Signaling	Cat# 9197; RRID: AB_331277
phospho-CREB (Ser133)	Cell Signaling	Cat# 9198; RRID: AB_2561044
PGGT1B	Abcam	Cat# ab122122; RRID: AB_11129941
RABGGTB	Abcam	Cat# ab187717; RRID: AB_2751007
GAPDH	Cell Signaling	Cat# 5174; RRID: AB_10622025
cleaved Caspase 3 (Asp175)	Cell Signaling	Cat# 9661; RRID: AB_2341188
RHOA	Cell Signaling	Cat# 2117; RRID: AB_10693922
RAC1/2/3	Cell Signaling	Cat# 2465; RRID: AB_10695732
CDC42	Cell Signaling	Cat# 2466; RRID: AB_2078082
RAP1A/RAP1B	Cell Signaling	Cat# 4938; RRID: AB_2177112
Na ⁺ /K ⁺ ATPase	Abcam	Cat# ab76020; RRID: AB_1310695
HMGCS2	Abcam	Cat# ab137043; RRID: AB_2749817
YAP1/TAZ	Cell Signaling	Cat# 8418; RRID: AB_10950494
PPAR _γ	Cell Signaling	Cat# 2443; RRID: AB_10694772
HMGCR	Abcam	Cat# ab174830; RRID: AB_2749818
anti-mouse HRP secondary	Millipore	Cat# 401253; RRID: AB_437779
anti-rabbit HRP secondary	Millipore	Cat# 401393; RRID: AB_10683386
Streptavidin-HRP	Cell Signaling	Cat# 3999; RRID: AB_10830897
Chemicals, Peptides, and Recombinant Proteins		
Hoechst 33342	Cell Signaling	Cat# 4082
Bodipy 493/503	Invitrogen	Cat# D3922
Syto60	Invitrogen	Cat# S11342
3-Isobutyl-1-methylxanthine	Sigma-Aldrich	Cat# I5879
Dexamethasone	Sigma-Aldrich	Cat# D4902
Indomethacin	Sigma-Aldrich	Cat# I7378
Insulin	Sigma-Aldrich	Cat# I9278
Rosiglitazone	Adipogen	Cat# 71740
Triiodo-L-Thyronine (T3)	Sigma-Aldrich	Cat# T6397
CL-316,243	Sigma-Aldrich	Cat# C5976
Collagen, Type I	Sigma-Aldrich	Cat# C3867
DMEM, low glucose	Lonza	Cat# BE12-707F
Ham's F12 medium	Lonza	Cat# BE12-615F
Penicillin-Streptomycin	Gibco	Cat# 15070063
DMEM, high glucose	Gibco	Cat# 41965062
L-glutamine	Gibco	Cat# 25030-024
Trizol reagent	Invitrogen	Cat# 15596026
DNase I (RNase-free)	NEB	Cat# M0303
Simvastatin	Sigma-Aldrich	Cat# S6196

(Continued on next page)



Continued		
REAGENT or RESOURCE	SOURCE	IDENTIFIER
Fluvastatin	Sigma-Aldrich	Cat# SML0038
Atorvastatin	Sigma-Aldrich	Cat# PZ0001
Rosuvastatin	Sigma-Aldrich	Cat# SML1264
Pravastatin	Sigma-Aldrich	Cat# P4498
Cerivastatin	Sigma-Aldrich	Cat# SML0005
GGTI-298	Sigma-Aldrich	Cat# G5169
FTI-277	Sigma-Aldrich	Cat# F9803
Farnesyl pyrophosphate	Sigma-Aldrich	Cat# F6892
Farnesol	Abcam	Cat# ab142428
Geranylgeranyl pyrophosphate	Sigma-Aldrich	Cat# G6025
Geranylgeraniol	Abcam	Cat# ab142436
Gallein	Santa Cruz	Cat# sc-202631
Rho inhibitor, Rhosin	Calbiochem	Cat# 555460
Squalene	Sigma-Aldrich	Cat# S3626
Coenzyme Q9	Sigma-Aldrich	Cat# 27597
Coenzyme Q10	Sigma-Aldrich	Cat# C9538
Tamoxifen	Sigma-Aldrich	Cat# T5648
4-Hydroxytamoxifen	Sigma-Aldrich	Cat# H7904
D-glucose	Sigma-Aldrich	Cat# G7021
Oligomycin	Adipogen	Cat# 11342
Isoproterenol	Sigma-Aldrich	Cat# I5627
Dibutyl-cAMP	Sigma-Aldrich	Cat# D0627
FCCP	Sigma-Aldrich	Cat# C2920
Rotenone	Sigma-Aldrich	Cat# R8875
Antimycin A	Sigma-Aldrich	Cat# A8674
Sodium pyruvate	Invitrogen	Cat# 11360070
Seahorse XF Base Medium	Agilent	Cat# 102353
Complete Protease Inhibitors	Roche	Cat# 05056489001
Halt Phosphatase Inhibitors	ThermoFischer	Cat# 78426
Click-IT Geranylgeranyl Alcohol, Azide	Invitrogen	Cat# C10249
Biotin Alkyne	Invitrogen	Cat# B10185
Phalloidin-iFluor 488 Reagent	Abcam	Cat# ab176753
Critical Commercial Assays		
High Capacity cDNA RT kit	Applied Biosystems	Cat# 4368814
TruSeq RNA library prep kit	Illumina	Cat# RS-122-2301
DC Protein Assay	Bio-Rad	Cat# 5000111
Click-IT Protein Reaction Kit	Invitrogen	Cat# C10276
XFE96 FluxPak	Agilent	Cat# 102416-100
Glycerol reagent	Sigma-Aldrich	Cat# F6428
QBT fatty acid uptake assay kit	Molecular Devices	Cat# R6132
Luciferase reporter system	Promega	Cat# E1501
Autokit Total Ketone Bodies R1 Set	Wako Chemicals	Cat# 415-73301
Autokit Total Ketone Bodies R2 Set	Wako Chemicals	Cat# 413-73601
Deposited Data		
RNA sequencing data for clinical transcriptome study	European Nucleotide Archive	PRJEB23275
Experimental Models: Cell Lines		
immortalized brown adipocytes	Christian Wolfrum	Klein et al., 2002
hMADS cells	Ez-Zoubir Amri	Elabd et al., 2009

(Continued on next page)

Continued		
REAGENT or RESOURCE	SOURCE	IDENTIFIER
Experimental Models: Organisms/Strains		
C57BL/6N mice	Charles River	C57BL/6NcrJ Strain code 027
<i>Ucp1</i> -CreERT2 x LoxP-Red mice	Christian Wolfrum	Rosenwald et al., 2013
<i>Pggt1b</i> ^{fl/fl} mice	Martin Bergo	Sjogren et al., 2007
<i>Adip</i> -CreERT2 mice	Christian Wolfrum	Rosenwald et al., 2013
Oligonucleotides		
qPCR primers	Microsynth	Listed in Table S4
siRNAs	Microsynth	Listed in Table S3
Software and Algorithms		
Harmony - Operetta software	Perkin Elmer	version 3.5
ImageJ	NIH, USA	version 1.50b
Phenomaster software	TSE systems	version 5.6.5
Wave - XF96 software	Agilent	version 2.3.0.19
ImageQuant LAS 4000	GE Healthcare	version 1.1
GraphPad Prism 7	GraphPad software	version 7.03
ViiA7 software	Applied Biosystems	version 1.2.3
Gen5	BioTek	version 1.10

CONTACT FOR REAGENT AND RESOURCE SHARING

Further information and requests for resources and reagents should be directed to and will be fulfilled by the Lead Contact, Professor Christian Wolfrum (christian-wolfrum@ethz.ch).

EXPERIMENTAL MODEL AND SUBJECT DETAILS

Clinical Transcriptome Study

The clinical study was approved by the Local Ethics Committee of the University Hospital in Bratislava, Slovakia and it conforms to the ethical guidelines of the 2000 Helsinki declaration. All study participants provided witnessed written informed consent prior entering the study. Deep neck brown and adjacent subcutaneous white adipose tissue samples were obtained from the lower third of the neck by an experienced ENT surgeon during neck surgery under general anesthesia. The deep neck adipose tissue sample was taken from pre- and paravertebral space between common carotid and trachea in case of thyroid surgery and just laterally to carotid sheath in case of branchial cleft cyst surgery. In all cases, the surgical approach was sufficient to reach and sample the deep neck adipose tissue without any additional morbidity. Patients with malignant disease and subjects younger than 18 years were excluded from participation in the study. Adipose tissue samples were immediately cleaned from blood and connective tissue, and frozen in liquid nitrogen until further processing. In order to identify patients with active BAT, we first quantified expression of brown adipocyte marker genes in individual biopsies using qPCR. By analyzing BAT and WAT biopsies of 18 patients, we identified 10 individuals with active BAT (2 male/8 female; 39.6 ± 4.7 years; BMI 23.5 ± 0.8 kg/m²; waist circumference 82.5 ± 4.3 cm; body fat 28.2 ± 2.0 %; thyroid surgery n=9 or branchial cleft cyst surgery n=1). Adipose tissue biopsies of these patients were subjected to RNA sequencing. Our cohort consists of 2 male and 8 female patients, which is mainly due to the fact that prevalence of BAT is higher in females than in males and also because more females were willing to participate in our study. We have analyzed BAT and WAT transcriptomes of all patients and could not find any difference between male and female tissues in Principal component analysis (Perdikari et al., 2018).

Retrospective ¹⁸F-FDG-PET/CT Cohort Study

The retrospective study was approved by the ethics committee of the canton of Zurich. 8409 ¹⁸F-FDG-PET scans were reviewed of patients who had been hospitalized in the winter months (Nov-Feb) at University Hospital of Zürich between November 2009 and February 2015. Of those, 2789 patients (1105 female/1684 male; mean age 60.0 ± 14.8 years; mean BMI 24.5 ± 4.9 kg/m²) were identified who had been hospitalized up to 12 months prior to the scan (median time to PET: 4.7 months) and had electronic patient files available. All scans were manually reviewed by specialized physicians for presence of active BAT, which was graded using a previously published anatomical system (Becker et al., 2016). Electronic patient files were searched for administered medication of the class of statins. Statistical analysis was performed with R version 3.4.4. The formula for the general linear model was 'BAT-Grade'[0-3] ~ Statin[binary] * age * BMI * sex. Step-wise model selection was performed with the function *stepAIC* from the package



MASS version 7.3-50. The according scatterplot was created with the package *ggplot2* version 2.2.1. Both males and females were included in the analysis, however, statin use was significantly associated with BAT inactivity even after adjustment for sex, age and BMI (Table S1).

Clinical Fluvastatin Study

The clinical study was approved by the ethics committee of the canton of Zurich. The study is registered under the [ClinicalTrials.gov](https://clinicaltrials.gov/ct2/show/study/NCT03189511) identifier NCT03189511, where the detailed study protocol can be accessed. In short, 16 healthy male Caucasian volunteers with a BMI of 19-27 kg/m² (23.1±1.7 kg/m²) and between 18 to 50 years of age (25.1±1.4 years) were included. We have focused on males in a non-overweight BMI range to reduce the variability of the observed effects. In female volunteers a potential variability for the menstrual cycle would have to be accounted for. In addition, the inclusion of female volunteers would include the need for negative pregnancy tests and safe contraception during the study period, since this study involved ionizing radiation. For a power of 80%, at a type one error level of 5% a minimal sample size of 10 participants is needed to detect a significant difference (50% drop in activity). In order to account for heterogeneity of the sample and dropouts, we recruited 16 participants. All participants were first screened by indirect calorimetry for an increase in cold-induced thermogenesis of at least 5% of resting energy expenditure at warm conditions. The schedule of both study visits spaced 14 days apart was identical: The volunteer arrived in a fasted state for oral administration of 200mg Mirabegron (Betmiga, Astellas Pharma, Switzerland). Volunteers were given standard hospital gowns for the entire duration of the study visit. After 90 minutes waiting time, standardized cold stimulation with water cooling pads (HiloTherm Clinic; 10°C setting) was commenced lasting another 120 minutes. Skin and room temperatures were monitored with surface temperature probes. No shivering was reported by any of the participants. At the end of the cooling period the participant was transferred to the PET/MR table (SIGMA PET/MR, GE Healthcare, Waukesha, WI, USA). The scan procedure was performed by experienced technicians and were compliant with EANM standards. Low blood sugar (<7 mM) was confirmed with a finger prick blood test. For the scan, the participants received 75 MBq of ¹⁸F-DG intravenously via the antecubital vein, with immediately following partial-body (vertex to mid-torso) PET/MR scan for 50±10 minutes. All scans were performed in the afternoon (between 2-4 pm). SUVlean was calculated using the Janmahasatian formulation (Janmahasatian et al., 2005). After the scan, the location of metabolically active brown fat in the supraclavicular region was determined qualitatively on the PET/MR images and targeted by an ultrasound-guided coaxial core-needle (18G size, 10mm core length, BARD Mission) biopsy under local anesthesia. Samples (~1-2 mg) were immediately frozen in dry ice. Volunteers remained in a fasted state until after the biopsy. At the end of the 1st visit, volunteers received the study medication and instructions for the intake over the next 14 days, until the 2nd study visit (2x40mg fluvastatin daily per os). The core-needle biopsy on the second visit was performed through the same access point as the first one, with the same anatomical landmarks with the help of a screenshot of the first biopsy (representative example in Figures S7A-S7D), and with the same depth of needle insertion (if possible), in order to ensure sampling as close as possible to the location of the first biopsy. Two volunteers were excluded from the analysis, one due to non-compliance (no change in cholesterol levels) and in the second we failed to obtain sufficient amount of tissue for the gene expression analysis.

Mouse Experiments

All animal procedures were approved by the Veterinary office of the Canton of Zürich. Sample size was determined based on previous experiments in our lab and similar studies reported in the literature. All mice used for the experiments were male, housed 3-4 littermates per cage in individually ventilated cages at standard housing conditions (22°C, 12 h reversed light/dark cycle, dark phase starting at 7am), with *ad libitum* access to chow (18 % proteins, 4.5 % fibers, 4.5 % fat, 6.3 % ashes, Provimi Kliba SA) and water. Health status of all mouse lines were regularly monitored according to FELASA guidelines. 12-14 weeks old male C57Bl6 mice (Charles River) were subjected to statins (10 mg/kg/day) or GGTI-298 (1 mg/kg/day) treatment for 6 consecutive days by oral gavage or intraperitoneal injection, respectively. Mice were kept for 2 days at 22°C, followed by 4 days of cold exposure at 8°C, or 2 days of CL-316.243 injection (0.1 mg/kg/day) to activate thermogenesis. GGOH (50 mg/kg/day) was administered to 10-week old C57Bl6 mice housed at 22°C for 4 consecutive days by IP injection. Neither acute cold exposure nor CL-316.243 was applied to investigate the effect of GGOH on browning of iWAT.

Pggt1b^{fl/fl} mice (Sjogren et al., 2007) were crossed to *Adip-CreERT2* mice (Rosenwald et al., 2013) to achieve inducible adipocyte-specific ablation of GGTase I. At 12 weeks of age, recombination of the floxed allele was induced by oral tamoxifen gavage (2mg/day in sunflower oil, Sigma-Aldrich). To induce thermogenesis, mice were injected with CL-316.243 (IP 0.1 mg/kg/day) or exposed to 8°C. All studies were performed on 12-14 week old male mice. In high fat diet cohorts (23.9 % proteins, 4.9 % fibers, 35 % fat, 5.0 % ashes, Provimi Kliba SA), the feeding regimen (8 weeks) was initiated at age of 6 weeks.

The *Ucp1*-tracer mouse line (*Ucp1-CreERT2* x *LoxP-Red*) was previously described (Rosenwald et al., 2013). To investigate the effect of statins on the number of UCP1⁺ cells, 14-week old male mice were treated with fluvastatin (10 mg/kg/day) by IP injection for 6 consecutive days. First two days, mice were kept at 22°C to achieve inhibition of mevalonate pathway before they were moved to 8°C (days 3-6). To induce *CreERT2* activity, mice were injected with tamoxifen (day 3-4, 2 mg/day).

Cell Culture – hMADS Cells

hMADS cells originating from the prepubic fat pad of a 4-month-old male were kindly provided by Dr. Amri and cultured as previously described (Elabd et al., 2009). Briefly, cells (between passage 14 and 16) were grown in low glucose DMEM supplemented with 15mM HEPES, 10% FBS, 2mM L-glutamine, 1% Penicillin/Streptomycin and 2.5ng/ml recombinant human FGF-2 (Peprotech) in



normoxic humidified cell culture incubator (5% CO₂ and 37°C). The medium was changed every other day and FGF-2 was omitted after cells reached confluence. Differentiation of 48 hours post-confluent cells was induced (day 0) by adipogenic medium (DMEM/Ham's F12 media (Lonza) containing 10 μg/ml Transferrin, 10 nM insulin and 0.2 nM triiodothyronine) supplemented with 1 μM dexamethasone and 500 μM isobutyl methylxanthine (IBMX) and from day 2 to 9, cells were cultured in adipogenic medium containing 100 nM rosiglitazone. All compounds were obtained from Sigma-Aldrich (specification in [Key Resources Table](#)), except for rosiglitazone (Adipogen). Cells were kept in culture until day 18 in absence of rosiglitazone to obtain mature white adipocytes. To obtain brown adipocytes, cells were exposed to an additional rosiglitazone pulse between days 14 - 18. To investigate the effect of pharmacological agents on browning of white adipocytes, treatment was performed between day 14 and 18 in combination with rosiglitazone. To knockdown candidate genes, 50 nM siRNA pools (Microsynth) were delivered into mature adipocytes on day 13 using Lipofectamine RNAiMAX (Invitrogen) according to manufacturer's instructions. A control siRNA pool was used in all experiments as a control. To make sure that the observed phenotypes are not due to off-target effects of the control siRNA pool, we validated the critical experiments using scrambled siRNA pools ([Figures S7E–S7J](#)). All siRNA sequences and corresponding knockdown efficiencies are listed in [Table S3](#). After 24 hours, transfection medium was replaced by fresh adipogenic medium containing 100 nM rosiglitazone. Adipocytes were cultured until day 18, when cellular respiration was determined or cells were harvested for RNA and protein analysis. All cell lines used were regularly tested negative for mycoplasma contamination throughout the whole duration of this study.

Cell Culture – Immortalized Murine Brown Adipocytes

Preadipocytes isolated from the iBAT stromal-vascular fraction of late fetal and newborn C57Bl/6 mice (both genders) and immortalized by introducing the SV40 antigen were kindly provided by Prof. Klein ([Klein et al., 2002](#)). Preadipocytes (between passage 4 and 6) were grown on collagen-coated plates in DMEM containing 10% FBS and 1% Pen/Strep (Gibco) in normoxic humidified cell culture incubator (5% CO₂ and 37°C). After reaching confluence, adipogenic differentiation was induced by supplementing the medium with IBMX (500 μM), dexamethasone (1 μM), insulin (20 nM), T3 (1 nM) and indomethacin (125 μM). All compounds were obtained from Sigma-Aldrich (specification in [Key Resources Table](#)). After 48 hours, medium was replaced by fresh maintenance medium containing (insulin and T3), which was replaced every other day. For siRNA-mediated knockdown, differentiating adipocytes (day 5) were trypsinized, counted and replated on collagen-coated multi-well plates to reduce cell density. Cells were allowed to attach, recover and mature before siRNA transfection (100 nM siRNA pools, day 6) or treatment with different compounds (day 7). Cells were harvested on day 9 for RNA and protein analysis, or cellular respiration measurements. All siRNA sequences are listed in [Table S3](#). All cell lines used were regularly tested negative for mycoplasma contamination throughout the whole duration of this study.

METHOD DETAILS

Intraperitoneal Glucose Tolerance Test

To measure glucose tolerance, mice were fasted for 6 hours by removal to a clean cage without food at the end of the dark (active) phase. Mice were weighed and after fasting glucose levels were obtained from a small tail clip using a standard glucometer (ACCU-CHEK Aviva, Roche), D-glucose (Sigma-Aldrich) was injected intraperitoneally at dose 1 mg/g body weight. Blood glucose levels were measured 15, 30, 60 and 120 minutes after glucose injection using glucometer.

Body Composition Measurement

Live mice body composition was measured with a magnetic resonance imaging technique (EchoMRI 130, Echo Medical Systems). Mice were fasted for 4 hours before measurement. Fat and lean mass was analyzed using Echo MRI 14 software.

Indirect Calorimetry

Indirect calorimetry measurements were performed with the Phenomaster (TSE Systems) according to the manufacturer's guidelines. O₂ and CO₂ levels were measured for 60s every 13 minutes continuously. Energy expenditure was calculated according to the manufacturer's guidelines. The respiratory quotient was estimated by calculating the ratio of CO₂ production to O₂ consumption. Animals were single-caged and acclimated to the metabolic cage for 48 hours prior metabolic recording. Locomotor activity, food and water intake were monitored throughout the whole measurement.

Tissue Harvest

Animals were euthanized singly in carbon dioxide atmosphere. All tissues were carefully dissected, weighed and snap frozen in liquid nitrogen until further processing. Popliteal lymph nodes were carefully removed from iWAT for all gene and protein expression analyses. For RNA and protein isolation, whole adipose tissue depot was homogenized.

Analysis of Preadipocyte Proliferation and Adipocyte Differentiation

To study the effect of statins on preadipocyte proliferation, immortalized murine preadipocytes were plated on 96-well Operetta plates at low density (2,000 cells/cm²) and allowed to attach and recover for 12 hours. Cells were treated for 48h with atorvastatin, cerivastatin, simvastatin, fluvastatin and rosuvastatin (all statins were purchased from Sigma-Aldrich) at two different concentrations (1 and 10 μM). Cells were fixed with 4% formaldehyde for 20 min and washed 3 times with PBS. Immediately after washing, cells were



stained with Hoechst (Cell Signaling) and Syto60 (Invitrogen), to visualize nuclei and cytosol, respectively. Differentiated adipocytes at day 9 were used for differentiation analysis. Briefly, cells in 96-well optical plate, exposed to statins for the last 48 hours (day 7–9), were fixed with 4% formaldehyde for 20 min and washed 3 times with PBS. Immediately after washing, cells were stained with Bodipy (Invitrogen) for lipid droplets and Hoechst (Cell Signaling) for nuclei. Twenty-five pictures per well were taken with an automated microscope imaging system (Operetta, PerkinElmer). Pictures were analyzed using the Harmony software. In differentiation assay, all cells (Hoechst stained nuclei) surrounded by lipid droplets were considered adipocytes. In proliferation assay, nuclei were counted.

Cellular Respiration

For measurement of cellular respiration, immortalized murine brown adipocytes were cultured on collagen-coated cell culture dishes. Differentiating adipocytes were trypsinized and replated on day 5 at density 7,000 cells per well and allowed to recover for 48 hours before treatment. Since hMADS cells grow in a monolayer, they were differentiated directly on collagen-coated 96-well Seahorse microplates. On the day of experiment, adipogenic medium was replaced with XF Assay Medium (pH 7.4, Seahorse Bioscience) supplemented with glucose (1g/L; Sigma-Aldrich), 2mM sodium pyruvate (Invitrogen) and 2mM L-glutamine (Invitrogen). The oxygen consumption rate (OCR) was measured using the Extracellular flux analyzer XF96 (Agilent). Test compounds were sequentially injected to obtain following concentrations: 1 μ g/ml Oligomycin, 1 μ M isoproterenol, (0.5mM dibutyl cAMP for hMADS), 1 μ g/ml FCCP, 3 μ M Rotenone with 2 μ g/ml Antimycin A. All compounds were purchased from Sigma-Aldrich, except for Oligomycin (Adipogen). OCR levels (pmol/min) were normalized to protein amount per well (μ g protein). Non-mitochondrial respiration was subtracted to obtain basal, basal uncoupled, stimulated uncoupled and maximal mitochondrial respiration.

Fatty Acid Uptake

Fatty acid uptake was measured by a fluorescence-based assay utilizing BODIPY dodecanoic acid fluorescent fatty acid analogue (QBTTM Fatty Acid Uptake Assay kit, Molecular Devices, USA). Briefly, the cells were fasted for 2 hours in serum free culture media prior analysis. Isoproterenol (1 μ M; Sigma-Aldrich) was added and plate was incubated for another 30 minutes at 37 $^{\circ}$ C in humidified CO₂ incubator. After stimulation, the cells were loaded with fatty acid analogue according to manufacturer's instructions and uptake kinetics was measured every 30s for 30 min with λ_{ex} = 485 nm and λ_{em} = 515 nm using the microplate reader Synergy MX and Gen5 software (BioTek). Linear phase of fluorescence signal corresponding to fatty acid uptake was used for calculation after normalization to background fluorescence and protein content. The data are presented as relative fluorescence per μ g protein per minute.

Lipolysis

Lipolytic activity of mature brown adipocytes was determined as glycerol release into culture media. Briefly, the cells were serum starved for 2 hours in low-glucose medium (Gibco) prior to the analysis. Isoproterenol (1 μ M; Sigma-Aldrich) was added and plate was incubated for another 30 minutes at 37 $^{\circ}$ C in humidified CO₂ incubator. Media were collected and spun down to pellet detached cells. Glycerol was assessed in the supernatant using the Glycerol reagent (Sigma-Aldrich) according to manufacturer's instructions and normalized to protein content in the well. Absorbance (at 540 nm) was measured using the microplate reader Synergy MX and Gen5 software (BioTek).

Glucose Uptake

Glucose uptake in mature brown adipocytes was determined as the amount of ¹⁴C-2-deoxyglucose taken up by cells per minute. Briefly, cells were starved in low glucose DMEM (Gibco) for 2 hours. Starved cells were washed twice warm PBS and incubated at 37 $^{\circ}$ C in low glucose DMEM for additional 50 minutes. Isoproterenol (1 μ M) was added to assess isoproterenol stimulated glucose uptake. Cells were washed twice with fresh Krebs–Ringer–HEPES buffer (50 mM HEPES, 137 mM NaCl, 4.7 mM KCl, 1.85 mM CaCl₂, 1.3 mM MgSO₄, pH 7.4) containing 0.1% fatty acid-free BSA and incubated in presence of ¹⁴C-2-deoxyglucose (0.1 μ Ci/well; PerkinElmer) for exactly 10 minutes. Cells were washed 4 times with ice cold PBS and lysed in 0.1M NaOH. Lysates were mixed with 3 ml scintillation cocktail and radioactivity was quantified in disintegrations per minute (DPM) using the Liquid Scintillation Analyzer TRI-CARB 2000CA (PerkinElmer) and normalized to protein content in the corresponding well.

Ketone Bodies Measurement

Levels of ketone bodies in cell lysate and cell-conditioned media were determined using a commercially available kit according to manufacturer's instructions (Wako Chemicals) and normalized to protein amount.

Ucp1 Promoter Activity

Ucp1 promoter activity was determined in a murine immortalized brown adipocytes expressing Luciferase under *Ucp1* promoter. Preadipocytes were cultured on collagen-coated plates in DMEM containing 10% FBS and 1% Pen/Strep (Gibco). Adipogenic differentiation was induced by supplementing the medium with IBMX (500 μ M), dexamethasone (1 μ M), insulin (20nM), T3 (1nM) and indomethacin (125 μ M) 2 days after reaching confluence. After 48 hours, medium was replaced by fresh maintenance medium containing 20nM insulin, 1nM T3 and 1 μ M 4-hydroxytamoxifen (to induce Cre), which was replaced every other day. All compounds were purchased from Sigma-Aldrich. The cells were treated with different concentration of simvastatin from day 7 for 48 hours. On day 9, cells were washed with PBS, lysed in passive lysis buffer and luciferase activity was measured using Dual Luciferase Reporter Assay (Promega) on Synergy MX (BioTek) and normalized to protein content.

e6 Cell Metabolism 29, 901–916.e1–e8, April 2, 2019



RNA Extraction, cDNA Synthesis, Quantitative RT-PCR

Total RNA was extracted from tissues or cells using Trizol reagent (Invitrogen) according to the manufacturer's instructions. DNase treatment (NEB BioLabs) was included to remove traces of genomic DNA. Reverse transcription was performed to generate cDNA library by using the High Capacity cDNA Reverse transcription kit (Applied Biosystems), with 1 μ g of RNA. Quantitative PCR was performed on a ViiA7 (Applied Biosystems) and relative mRNA concentrations normalized to the expression of *RPL13A1* (human fat samples) or *TBP* (cell culture) were calculated by the $\Delta\Delta$ Ct method. Primer sequences are found in [Table S4](#).

Protein Extraction and Western Blot

Adipose tissue samples and *in vitro* differentiated adipocytes were homogenized in RIPA buffer (50mM Tris-HCl pH 7.4, 150mM NaCl, 2mM EDTA, 1.0% Triton X100, 0.5% sodium deoxycholate) supplemented with protease (Complete, Roche) and phosphatase (Halt phosphatase inhibitor cocktail, ThermoFisher) inhibitor cocktails. Lysates were cleared by centrifugation at 12,000g for 15 minutes at 4°C. Protein concentration of the supernatants was determined by DC Protein Assay (Bio-Rad). Equal amount of proteins (5–20 μ g) were separated on 12% SDS-polyacrylamide gel, transferred to a nitrocellulose membrane (Bio-Rad) and stained for UCP1 (1:1000, Pierce), phospho-HSL (Ser660; 1:1000, Cell Signaling), total HSL, phospho-CREB (Ser133; 1:1000, Cell Signaling), total CREB (1:1000, Cell Signaling), phospho-AKT (Thr308; 1:1000, Cell Signaling), AKT (1:1000, Cell Signaling), HMGCS2 (1:1000, Abcam), HMGR (1:1000, Abcam), cleaved Caspase 3 (1:1000, Cell Signaling), GAPDH (1:1000, Cell Signaling), Na⁺/K⁺ ATPase (1:10,000, Abcam), PPAR γ (1:1000, Cell Signaling), RHOA (1:1000, Cell Signaling), RHO (1:1000, Cell Signaling), CDC42 (1:1000, Cell Signaling), RAP1A/B (1:1000, Cell Signaling), RAC1/2/3 (1:1000, Cell Signaling), PGGT1B (1:1000, Abcam), RABGGTB (1:1000, Abcam), YAP1/TAZ (1:1000, Cell Signaling), HSP90 (1:1000, Cell Signaling) and γ -tubulin (1:10,000, Sigma-Aldrich). Signal of the HRP-conjugated secondary antibodies (1:10,000, Calbiochem) was visualized by the Image Quant system (GE Healthcare Life Sciences). All antibodies are listed in the [Key Resources Table](#).

Click Chemistry

To identify proteins incorporating the geranylgeranyl group, mature immortalized brown adipocytes were treated for 24 h with simvastatin to block mevalonate pathway and endogenous GGPP production. Maintenance medium was supplemented with GGOH (Abcam) or geranylgeranyl alcohol azide (Invitrogen) and cells were allowed to incorporate the regular/labeled isoprenoid group for 24 hours. Cells were washed 3 times with PBS, scraped in ice-cold RIPA buffer and extracted proteins were precipitated using methanol/chloroform. Proteins were resuspended in 0.1M Tris-HCl (pH 8.0) containing 1% SDS. The click reaction was performed using the Click labeling kit (Invitrogen) according to manufacturer's instructions. Biotin-alkyne was used as substrate for this reaction. Proteins were precipitated and washed to remove unbound biotin, dissolved in Laemmli buffer, heat denatured for 10 minutes at 70°C and separated on PAGE. Proteins were transferred to nitrocellulose membrane and geranylgeranyl-biotin complexes were detected using Streptavidine-HRP (Cell Signaling).

Subcellular Fractionation

In order to analyze subcellular distribution of small GTP-binding proteins, cells were fractionated using differential centrifugation. Mature adipocytes cultured on P10 dishes were treated with statins or GGTI-298 inhibitor, washed 3 times with ice-cold PBS and scraped in fractionation buffer (250mM Sucrose, 20mM HEPES (pH 7.4), 10mM KCl, 1.5mM MgCl₂, 1mM EDTA, 1mM EGTA) supplemented with 1mM DTT (Sigma-Aldrich) protease (Complete, Roche) and phosphatase (Halt phosphatase inhibitor cocktail, Thermo Fisher) inhibitors cocktails. Cells were passed through a 25 gauge needle 10 times and incubated on ice for 20 min. In the first centrifugation step (500g/5min/4°C) nuclei were pelleted. Supernatant containing cytosol, membranes and organelles was transferred into a clean Eppendorf tube and centrifuged (10,000g/5min/4°C) to pellet mitochondria and other organelles. Supernatant containing cytosol and membranes was transferred into an ultracentrifugation tube and membranes were pelleted by ultracentrifugation (100,000g/60min/4°C; Optima MAX-XP, Beckman Coulter). Supernatant was saved as cytosolic fraction. After washing the membrane pellet twice with fresh fractionation buffer, pellet containing membranes was resuspended in ice-cold RIPA buffer.

F-actin Staining

F-actin was stained in both cell lines using Phalloidin-iFluor 488 Reagent (Abcam). Cells were treated with statins for 48 hours, washed with PBS and fixed 20 minutes with 4% Formaldehyde (Sigma-Aldrich). Fixed cells were permeabilized for 5 minutes using 0.1% Triton and washed 3 times with PBS. F-actin fibers were stained for 1 hour with Phalloidin dye diluted 1:1000 in PBS with 0.1% BSA (Sigma-Aldrich). Nuclei were stained in parallel using Hoechst (Cell Signaling). After cells were washed 3 times with PBS, pictures were obtained using the automated Operetta imaging system (PerkinElmer).

RNA Sequencing, Mapping and Analysis

RNA extracted from brown and white adipose tissue biopsies was quality checked by TapeStation (Agilent). All samples had a RIN value of greater than 8. For the preparation of libraries the TruSeq mRNA sample preparation kit (Illumina) was used. Sequencing was performed as 50 bp, single reads and 7 bases index read on an Illumina HiSeq2000 instrument. Approximately 20–30 million reads per sample were obtained. The raw reads were first cleaned by removing adapter sequences, trimming low quality ends, and filtering reads with low quality (phred quality <20). Sequence alignment of the resulting high-quality reads to the human genome (build



GRCh38) and quantification of gene level expression was carried out using RSEM (version 1.2.18). To detect differentially expressed genes, we applied a count based negative binomial model implemented in the software package edgeR (R-version 3.1.2, edgeR 3.8.5). The gene-wise dispersions were estimated by conditional maximum likelihood and an empirical Bayes procedure was used to shrink the dispersions towards a consensus value. The differential expression was assessed using an exact test adapted for over-dispersed data. The genes were filtered for significant differential expression using an adjusted P-value cutoff at 0.05 (after Benjamini–Hochberg multiple testing correction).

Quantification of Cre Recombination in Mouse Tissues

Genomic DNA was prepared by following protocol. The tissue was crushed in a Thermolyser LT (Qiagen) in 1 ml 50mM NaOH, 250 μ l of 1 M Tris-HCl was added to neutralize the tissue lysate. The samples were centrifuged and the supernatant was diluted in MQ water. Quantification of the number of recombined LoxP-Red and non-recombined *ApoB* genomic loci copies was performed by qPCR. Absolute standard curves were prepared from synthesized pUC57recloxPRed-ApoB plasmid. Reactions were performed with following primers at final concentration 250 nM and Fast SYBR Green master mix (Applied Biosystems). Recombined ^{fl}stop^{fl} tdRFP: FW GCGCATGAACTCTTTGATGAC, RV TCGCGGTTGAGGACAAACTC; *ApoB*: FW GTCCAGGTTGAATCACGGGT, RV AGGATCCTGCAAGGCAAGC.

Metabolomic Analysis

For metabolomic analysis, tissue samples were weighed and homogenized in 10 volumes of extraction solvent, acetonitrile: methanol: water (40:40:20) pre-chilled to -20°C. All samples were kept on dry ice during processing. Homogenates were briefly spun down and supernatants were subjected to metabolomic analysis by flow-injection – time of flight mass spectrometry (Führer et al., 2011) on an Agilent 6550 QTOF instrument. Metabolites were identified by matching measured and theoretical m/z within a tolerance of 0.001 amu.

QUANTIFICATION AND STATISTICAL ANALYSIS

For *in vivo* studies, littermates randomly assigned to treatment groups were used for all experiments. Sample sizes were determined on the basis of previous experiments using similar methodologies. The animal numbers used for all experiments are indicated in the corresponding figure legends. In the clinical transcriptomic study, only volunteers with active BAT (enrichment of brown adipocyte marker genes in BAT compared to WAT) were included. In the clinical fluvastatin trial, 2 volunteers were excluded from the analysis, one due to non-compliance (no change in cholesterol levels) and in the second we failed to obtain sufficient amount of tissue for the gene expression analysis. All animals were included in statistical analyses, and the investigators were not blinded. All cell culture experiments were performed with 2-3 technical replicates for RNA and protein analysis, 5-6 replicates for measurement of cellular respiration and *Ucp1* promoter activity, and independently reproduced 2-4 times. No Results are reported as mean \pm SEM for mouse and cell culture data and mean \pm SD for the clinical trial. Two-tailed unpaired Student's T-test was applied on comparison of two groups. In case of non-normal data distribution, a non-parametric Wilcoxon test was performed. ANOVA was applied on comparisons of multiple groups. Pearson's correlation coefficient was calculated and all statistical analyses were performed using GraphPad Prism 7 and R version 3.4.4. Statistical differences are indicated as * for $P < 0.05$, ** for $P < 0.01$ and *** for $P < 0.001$.

DATA AND SOFTWARE AVAILABILITY

The accession number for the RNA sequencing data from the clinical transcriptome study reported in this paper is The European Nucleotide Archive: PRJEB23275.

Antioxidants protect against diabetes by improving glucose homeostasis in mouse models of inducible insulin resistance and obesity

Leon G. Straub, Vissarion Efthymiou, Gerald Grandl, Miroslav Balaz, Tenagne Delessa Challa, Luca Truscello, Carla Horvath, Caroline Moser, Yael Rachamin, Myrtha Arnold, Wenfei Sun, Salvatore Modica, Christian Wolfrum

Published in Diabetologia, 2019

Contribution:

Caroline Moser assisted in the hyperinsulinemic euglycemic clamp study and in the experiments for the adipose tissue quantification.

This article is a reprint of the original published article with kind permission of the publisher, Springer Nature. Supplementary material is available online under:

<https://doi.org/10.1007/s00125-019-4937-7>

Diabetologia (2019) 62:2094–2105
<https://doi.org/10.1007/s00125-019-4937-7>

ARTICLE



Antioxidants protect against diabetes by improving glucose homeostasis in mouse models of inducible insulin resistance and obesity

Leon G. Straub^{1,2} · Vissarion Efthymiou¹ · Gerald Grandl^{1,3} · Miroslav Balaz¹ · Tenagne Delessa Challa¹ · Luca Truscello¹ · Carla Horvath¹ · Caroline Moser¹ · Yael Rachamin¹ · Myrtha Arnold¹ · Wenfei Sun¹ · Salvatore Modica¹ · Christian Wolfrum¹

Received: 15 February 2019 / Accepted: 16 May 2019 / Published online: 15 July 2019
© The Author(s) 2019

Abstract

Aims/hypothesis In the context of diabetes, the health benefit of antioxidant treatment has been widely debated. In this study, we investigated the effect of antioxidant treatment during the development of insulin resistance and hyperphagia in obesity and partial lipodystrophy.

Methods We studied the role of antioxidants in the regulation of insulin resistance using the tamoxifen-inducible fat-specific insulin receptor knockout (iFIRKO) mouse model, which allowed us to analyse the antioxidant's effect in a time-resolved manner. In addition, leptin-deficient *ob/ob* mice were used as a hyperphagic, chronically obese and diabetic mouse model to validate the beneficial effect of antioxidants on metabolism.

Results Acute induction of insulin receptor knockout in adipocytes changed the substrate preference to fat before induction of a diabetic phenotype including hyperinsulinaemia and hyperglycaemia. In healthy chow-fed animals as well as in morbidly obese mice, this diabetic phase could be reversed within a few weeks. Furthermore, after the induction of insulin receptor knockout in mature adipocytes, iFIRKO mice were protected from subsequent obesity development through high-fat diet feeding. By genetic tracing we show that the persistent fat mass loss in mice after insulin receptor knockout in adipocytes is not caused by the depletion of adipocytes. Treatment of iFIRKO mice with antioxidants postponed and reduced hyperglycaemia by increasing insulin sensitivity. In *ob/ob* mice, antioxidants rescued both hyperglycaemia and hyperphagia.

Conclusions/interpretation We conclude that fat mass reduction through insulin resistance in adipocytes is not reversible. Furthermore, it seems unlikely that adipocytes undergo apoptosis during the process of extreme lipolysis, as a consequence of insulin resistance. Antioxidants have a beneficial health effect not only during the acute phase of diabetes development, but also in a temporary fashion once chronic obesity and diabetes have been established.

Keywords Acetovanillone · Adipocyte · Adipocyte quantification · Adipocyte-specific · Adipose tissue · Antioxidants · Apocynin · CreERT2 · Diet-induced obesity · Fat · Hyperglycaemia · Hyperinsulinaemic–euglycaemic clamp · Hyperphagia · iFIRKO · Insulin receptor · Insulin resistance · Leptin deficiency · Lipolysis · *N*-acetylcysteine · *ob/ob* · Obesity resistance · Polydipsia obesity · Tamoxifen · Type 2 diabetes

Leon G. Straub and Vissarion Efthymiou contributed equally to this study.

Electronic supplementary material The online version of this article (<https://doi.org/10.1007/s00125-019-4937-7>) contains peer-reviewed but unedited supplementary material, which is available to authorised users.

✉ Christian Wolfrum
christian-wolfrum@ethz.ch

¹ Laboratory of Translational Nutrition Biology, Institute of Food, Nutrition and Health, Swiss Federal Institute of Technology, ETH Zürich, CH-8603 Schwerzenbach, Switzerland

² Touchstone Diabetes Center, UT Southwestern Medical Center, Dallas, TX, USA

³ Institute for Diabetes and Obesity, Helmholtz Diabetes Center, Helmholtz Zentrum München, Neuherberg, Germany

Springer

Research in context

What is already known about this subject?

- Insulin resistance in adipocytes causes hyperglycaemia
- Antioxidants are proposed to reduce insulin resistance in adipose tissue and thereby inhibit hyperglycaemia

What is the key question?

- What is the effect of antioxidants during the acute development of type 2 diabetes that is triggered by insulin resistance in adipocytes?

What are the new findings?

- The extreme lipolysis caused by insulin resistance in adipocytes does not reduce adipocyte number when hyperglycaemia is at a high level
- Hyperglycaemia caused by adipocyte-specific insulin resistance is reversible, but adipose tissue mass loss is irreversible, which we found to be the case even in a mouse model of high-fat-diet-induced obesity
- Antioxidants can have a beneficial health effect in mouse models of acute and chronic hyperglycaemia by regulating food intake

How might this impact on clinical practice in the foreseeable future?

- This reported effect of antioxidants suggests that treating oxidative stress during the development of type 2 diabetes might be considered as a supplemental option to existing therapies

Abbreviations

ApoB	Apolipoprotein B
epiWAT	Epididymal white adipose tissue
HFD	High-fat diet
iBAT	Interscapular brown adipose tissue
iFIRKO	Inducible fat-specific insulin receptor knockout
ingWAT	Inguinal white adipose tissue
IR	Insulin receptor
NAc	<i>N</i> -acetylcysteine
qPCR	Quantitative PCR
RER	Respiratory exchange ratio

Introduction

Type 2 diabetes is defined as a metabolic disorder characterised by systemic insulin resistance which results in hyperglycaemia. Epidemiological studies identified high BMI as a risk factor for developing diabetes [1]. Insulin resistance of adipose tissue leads to increased plasma NEFA levels through aberrant regulation of lipolysis. In humans, lipoatrophy was shown to drive systemic insulin resistance [2], while disruption of the insulin signalling cascade in adipocytes in mice causes lipoatrophy and promotes the development of type 2 diabetes [3, 4]. Thus, it has been proposed that elevated NEFA concentrations in blood are the primary cause of insulin resistance through lipid accumulation in non-adipose tissues [5]. In recent years, a new generation of

genetic insulin receptor (IR) knockout mouse models enabled researchers to establish the causal link between adipose tissue insulin resistance and the development of type 2 diabetes [3, 6]. The tamoxifen-inducible fat-specific IR knockout (iFIRKO) mouse model established for the first time a causal relationship between insulin resistance in adipocytes and early stages of type 2 diabetes development [6]. Interestingly, IR ablation in adipocytes not only promotes lipolysis but also reduces blood leptin concentrations, which has been suggested to cause the hyperglycaemic phenotype of iFIRKO mice. Leptin informs the brain on the body's energy reserves [7]. Low blood leptin concentrations indicate imminent depletion of fat stores and trigger responses that aim at acquiring and preserving energy [8]. In consequence, congenital leptin deficiency causes overeating which leads to obesity in early life in humans [9, 10], as well as in mice [11]. Another factor reported to contribute to insulin resistance in the adipose tissue is oxidative stress [12–14]; however, this concept has been widely criticised for the lack of evidence and negative outcomes in both human correlative food supplementation studies and mouse experiments [15].

Methods

Animal work *Adipoq*-CreERT2 animals were created by bacterial artificial chromosome (BAC) cloning of CreERT2 into

the RPCI-24-69M4 BAC vector (BACPAC, Oakland, CA, USA) and pronuclear injection. iFIRKO mice were created by breeding *Adipoq-CreERT2* with *IR^{f1/f1}* mice (B6.129S4(FVB)-*Insr^{tm1Khn}/J*) [16], which had been backcrossed to C57BL6 mice for 10 generations. Breeding with *Rosa26-tdRFP* mice (*Gt(ROSA)26Sor^{tm1Hjf}*) [17] resulted in the iFIRKO-chaser mouse (loxPStoploxP-tdRFP transgene). Male mice of 10–14 weeks of age were used for all experiments and unless stated otherwise were housed at 23°C on an inverted light cycle. *ob/ob* (B6.Cg-*Lep^{ob}/J*) mice were purchased from Jackson Laboratory (Bar Harbor, ME, USA). Breeding and experiments were performed in the SLA-Schwerzenbach animal facility of ETH Zurich. Feeding a high-fat diet (HFD) with 60% of energy derived from fat (purified diet #2127; Kliba-Nafag, Kaiseraugst, Switzerland) induced obesity. CreERT2 activity was induced by gavage of 2 mg tamoxifen (Sigma-Aldrich, St. Louis, MO, USA) per mouse in 100 µl sunflower oil for 3 consecutive days. The antioxidants *N*-acetylcysteine (NAC) and apocynin (also known as acetovanillone) were dissolved in drinking water at concentrations of 15 mmol/l and 40 mmol/l, respectively. Body composition was measured with NMR scanning (EchoMRI, Houston, TX, USA). GTT and ITT were performed after a 4–5 h fast. Fasting blood glucose was measured from the tail vein with ACCU-Check Aviva Blood Glucose Meter System (Roche, Basel, Switzerland). Glucose solution (1 g glucose per kg body weight, in 0.9% NaCl, Braun, Kronberg, Germany) or insulin solution (0.6, 1, 1.5 or 2 U insulin Actrapid HM per kg body weight, Novo Nordisk [Bagsvaerd, Denmark], in 0.9% NaCl) was injected intraperitoneally. All experiments were performed according to national and institutional guidelines, which are in line with Animal Research: Reporting of In Vivo Experiments (ARRIVE) guidelines and the EU directive 2010/63/EU.

Indirect calorimetry Indirect calorimetry was performed with a metabolic cage system (PhenoMaster, TSE Systems, Bad Homburg, Germany). O₂ consumption ($\dot{V}O_2$) and CO₂ production ($\dot{V}CO_2$) were calculated using TSE PhenoMaster V5.6.5 with corresponding coefficients of 3.941 (CVO₂) and 1.106 (CVCO₂). Respiratory exchange ratio (RER) was calculated as the ratio of $\dot{V}CO_2$ to $\dot{V}O_2$. Mice were acclimated to the system for 24 h before measurements.

Blood plasma content measurement Insulin concentration was measured using the Mouse/Rat Insulin kit (Meso Scale Discovery, Rockville, MD, USA). NEFA levels were measured using the NEFA-C kit (Wako Chemicals, Neuss, Germany). Leptin concentrations were measured with the leptin Mouse/Rat ELISA (BioVendor, RD291001200R, Heidelberg, Germany) and T₄ concentrations with the T₄ ELISA kit (Invitrogen, EIAT4C, Carlsbad, CA, USA).

Hyperinsulinaemic–euglycaemic clamp Before the hyperinsulinaemic–euglycaemic clamp, mice were fasted for 5 h. The surgery as well as overall clamp procedure were performed as previously published [18].

Western blots IR-β subunit (Santa Cruz Biotechnology, #SC-711, Dallas, TX, USA) and Pan-Actin (Cell Signaling Technology, #8456, Danvers, MA, USA), were used in western blots. Band intensity was quantified using the ImageJ 1.52a function ‘Analyse→Measure’. The western blot protein band signal was calculated as ([integrated density of IR-β / integrated density of Pan-Actin] – background signal) normalised to the *IR^{f1/f1}* sample.

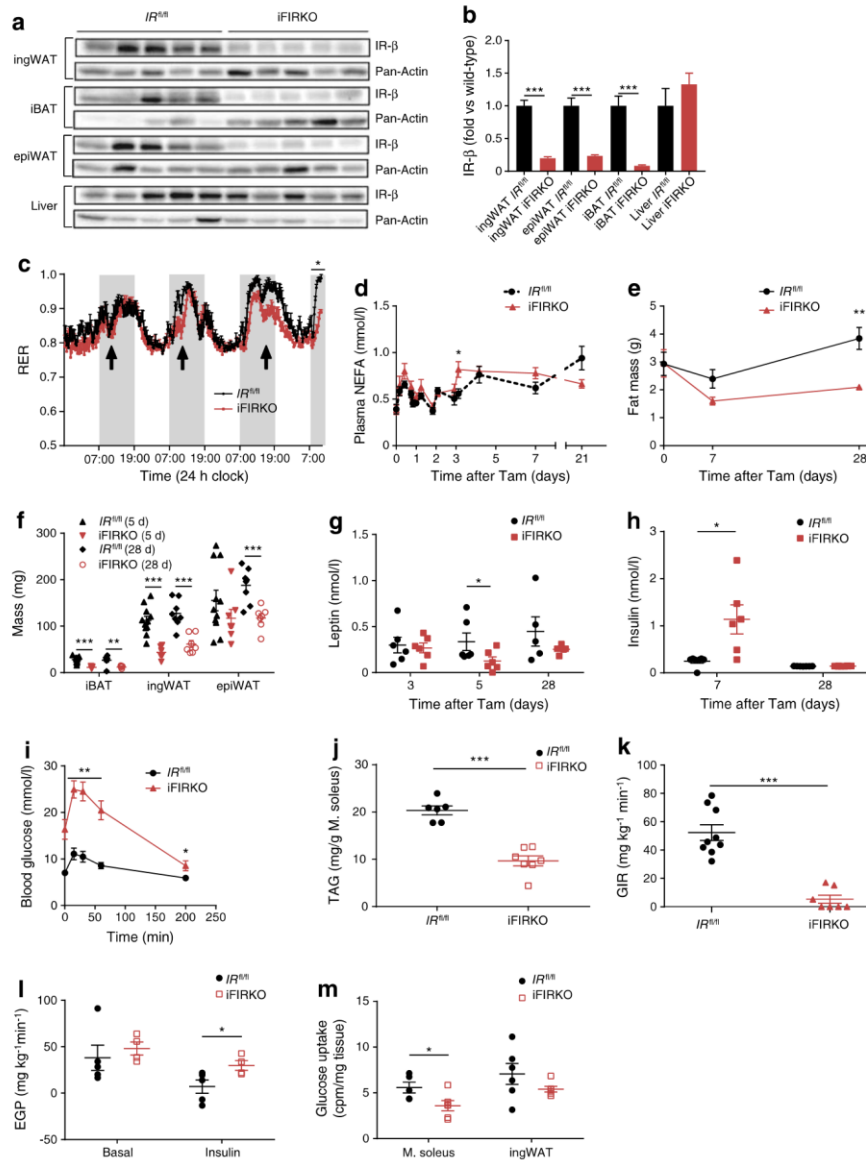
mRNA analysis Total RNA was isolated with TRIzol (Invitrogen, Carlsbad, CA, USA), then reverse-transcribed with the High Capacity cDNA Reverse Transcription kit (Applied Biosystems, Foster City, CA, USA). Sybr Green quantitative PCR (qPCR) was used (Thermo Fisher Scientific, Waltham, MA, USA). Primer sequences are listed in electronic supplementary material (ESM) Tables 1, 2. Gene expression was referenced to that of TATA-box binding protein (encoded by *Tbp*).

Quantification of Cre recombination in mouse tissues Tissue was homogenised in 1 ml of 50 mmol/l NaOH (Sigma-Aldrich) with Thermolyser LT (Qiagen, Hilden, Germany) and 250 µl of 1 mmol/l Tris/HCl (Sigma-Aldrich) was added to neutralise the pH. Samples were centrifuged twice at 12,000 g for 5 min and the aqueous phase was transferred to a fresh tube. To quantify labelled adipocytes, primers (ESM Table 2) were designed to identify recombined loxP sites in tandem red fluorescent protein (tdRFP) transgene (loxPStoploxP-tdRFP) [17], which reflects the amount of adiponectin-positive cells. Apolipoprotein B (ApoB) was used for total cells. Absolute recombined loci were quantified by quantitative PCR of genomic DNA using a standard curve generated from synthesised plasmid pUC57recloxPRFP-ApoB.

Statistical analysis All results are expressed as mean ± SEM; all graphics and statistical analyses were performed using GraphPad Prism 7. Statistical significance was calculated using multiple two-tailed unpaired Student’s *t* tests, or two-way ANOVA with Sidak’s multiple comparisons test. Statistical significance is indicated as: **p* < 0.05, ***p* < 0.01, ****p* < 0.001.

Results

iFIRKO mice show impaired glucose homeostasis In order to investigate the effect of adipose tissue insulin resistance on whole-body metabolism, we studied inducible adipocyte-



specific IR knockout mice, also called iFIRKO mice ($IR^{fl/fl} \times Adipoq-CreERT2$). One week after tamoxifen gavage, iFIRKO mice showed a marked reduction of IR-β protein

levels in adipose tissue depots (inguinal white adipose tissue [ingWAT], interscapular brown adipose tissue [iBAT] and epididymal white adipose tissue [epiWAT]), but not in liver

Fig. 1 Inducible fat-specific IR knockout first reduces RER then leads to hyperinsulinaemia that correlates with hypoleptinaemia and insulin resistance, before it reduces the mass of all adipose tissue depots. **(a)** Western blot of IR- β and Pan-Actin in adipose tissue and liver lysates ($n = 5$ for $IR^{fl/fl}$ and iFIRKO). **(b)** Quantification of western blot band intensity of IR- β normalised to Pan-Actin and expressed as fold vs wild-type ($IR^{fl/fl}$) in adipose tissue and liver lysates ($n = 5$ for $IR^{fl/fl}$ and iFIRKO). **(c)** Time course of RER ($\dot{V}CO_2/\dot{V}O_2$) during induction of IR knockout by tamoxifen (arrows indicate tamoxifen gavage) ($n = 5$ for $IR^{fl/fl}$; $n = 6$ for iFIRKO). **(d)** Time course of NEFA concentration in mice fed ad libitum ($n = 6$ –13 for $IR^{fl/fl}$; $n = 6$ for iFIRKO). **(e)** Total fat mass measured by EchoMRI 0, 7 and 28 days after tamoxifen ($n = 8$ for $IR^{fl/fl}$; $n = 6$ for iFIRKO). **(f)** iBAT, ingWAT and epiWAT wet weight 5 days (5 d) or 28 days (28 d) after tamoxifen ($n = 11$ for $IR^{fl/fl}$ (5 d); $n = 6$ for iFIRKO (5 d); $n = 8$ for $IR^{fl/fl}$ (28 d); $n = 7$ for iFIRKO (28 d)). **(g)** Plasma leptin concentration measured with ELISA 3, 5 and 28 days after tamoxifen ($n = 5$ –6 for $IR^{fl/fl}$; $n = 5$ –7 for iFIRKO). **(h)** Plasma insulin concentration measured by ELISA 7 and 28 days after tamoxifen ($n = 6$ –7 for $IR^{fl/fl}$; $n = 6$ –8 for iFIRKO). **(i)** IPGTT in 4 h-fasted iFIRKO and $IR^{fl/fl}$ littermate controls, 7 days after tamoxifen administration ($n = 8$ for $IR^{fl/fl}$; $n = 6$ for iFIRKO). **(j)** Amount of triacylglycerol in soleus muscle, 2 weeks after tamoxifen administration ($n = 6$ for $IR^{fl/fl}$; $n = 7$ for iFIRKO). **(k)** Glucose infusion rate during steady state of hyperinsulinaemic–euglycaemic glucose clamping in iFIRKO and $IR^{fl/fl}$ littermate controls ($n = 9$ for $IR^{fl/fl}$; $n = 7$ for iFIRKO). **(l)** Endogenous glucose production rate under basal and insulin-stimulated conditions ($n = 5$ for $IR^{fl/fl}$; $n = 4$ for iFIRKO). **(m)** Uptake of ^{14}C -glucose per mg tissue into soleus muscle and ingWAT ($n = 5$ –6 for $IR^{fl/fl}$; $n = 6$ for iFIRKO). In **(k–m)** hyperinsulinaemic–euglycaemic clamps were performed 7 days after tamoxifen administration. Data are mean \pm SEM. Student's *t* test: * $p < 0.05$, ** $p < 0.01$, *** $p < 0.001$ for iFIRKO vs $IR^{fl/fl}$ or as shown. In **(f)** difference is significant for all time points below the line. d, days; EGP, endogenous glucose production rate; GIR, glucose infusion rate; M, soleus, soleus muscle; TAG, triacylglycerol; Tam, tamoxifen

(Fig. 1a, b). Three days after tamoxifen treatment, we measured $\dot{V}CO_2$ and $\dot{V}O_2$ and observed a decrease in the RER in iFIRKO mice (Fig. 1c), while $\dot{V}O_2$ and activity levels of mice remained unchanged (ESM Fig. 1a, b). Thyroid hormones are supposed to be plasma markers for increased basal metabolic rates. We found an increase in T_4 , which is the precursor of T_3 , in iFIRKO mice (ESM Fig. 1c). To resolve the timeline, we measured plasma NEFA concentrations in randomly fed mice after induction of the IR knockout. Coinciding with the change in RER, NEFA concentration increased by 40% in plasma of iFIRKO mice 3 days after induction (Fig. 1d). One week of IR ablation in adipocytes did not change the overall fat mass, while 4 weeks post induction we observed a significant change in adipose tissue mass (Fig. 1e). Interestingly, at day 5 of IR knockout in adipocytes, a reduction in iBAT and ingWAT but not in epiWAT mass was seen (Fig. 1f). The reduction of ingWAT mass was accompanied by reduced *Lep*, *Adipoq* and *Retn* gene expression in this fat depot (ESM Fig. 1d) in conjunction with a 70% reduction of plasma leptin levels (Fig. 1g), while plasma insulin concentration increased fourfold in iFIRKO mice at day 7 (Fig. 1h). At 7 days of IR knockout, we performed an IPGTT to avoid

confounding effects from gut glucose absorption and an ITT, which showed that iFIRKO mice were glucose intolerant and insulin resistant (Fig. 1i and ESM Fig. 1e).

Four weeks after knockout, a normalisation of insulin and leptin plasma concentrations (Fig. 1g, h) and adipokine gene expression (ESM Fig. 1d) was observed. iFIRKO mice had half as much fat as the $IR^{fl/fl}$ control mice (Fig. 1e) and the decrease in fat mass correlated with an increase in lean mass (ESM Fig. 1f), while total body mass remained unchanged (ESM Fig. 1g). During the same course of time, epiWAT mass was also reduced (Fig. 1f). The increase in liver mass could only account for a minor part of lean mass changes (ESM Fig. 1f). Unexpectedly, we observed no significant increase in liver triacylglycerol content (ESM Fig. 1i), while muscle triacylglycerol was reduced in iFIRKO mice (Fig. 1k and ESM Fig. 1j).

To further dissect the pathophysiology of adipose-specific deletion of IR, we performed hyperinsulinaemic–euglycaemic clamps in iFIRKO mice and their littermate $IR^{fl/fl}$ controls. At 7 days, we observed a glucose infusion rate of close to zero in iFIRKO mice (Fig. 1k and ESM Fig. 1k, l). Furthermore, iFIRKO mice demonstrated higher hepatic glucose output (Fig. 1l) and lower glucose uptake by the soleus muscle and the ingWAT (Fig. 1m and ESM Fig. 1m). Blood glycerol concentrations remained unchanged during the course of IR knockout (ESM Fig. 1n, o).

Fat loss after IR knockout induction in adipocytes is chronic, but not caused by adipocyte loss

To study the effect of adipocyte-specific IR ablation on adipose tissue mass under obesogenic conditions, we induced the knockout after 16 weeks of HFD (Fig. 2). In diet-induced obese mice, the genetic ablation of IR strongly reduced body weight (Fig. 2a). We observed that following IR knockout in adipocytes, 10.4 g loss of body weight was due to a 12.7 g loss in fat mass (Fig. 2b), which was paralleled by a reduction in the size of all adipose depots analysed (ESM Fig. 2a). Along with this, lean mass increased in iFIRKO mice (ESM Fig. 2b). Similar to previous findings in chow-fed iFIRKO mice, leptin concentration was reduced in diet-induced obese mice after induction of IR knockout in adipocytes by 70% (ESM Fig. 2c), and liver weight was increased by 0.8 g 4 weeks after induction of IR knockout in adipocytes (ESM Fig. 2d).

Subsequently, we sought to metabolically characterise already obese iFIRKO and $IR^{fl/fl}$ mice that were on an HFD. We observed that obese iFIRKO mice developed extreme hyperglycaemia 1 week after induction of IR knockout in adipocytes and returned to normoglycaemia at 4 weeks, a pattern that was similar to the aforementioned development of glucose levels in chow-fed iFIRKO mice (Fig. 2c). Additionally, 1 week after induction of IR knockout in

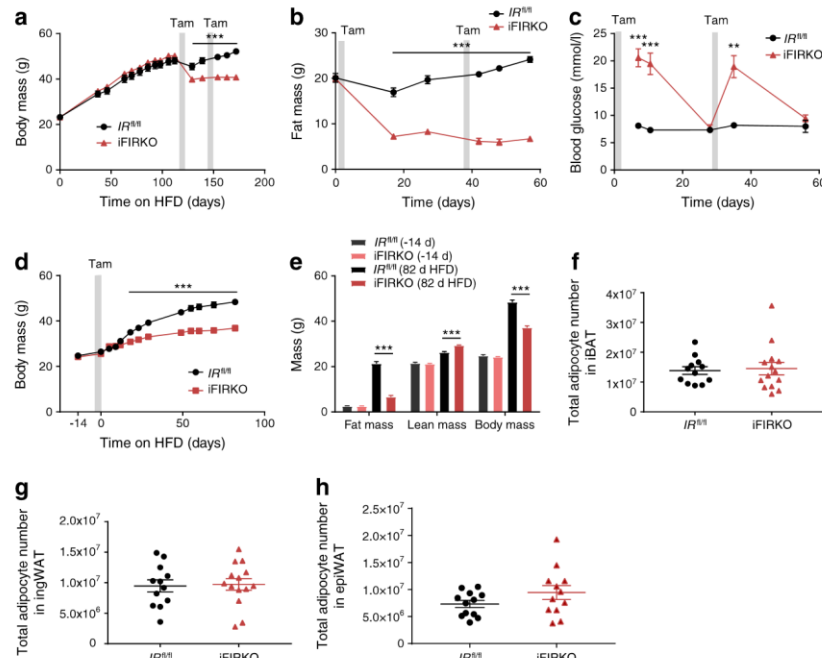


Fig. 2 Diet-induced obese mice chronically lose fat tissue mass by induction of adipose tissue-specific IR knockout while, in parallel, mice are protected from diet-induced obesity when knockout is carried out before the initiation of HFD feeding. **(a)** Body mass and **(b)** fat mass of HFD-induced obese mice before and after induction of IR knockout by tamoxifen in adipose tissue ($n = 5-16$ for $IR^{fl/fl}$; $n = 5-16$ for $iFIRKO$). **(c)** Ad libitum-fed blood glucose after two consecutive periods of induction of IR knockout in HFD-induced obese mice ($n = 4-7$ for $IR^{fl/fl}$; $n = 5-9$ for $iFIRKO$). **(d)** Effect of HFD on body mass of lean mice after induction of adipose tissue-specific IR deletion ($n = 11$ for $IR^{fl/fl}$; $n = 5$ for $iFIRKO$). **(e)** Evaluation of body composition and EchoMRI measurements of lean

and fat mass in $iFIRKO$ and $IR^{fl/fl}$ littermate controls before and after an 11 week HFD challenge. Adipose tissue-specific IR knockout was induced at the initiation of the HFD challenge ($n = 11$ for $IR^{fl/fl}$; $n = 5$ for $iFIRKO$; d, days). **(f-h)** Total adipocyte number in whole iBAT, ingWAT and epiWAT depots 1 week after tamoxifen induction, as measured by quantitative PCR for the evaluation of all cells that demonstrated the loxPStoploxP-tDRFP recombination ($n = 12$ for $IR^{fl/fl}$; $n = 14$ for $iFIRKO$). Grey bars in **(a-d)** indicate time period of tamoxifen gavage. Data are mean \pm SEM. Student's t test: ** $p < 0.01$, *** $p < 0.001$ for $iFIRKO$ vs $IR^{fl/fl}$ or as shown. In **(a, b, d)** difference is significant for all time points below the line. d, days; Tam, tamoxifen

adipocytes, obese $iFIRKO$ mice were insulin resistant (ESM Fig. 2e). While obese $iFIRKO$ mice showed no difference in ambulatory activity (ESM Fig. 2f), the development of whole-body insulin resistance coincided with a reduced RER (ESM Fig. 2g, h). To our surprise, IR knockout in adipocytes of obese mice led to an increased $\dot{V}O_2$ rate, which lasted from day 3 to day 10 (ESM Fig. 2i, j).

Because blood glucose levels in $iFIRKO$ mice normalised 4 weeks after induction of IR knockout in adipocytes, while fat mass did not, we induced the knockout for a second time in the same mouse cohort in order to test whether fat mass could be reduced even further. Interestingly, renewed ablation of IR further reduced fat mass (Fig. 2b). Furthermore, the second induction of knockout led to the development of another hyperglycaemic phase, which again reversed within 4 weeks

(Fig. 2c). This second knockout induction did not lead to liver mass alterations in hyperglycaemic $iFIRKO$ mice, and only when normoglycaemia had already developed was an additional increase of liver mass observed. This indicates that normalisation of blood glucose levels might be independent of ectopically stored fat in the liver (ESM Fig. 2d).

In a different experimental approach, we induced IR knockout in adipocytes of adult chow-fed mice and subsequently changed their diet to an obesogenic HFD, to test the potential of re-growth of adipose tissue after it was rendered insulin resistant. Because of the inducible character of our adipocyte-specific insulin-resistant mouse model, newly differentiated cells will contain an unrecombined IR gene once tamoxifen is washed out. Starting at equal body and fat mass before the induction of knockout, $iFIRKO$ mice gained less

weight on HFD than $IR^{fl/fl}$ control mice (Fig. 2d) and stayed protected from the obesogenic effect of HFD throughout week 12 (Fig. 2e). The difference in fat mass was even higher than that of body weight, because the lean mass was increased in iFIRKO mice (ESM Fig. 2b).

To address the question of whether IR knockout in adipocytes leads to their loss, we applied a new mouse model specifically generated to count adipocyte cells in iFIRKO mice. This triple-transgenic model, called the iFIRKO-chaser mouse, was created by combining the transgenes *Adipoq-CreERT2* and $IR^{fl/fl}$ with the floxed stop tdRFP allele (*loxPStoploxP-tdRFP*). After quantification of the recombination events in all cells of the adipose tissue depots iBAT, ingWAT and epiWAT, we could demonstrate that, 1 week after the induction of IR knockout, the total adipocyte number remained unchanged between $IR^{fl/fl}$ control and iFIRKO mice (Fig. 2f–h). This suggests that adipose tissue mass reduction is due to lipid content reduction per adipocyte and not to disappearance of adipocytes.

Antioxidants improve glucose intolerance of iFIRKO mice To elucidate the cause of hyperglycaemia in the iFIRKO animals, we analysed the development of glucose levels in a time course experiment, *in vivo*. We could show that hyperglycaemia development started 4 days after the induction of IR knockout in adipocytes (Fig. 3a), which notably is 1 day after the observed switch in energy substrate from glucose to fat. More specifically, the ad libitum random-fed blood glucose concentration increased from 8.96 ± 0.3 mmol/l in $IR^{fl/fl}$ control mice to 26.5 ± 1.6 mmol/l in iFIRKO mice, 6 days after the induction of IR knockout time point when the peak of hyperglycaemia was observed. Throughout the time course experiment, hyperglycaemia (>19 mmol/l) in iFIRKO mice persisted for 7 days (until day 12 post induction of IR knockout) and subsequently decreased for 3 days, until similar levels were observed compared with $IR^{fl/fl}$ control littermates on day 15 of IR knockout induction.

Despite reduced circulating leptin levels, iFIRKO mice did not consume more food than $IR^{fl/fl}$ control mice after induction of IR knockout in adipocytes (Fig. 3b). Only on day 9 could food consumption be linked to blood glucose levels. When measuring random-fed blood glucose levels in mice, which were pair-fed to $IR^{fl/fl}$ littermate controls, we observed that adipocyte-specific IR deletion-induced hyperglycaemia resolved faster in pair-fed iFIRKO mice (Fig. 3c). With a 2 day delay after the development of hyperglycaemia, iFIRKO mice showed an increase in water consumption (Fig. 3d).

Since many studies have reported that oxidative stress can cause insulin resistance by modulating lipotoxicity, we sought to evaluate whether antioxidants could have a beneficial role in our adipocyte-specific insulin-resistant model. As an antioxidant treatment, we chose the combination of NAc and apocynin. When mice were treated with antioxidants 1 day

before induction of IR knockout, the development of hyperglycaemia in the iFIRKO mice was delayed by 1 day. Furthermore, antioxidant treatment reduced the random-fed hyperglycaemia to 17.0 ± 1.7 mmol/l compared with 26.5 ± 1.6 mmol/l in the untreated iFIRKO mice 6 days post induction of IR knockout (Fig. 3a). Acute administration of apocynin alone could not reproduce the beneficial effect of both antioxidants (Apo+NAc cocktail) (ESM Fig. 3a, b). Another effect of the antioxidant cocktail on iFIRKO mice was the reduction of food intake by 40% (Fig. 3b). The increase in water intake, which developed in iFIRKO mice 7 days after IR knockout, was blunted by the antioxidant cocktail (Fig. 3d). The reduction of fat mass caused by IR knockout was unchanged by antioxidant treatment (Fig. 3e). Although antioxidant administration did not lead to a reduction of fat mass in $IR^{fl/fl}$ control mice, it counteracted the increase in fat mass observed in $IR^{fl/fl}$ control mice. Body mass was reduced in both iFIRKO and $IR^{fl/fl}$ control mice by antioxidant treatment (ESM Fig. 3c). This reduction in body mass on day 7 of treatment is due to a comparable reduction in lean mass of both iFIRKO and $IR^{fl/fl}$ mice (ESM Fig. 3d).

To delineate the adipose-specific IR knockout-induced hyperglycaemia as well as the improvement in glucose tolerance caused by antioxidant supplementation, we evaluated substrate preference and energy expenditure in iFIRKO and littermate $IR^{fl/fl}$ control mice. As mentioned above, iFIRKO mice had a significantly lower RER compared with littermate controls (Fig. 1b). Surprisingly, we observed that antioxidant supplementation reduced RER in wild-type mice but not in iFIRKO mice (Fig. 3f, g). Most importantly, the $IR^{fl/fl}$ control group that was not supplemented with antioxidants did not demonstrate any significant RER differences compared with the other groups after fasting (Fig. 3f, g). Physical activity was similar in all groups (ESM Fig. 3e) and both iFIRKO and $IR^{fl/fl}$ mice supplemented with antioxidants showed reduced $\dot{V}O_2$ compared with the non-supplemented controls (ESM Fig. 3f, g). Along with the $\dot{V}O_2$ rate, energy expenditure was reduced in the antioxidant-treated mice (ESM Fig. 3h, i). Interestingly, while the $\dot{V}O_2$ and $\dot{V}CO_2$ rates remained unchanged after IR knockout in adipocytes, the supplementation of antioxidants reduced $\dot{V}CO_2$ during the dark phase more strongly in iFIRKO mice than in $IR^{fl/fl}$ controls (ESM Fig. 3j, k).

As we could show that supplementation of antioxidants in iFIRKO mice led to a reduction in daily food intake (Fig. 3b), we measured random-fed and fasted blood glucose levels in wild-type and iFIRKO mice, which were not supplemented with antioxidants. Notably, we observed that the effect of antioxidants of reducing hyperglycaemia was present only in the random-fed and not in the fasted iFIRKO animals (Fig. 3h). To investigate the effect of antioxidants on insulin sensitivity, we performed an ITT 1 week after the induction of IR knockout in adipocytes. Similar to our previous results, we observed

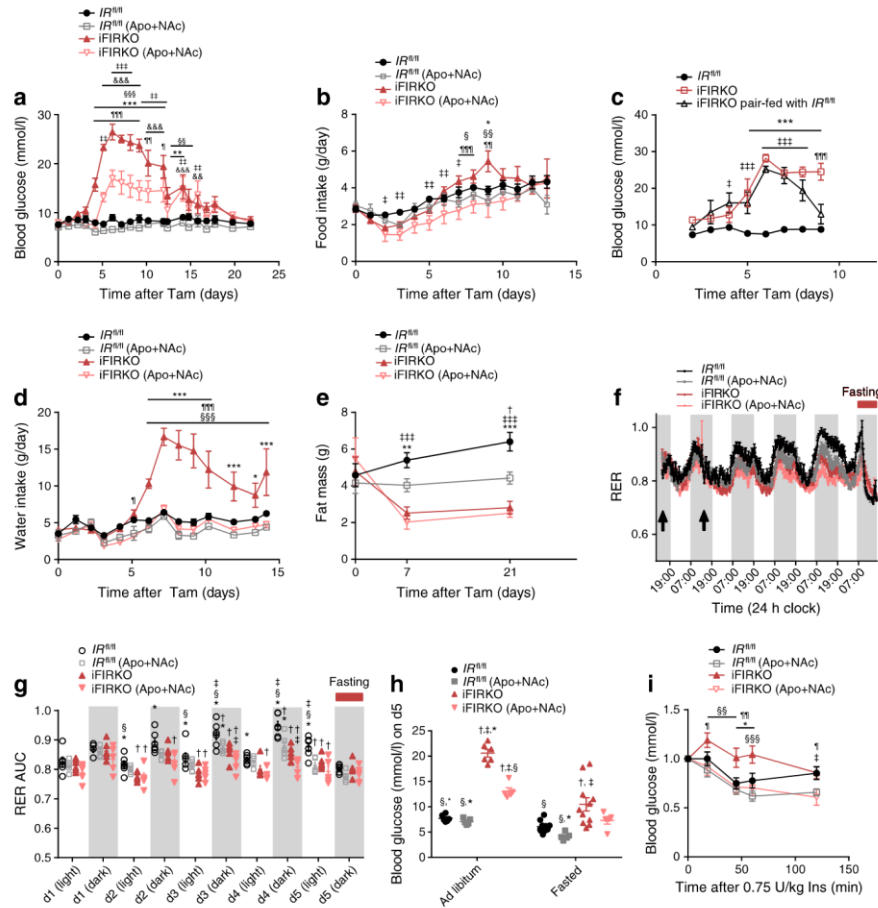


Fig. 3 Supplementation of drinking water with apocynin (Apo, 40 mmol/l) and NAc (15 mmol/l) postpones and reduces hyperglycaemia, reduces food intake and enhances insulin sensitivity. **(a)** Blood glucose in ad libitum-fed iFIRKO and $IR^{fl/fl}$ mice in either the presence or absence of Apo+Nac supplementation ($n = 6$ for $IR^{fl/fl}$, $n = 6$ for $IR^{fl/fl}$ (Apo+Nac); $n = 6$ for iFIRKO; $n = 5$ for iFIRKO (Apo+Nac)). **(b)** Recording of food intake in ad libitum-fed iFIRKO and $IR^{fl/fl}$ mice in either the presence or absence of Apo+Nac supplementation ($n = 6-13$ for $IR^{fl/fl}$, $n = 6$ for $IR^{fl/fl}$ (Apo+Nac); $n = 6$ for iFIRKO; $n = 5-12$ for iFIRKO (Apo+Nac)). **(c)** Blood glucose from pair-fed iFIRKO mice upon pair-feeding with $IR^{fl/fl}$, ad libitum-fed iFIRKO mice were used as controls ($n = 7$ for $IR^{fl/fl}$, $n = 4$ for iFIRKO ad libitum-fed; $n = 6$ for iFIRKO pair-fed). **(d)** Water intake in ad libitum-drinking iFIRKO and $IR^{fl/fl}$ mice in either the presence or absence of Apo+Nac supplementation ($n = 6$ for $IR^{fl/fl}$, $n = 6$ for $IR^{fl/fl}$ (Apo+Nac); $n = 6$ for iFIRKO; $n = 5$ for iFIRKO (Apo+Nac)). **(e)** Fat mass measured with EchoMRI in iFIRKO and $IR^{fl/fl}$ mice either in the presence or absence of Apo+Nac supplementation ($n = 6$ for $IR^{fl/fl}$, $n = 6$ for $IR^{fl/fl}$ (Apo+Nac); $n = 6$ for iFIRKO; $n = 5$ for iFIRKO (Apo+Nac)). **(f)** RER (VCO_2/VO_2) time course (adipose tissue-specific IR knockout was induced where indicated with the arrows) and **(g)** RER AUC of dark/light cycle for iFIRKO and $IR^{fl/fl}$ mice in either the presence or absence of Apo+Nac supplementation ($n = 6$ for $IR^{fl/fl}$, $n = 5$ for iFIRKO; d, day). **(h)** Blood glucose levels in ad libitum-fed and fasted iFIRKO and $IR^{fl/fl}$ mice in either the presence or absence of Apo+Nac supplementation ($n = 6-11$ for $IR^{fl/fl}$, $n = 5$ for $IR^{fl/fl}$ (Apo+Nac); $n = 6-11$ for iFIRKO; $n = 5$ for iFIRKO (Apo+Nac)). **(i)** ITT using 0.75 U insulin per kg body mass ($n = 6-11$ for $IR^{fl/fl}$, $n = 5$ for $IR^{fl/fl}$ (Apo+Nac); $n = 5$ for iFIRKO; $n = 6-11$ for iFIRKO (Apo+Nac)). Data are mean \pm SEM. Two-way ANOVA with Tukey's multiple comparisons test: in **(a, b, d, e, g-i)** $^{\dagger}p < 0.05$ for $IR^{fl/fl}$ vs $IR^{fl/fl}$ (Apo+Nac); $^*p < 0.05$, $^{**}p < 0.01$, $^{***}p < 0.001$ for $IR^{fl/fl}$ vs iFIRKO; $^{\ddagger}p < 0.05$, $^{\ddagger\ddagger}p < 0.01$, $^{\ddagger\ddagger\ddagger}p < 0.001$ for $IR^{fl/fl}$ vs iFIRKO (Apo+Nac); $^{\S}p < 0.05$, $^{\S\S}p < 0.01$, $^{\S\S\S}p < 0.001$ for $IR^{fl/fl}$ (Apo+Nac) vs iFIRKO; $^{\parallel}p < 0.01$, $^{\parallel\parallel\parallel}p < 0.001$ for iFIRKO vs iFIRKO (Apo+Nac), $^{\&\&}p < 0.01$, $^{\&\&\&}p < 0.001$ for $IR^{fl/fl}$ (Apo+Nac) vs iFIRKO (Apo+Nac). In **(c)** $^{***}p < 0.001$ for $IR^{fl/fl}$ vs iFIRKO; $^{\ddagger}p < 0.05$, $^{\ddagger\ddagger}p < 0.01$ vs iFIRKO pair-fed; $^{\parallel\parallel\parallel}p < 0.001$ for iFIRKO vs iFIRKO pair-fed. In **(a-d)** and **(i)** difference is significant for all time points below the line. d, day; Ins, insulin; Tam, tamoxifen

that antioxidants improved insulin sensitivity in iFIRKO mice but had no significant effect in wild-type mice (Fig. 3i).

Antioxidants reduce hyperphagia and improve glucose homeostasis in *ob/ob* mice After demonstrating a protective role of the antioxidant cocktail in hyperglycaemic iFIRKO mice, we evaluated whether this phenomenon is observed in other mouse models. Therefore, we examined the effect of supplementation of antioxidants in leptin-deficient *ob/ob* mice. At 12 weeks of age, *ob/ob* mice had developed hyperglycaemia (Fig. 4a), accompanied by hyperphagia (Fig. 4b) and polydipsia (Fig. 4c). We observed that after 24 h of antioxidant supplementation, there was already a significant reduction in the levels of random-fed blood glucose in *ob/ob* mice, compared with the control *ob/ob* mice which did not receive any antioxidant supplementation (Fig. 4a). In accordance with the effect of antioxidants in the iFIRKO mouse model, we observed that antioxidant supplementation did not acutely improve insulin

sensitivity in this diabetic mouse model. (Fig. 4d). Therefore, we assume that regulation of food intake could be responsible for the observed beneficial hypoglycaemic effect of antioxidant supplementation. By measuring the daily food intake of *ob/ob* and wild-type mice, in combination with antioxidant supplementation, we confirmed that antioxidants significantly reduced food intake in *ob/ob* but not in wild-type mice (Fig. 4b and ESM Fig. 4a). Food over-consumption of heavily obese *ob/ob* mice (Fig. 4b) normalised to that of the control group by 2 days of treatment with antioxidant cocktail supplemented into the drinking water (Fig. 4b). We assume no taste aversion since antioxidant cocktail supplementation did not change daily water intake (Fig. 4c). Additionally, supplementation of apocynin alone could not reproduce the same effect as the administration of both antioxidants in parallel (ESM Fig. 4b, c). Finally, the short-term antioxidant supplementation did not demonstrate any effect on the fat or lean mass of *ob/ob* mice (Fig. 4e).

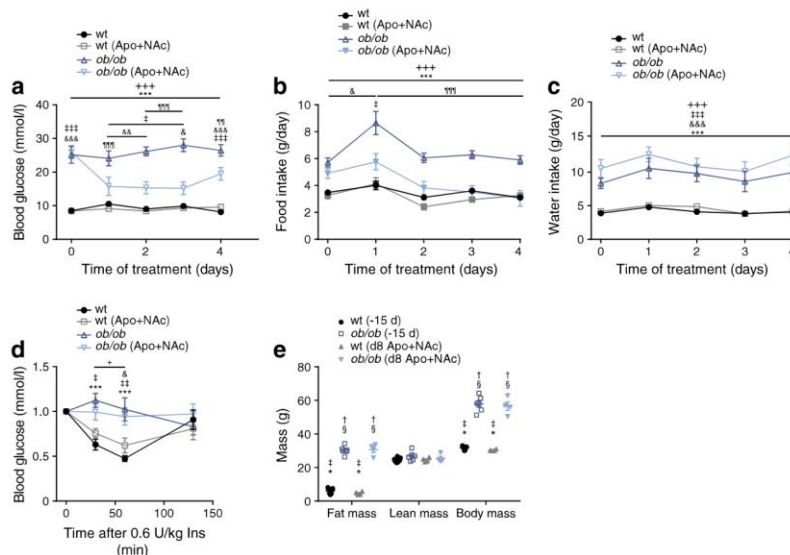


Fig. 4 Supplementation of drinking water with apocynin (Apo, 40 mmol/l) and Nac (15 mmol/l) reduces hyperphagia and improves glucose homeostasis in leptin-deficient *ob/ob* mice. Apo+Nac supplementation was continuous and started on day 0 after measurement. (a) Blood glucose levels in ad libitum-fed *ob/ob* mice during treatment with antioxidants ($n = 9$ for wt; $n = 8$ for wt (Apo+Nac); $n = 7$ for *ob/ob*; $n = 8$ for *ob/ob* (Apo+Nac)). (b) Daily food intake in *ob/ob* mice during antioxidant treatment ($n = 9$ for wt; $n = 8$ for wt (Apo+Nac); $n = 6$ for *ob/ob*; $n = 9$ for *ob/ob* (Apo+Nac)). (c) Daily water intake in *ob/ob* mice during antioxidant treatment ($n = 11$ for WT; $n = 11$ for WT (Apo+Nac); $n = 4$ for *ob/ob*; $n = 3$ for *ob/ob* (Apo+Nac)). (d) ITT blood glucose over time, in min, after intraperitoneal injection of 0.6 U insulin per kg after 8 h fasting. Values normalised to blood glucose levels at injection ($n = 6$ for WT; $n =$

7 for WT (Apo+Nac); $n = 7$ for *ob/ob*; $n = 8$ for *ob/ob* (Apo+Nac)). (e) Body composition 15 days (-15 d) before and 8 days after (d8) antioxidant treatment ($n = 7$ for wt (-15 d); $n = 4$ for wt (d8 Apo+Nac); $n = 6$ for *ob/ob* (-15 d); $n = 4$ for *ob/ob* (d8 Apo+Nac)). Data are mean \pm SEM. Two-way ANOVA with Tukey's multiple comparisons test: in (a-d) $^{\#}p < 0.05$, $^{***}p < 0.001$ for wt vs *ob/ob*; $^{\ddagger}p < 0.05$, $^{\dagger\dagger}p < 0.01$, $^{\dagger\dagger\dagger}p < 0.001$ for wt vs *ob/ob* (Apo+Nac); $^{\ddagger}p < 0.05$, $^{***}p < 0.001$ for wt (Apo+Nac) vs *ob/ob*; $^{\ddagger}p < 0.05$, $^{***}p < 0.001$ for *ob/ob* vs *ob/ob* (Apo+Nac); $^{\&}p < 0.05$, $^{\&\&}p < 0.01$, $^{\&\&\&}p < 0.001$ for wt (Apo+Nac) vs *ob/ob* (Apo+Nac). In (e) $^{\ddagger}p < 0.05$ vs wt (-15 d); $^{\ddagger}p < 0.05$ vs *ob/ob* (-15 d); $^{\ddagger}p < 0.05$ vs wt (d8 Apo+Nac); $^{\ddagger}p < 0.05$ vs *ob/ob* (d8 Apo+Nac). In (a-d) difference is significant for all time points below the line. d, day; Ins, insulin; WT, wild-type

Discussion

Based on the use of the new iFIRKO-tracer mouse model, we conclude that the iFIRKO mouse model does not resemble the typical lipotrophic mouse models such as the FAT-ATTAC [19] or the A-Zip/F-1 mouse models [20], which exhibit a loss of adipocytes and ectopic deposition of lipids. The finding that adipose tissue can re-establish its storage function within a few weeks supports the notion of its high plasticity [21]. Importantly, in iFIRKO mice there seems to be no full compensation for the reduction of adipocyte size and mass of the various adipose tissue depots, because they are protected from excessive weight gain when mice are fed an obesogenic diet after the induction of IR knockout.

The adiponectin gene regulatory elements that we used to target adipocytes are currently the most specific known [22, 23]. The inducible nature of our iFIRKO mouse model allowed us to study different phases of the development of type 2 diabetes. At the start of the initial phase, insulin resistance could arise as a consequence of lipolysis-induced hyperinsulinaemia through lipotoxicity [24–27]. Our pair-feeding experiment indicates that hyperphagia of iFIRKO mice is not causative for the initial hyperglycaemia development, but rather that it contributes at a later phase. Results of hyperinsulinaemic–euglycaemic clamp experiments suggest that the subsequent development of hyperglycaemia in iFIRKO mice might be due to reduced hepatic insulin sensitivity of liver, which results in an increased endogenous glucose production [28]. One important conclusion is that lipids released from adipose tissue can be utilised by the respective tissues, which is supported by our finding of reduced lipid content in muscle, the observed switch in energy substrate and the reversibility of the type 2 diabetes symptoms in iFIRKO mice. While in lean iFIRKO mice an increase of T_4 was detectable, in obese iFIRKO mice the increased lipid metabolising led to higher $\dot{V}O_2$ rates. Further experiments at thermoneutrality or in the absence of Ucp1 could help to delineate the contribution of brown adipose tissue to this elevated basal metabolic rate.

One key molecular mechanism behind lipotoxicity is lipid-induced mitochondrial oxidative stress [13, 29]. Ethnological studies suggest that plants with antioxidant capacity can be used to treat diabetes-like symptoms [30, 31]. However, more recent clinical studies, which tested food supplementation with different antioxidants in the context of human diabetes, have questioned their beneficial effects [32, 33]. Unlike other studies [12, 34], we used a combination of the potent antioxidants NAc [35, 36] and apocynin [37, 38] to treat mice briefly before and while they were developing diabetes. The proposed targets of antioxidants are reactive oxygen species; however, as reactive oxygen species are very unstable molecules and oxidative stress is tightly regulated by antioxidant enzymes [39, 40], the exact contribution is hard to define. A few reports exist which

demonstrate an improvement in insulin resistance in leptin-deficient *ob/ob* mice, while other studies supplementing food with antioxidants (e.g. apple polyphenol extracts or melatonin) have failed to report an effect on food intake [41, 42]. A blood glucose-lowering effect of apocynin, structurally related to vanillin [43], was reported in morbidly chronically obese KKAY mice [12]. In our system, acute treatment with apocynin reduced hyperglycaemia in neither iFIRKO mice nor *ob/ob* mice. The suggestion that the effect of the antioxidants NAc and apocynin is leptin independent is further supported by our observation that they mediate an effect during the early phase of diabetes development in iFIRKO mice in which leptin is almost absent.

Melatonin in its function as an antioxidant was reported to improve non-alcoholic fatty liver disease symptoms [42]. Additionally, the supplementation of apple polyphenol extracts reduced inflammation in *ob/ob* mouse liver, which was suggested as the site of its action [41]. We demonstrated here that iFIRKO mice are insulin resistant even under fasting conditions; however, as fasting lowered the RER of the control groups, we conclude that the substrate change from glucose to lipids observed after antioxidant treatment is not directly causal for the alterations of insulin resistance. Rather, we propose that the accumulation of oxidative damage over several days is required to cause insulin resistance. Unfortunately, the identification of factors that are secreted from tissues damaged by oxidative stress is beyond the scope of this study.

Acknowledgements We thank J. Krützfeldt and M. Stoffel for helpful criticism. We also thank M. Geiger and E. Kiehlmann for technical help, as well as H. Sengül and members of the SLA-Schwerzenbach animal facility for help with animal work. Furthermore, we would like to thank S. Turner for administrative support.

Data availability Primary data are available upon request. Please contact the corresponding author.

Funding Funding was provided by the Schweizer Nationalfonds (SNF).

Duality of interest The authors declare that there is no duality of interest associated with this manuscript.

Contribution statement LGS developed the hypothesis and project, performed the experiments, analysed the data and wrote the manuscript. VE co-supervised the project and performed experiments, analysed data and wrote the manuscript. GG, MB, TDC, LT, CH, CM, YR, MA, WS, SM and CW have all substantially contributed to concept and design, acquisition of data, or analysis and interpretation of data, and drafting the article or revising it critically for important intellectual content. All authors gave their final approval of the present version to be published. CW is the study guarantor and is responsible for the integrity of the work as a whole.

Open Access This article is distributed under the terms of the Creative Commons Attribution 4.0 International License (<http://creativecommons.org/licenses/by/4.0/>), which permits unrestricted use, distribution, and reproduction in any medium, provided you give appropriate credit to the original author(s) and the source, provide a link to the Creative Commons license, and indicate if changes were made.

References

1. Collaborators GBDO, Afshin A, Forouzanfar MH et al (2017) Health effects of overweight and obesity in 195 countries over 25 years. *N Engl J Med* 377(1):13–27. <https://doi.org/10.1056/NEJMoa1614362>
2. O'Rahilly S (2002) Insights into obesity and insulin resistance from the study of extreme human phenotypes. *Eur J Endocrinol* 147(4):435–441. <https://doi.org/10.1530/eje.0.1470435>
3. Softic S, Boucher J, Solheim MH et al (2016) Lipodystrophy due to adipose tissue-specific insulin receptor knockout results in progressive NAFLD. *Diabetes* 65(8):2187–2200. <https://doi.org/10.2337/db16-0213>
4. George S, Rochford JJ, Wolfrum C et al (2004) A family with severe insulin resistance and diabetes due to a mutation in AKT2. *Science* 304(5675):1325–1328. <https://doi.org/10.1126/science.1096706>
5. Roden M, Price TB, Perseghin G et al (1996) Mechanism of free fatty acid-induced insulin resistance in humans. *J Clin Invest* 97(12):2859–2865. <https://doi.org/10.1172/Jci118742>
6. Sakaguchi M, Fujisaka S, Cai W et al (2017) Adipocyte dynamics and reversible metabolic syndrome in mice with an inducible adipocyte-specific deletion of the insulin receptor. *Cell Metab* 25(2):448–462. <https://doi.org/10.1016/j.cmet.2016.12.008>
7. Morton GJ, Blevins JE, Williams DL et al (2005) Leptin action in the forebrain regulates the hindbrain response to satiety signals. *J Clin Invest* 115(3):703–710. <https://doi.org/10.1172/JCI22081>
8. Funcke JB, von Schnurbein J, Lennerz B et al (2014) Monogenic forms of childhood obesity due to mutations in the leptin gene. *Mol Cell Pediatr* 1(1):3. <https://doi.org/10.1186/s40348-014-0003-1>
9. Montague CT, Farooqi IS, Whitehead JP et al (1997) Congenital leptin deficiency is associated with severe early-onset obesity in humans. *Nature* 387(6636):903–908. <https://doi.org/10.1038/43185>
10. Wabitsch M, Funcke JB, Lennerz B et al (2015) Biologically inactive leptin and early-onset extreme obesity. *N Engl J Med* 372(1):48–54. <https://doi.org/10.1056/NEJMoal406653>
11. Coleman DL (1978) Obese and diabetes: two mutant genes causing diabetes-obesity syndromes in mice. *Diabetologia* 14(3):141–148. <https://doi.org/10.1007/BF00429772>
12. Furukawa S, Fujita T, Shimabukuro M et al (2004) Increased oxidative stress in obesity and its impact on metabolic syndrome. *J Clin Invest* 114(12):1752–1761. <https://doi.org/10.1172/JCI21625>
13. Lee HY, Lee JS, Alves T et al (2017) Mitochondrial-targeted catalase protects against high-fat diet-induced muscle insulin resistance by decreasing intramuscular lipid accumulation. *Diabetes* 66(8):2072–2081. <https://doi.org/10.2337/db16-1334>
14. Sies H (1986) Biochemistry of oxidative stress. *Angew Chem Int Ed* 25(12):1058–1071. <https://doi.org/10.1042/Bst0351147>
15. Yancy WS, Dunbar SA, Boucher JL et al (2014) Nutrition therapy recommendations for the management of adults with diabetes. *Diabetes Care* 2013 36:3821–3842 RESPONSE. *Diabetes Care* 37(5):E102–E103. <https://doi.org/10.2337/dc14-0077>
16. Bruning JC, Michael MD, Winnay JN et al (1998) A muscle-specific insulin receptor knockout exhibits features of the metabolic syndrome of NIDDM without altering glucose tolerance. *Mol Cell* 2(5):559–569. [https://doi.org/10.1016/S1097-2765\(00\)80155-0](https://doi.org/10.1016/S1097-2765(00)80155-0)
17. Luche H, Weber O, Nageswara Rao T, Blum C, Fehling HJ (2007) Faithful activation of an extra-bright red fluorescent protein in “knock-in” Cre-reporter mice ideally suited for lineage tracing studies. *Eur J Immunol* 37(1):43–53. <https://doi.org/10.1002/eji.200636745>
18. Grandl G, Straub L, Rudigier C et al (2018) Short-term feeding of a ketogenic diet induces more severe hepatic insulin resistance than an obesogenic high-fat diet. *J Physiol* 596(19):4596–4609. <https://doi.org/10.1113/JP275173>
19. Pajvani UB, Trujillo ME, Combs TP et al (2005) Fat apoptosis through targeted activation of caspase 8: a new mouse model of inducible and reversible lipatrophy. *Nat Med* 11(7):797–803. <https://doi.org/10.1038/nm1262>
20. Moitra J, Mason MM, Olive M et al (1998) Life without white fat: a transgenic mouse. *Genes Dev* 12(20):3168–3181. <https://doi.org/10.1101/gad.12.20.3168>
21. Ghaben AL, Scherer PE (2019) Adipogenesis and metabolic health. *Nat Rev Mol Cell Biol* 20(4):242–258. <https://doi.org/10.1038/s41580-018-0093-z>
22. Wolfrum C, Straub LG (2018) Lessons from Cre-mice and indicator mice. *Handb Exp Pharmacol* 251:37–54. https://doi.org/10.1007/164_2018_146
23. Straub LG, Scherer PE (2019) Metabolic messengers: adiponectin. *Nature Metabolism* 1(3):334–339. <https://doi.org/10.1038/s42255-019-0041-z>
24. Heine M, Fischer AW, Schlein C et al (2018) Lipolysis triggers a systemic insulin response essential for efficient energy replenishment of activated brown adipose tissue in mice. *Cell Metab* 28(4):644–655. <https://doi.org/10.1016/j.cmet.2018.06.020>
25. Unger RH, Clark GO, Scherer PE, Orci L (2010) Lipid homeostasis, lipotoxicity and the metabolic syndrome. *Biochim Biophys Acta* 1801(3):209–214. <https://doi.org/10.1016/j.bbaplp.2009.10.006>
26. Unger RH (1995) Lipotoxicity in the pathogenesis of obesity-dependent NIDDM. Genetic and clinical implications. *Diabetes* 44(8):863–870. <https://doi.org/10.2337/diab.44.8.863>
27. Berson A, De Beco V, Letteron P et al (1998) Steatohepatitis-inducing drugs cause mitochondrial dysfunction and lipid peroxidation in rat hepatocytes. *Gastroenterology* 114(4):764–774. [https://doi.org/10.1016/S0016-5085\(98\)70590-6](https://doi.org/10.1016/S0016-5085(98)70590-6)
28. Day CP, James OF (1998) Steatohepatitis: a tale of two “hits”? *Gastroenterology* 114(4):842–845. [https://doi.org/10.1016/S0016-5085\(98\)70599-2](https://doi.org/10.1016/S0016-5085(98)70599-2)
29. Koves TR, Ussher JR, Noland RC et al (2008) Mitochondrial overload and incomplete fatty acid oxidation contribute to skeletal muscle insulin resistance. *Cell Metab* 7(1):45–56. <https://doi.org/10.1016/j.cmet.2007.10.013>
30. Scartezzini P, Speroni E (2000) Review on some plants of Indian traditional medicine with antioxidant activity. *J Ethnopharmacol* 71(1–2):23–43. [https://doi.org/10.1016/S0378-8741\(00\)00213-0](https://doi.org/10.1016/S0378-8741(00)00213-0)
31. Djukanovic V, Mach EP, WHO, UNICEF (1975) Alternative approaches to meeting basic health needs in developing countries: a joint UNICEF/WHO study. WHO, Geneva
32. Heart Protection Study Collaborative G (2002) MRC/BHF Heart Protection Study of antioxidant vitamin supplementation in 20,536 high-risk individuals: a randomised placebo-controlled trial. *Lancet* 360(9326):23–33. [https://doi.org/10.1016/S0140-6736\(02\)09328-5](https://doi.org/10.1016/S0140-6736(02)09328-5)
33. Pazdro R, Burgess JR (2010) The role of vitamin E and oxidative stress in diabetes complications. *Mech Ageing Dev* 131(4):276–286. <https://doi.org/10.1016/j.mad.2010.03.005>
34. Saha MR, Dey P, Sarkar I et al (2018) Acacia nilotica leaf improves insulin resistance and hyperglycemia associated acute hepatic injury and nephrotoxicity by improving systemic antioxidant status in diabetic mice. *J Ethnopharmacol* 210:275–286. <https://doi.org/10.1016/j.jep.2017.08.036>
35. Flora SD, Bencicelli C, Camoirano A et al (1985) In vivo effects of N-acetylcysteine on glutathione metabolism and on the biotransformation of carcinogenic and/or mutagenic compounds. *Carcinogenesis* 6(12):1735–1745. <https://doi.org/10.1093/carcin/6.12.1735>
36. Perchellet EM, Maatta EA, Abney NL, Perchellet JP (1987) Effects of diverse intracellular thiol delivery agents on glutathione peroxidase activity, the ratio of reduced/oxidized glutathione, and ornithine decarboxylase induction in isolated mouse epidermal cells

- treated with 12-O-tetradecanoylphorbol-13-acetate. *J Cell Physiol* 131(1):64–73. <https://doi.org/10.1002/jcp.1041310111>
37. Stefanska J, Pawliczak R (2008) Apocynin: molecular aptitudes. *Mediat Inflamm* 2008:1–10. <https://doi.org/10.1155/2008/106507>
 38. Petronio MS, Zeraik ML, Fonseca LM, Ximenes VF (2013) Apocynin: chemical and biophysical properties of a NADPH oxidase inhibitor. *Molecules* 18(3):2821–2839. <https://doi.org/10.3390/molecules18032821>
 39. Ristow M (2014) Unraveling the truth about antioxidants: mitohormesis explains ROS-induced health benefits. *Nat Med* 20(7):709–711. <https://doi.org/10.1038/nm.3624>
 40. Ristow M, Schmeisser K (2014) Mitohormesis: promoting health and lifespan by increased levels of reactive oxygen species (ROS). *Dose-Response* 12(2):288–341. <https://doi.org/10.2203/dose-response.13-035.Ristow>
 41. Ogura K, Ogura M, Shoji T et al (2016) Oral administration of apple procyanidins ameliorates insulin resistance via suppression of pro-inflammatory cytokine expression in liver of diabetic *ob/ob* mice. *J Agric Food Chem* 64(46):8857–8865. <https://doi.org/10.1021/acs.jafc.6b03424>
 42. Stacchiotti A, Favero G, Lavazza A et al (2016) Hepatic macrosteatosis is partially converted to microsteatosis by melatonin supplementation in *ob/ob* mice non-alcoholic fatty liver disease. *PLoS One* 11(1):e0148115. <https://doi.org/10.1371/journal.pone.0148115>
 43. Heumüller S, Schreiber JG, Scholich K, Brandes RP (2009) Apocynin is activated by several peroxidases. *Free Radical Bio Med* 47:S143–S144

Publisher's note Springer Nature remains neutral with regard to jurisdictional claims in published maps and institutional affiliations.

A Genetic Model to Study the Contribution of Brown and Brite Adipocytes to Metabolism

Tenagne D. Challa, Dianne H. Dapito, Elisabeth Kulenkampff, Elke Kiehlmann, Caroline Moser, Leon Straub, Wenfei Sun, Christian Wolfrum

Published in Cell Reports, 2020

Contribution:

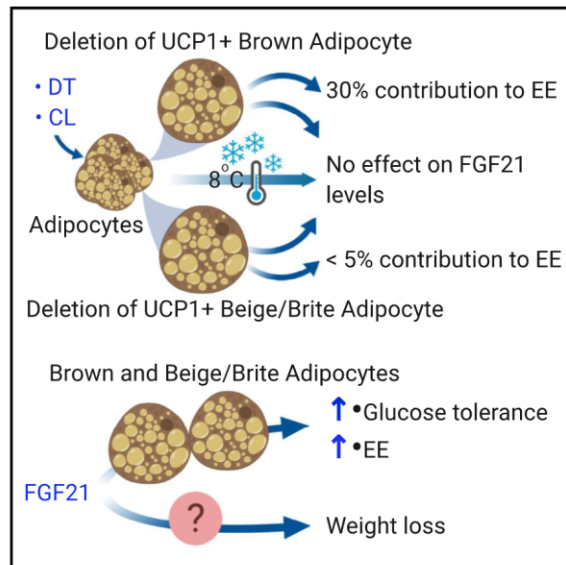
Caroline Moser performed and analyzed the adipocyte quantification experiment

This article is a reprint of the original published article with kind permission of the publisher, Elsevier GmbH. Supplementary material is available online under:
<https://doi.org/10.1016/j.celrep.2020.02.055>

Cell Reports

A Genetic Model to Study the Contribution of Brown and Brite Adipocytes to Metabolism

Graphical Abstract



Authors

Tenagne D. Challa, Dianne H. Dapito, Elisabeth Kulenkampff, ..., Leon Straub, Wenfei Sun, Christian Wolfrum

Correspondence

christian-wolfrum@ethz.ch

In Brief

Challa et al. develop a mouse model to ablate UCP1⁺ adipocytes and demonstrate that activated brown adipocytes contribute 30% to energy expenditure (EE), while the contribution of brite/beige cells is low. The effect of FGF21 on EE and glucose homeostasis is in part dependent on the presence of UCP1⁺ cells.

Highlights

- Generation of a mouse model to ablate UCP1⁺ cells in mice using diphtheria toxin
- Deletion of UCP1⁺ cells does not change energy expenditure at room temperature
- UCP1⁺ cells do not contribute to circulating FGF21 levels after cold exposure
- FGF21-dependent increase in EE and glucose tolerance is dependent on UCP1⁺ cells



Challa et al., 2020, Cell Reports 30, 3424–3433
March 10, 2020 © 2020 The Author(s).
<https://doi.org/10.1016/j.celrep.2020.02.055>

CellPress



A Genetic Model to Study the Contribution of Brown and Brite Adipocytes to Metabolism

Tenagne D. Challa,^{1,2} Dianne H. Dapito,^{1,2} Elisabeth Kulenkampff,^{1,2} Elke Kiehlmann,¹ Caroline Moser,¹ Leon Straub,¹ Wenfei Sun,¹ and Christian Wolfrum^{1,3,*}

¹Institute of Food Nutrition and Health and Department of Health Sciences and Technology, Eidgenössische Technische Hochschule Zürich (ETH), 8603 Schwerzenbach, Switzerland

²These authors contributed equally

³Lead Contact

*Correspondence: christian-wolfrum@ethz.ch
<https://doi.org/10.1016/j.celrep.2020.02.055>

SUMMARY

UCP1-dependent thermogenesis is studied to define new strategies to ameliorate obesity and type 2 diabetes; however, animal models are mostly limited to germline mutations of UCP1, which can effect adaptive changes in UCP1-independent pathways. We develop an inducible mouse model for the sequential ablation of UCP1⁺ brown and brite/beige adipocytes in adult mice. We demonstrate that activated brown adipocytes can increase systemic energy expenditure (EE) by 30%, while the contribution of brite/beige UCP1⁺ cells is <5%. Notably, UCP1⁺ adipocytes do not contribute to circulating FGF21 levels, either at room temperature or after cold exposure. We demonstrate that the FGF21-mediated effects on EE and glucose homeostasis are partially dependent on the presence of UCP1⁺ cells, while the effect on weight loss is not. In conclusion, acute UCP1⁺ cell deletion may be a useful model to study the impact of brown and brite/beige adipocytes on metabolism.

INTRODUCTION

Brown adipose tissue (BAT) generates heat by dissipating the inner mitochondrial proton gradient, thereby uncoupling oxidative phosphorylation from ATP production through uncoupling protein 1 (UCP1). UCP1 converts glucose and lipids to heat and thereby increases energy expenditure (EE) to maintain body temperature (Cannon and Nedergaard, 2004). The finding that active BAT can be found in cold-exposed adult humans has increased scientific interest in its therapeutic potential to counter diabetes and obesity (Hany et al., 2002; Nedergaard et al., 2007; Saito et al., 2009; van Marken Lichtenbelt et al., 2009; Virtanen et al., 2009). In fact, pharmacological and genetic activation of UCP1 in rodents has been shown to protect them from diet-induced obesity (DIO) (Liu et al., 2003; Poher et al., 2015; Wankhade et al., 2016).

Various transgenic mice models lacking UCP1 were generated to understand the importance of UCP1 and brown adipocytes. For instance, the deletion of brown cells by the specific expression of diphtheria toxin A chain in brown adipocytes resulted

in increased body weight and insulin resistance (Dulloo and Miller, 1984; Lowell et al., 1993). In another model in which UCP1 expression was specifically induced by the use of an aP2-UCP1 transgenic allele, high levels of UCP1 in adipocytes led to cytotoxicity and resulted in the ablation of UCP1⁺ brown adipocytes (Kopecky et al., 1995). These mice were cold sensitive and protected from DIO (Kozak, 2010). Other studies reported reduced cold-induced thermogenesis in UCP1-deficient mice (Enerbäck et al., 1997).

These conflicting results in UCP1-deficient models were addressed in a study by Feldmann et al. (2009), in which they reported that chow diet-fed UCP1-deficient mice housed at thermoneutrality became obese. Based on their findings, they postulated that housing at ambient temperatures induced thermal stress and consequently increased the metabolic rate and food intake to maintain body temperature (Golozoubova et al., 2004). Deletion of UCP1 resulted in compensatory mechanisms to maintain body temperature in mice at ambient temperatures, thus explaining the lack of an obesogenic effect in UCP1-knockout mice (Feldmann et al., 2009). To circumvent the problems associated with compensatory mechanisms in UCP1-deficient mice, we generated a model to acutely ablate UCP1⁺ brown adipocytes in adult mice. Using this model, we investigated the contribution of brown and recruited brite/beige cells to total EE at ambient temperatures, as well as the dependency of fibroblast growth factor 21 (FGF21) on brown adipocytes to achieve its beneficial metabolic effects.

RESULTS

An Efficient Deletion of UCP1-Expressing Adipocytes in an Inducible Adult Mouse Model

Considering the limitations presented by the use of UCP1-deficient mice, we sought to use a model that allows for inducible and transient deletion of UCP1⁺ cells. Therefore, we generated the UCP1DTR2GFP mouse line (UCP-DTR) (Rosenwald et al., 2013) to investigate the impact of acute and transient deletion of cells expressing UCP1. These mice carry a diphtheria toxin receptor (DTR) and an EGFP cassette under the control of the UCP1 promoter. To test the efficacy of DT-mediated ablation, 8- to 12-week-old wild-type (WT) littermates and UCP1-DTR mice were treated with DT at room temperature (RT; 23°C) (Figure 1A). We observed that interscapular BAT (iBAT) of UCP1-DTR mice appeared to be much paler brown compared



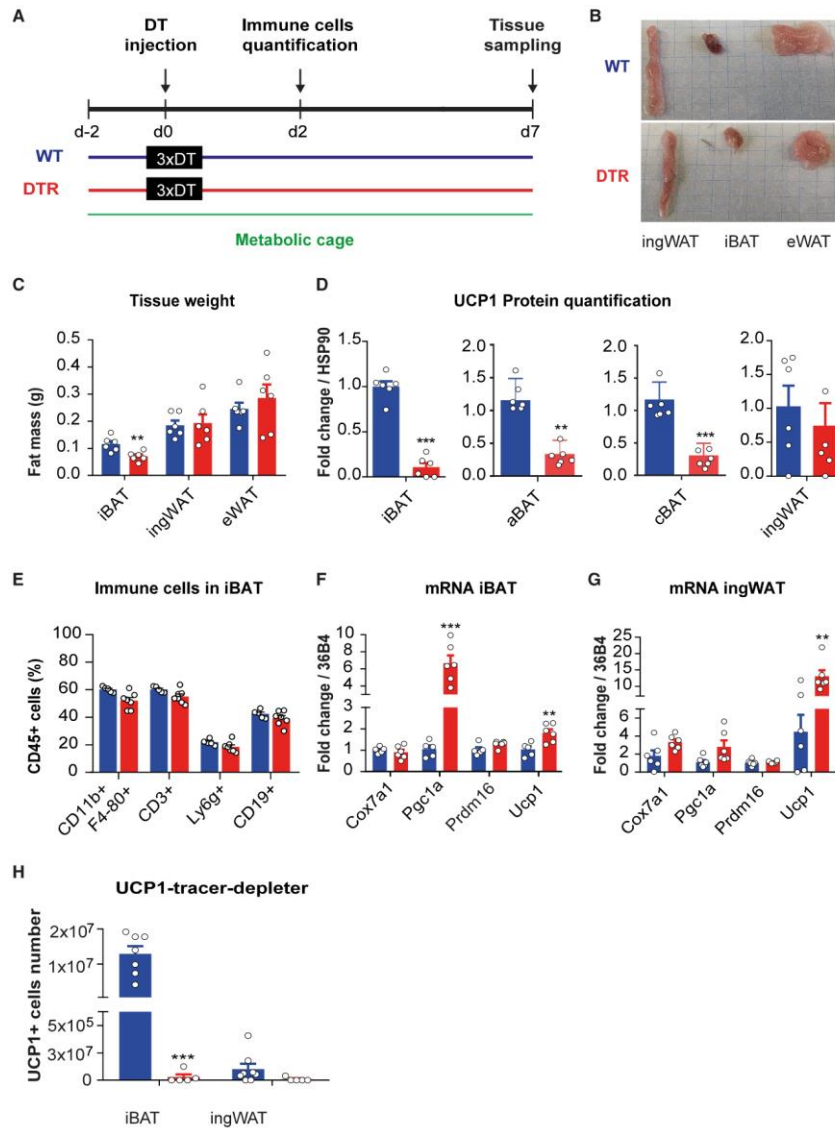


Figure 1. Ablation of UCP1⁺ Cells in an Inducible Adult Mouse at Room Temperature (RT)

(A) Experimental scheme for the ablation of UCP1⁺ cells at RT (23°C, mild cold stress). WT littermates group (blue); did not carry the UCP1-DTR transgene. DTR group (red); carried the UCP1-DTR transgene. At 9 to 12 weeks old, the mice were given 3 consecutive doses of 100 ng DT every 6 h on day 0 to ablate UCP1⁺ cells in the DTR group, and tissues were harvested after 7 days.

(legend continued on next page)



to the iBAT of WT littermates (Figure 1B), which is in line with reduced iBAT weight (Figure 1C). Notably, the appearance and weight of inguinal white adipose tissue (ingWAT) and epididymal WAT (eWAT) remained unchanged, and similar lean mass (Figures 1B, 1C, and S1A) was observed. As expected, protein levels of UCP1 in iBAT, axillary BAT (aBAT), and cervical BAT (cBAT) were decreased in UCP1-DTR mice compared to WT littermates, demonstrating the efficient deletion of brown adipocytes (Figures 1D and S1B) (Sun et al., 2018). In contrast, UCP1 protein levels in ingWAT showed a high variance and no reduction in UCP1-DTR mice (Figures 1D and S1B). To test whether the ablation of UCP1⁺ cells upon DT injection resulted in an immune response in iBAT, we analyzed the immune cell composition of iBAT, which was unchanged (Figures 1E and S1C). This is in line with a previous report that demonstrated that DT injection did not lead to changes in serum C-reactive protein (CRP), tumor necrosis factor α (TNF- α), and interleukin-6 (IL-6) (Sun et al., 2018).

To determine whether the loss of UCP1⁺ brown cells under mild cold stress (23°C) would force the recruitment of UCP1⁺ brite/beige adipocytes in ingWAT, we examined thermogenic gene expression in adipose tissue. *Ucp1* expression was upregulated in both ingWAT and iBAT of UCP1-DTR mice, indicating a compensatory reaction to the loss of functional UCP1⁺ cells (Figures 1F and 1G). In parallel, we observed a significant upregulation of *Pgc1a* in iBAT, suggesting increased mitochondrial biogenesis (Figure 1F).

As an alternate approach to quantify the deletion of Ucp1⁺ adipocytes, we used the UCP1 tracer-deleter mice (UCP1-DTR \times UCP1-CreER \times ROSA-tdRFP) (Rosenwald et al., 2013), which enabled us to quantify the numbers of UCP1⁺ cells based on the recombined alleles. Therefore, UCP1 tracer-deleter mice were injected with tamoxifen to label all UCP1⁺ cells with red fluorescent protein (RFP). After 3 weeks, DT was injected to induce the ablation of UCP1-expressing cells. In line with the protein data, we observed a 95% reduction in UCP1⁺ cells in iBAT upon DT injection relative to those injected with saline (Figure 1H). As reported previously, ingWAT contained substantially fewer UCP1-expressing cells, and in agreement with our protein expression data, the numbers were not significantly reduced after DT injection (Figure 1H). Here, we show that the UCP-DTR mouse is an efficient model for ablating UCP1⁺ cells in iBAT, aBAT, and cBAT in adult mice and allows the study of the contribution of UCP1-expressing adipocytes to metabolism.

Ablation of UCP1⁺ Cells Has No Impact on EE at RT Conditions

To determine whether the efficient deletion of UCP1-expressing cells in iBAT affects energy metabolism and glucose tolerance,

8-week-old mice were fed either a standard chow or a high-fat diet (HFD) for 6 weeks at 23°C and were treated with DT or saline (non-DT) twice per week (Figure 2A). While HFD-fed mice revealed higher body weight compared to chow-fed mice, UCP1-DTR and WT littermates showed a similar body weight gain, regardless of diet (Figures S2A and S2B). DT and non-DT treatment did not affect body weight gain in both UCP1-DTR and WT mice either under chow or HFD feeding (Figures S2A and S2B). Glucose tolerance was unchanged in UCP1⁺ brown adipocyte-deleted UCP1-DTR mice, regardless of diet (Figures 2B and S2C), indicating that UCP1⁺ brown cells do not influence HFD-induced glucose intolerance. Moreover, plasma insulin, leptin, adiponectin, triglyceride, free fatty acids, and cholesterol levels were unchanged (Figures 2C and S2D–S2I).

To assess whether UCP1⁺ brown adipocyte-deleted mice are able to maintain their body temperature, chow diet-fed mice were treated with DT. We observed a similar body temperature under fed and fasting conditions between both genotypes at RT (Figure 2D), indicating that UCP1⁺ brown cells have no impact on body temperature under mild stress conditions (23°C) (Figure 2D). Furthermore, at basal conditions, no changes in any of the measured parameters of EE, oxygen consumption (VO₂), carbon dioxide production (VCO₂), respiratory exchange ratio (RER), food intake, or physical activity were observed between the two genotypes (Figures 2E–2I and S2J), suggesting that the contribution of brown adipocytes to EE and fuel selection at mild cold stress conditions (23°C) was below the detection limit of our system (observable effect size is $\geq 5\%$) (Sun et al., 2018). These data demonstrate that UCP1⁺ cells in iBAT, aBAT, and cBAT in adult mice do not contribute to energy metabolism in RT conditions.

Activation of ingWAT UCP1 Has a Negligible Effect in EE

Based on our findings that at RT, DT injection did only ablate UCP1⁺ cells in iBAT, we next developed a strategy to deplete UCP1⁺ brite/beige cells to study their contribution to energy metabolism. Therefore, UCP1-DTR mice were treated with β -3-adrenergic receptor (β 3-AR) agonist (CL316, 243) (CL) to activate the expression of the transgene. Mice were divided into 3 groups: (1) WT littermates, which have UCP1⁺ brown and brite/beige cells; (2) UCP1-DTR mice, which were injected with DT only at the beginning of the experiment to delete preexisting brown cells (DTR group, expected to have no UCP1⁺ brown cells, but to recruit UCP1⁺ brite/beige cells upon β -adrenergic activation); and (3) UCP1-DTR mice, which received DT with each injection of CL to constantly ablate newly formed brite/beige cells (DTR+DT group, expected to have neither UCP1⁺ brown nor brite/beige cells) (Figure 3A).

(B) Representative tissue images of WT and DTR mice.

(C) Tissue weights (n = 6 in each group).

(D) Quantification of UCP1 protein levels in iBAT, aBAT, cBAT, and ingWAT (n = 6 each group).

(E) Fluorescence-activated cell sorting (FACS) analysis of immune cells in iBAT 2 days after DT injections (WT n = 5; DTR n = 7).

(F and G) Gene expression of thermogenic genes *Cox7a1*, *Pgc1a*, *Prdm16*, and *Ucp1* in iBAT and ingWAT (WT n = 5; DTR n = 6).

(H) Percentage of recombined cells in UCP1 tracer-deleter mice 1 week after saline or DT injection (WT n = 7; DTR n = 5).

Values are presented as means \pm SEMs. **p < 0.01 and ***p < 0.001 by Student's t test. n = number of mice. aBAT, axillary BAT; BAT, brown adipose tissue; cBAT, cervical BAT; DTR, diphtheria toxin receptor; iBAT, intrascapular brown adipose tissue; ingWAT, inguinal white adipose tissue; WT, wild type.

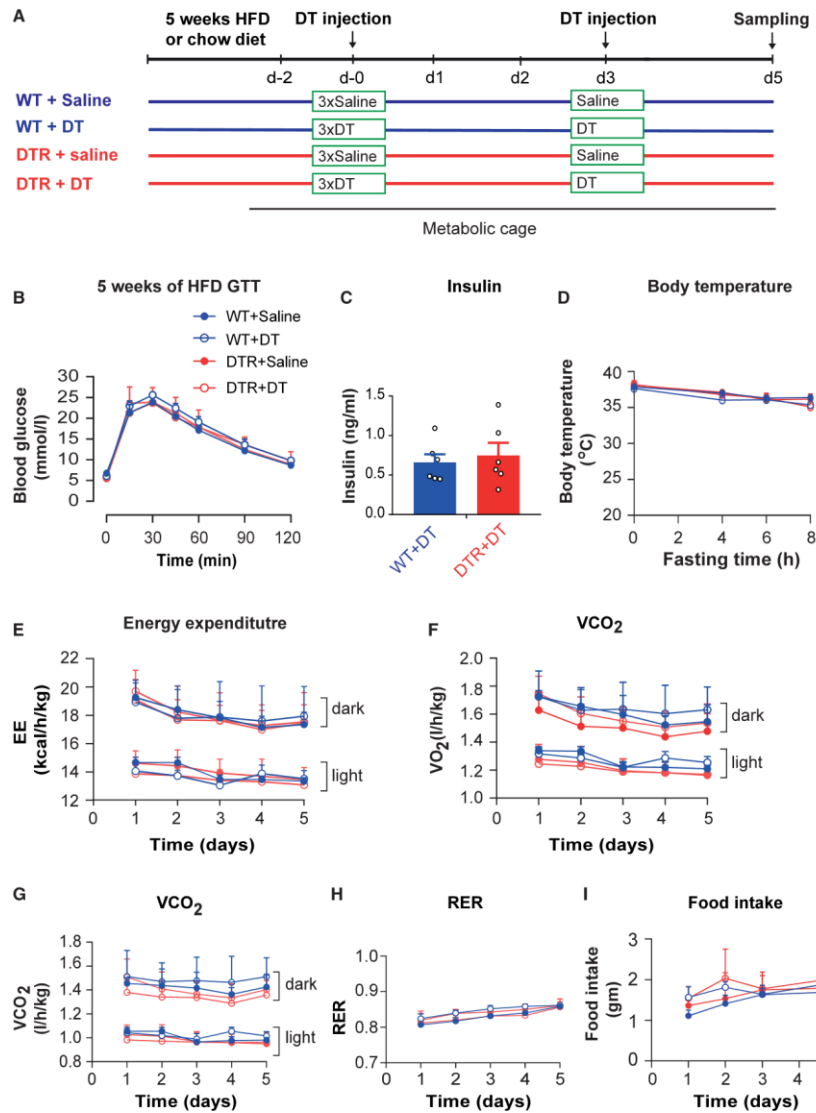


Figure 2. UCP1⁺ Cell Deletion Has No Impact on Energy Expenditure (EE) at Basal Conditions

(A) Experimental scheme for DT and saline (non-DT) treatment at RT (23°C). Eight-week-old WT littermates group (blue) and UCP1-DTR transgene (red) mice were fed either a standard chow or a high-fat diet (HFD) for 6 weeks, and 3 consecutive doses of 100 ng DT (chow) and 200 ng (HFD) were injected every 6 h on day 0 and once on day 3. Tissue were harvested on day 5.

(B) Intraperitoneal glucose tolerance test (ipGTT) in mice fed an HFD for 5 weeks (WT+saline n = 5; WT+DT n = 7, DTR+saline n = 5, DTR+DT n = 5).

(legend continued on next page)



The significant reduction in UCP1 protein levels in iBAT of DTR and DTR+DT groups illustrated that the initial DT injections efficiently ablated preexisting UCP1⁺ cells in iBAT; but more important, CL treatment was not sufficient to induce the formation of new UCP1⁺ cells in this tissue (Figures 3B and 3C). Conversely, UCP1⁺ brite/beige cells formed in ingWAT upon CL treatment in the WT and DTR, but were efficiently ablated by additional injections of DT in the DTR+DT group (Figures 3B and 3C). Moreover, *Ucp1* mRNA was reduced in iBAT of the DTR and DTR+DT groups relative to WT mice (Figure 3D). In ingWAT, increased *Ucp1* and *Pgc1a* in the DTR group indicated the formation of brite/beige cells and were significantly decreased after continued DT injection in the DTR+DT group (Figure 3E).

Since our model allowed the formation of brite/beige cells in ingWAT in the absence of iBAT under stimulated conditions, we assessed the contribution of the newly formed brite/beige cells to energy metabolism. Tissue weight and fasted blood parameters were not different between the 3 groups (Figures S3C–S3G, data not shown). As expected, CL administration resulted in higher oxygen consumption (VO₂) and changes in RER in WT mice (Figures 3F and 3G). In contrast, CL-treated DTR and DTR+DT groups showed VO₂ and RER comparable to basal levels (Figures 3F and 3G), suggesting the efficient ablation of functional UCP1⁺ brown adipocytes. We failed to observe an increase in VO₂ or changes in RER between DTR and DTR+DT groups after CL stimulation (Figures 3F and 3G), despite increased UCP1 levels in ingWAT in DTR mice. These results indicate that the contribution of the newly formed UCP1⁺ brite/beige cells to EE is below the detection limit of the system (Sun et al., 2018).

As it has been debated that brown and brite/beige cells contribute to circulating FGF21 levels, we determined the levels of circulating FGF21 in mice with or without UCP1⁺ cells housed at 23°C (RT) or 8°C (cold) (Figure 3H). Notably, circulating FGF21 levels were similar between both genotypes at RT and under cold exposure (Figure 3H).

UCP1 Is Required for Some of the FGF21-Mediated Metabolic Effects

FGF21 reduces body weight and improves glucose metabolism in DIO independently of UCP1 (BonDurant et al., 2017; Samms et al., 2015; Véniant et al., 2015). Thus, mice with an acute ablation of UCP1⁺ cells were used to examine whether FGF21-mediated weight loss and energy metabolism are dependent on the presence of UCP1⁺ cells. HFD-fed UCP1-DTR mice and WT littermates were treated with DT to ablate UCP1⁺ cells and subsequently subjected to the continuous administration of recombinant FGF21 or saline using mini-osmotic pumps (Figure 4A). To delete newly formed UCP1⁺ brite/beige cells that can be attributable to FGF21 treatment, mice were further injected with a bolus of DT 2 days after pump implantation.

Expectedly, UCP1⁺ cells were deleted in FGF21-treated UCP1-DTR mice, as demonstrated by a significant reduction in UCP1 protein levels in iBAT and ingWAT (Figures 4B and 4C). In iBAT and ingWAT, mRNA expression of *Ucp1* was significantly increased in FGF21-treated WT mice compared to WT mice treated with saline (Figures 4D and 4E), indicating that FGF21 enhances browning. FGF21 administration in both WT and UCP1-DTR mice resulted in the loss of 20% of their initial body weight after 8 days, suggesting that this weight loss effect is independent of UCP1⁺ cells (Figure 4F). This decrease was partly attributed to slightly reduced food intake (Figure S4B). Notably, FGF21 treatment increased oxygen consumption in the WT mice (Figure 4G). However, we did not observe an increase in oxygen consumption in the DTR+FGF21 compared to the WT+saline group (Figure 4G), suggesting that the increased oxygen consumption upon FGF21 treatment is dependent on the presence of UCP1⁺ brown adipocytes. RER was unchanged between the groups (Figure 4H), and DTR+FGF21 mice showed a substantial increase in activity in light and dark phases (Figure 4I). FGF21 signaling has been shown to improve glucose homeostasis and to lower circulating lipids (Véniant et al., 2012). In line with these findings, FGF21-treated WT (5.533 ± 0.423) and UCP1-DTR (5.683 ± 0.452) mice exhibited a lowering of fasting blood glucose compared to WT+saline (8.3 ± 1.372) (Figure 4J). Glucose clearance as assessed by the glucose tolerance test (GTT) showed that DTR+FGF21 mice exhibit significantly impaired glucose tolerance compared to WT+FGF21 mice (area under the curve [AUC]: WT+saline, 998.8 ± 76.89; WT+FGF21, 638 ± 38.83; DTR+FGF21, 886 ± 102.4) (Figure 4K), indicating that the positive effect of FGF21 on glucose metabolism is partly dependent on the presence of UCP1⁺ cells. However, plasma insulin and triacylglycerol (TAG) levels were lower in WT and UCP1-DTR groups treated with FGF21 relative to saline controls (Figures 4L and S3D). Our results suggest that the main beneficial effects of FGF21 such as weight reduction are not directly dependent on UCP1⁺ cells, whereas its effects on glucose metabolism are dependent on UCP1⁺ cells.

DISCUSSION

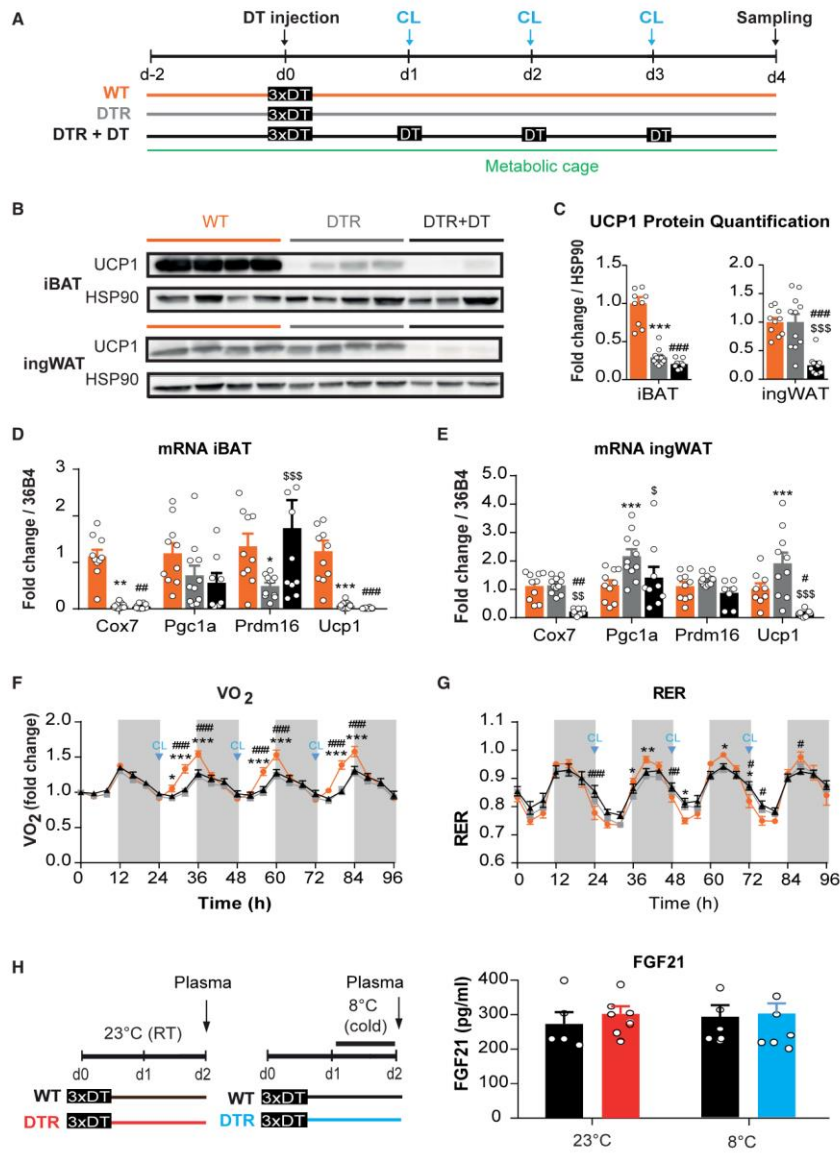
The UCP1-DTR mouse line reported here is, to our knowledge, the first mouse line with an inducible system that allows the efficient ablation of UCP1⁺ cells in adult mice, which can be used to determine the contribution of brown and brite/beige adipocytes to systemic metabolism. In UCP1-deficient mice, which are mainly used to study the contribution of BAT to metabolism (Enerbäck et al., 1997), BAT is still present. Thus, brown/brite/beige cells may still be able to contribute to alternate thermogenic mechanisms, and furthermore, adipokine-mediated signaling would remain active in these mice (Kazak et al., 2015). Contrary to UCP1-deficient mice, our model allows for an acute and transient deletion of UCP1⁺ brown adipocytes by

(C) Plasma insulin levels were measured in mice fed a chow diet (n = 6 in each group).

(D) Body temperature measurement in mice fed a chow diet (WT+saline n = 4; WT+DT n = 5, DTR+saline n = 4, DTR+DT n = 5).

(E–I) EE (E), oxygen consumption (VO₂) (F), carbon dioxide production (VCO₂) (G), respiratory exchange ratio (RER) (H), and food intake (I) were monitored over 6 days in mice fed a chow diet (WT+saline n = 6; WT+DT n = 5, DTR+saline n = 6, DTR+DT n = 7).

Values are expressed as means ± SEMs. The statistical tests used were t test (B and C) and ANOVA (D–I).



(legend on next page)



DT treatment. As DT is efficiently cleared from the blood in ~6 h (Wrobel et al., 1990), our model can be used to study new UCP1⁺ cell formation in ingWAT (Barbatelli et al., 2010; Lee et al., 2015; Rosenwald et al., 2013). While iBAT is to a large extent already functional at RT (21°C), UCP1 expression in brite/beige cells is substantially increased upon cold induction in ingWAT (Kalimovich et al., 2017). In agreement with these findings, ablation of UCP1⁺ cells at RT in iBAT is very efficient, whereas UCP1⁺ brite/beige cells in ingWAT are not ablated. Upon β3-AR agonist activation, UCP1⁺ brite/beige cells in ingWAT express higher levels of both UCP1 protein and DTR protein, which enables the ablation of these cells.

Several studies have suggested compensations by other tissues to account for the loss of non-shivering thermogenesis in different model systems of chronic ablation (Schulz et al., 2013). One argument against such an effect in the acute model presented here is the fact that we observe a reduction in EE under cold stimulation, but not at RT, which is in line with the calculated contribution of iBAT to systemic EE. Furthermore, we recently demonstrated (Sun et al., 2018) that ablation in a model of increased EE is normalized by the ablation of BAT, suggesting that no compensation is observed in the acute modulation. Lastly, an increasing number of publications suggest possible cross-talk between skeletal muscle and BAT via humoral-mediated factors including cytokines in the regulation of energy homeostasis (Bal et al., 2017). The role of FGF21 in cross-communication between BAT and muscle has been proposed (Li et al., 2017; Rodríguez et al., 2017); however, we show here that there was no difference in circulating FGF21 levels in WT and UCP1⁺ at RT and after cold exposure. Similarly, it has been reported that mild cold adaptation resulted in a significant upregulation of IL-6 (Jansky et al., 1996; Liu et al., 2007). In addition, the serum of mice acclimatized to severe cold exhibited higher TNF-α compared to thermoneutrality, while leptin levels were significantly downregulated after mild and severe cold adaptation (Bal et al., 2017). We show here that the deletion of UCP1-expressing adipocytes in an inducible adult mouse model has no impact on the plasma leptin level at mild cold adaptation, regardless of diet. Furthermore, TNF-α levels were unchanged, and IL-6 levels were significantly decreased in UCP1-DTR mice treated with DT in cold (Sun et al., 2018).

UCP1-deficient mice exhibited similar EE at RT with WT animals and blunted response to a β3-AR agonist treatment (Enerbäck et al., 1997; Lowell et al., 1993). In accordance with these observations, the UCP1-DTR model shows no changes in oxygen consumption and RER at RT. It has been recently

reported that UCP1⁺ brite/beige cells contribute only ~10% of the thermogenic capacity of BAT (Nedergaard and Cannon, 2013). Accordingly, our data demonstrate that oxygen consumption is mainly regulated by UCP1⁺ cells in iBAT and that UCP1⁺ brite cells under physiological conditions do not contribute to oxygen consumption or weight gain on an HFD. It should be noted that enhanced induction through alternate pathways may induce both formation and activity of these cells; thus, every model would need to be tested independently for the contribution of brown and brite/beige cells to energy metabolism.

FGF21 has been identified as a novel circulating hormone that controls EE, and treatment with FGF21 can induce enhanced EE and lead to weight loss that is concomitant with improved systemic metabolism (Straub and Wolfrum, 2015). Since FGF21 is expressed in UCP1⁺ cells and FGF21 levels are induced upon cold, it has been suggested that circulating FGF21 may in part be derived from brown adipocytes (Hondares et al., 2011; Keipert et al., 2015, 2017). We show here that the acute deletion of UCP1⁺ cells has no impact on circulating FGF21 levels either at RT or in cold, indicating that brown adipocytes do not contribute to circulating FGF21 levels. In UCP1-deficient mice, FGF21 levels in BAT are substantially higher as part of a compensatory response (Keipert et al., 2015, 2017). Whether under these conditions BAT is a source of FGF21 would require the generation of a UCP1-DTR, UCP1-deficient double-knockout (KO) animal.

Previous studies using the UCP1-KO model system have proposed that the effects of FGF21 on body weight are independent of UCP1 (Samms et al., 2015; Véniant et al., 2015). In agreement with these studies, we show here that the ablation of both brown and brite adipocytes does not alter weight loss, which can be achieved by chronic FGF21 infusion. This finding would foment the simple conclusion that FGF21 acts independently of BAT to affect energy metabolism, which is supported by a careful analysis of the data. In agreement with the study by Samms et al. (2015), we could show that the induction of EE upon FGF21 infusion is not observed in mice lacking UCP1⁺ cells, which is in contrast to the finding of Véniant et al. (2015). Similarly, we did not observe any differences in basal EE in mice lacking UCP1⁺ cells. Why then is weight gain not affected? Samms et al. (2015) reported that food intake was lower in UCP1-KO mice infused with FGF21, for which we observed a trend in our infusion model. In contrast to all other studies, we observed that FGF21 also increased voluntary movement of the mice only upon the infusion of FGF21. These data indicate that BAT is affected by FGF21

Figure 3. Ablation of UCP1⁺ Brite Cells after CL Injection

(A) Experimental scheme for ablation of UCP1⁺ cells after CL treatment. WT group (orange): mice not carrying the UCP1-DTR transgene obtained DT on day 0. DTR group (gray): UCP1-DTR mice receiving DT only on day 0. DTR+DT group (black): UCP1-DTR mice receiving DT continuously. All of the mice were treated with β3-adrenergic receptor agonist (CL316, 243) (CL) every 24 h, and tissue was harvested 24 h after last CL/CL+DT injection.

(B and C) Representative western blot and quantification of UCP1 in iBAT and ingWAT (WT n = 10; DTR n = 11; DTR+DT n = 10).

(D and E) Gene expression of thermogenic genes *Cox7a1*, *Pgc1a*, *Prdm16*, and *Ucp1* in iBAT and ingWAT (WT n = 10; DTR n = 11; DTR+DT n = 10).

(F and G) $\dot{V}O_2$ (F) and RER (G) were monitored (WT n = 10; DTR n = 11; DTR+DT n = 10).

(H) Plasma FGF21 levels (WT n = 5; DTR n = 6).

Values represented as means ± SEMs. *, #, or § p < 0.05, **, ##, or §§ p < 0.01, and ***, ###, or §§§ p < 0.001 by 2-way ANOVA + Tukey's multiple comparison. *, WT versus DTR; #, WT versus DTR+DT; §, DTR versus DTR+DT. Unless indicated otherwise, n denotes individual mice.

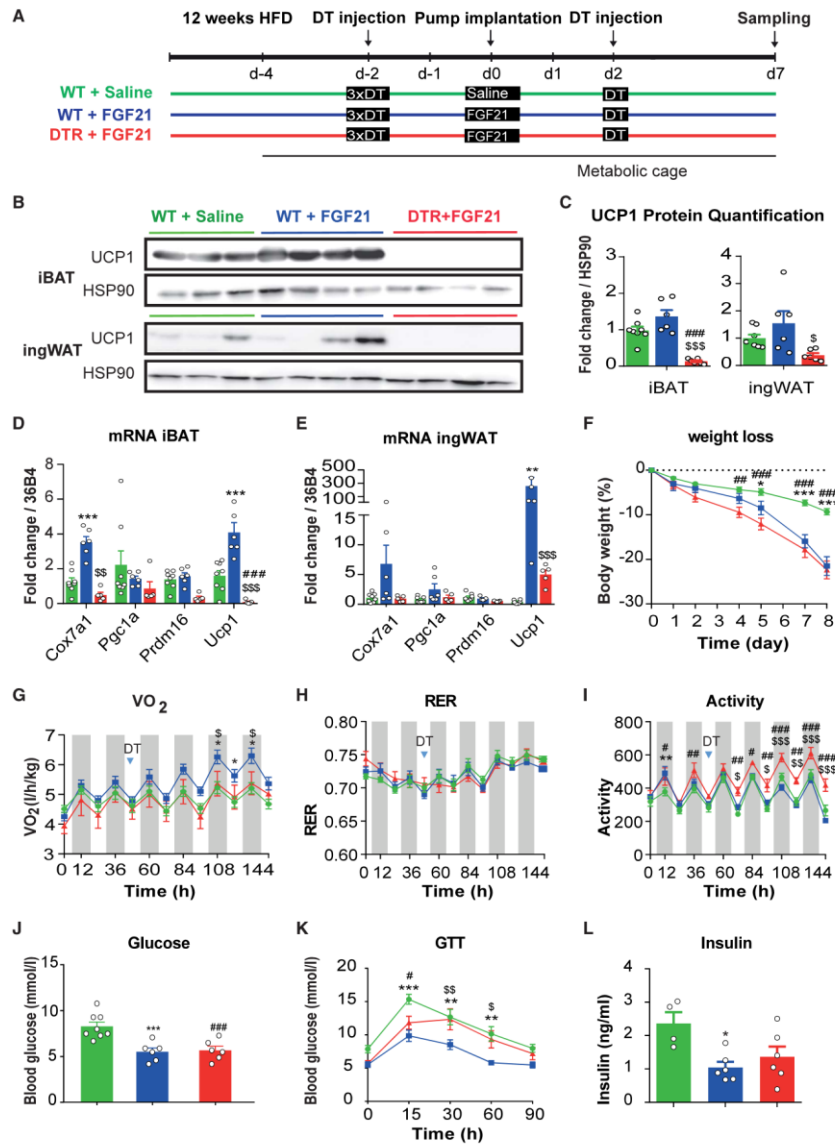


Figure 4. UCP1 Is Required for Some of the FGF21-Mediated Metabolic Effects

(A) Experimental scheme. HFD-fed UCP1-DTR mice and WT littermates for 12 weeks treated with DT on day -2 before pump implantation on day 0. Pumps containing saline or recombinant human FGF21 were implanted on day 0, DT treatment was repeated on day 2, and tissue was harvested on day 7. WT+saline

(legend continued on next page)



and that the absence of this tissue leads to compensatory changes in basal metabolism, food intake, and ambulatory behavior, resulting in a similar net body weight loss. In addition to its beneficial effect on weight reduction, FGF21 has been reported to lower plasma glucose and triglyceride levels independent of UCP1 (Samms et al., 2015; Véniant et al., 2015). Contrary to these findings, we show here that FGF21-treated UCP1-DTR mice exhibited impaired glucose tolerance compared to control mice, indicating that UCP1⁺ cells are partially required for the beneficial effects of FGF21 on blood glucose levels. Supporting our findings, Lan et al. (2017) showed that the acute insulin-sensitizing effects of FGF21 require direct binding to adipose tissue, whereas long-term effects such as weight loss are more centrally regulated and depend on the binding of FGF21 in the hypothalamus, but not on adipose tissue. These findings clearly demonstrate that signals that originate from BAT are important modulators of various mechanisms regulating energy and glucose metabolism. This in turn has important implications for the study of the effects of FGF21 in humans.

STAR+METHODS

Detailed methods are provided in the online version of this paper and include the following:

- KEY RESOURCES TABLE
- LEAD CONTACT AND MATERIALS AVAILABILITY
- EXPERIMENTAL MODEL AND SUBJECT DETAILS
- METHOD DETAILS
 - Quantification of UCP1 ablation with UCP1-tracer mouse
 - Diphtheria toxin (DT)-mediated brown and brite adipocytes ablation
 - Beta-3-adrenergic receptor agonist (CL316, 243) (CL) stimulation
 - Indirect calorimetry
 - Osmotic Pump Implantation and FGF21 Treatment
 - Glucose tolerance test
 - Plasma parameters
 - Body temperature
 - SVF isolation and FACS
 - Western blot analysis
 - RNA extraction and quantitative real-time PCR
- QUANTIFICATION AND STATISTICAL ANALYSIS
- DATA AND CODE AVAILABILITY

SUPPLEMENTAL INFORMATION

Supplemental Information can be found online at <https://doi.org/10.1016/j.celrep.2020.02.055>.

ACKNOWLEDGMENTS

We gratefully thank S. Freederich for help with the mice work and the PhenoMaster. We thank Eli Lilly for providing the recombinant human FGF21 used in the study. This work was supported by a grant from the Swiss National Science Foundation.

AUTHOR CONTRIBUTIONS

T.D.C., E. Kulenkampff, D.H.D., and C.W. wrote the manuscript. T.D.C., E.K., and D.H.D. performed most of the experiments. C.M. and L.S. performed the UCP1 tracer-deleter experiments. E. Kiehlmann performed the western blot experiments. W.S. helped with the injections of CL.

DECLARATION OF INTERESTS

The authors declare no competing interests.

Received: May 20, 2019
Revised: December 20, 2019
Accepted: February 13, 2020
Published: March 10, 2020

REFERENCES

- Bal, N.C., Maurya, S.K., Pani, S., Sethy, C., Banerjee, A., Das, S., Patnaik, S., and Kundu, C.N. (2017). Mild cold induced thermogenesis: are BAT and skeletal muscle synergistic partners? *Biosci. Rep.* 37, BSR20171087.
- Barbatelli, G., Murano, I., Madsen, L., Hao, Q., Jimenez, M., Kristiansen, K., Giacchino, J.P., De Matteis, R., and Cinti, S. (2010). The emergence of cold-induced brown adipocytes in mouse white fat depots is determined predominantly by white to brown adipocyte transdifferentiation. *Am. J. Physiol. Endocrinol. Metab.* 298, E1244–E1253.
- BonDurant, L.D., Ameka, M., Naber, M.C., Markan, K.R., Idiga, S.O., Acevedo, M.R., Walsh, S.A., Ornitz, D.M., and Potthoff, M.J. (2017). FGF21 Regulates Metabolism Through Adipose-Dependent and -Independent Mechanisms. *Cell Metab.* 25, 935–944.e4.
- Cannon, B., and Nedergaard, J. (2004). Brown adipose tissue: function and physiological significance. *Physiol. Rev.* 84, 277–359.
- Dulloo, A.G., and Miller, D.S. (1984). Energy balance following sympathetic denervation of brown adipose tissue. *Can. J. Physiol. Pharmacol.* 62, 235–240.
- Enerbäck, S., Jacobsson, A., Simpson, E.M., Guerra, C., Yamashita, H., Harper, M.E., and Kozak, L.P. (1997). Mice lacking mitochondrial uncoupling protein are cold-sensitive but not obese. *Nature* 387, 90–94.
- Feldmann, H.M., Golozubova, V., Cannon, B., and Nedergaard, J. (2009). UCP1 ablation induces obesity and abolishes diet-induced thermogenesis in

group (green): received pumps with saline; WT+FGF21 (blue): received pumps delivering recombinant human FGF21; DTR+FGF21 (red): carried the UCP1-DTR transgene and received pumps delivering recombinant human FGF21.

(B and C) Representative western blot and protein quantification of UCP1 in iBAT and ingWAT (WT+saline n = 8; WT+FGF21 n = 6; DTR+FGF21 n = 6).

(D and E) Expression of thermogenic genes *Cox7a1*, *Pgc1a*, *Prdm16*, and *Ucp1* in iBAT and ingWAT (WT+saline n = 8; WT+FGF21 n = 6; DTR+FGF21 n = 6).

(F) Percentage of body weight reduction after pump implantation (WT+saline n = 8; WT+FGF21 n = 6; DTR+FGF21 n = 6).

(G–I) VO₂ (G), RER (H), and activity (I) were monitored over 6 days (WT+saline n = 8; WT+FGF21 n = 6; DTR+FGF21 n = 6).

(J and K) Fasted blood glucose (J; WT+saline n = 8; WT+FGF21 n = 6; DTR+FGF21 n = 6) and ipGTT (K) 7 days after pump implantation (WT+saline n = 4; WT+FGF21 n = 6; DTR+FGF21 n = 6).

(L) Insulin levels 7 days after pump implantation (WT+saline n = 4; WT+FGF21 n = 6; DTR+FGF21 n = 6).

Values represented as means ± SEMs. *p < 0.05, **p < 0.01, and ***p < 0.001 by 2-way ANOVA + Tukey's multiple comparison. #, WT+saline versus WT+FGF21; #, WT+saline versus DTR+FGF21; \$, WT+FGF21 versus DTR+FGF21. n denotes individual mice.

- mice exempt from thermal stress by living at thermoneutrality. *Cell Metab.* 9, 203–209.
- Golozoubova, V., Gullberg, H., Matthias, A., Cannon, B., Vennström, B., and Nedergaard, J. (2004). Depressed thermogenesis but competent brown adipose tissue recruitment in mice devoid of all hormone-binding thyroid hormone receptors. *Mol. Endocrinol.* 18, 384–401.
- Hany, T.F., Gharehpapagh, E., Kamel, E.M., Buck, A., Himms-Hagen, J., and von Schulthess, G.K. (2002). Brown adipose tissue: a factor to consider in symmetrical tracer uptake in the neck and upper chest region. *Eur. J. Nucl. Med. Mol. Imaging* 29, 1393–1398.
- Hondares, E., Iglesias, R., Giralt, A., Gonzalez, F.J., Giralt, M., Mampel, T., and Villarroya, F. (2011). Thermogenic activation induces FGF21 expression and release in brown adipose tissue. *J. Biol. Chem.* 286, 12983–12990.
- Janský, L., Pospíšilová, D., Honzová, S., Uličný, B., Srámek, P., Zeman, V., and Kamínková, J. (1996). Immune system of cold-exposed and cold-adapted humans. *Eur. J. Appl. Physiol. Occup. Physiol.* 72, 445–450.
- Kalinovich, A.V., de Jong, J.M., Cannon, B., and Nedergaard, J. (2017). UCP1 in adipose tissues: two steps to full browning. *Biochimie* 134, 127–137.
- Kazak, L., Chouchani, E.T., Jedrychowski, M.P., Erickson, B.K., Shinoda, K., Cohen, P., Vetrivelan, R., Lu, G.Z., Laznik-Bogoslavski, D., Hasenfuss, S.C., et al. (2015). A creatine-driven substrate cycle enhances energy expenditure and thermogenesis in beige fat. *Cell* 163, 643–655.
- Keipert, S., Kutschke, M., Lamp, D., Brachthäuser, L., Neff, F., Meyer, C.W., Oelkrug, R., Kharitonov, A., and Jastroch, M. (2015). Genetic disruption of uncoupling protein 1 in mice renders brown adipose tissue a significant source of FGF21 secretion. *Mol. Metab.* 4, 537–542.
- Keipert, S., Kutschke, M., Ost, M., Schwarzmayr, T., van Schothorst, E.M., Lamp, D., Brachthäuser, L., Hamp, I., Mazubuko, S.E., Hartwig, S., et al. (2017). Long-Term Cold Adaptation Does Not Require FGF21 or UCP1. *Cell Metab.* 26, 437–446.e5.
- Kopecky, J., Clarke, G., Enerbäck, S., Spiegelman, B., and Kozak, L.P. (1995). Expression of the mitochondrial uncoupling protein gene from the *aP2* gene promoter prevents genetic obesity. *J. Clin. Invest.* 96, 2914–2923.
- Kozak, L.P. (2010). Brown fat and the myth of diet-induced thermogenesis. *Cell Metab.* 11, 263–267.
- Kulenkampff, E., and Wolfrum, C. (2018). Proliferation of nutrition sensing pre-adipocytes upon short term HFD feeding. *Adipocyte* 8, 16–25.
- Lan, T., Morgan, D.A., Rahmouni, K., Sonoda, J., Fu, X., Burgess, S.C., Holland, W.L., Kilewer, S.A., and Mangelsdorf, D.J. (2017). FGF19, FGF21, and an FGFFR1/beta-Klotho-Activating Antibody Act on the Nervous System to Regulate Body Weight and Glycemia. *Cell Metab.* 26, 709–718.e3.
- Lee, Y.H., Petkova, A.P., Konkar, A.A., and Granneman, J.G. (2015). Cellular origins of cold-induced brown adipocytes in adult mice. *FASEB J.* 29, 286–299.
- Li, F., Li, Y., Duan, Y., Hu, C.A.A., Tang, Y., and Yin, Y. (2017). Myokines and adipokines: involvement in the crosstalk between skeletal muscle and adipose tissue. *Cytokine Growth Factor Rev.* 33, 73–82.
- Liu, X., Rossmel, M., McClaine, J., Riachi, M., Harper, M.E., and Kozak, L.P. (2003). Paradoxical resistance to diet-induced obesity in UCP1-deficient mice. *J. Clin. Invest.* 111, 399–407.
- Liu, Y.L., Bi, H., Chi, S.M., Fan, R., Wang, Y.M., Ma, X.L., Chen, Y.M., Luo, W.J., Pei, J.M., and Chen, J.Y. (2007). The effect of compound nutrients on stress-induced changes in serum IL-2, IL-6 and TNF- α levels in rats. *Cytokine* 37, 14–21.
- Lowell, B.B., S-Sulic, V., Hamann, A., Lawitts, J.A., Himms-Hagen, J., Boyer, B.B., Kozak, L.P., and Flier, J.S. (1993). Development of obesity in transgenic mice after genetic ablation of brown adipose tissue. *Nature* 366, 740–742.
- Nedergaard, J., and Cannon, B. (2013). UCP1 mRNA does not produce heat. *Biochim. Biophys. Acta* 1831, 943–949.
- Nedergaard, J., Bengtsson, T., and Cannon, B. (2007). Unexpected evidence for active brown adipose tissue in adult humans. *Am. J. Physiol. Endocrinol. Metab.* 293, E444–E452.
- Poher, A.L., Altirriba, J., Veyrat-Durebex, C., and Rohrer-Jeanrenaud, F. (2015). Brown adipose tissue activity as a target for the treatment of obesity/insulin resistance. *Front. Physiol.* 6, 4.
- Rodríguez, A., Becerril, S., Ezquerro, S., Méndez-Giménez, L., and Frühbeck, G. (2017). Crosstalk between adipokines and myokines in fat browning. *Acta Physiol. (Oxf.)* 219, 362–381.
- Rosenwald, M., Perdikari, A., Rülcke, T., and Wolfrum, C. (2013). Bi-directional interconversion of brite and white adipocytes. *Nat. Cell Biol.* 15, 659–667.
- Saito, M., Okamatsu-Ogura, Y., Matsushita, M., Watanabe, K., Yoneshiro, T., Nio-Kobayashi, J., Iwanaga, T., Miyagawa, M., Kameya, T., Nakada, K., et al. (2009). High incidence of metabolically active brown adipose tissue in healthy adult humans: effects of cold exposure and adiposity. *Diabetes* 58, 1526–1531.
- Samms, R.J., Smith, D.P., Cheng, C.C., Antonellis, P.P., Perfield, J.W., 2nd, Kharitonov, A., Gimeno, R.E., and Adams, A.C. (2015). Discrete Aspects of FGF21 In Vivo Pharmacology Do Not Require UCP1. *Cell Rep.* 11, 991–999.
- Schulz, T.J., Huang, P., Huang, T.L., Xue, R., McDougall, L.E., Townsend, K.L., Cypess, A.M., Mishina, Y., Gussoni, E., and Tseng, Y.H. (2013). Brown-fat paucity due to impaired BMP signalling induces compensatory browning of white fat. *Nature* 495, 379–383.
- Straub, L., and Wolfrum, C. (2015). FGF21, energy expenditure and weight loss - How much brown fat do you need? *Mol. Metab.* 4, 605–609.
- Sun, W., Dong, H., Becker, A.S., Dapito, D.H., Modica, S., Grandl, G., Opitz, L., Efthymiou, V., Straub, L.G., Sarker, G., et al. (2018). Cold-induced epigenetic programming of the sperm enhances brown adipose tissue activity in the offspring. *Nat. Med.* 24, 1372–1383.
- van Marken Lichtenbelt, W.D., Vanhommerig, J.W., Smulders, N.M., Drossaerts, J.M., Kemerink, G.J., Bouvy, N.D., Schrauwen, P., and Teule, G.J. (2009). Cold-activated brown adipose tissue in healthy men. *N. Engl. J. Med.* 360, 1500–1508.
- Véniant, M.M., Hale, C., Helmering, J., Chen, M.M., Stanislaus, S., Busby, J., Vonderfecht, S., Xu, J., and Lloyd, D.J. (2012). FGF21 promotes metabolic homeostasis via white adipose and leptin in mice. *PLoS One* 7, e40164.
- Véniant, M.M., Sivits, G., Helmering, J., Komorowski, R., Lee, J., Fan, W., Moyer, C., and Lloyd, D.J. (2015). Pharmacologic Effects of FGF21 Are Independent of the “Browning” of White Adipose Tissue. *Cell Metab.* 21, 731–738.
- Virtanen, K.A., Lidell, M.E., Orava, J., Heglind, M., Westergren, R., Niemi, T., Taittonen, M., Laine, J., Savisto, N.J., Enerbäck, S., and Nuutila, P. (2009). Functional brown adipose tissue in healthy adults. *N. Engl. J. Med.* 360, 1518–1525.
- Wankhade, U.D., Shen, M., Yadav, H., and Thakali, K.M. (2016). Novel Browning Agents, Mechanisms, and Therapeutic Potentials of Brown Adipose Tissue. *BioMed Res. Int.* 2016, 2365609.
- Wrobel, C.J., Wright, D.C., Dedrick, R.L., and Youle, R.J. (1990). Diphtheria toxin effects on brain-tumor xenografts. Implications for protein-based brain-tumor chemotherapy. *J. Neurosurg.* 72, 946–950.



STAR★METHODS

KEY RESOURCES TABLE

REAGENT or RESOURCE	SOURCE	IDENTIFIER
Antibodies		
UCP1 antibody	Abcam	Cat# ab10983; RRID: AB_2241462
HSP90 (C45G5) Rabbit mAb antibody	Cell Signaling	Cat# 4877; RRID: AB_2233307
APC/Cy7 anti-mouse CD45 antibody	Biolegend	Cat# 103115; RRID: AB_312980
Brilliant V71 anti-mouse CD3 antibody	Biolegend	Cat# 100241; RRID: AB_2563945
PE/Cy7 anti-mouse CD19 antibody	Biolegend	Cat# 115519; RRID: AB_313654
FITC anti-mouse Ly-6G antibody	Biolegend	Cat# 127605; RRID: AB_1236488
PE anti-mouse/human CD11b antibody	Biolegend	Cat# 101208; RRID: AB_312791
Pacific Blue anti-mouse F4/80 antibody	Biolegend	Cat# 123123; RRID: AB_893487
Chemicals, Peptides, and Recombinant Proteins		
Diphtheria toxin	Millipore,	Cat#322326-1MG
Tamoxifen (#T564, Sigma-Aldrich)	Sigma-Aldrich	Cat#T564
Recombinant human FGF21	Elli Lilly	N/A
CL 316243	Sigma-Aldrich	Cat#C5976
Trizol reagent	Invitrogen	Cat# 15596026
-2147483641-1359662100Live/dead fixable dead cell stains	Thermofisher	Cat# L34960
Critical Commercial Assays		
FGF 21 Mouse/Rat ELISA	R&D SYSTEMS	cat#MF2100
Ultra-sensitive mouse insulin ELISA kit	Crystal Chem,	Cat#90080
FGF 21 Mouse/Rat ELISA	R&D SYSTEMS	Cat#MF2100
Mouse Leptin ELISA Kit	Crystal Chem	Cat#90030
Mouse Adiponectin ELISA Kit	Crystal Chem	Cat#80569
Triglycerides	Roche	Cat#11489232
Cholesterol	Roche	Cat#11877771
Free fatty acids	Wako Nefa	Cat#9196
High Capacity cDNA RT kit	Applied Biosystems	Cat# 4368814
Pierce BCA Protein assay Kit	Thermo Fisher	Cat#23225
Experimental Models: Organisms/Strains		
UCP1-DTR-eGFP	Christian Wolfrum	Rosenwald et al., 2013
UCP1-CreER	Christian Wolfrum	Rosenwald et al., 2013
8.58.5ROSA-tDrFP	Christian Wolfrum	Rosenwald et al., 2013
Oligonucleotides		
Primers for qRT-PCR	N/A	Microsynth
Mouse Cox7a1 primer sequence Forward:	CAGCGTCATGGTCAGTCTGT	N/A
Mouse Cox7a1 primer sequence Reverse:	AGAAAACCGTGTGGCAGAGA	N/A
Mouse PGC1a primer sequence Forward:	ACCCCAAAGGATGCGCTCTCGTT	N/A
Mouse PGC1a primer sequence Reverse:	TGCGGTGTCTGTAGTGGCTTGATT	N/A
Mouse PRDM16 primer sequence Forward:	CGCTTCGAATGTGAAAACCTG	N/A
Mouse PRDM16 primer sequence Reverse:	AAGGTCTTGCCACAGTCAGG	N/A
Mouse UCP1 primer sequence Forward:	GGGCATTGAGAGGCAAATCAGCTT	N/A
Mouse UCP1 primer sequence Reverse:	ACACTGCCACACCTCCAGTCATTA	N/A
Mouse 36B4 primer sequence Forward:	GCCGTGATGCCAGGGAAGA	N/A
Mouse 36B4 primer sequence Reverse:	CATCTGCTTGGAGCCACGTT	N/A

(Continued on next page)

Continued		
REAGENT or RESOURCE	SOURCE	IDENTIFIER
Software and Algorithms		
TSE PhenoMaster software	TSE PhenoMaster	Version 5.6.5
GraphPad Prism 8 software	GraphPad Prism	Version 8.2.0
ViiA7 software	Applied Biosystems	Version 1.2.3
Other		
Standard chow	Kliba-Nafag, Kaiseraugst	#2222
60% calories from fat high-fat diet	Kliba-Nafag	#2127

LEAD CONTACT AND MATERIALS AVAILABILITY

UCP1-DTR mice line generated in this study are available under request for distribution through a completed Material Transfer Agreement. Further information and requests for resources and reagents should be directed to and will be fulfilled by the Lead Contact, Christian Wolfrum (christian-wolfrum@ethz.ch).

EXPERIMENTAL MODEL AND SUBJECT DETAILS

UCP1-DTR-eGFP mice were generated as previously described (Rosenwald et al., 2013). Mice were kept on a C57/B6N background and housed at 23°C under a 12-hour light/dark cycle with free access to water and standard chow (purified diet #2222; Kliba-Nafag, Kaiseraugst, Switzerland; 18% protein, 7% fat, 58% carbohydrate by mass) or a 60% calories from fat high-fat diet (purified diet #2127; Kliba-Nafag; 23.9% protein, 35% fat, 23.2% carbohydrate by mass) the latter was started at the age of eight weeks and maintained for 6 to 12 weeks on HFD. In chow-fed experiments, 8-12 weeks old UCP1-DTR-eGFP and littermate WT controls male mice were used. Body weight was monitored weekly. All animal studies conformed to the Swiss animal protection laws and were approved by the cantonal Veterinary Office in Zurich, Switzerland.

METHOD DETAILS

Quantification of UCP1 ablation with UCP1-tracer mouse

According to standard protocol, CreERT2 activity was induced by gavaging UCP1-tracer-deleter (UCP1-DTR x UCP1-CreER x ROSA-tdRFP) mice with 2 mg (80 mg/kg mouse) of Tamoxifen (#T564, Sigma-Aldrich) in 100ul sun flower oil per day for two consecutive days to label all UCP1+ cells with RFP. Quantification of recombination was performed as described previous (Rosenwald et al., 2013). The UCP1-tracer-deleter mouse model allows labeling of brown and brite adipocytes up on tamoxifen treatment. To quantify labeled cells, iBAT and ingWAT were excised and genomic DNA (gDNA) was prepared by lysing the tissue in 1 mL of 50 mM NaOH (Sigma-Aldrich) with metal beads for 6 minutes with the Thermolyser LT (QIAGEN). Subsequently, tissues were rotated (1000 rpm) at 92°C for 1 h and neutralized with 250 µl of 1 M TrisHCl (Sigma-Aldrich). The samples were centrifuged twice at 12000 rpm for 5 minutes and the aqueous phase was transferred to a new tube and diluted at a ratio of 1:30. To quantify the exact number of labeled adipocytes, the number of recombined loxP site loci in genomic DNA was quantified by qPCR (Rosenwald et al., 2013). The apolipoprotein B gene (*ApoB*) used as an internal control, to quantify the total cell number.

Diphtheria toxin (DT)-mediated brown and brite adipocytes ablation

To ablate UCP1+ cells, littermate WT or UCP1-DTR mice were subjected to three subcutaneous doses of 100ng (for mice on chow) or 200ng (for mice on HFD) Diphtheria toxin (#322326-1MG, Millipore, Zug, Switzerland) or saline (non-DT) injection every 6h. Three days later DT or saline was also administrated once per day depending on the experimental setup. Body weight was measured every second day after DT or non-DT injection to monitor the effect of DT on body weight gain.

Beta-3-adrenergic receptor agonist (CL316, 243) (CL) stimulation

UCP1-DTR or littermate control WT mice were received three intra-peritoneal (i.p.) injections of 0.1mg/kg CL-316243 (# C5976, Sigma-Aldrich) 18h after the third initial DT injection. Repeated CL/CL+DT injections were given every 24h for consecutive 3 days.

Indirect calorimetry

Indirect calorimetry measurements were performed with the Phenomaster (TSE Systems; TSE systems, Bad Homburg, Germany) or with the Promethion High-Definition Behavioral Phenotyping System for Mice. UCP1-DTR or littermate WT mice were acclimated to metabolic cages for two days prior to DT-mediated ablation and subsequent measurement. Mice had free access to water and food weight was measured daily. For 60 s every 10 min, Oxygen consumption (O₂) and CO₂ volumes were measured continuously using



the manufacturer's software (TSE PhenoMaster, version 5.6.5) with the coefficients of 3.941 (CVO2) and 1.106 (CVCO2) and normalized to the lean body mass. Lean and fat body mass was measured by a magnetic resonance imaging technique (EchoMRI 130, Body Composition Analyzer, Echo Medical Systems) before DT administration. RER was calculated by volume CO₂/volume O₂. Analyses were conducted on averaged measurements over the course of 12h representing the light or dark cycles for 4 to 10 days, unless otherwise indicated.

Osmotic Pump Implantation and FGF21 Treatment

For FGF21 experiments, mice were fed HFD for 12 weeks and UCP1-DTR or littermate WT mice were acclimated to metabolic cages for two days before DT injection. Then treated with 3x200ng of DT every 6h, after 48h from the initial DT injection, mice were subcutaneously given 5mg/kg bodyweight of carprofen (Novocarp) as an analgesic prior to osmotic pump implantation. Mice were subcutaneously implanted with mini osmotic pumps (Alzet Model 1002, 0.25ul/h infusion rate) containing saline or recombinant human FGF21 (Elli Lilly; dose 1mg/kg/day). Mice were monitored post-surgery and allowed to recover for 2 days during which they received a daily i.p. injection of carprofen (5mg/kg) for three days. Two days after FGF21/saline pump implantation, mice were given a booster dose of 200ng DT to further ablate newly formed UCP1+ cells induced by FGF21 infusion for indirect calorimetry measurements and analyzing of metabolic parameters.

Glucose tolerance test

Mice were fasted for 6h and baseline glucose levels were measured. Thereafter, glucose (2 g/kg body weight (D-glucose, Sigma in 0.9% saline)) was injected i.p. and blood glucose concentration was measured from tail-tip blood after 15, 30, 45, 60, 90, and 120 min by using a glucometer (Accu-Check Aviva glucose strip system, #07400918016, #06453988016; Roche Diagnostics International, Basel, Switzerland).

Plasma parameters

Mice were fasted for 6h before tissue and blood sampling. Circulating insulin concentration was measured by using ultra-sensitive mouse insulin ELISA kit (Crystal Chem, #90080), FGF21 concentration was measured by using the FGF21 Mouse/Rat ELISA kit (R&D SYSTEMS, #MF2100). Plasma triglycerides (Cobas Roche/Hitachi Kit #11489232, Roche Diagnostics International), Cholesterol (Cobas Roche/Hitachi Kit #11877771, Roche Diagnostics International) and free fatty acids (Wako Nefa kit #9196, Wako Pure Chemical Industries, Tokyo, Japan) were measured by colorimetric assays as per manufacturer's instructions. Circulating adiponectin (Crystal Chem, #80569) and leptin (Crystal Chem, #90030) concentrations were measured by mouse leptin and adiponectin ELISA Kit according to the manufacturer's protocols.

Body temperature

Eight to ten weeks old chow-diet fed WT and UCP1-DTR mice were injected with saline (non-DT) or 100ng DT every 6 hours (3x) on day 0, after 72 h of last DT or saline injection, fed-state rectal body temperature was measured and the mice were fasted for 2, 4, 6 and 8 hours for fasting rectal body temperature measurement.

SVF isolation and FACS

For SVF (stromal vascular fraction) isolation, iBAT was obtained from UCP1-DTR or littermate WT mice and prepared as previously described (Kulenkampff and Wolfrum, 2018). Surface antigens such as APC/Cy7 anti-mouse CD45 Antibody #103115, Brilliant Violet 711 anti-mouse CD3 Antibody # 100241, PE/Cy7 anti-mouse CD19 Antibody #115519, FITC anti-mouse Ly-6G Antibody #127605, PE anti-mouse/human CD11b Antibody#101207 and Pacific Blue anti-mouse F4/80 Antibody #123123 were obtained from BioLegend and the cells were stained for 15min on ice. Live/dead staining was performed by using live/dead fixable dead cell stains (# L34960, ThermoFisher). Cells were fixed with 4% PFA for 15min, diluted in FACS buffer (PBS, 3% FBS, 1% P/S, 1mM EDTA) and FACS analysis was performed on BD LSRFortessa. All antibodies are listed in the key Resource table.

Western blot analysis

Tissue samples were lysed in cold RIPA buffer (50mM Tris-HCl pH 7.4, 150mM NaCl, 2mM EDTA, 1.0% Triton X-100, 0.5% sodium deoxycholate) containing protease (Complete, Roche) and phosphatase (Thermo Fisher) inhibitor cocktails. The samples were centrifuged at 24,000 g for 10 min at 4°C, and protein concentrations were measured by using Pierce BCA Protein assay Kit (#23225, Thermo Fisher Scientific). Equal amounts of proteins (10-20 μg) were resolved on 10% SDS-polyacrylamide gel (PAGE) gel and transferred onto a nitrocellulose membrane (Bio-Rad). The following primary antibodies were used: UCP1 (1:1,000, # ab10983, Abcam) and HSP90 (1:1000, # 4877, Cell signaling). Thereafter, membranes were incubated with corresponding secondary HRP-conjugated antibodies (1:10,000, Calbiochem) and signals were detected by an LAS 4000 mini Image Quant system (GE Healthcare Life Sciences).

RNA extraction and quantitative real-time PCR

Total RNA was extracted from tissue using Trizol reagent (# 15596026, Invitrogen) according to the manufacturer's protocol. Genomic DNA was treated by DNase (NEB BioLabs). Reverse transcription was performed using the High Capacity cDNA Reverse



transcription kit (# 4368814, Applied Biosystems) with 0.5-1ug of the total RAN. Quantitative PCR was performed on a ViiA7 (Applied Biosystems) using Sybergreen (Themofisher). Relative mRNA concentrations normalized to the expression of 36B4 were calculated by the $\Delta\Delta C_t$ method. Primer sequences are listed in the [Key Resources Table](#).

QUANTIFICATION AND STATISTICAL ANALYSIS

All data are expressed as mean \pm standard error of the mean (SEM). The significance was determined using a two-tailed, unpaired Student's *t*-test, one-way ANOVA with Newman-Keuls correction for multiple group comparisons, or two-way ANOVA with Bonferroni multiple comparisons/Tukey's multiple comparison. Statistical tests were calculated using the GraphPad Prism 8.0 (GraphPad Software, San Diego, CA, USA). *P*-values < 0.05 were considered significant. All statistical details can be found in the figure legends. Power calculation analysis was not performed. Sample size was determined based on previous experiments performed in our laboratory. The evaluator was blinded to the identity of a specific sample as far as the nature of the experiment allowed it.

DATA AND CODE AVAILABILITY

Original data for uncropped and unmodified images in this paper are available upon request.

Acknowledgements

Foremost, I would like to thank Prof. Christian Wolfrum, my supervisor and mentor during this journey of a PhD. His passion and enthusiasm for science will always stay with me and inspire me. Thank you for supporting me in my development as a researcher, thank you for giving me guidance when I needed it, but also thank you for the freedom I had to pursue my own ideas. Thank you to my committee member Katrien De Bock, your input during my committee meetings, but also during various other meetings, or chats at the coffee machine were always valuable. Thanks for your open ear and support whenever my projects drifted into the field of skeletal muscle or endothelial cells. Further, I would like to thank Brice Emanuelli for being part of my committee. I was hoping that at least for my defense I would get the chance to meet you once in person. But nonetheless, your suggestions and your perspective on my projects were always extremely helpful.

A big thank you goes to all people of the Böhringer Ingelheim collaboration. Our discussions during the regular meetings were very essential for the FAM3D project. Special thanks goes to Torsten and his team for producing endless amounts of AAV and recombinant protein. Thanks to Brad and his team for supporting me with the Sally Sue and letting me experience how science is done in the pharmaceutical industry. A big thank you also to Heike, who accompanied this project even beyond the collaboration.

Next, my thank you goes to all the current and past members of the awesome Wolfrum group, without the wonderful environment and spirit we have in the lab, my PhD would have not been the same. Carla, thank you for being my glucose metabolism buddy. Thank you for the endless hours spend together in the lab doing crazy experiments. But more importantly thank you for the good times drinking gin tonic, having good funny lunch breaks and wonderful runs through the fields of Schwerzenbach. Lucy and Miro, thank you for being awesome parents, not only for your little one, but also for lost PhD students. Thank you to both of you for all the support whenever I needed somebody helping me finding the right path to continue my projects. I might have even learned my lesson of not "overdoing" it, thanks Lucy ;). Matthias, what would we do without you? One is for sure, there would be less cake ;), so thanks for making our life more cakefull. Thanks for all the organization, ordering etc. and making sure that everything runs smoothly in the lab. Sylvia, thank you for always having an open ear, it is good to know that your door is always open. Manuel, what would have I done with all my mice without you? Actually, I have no clue. Thank you for the endless hours you helped me during clamps, dissections, GTTs and so on. Also a huge thank you to all the other members of the animal facility, you always kept my mice happy. Whenever I had

a special request or needed a something out of the row you were there and tried your best to help me. A big thank you also to Myrtha for being such an awesome mouse surgeon. Thank you to Elke, for cutting all my histology slides and preparing endless amounts of buffers, so that we can go crazy in the Westernblot room. Lianggong, thanks for your help, it was great to have you in the office, and sorry if my many questions were sometimes too annoying ;). Thank you Salvo for you AAV knowledge, thank you Anand for your cross-linker skills, thank you Hua and Wenfei for all your little tips and tricks and thank you Tongtong for your histology knowledge. Thanks to Ian and Gillian for proof reading this thesis. A huge shout out to the whole von Meyen group, it is really nice to have you around guys and I definitely learned a lot from you guys. Special notice to Eva, I would have never ever thought that I will ever run so fast. To the former members of the Wolfrum Group, Lisi, Gitalee, Ania, Anne, Amy and Arionas thanks for all the good coffee talks and very delicious dinners. Thank you Katherine for taking me under your wings especially during the first time of my PhD and handing me over the FAM3D project. Thank you Leon for the good collaboration in the Fataccounting story and all the mouse stuff I learned from you. Thank you Gerald, for teaching me my first steps in science.

A big thank you also to the rest of the whole SLA building. It was always amazing to experience the support of all the other groups whenever help in dissecting muscles or brain was needed or you wanted to test antibodies, primers, cells etc. Thank you also to the SLA-Service, especially Roland who always found a solution for everything. Thank you to our IT guys David and Aryan, for always being there whenever I messed up my computer (believe me this happened more often than I preferred it).

Lastly, I would like to thank my family. Mama thank you for everything, from calling me to hear how I'm doing until taking me to super nice hikes on scary rims in the mountains. Papa even though you sometimes wondered what you daughter is doing there in her PhD, you were always interested and supported me. A big thank you to brothers Linus, Levin, Tim and Benno, it is good to have all of you around and it is always good fun with you guys when we see each other. Last but not least THANK YOU Tobi, my favorite partner in crime, my one and only, thank you for always being there for me. Thank you for supporting me and my dreams, dealing with my bumblebees and spending great times with me in the mountains – yes you definitely have the best powder nose ;). Now I'm looking forward to the next adventures with you, I'm sure they are going to be awesome!

Bibliography

- [1] Chen Y, Pan R, Pfeifer A. Fat tissues, the brite and the dark sides. *Pflüg Arch - Eur J Physiol* 2016;468:1803–7. <https://doi.org/10.1007/s00424-016-1884-8>.
- [2] Carper D, Coué M, Nascimento EBM, Barquissau V, Lagarde D, Pestourie C, et al. Atrial Natriuretic Peptide Orchestrates a Coordinated Physiological Response to Fuel Non-shivering Thermogenesis. *Cell Rep* 2020;32:108075. <https://doi.org/10.1016/j.celrep.2020.108075>.
- [3] Stanford KI, Middelbeek RJW, Goodyear LJ. Erratum. Exercise Effects on White Adipose Tissue: Beiging and Metabolic Adaptations. *Diabetes* 2015;64:2361-2368. *Diabetes* 2015;64:3334. <https://doi.org/10.2337/db15-er09>.
- [4] Feldmann HM, Golozoubova V, Cannon B, Nedergaard J. UCP1 ablation induces obesity and abolishes diet-induced thermogenesis in mice exempt from thermal stress by living at thermoneutrality. *Cell Metab* 2009;9:203–9. <https://doi.org/10.1016/j.cmet.2008.12.014>.
- [5] Harms M, Seale P. Brown and beige fat: development, function and therapeutic potential. *Nat Med* 2013;19:1252–63. <https://doi.org/10.1038/nm.3361>.
- [6] de Jong JM, Larsson O, Cannon B, Nedergaard J. A stringent validation of mouse adipose tissue identity markers. *Am J Physiol Endocrinol Metab* 2015;308:E1085-105. <https://doi.org/10.1152/ajpendo.00023.2015>.
- [7] van Marken Lichtenbelt WD, Vanhomerig JW, Smulders NM, Drossaerts JMAFL, Kemerink GJ, Bouvy ND, et al. Cold-activated brown adipose tissue in healthy men. *N Engl J Med* 2009;360:1500–8. <https://doi.org/10.1056/NEJMoa0808718>.
- [8] Cypess AM, Williams G, Goldfine AB, Tseng Y-H, Kolodny GM. Identification and Importance of Brown Adipose Tissue in Adult Humans. *N Engl J Med* 2009;9.
- [9] Virtanen KA, Lidell ME, Orava J, Heglind M, Westergren R, Niemi T, et al. Functional brown adipose tissue in healthy adults. *N Engl J Med* 2009;360:1518–25. <https://doi.org/10.1056/NEJMoa0808949>.
- [10] Wang QA, Tao C, Gupta RK, Scherer PE. Tracking adipogenesis during white adipose tissue development, expansion and regeneration. *Nat Med* 2013;19:1338–44. <https://doi.org/10.1038/nm.3324>.
- [11] Berry DC, Jiang Y, Graff JM. Mouse strains to study cold-inducible beige progenitors and beige adipocyte formation and function. *Nat Commun* 2016;7:10184. <https://doi.org/10.1038/ncomms10184>.
- [12] Lee YH, Petkova AP, Konkar AA, Granneman JG. Cellular origins of cold-induced brown adipocytes in adult mice. *Faseb J* 2015;29:286–99. <https://doi.org/10.1096/fj.14-263038>.
- [13] Cinti S. Transdifferentiation properties of adipocytes in the adipose organ. *Am J Physiol Endocrinol Metab* 2009;297:E977-986. <https://doi.org/10.1152/ajpendo.00183.2009>.
- [14] Rosenwald M, Perdikari A, Rulicke T, Wolfrum C. Bi-directional interconversion of brite and white adipocytes. *Nat Cell Biol* 2013;15:659–67. <https://doi.org/10.1038/ncb2740>.
- [15] Sanchez-Gurmaches J, Hung C-M, Guertin DA. Emerging Complexities in Adipocyte Origins and Identity. *Trends Cell Biol* 2016;26:313–26. <https://doi.org/10.1016/j.tcb.2016.01.004>.

- [16] Leushacke M, Barker N. Ex vivo culture of the intestinal epithelium: strategies and applications. *Gut* 2014;63:1345–54. <https://doi.org/10.1136/gutjnl-2014-307204>.
- [17] Clevers HC, Bevins CL. Paneth cells: maestros of the small intestinal crypts. *Annu Rev Physiol* 2013;75:289–311. <https://doi.org/10.1146/annurev-physiol-030212-183744>.
- [18] Kim YS, Ho SB. Intestinal Goblet Cells and Mucins in Health and Disease: Recent Insights and Progress. *Curr Gastroenterol Rep* 2010;12:319–30. <https://doi.org/10.1007/s11894-010-0131-2>.
- [19] Snoeck V, Goddeeris B, Cox E. The role of enterocytes in the intestinal barrier function and antigen uptake. *Microbes Infect* 2005;7:997–1004. <https://doi.org/10.1016/j.micinf.2005.04.003>.
- [20] Gribble FM, Reimann F. Function and mechanisms of enteroendocrine cells and gut hormones in metabolism. *Nat Rev Endocrinol* 2019;15:226–37. <https://doi.org/10.1038/s41574-019-0168-8>.
- [21] Gribble FM, Reimann F. Enteroendocrine Cells: Chemosensors in the Intestinal Epithelium. *Annu Rev Physiol* 2016;78:277–99. <https://doi.org/10.1146/annurev-physiol-021115-105439>.
- [22] Latorre R, Sternini C, De Giorgio R, Greenwood-Van Meerveld B. Enteroendocrine Cells: A Review of Their Role In Brain-Gut Communication. *Neurogastroenterol Motil Off J Eur Gastrointest Motil Soc* 2016;28:620–30. <https://doi.org/10.1111/nmo.12754>.
- [23] Cresci GA, Bawden E. Gut Microbiome: What We Do and Don't Know. *Nutr Clin Pract Off Publ Am Soc Parenter Enter Nutr* 2015;30:734–46. <https://doi.org/10.1177/0884533615609899>.
- [24] Alberti KGMM, Zimmet PZ. Definition, diagnosis and classification of diabetes mellitus and its complications. Part 1: diagnosis and classification of diabetes mellitus. Provisional report of a WHO Consultation. *Diabet Med* 1998;15:539–53. [https://doi.org/10.1002/\(SICI\)1096-9136\(199807\)15:7<539::AID-DIA668>3.0.CO;2-S](https://doi.org/10.1002/(SICI)1096-9136(199807)15:7<539::AID-DIA668>3.0.CO;2-S).
- [25] Zimmet P, Magliano D, Matsuzawa Y, Alberti G, Shaw J. The metabolic syndrome: a global public health problem and a new definition. *J Atheroscler Thromb* 2005;12:295–300. <https://doi.org/10.5551/jat.12.295>.
- [26] Obesity and overweight n.d. <https://www.who.int/news-room/fact-sheets/detail/obesity-and-overweight> (accessed March 25, 2020).
- [27] Kim CH. Measurements of Adiposity and Body Composition. *Korean J Obes* 2016;25:115–20. <https://doi.org/10.7570/kjo.2016.25.3.115>.
- [28] Ogden CL, Carroll MD, Kit BK, Flegal KM. Prevalence of childhood and adult obesity in the United States, 2011–2012. *JAMA* 2014;311:806–14. <https://doi.org/10.1001/jama.2014.732>.
- [29] von Ruesten A, Steffen A, Floegel A, van der A DL, Masala G, Tjønneland A, et al. Trend in obesity prevalence in European adult cohort populations during follow-up since 1996 and their predictions to 2015. *PloS One* 2011;6:e27455. <https://doi.org/10.1371/journal.pone.0027455>.
- [30] Stevens GA, Singh GM, Lu Y, Danaei G, Lin JK, Finucane MM, et al. National, regional, and global trends in adult overweight and obesity prevalences. *Popul Health Metr* 2012;10:22. <https://doi.org/10.1186/1478-7954-10-22>.

- [31] Kelly T, Yang W, Chen C-S, Reynolds K, He J. Global burden of obesity in 2005 and projections to 2030. *Int J Obes* 2008;32:1431–7. <https://doi.org/10.1038/ijo.2008.102>.
- [32] Stunkard AJ, Foch TT, Hrubec Z. A twin study of human obesity. *JAMA* 1986;256:51–4.
- [33] Börjeson M. The aetiology of obesity in children. A study of 101 twin pairs. *Acta Paediatr Scand* 1976;65:279–87. <https://doi.org/10.1111/j.1651-2227.1976.tb04887.x>.
- [34] Neel JV. Diabetes Mellitus: A “Thrifty” Genotype Rendered Detrimental by “Progress”? *Am J Hum Genet* 1962;14:353–62.
- [35] Southam L, Soranzo N, Montgomery SB, Frayling TM, McCarthy MI, Barroso I, et al. Is the thrifty genotype hypothesis supported by evidence based on confirmed type 2 diabetes- and obesity-susceptibility variants? *Diabetologia* 2009;52:1846–51. <https://doi.org/10.1007/s00125-009-1419-3>.
- [36] Koh X-H, Liu X, Teo Y-Y. Can Evidence from Genome-Wide Association Studies and Positive Natural Selection Surveys Be Used to Evaluate the Thrifty Gene Hypothesis in East Asians? *PLOS ONE* 2014;9:e110974. <https://doi.org/10.1371/journal.pone.0110974>.
- [37] Locke AE, Kahali B, Berndt SI, Justice AE, Pers TH, Day FR, et al. Genetic studies of body mass index yield new insights for obesity biology. *Nature* 2015;518:197–206. <https://doi.org/10.1038/nature14177>.
- [38] Loos RJF, Janssens ACJW. Predicting Polygenic Obesity Using Genetic Information. *Cell Metab* 2017;25:535–43. <https://doi.org/10.1016/j.cmet.2017.02.013>.
- [39] Albuquerque D, Nóbrega C, Manco L, Padez C. The contribution of genetics and environment to obesity. *Br Med Bull* 2017;123:159–73. <https://doi.org/10.1093/bmb/ldx022>.
- [40] Herman CP, Polivy J, Vartanian LR, Pliner P. Are large portions responsible for the obesity epidemic? *Physiol Behav* 2016;156:177–81. <https://doi.org/10.1016/j.physbeh.2016.01.024>.
- [41] Vandelanotte C, Sugiyama T, Gardiner P, Owen N. Associations of Leisure-Time Internet and Computer Use With Overweight and Obesity, Physical Activity and Sedentary Behaviors: Cross-Sectional Study. *J Med Internet Res* 2009;11:e28. <https://doi.org/10.2196/jmir.1084>.
- [42] Crawford DA, Jeffery RW, French SA. Television viewing, physical inactivity and obesity. *Int J Obes* 1999;23:437–40. <https://doi.org/10.1038/sj.ijo.0800845>.
- [43] Shrewsbury V, Wardle J. Socioeconomic status and adiposity in childhood: a systematic review of cross-sectional studies 1990–2005. *Obes Silver Spring Md* 2008;16:275–84. <https://doi.org/10.1038/oby.2007.35>.
- [44] Fock KM, Khoo J. Diet and exercise in management of obesity and overweight. *J Gastroenterol Hepatol* 2013;28:59–63. <https://doi.org/10.1111/jgh.12407>.
- [45] Wadden TA, Webb VL, Moran CH, Bailer BA. Lifestyle Modification for Obesity. *Circulation* 2012;125:1157–70. <https://doi.org/10.1161/CIRCULATIONAHA.111.039453>.
- [46] Donnelly JE, Blair SN, Jakicic JM, Manore MM, Rankin JW, Smith BK, et al. American College of Sports Medicine Position Stand. Appropriate physical activity intervention strategies for weight loss and prevention of weight regain for adults. *Med Sci Sports Exerc* 2009;41:459–71. <https://doi.org/10.1249/MSS.0b013e3181949333>.

- [47] Bouchard C, Depres J-P, Tremblay A. Exercise and Obesity. *Obes Res* 1993;1:133–47. <https://doi.org/10.1002/j.1550-8528.1993.tb00603.x>.
- [48] Hainer V, Toplak H, Mitrakou A. Treatment Modalities of Obesity: What fits whom? *Diabetes Care* 2008;31:S269–77. <https://doi.org/10.2337/dc08-s265>.
- [49] Jacob JJ, Isaac R. Behavioral therapy for management of obesity. *Indian J Endocrinol Metab* 2012;16:28–32. <https://doi.org/10.4103/2230-8210.91180>.
- [50] Daneschvar HL, Aronson MD, Smetana GW. FDA-Approved Anti-Obesity Drugs in the United States. *Am J Med* 2016;129:879.e1-879.e6. <https://doi.org/10.1016/j.amjmed.2016.02.009>.
- [51] Sweeting AN, Hocking SL, Markovic TP. Pharmacotherapy for the treatment of obesity. *Mol Cell Endocrinol* 2015;418 Pt 2:173–83. <https://doi.org/10.1016/j.mce.2015.09.005>.
- [52] Moini J. Type 2 Diabetes. *Epidemiol. Diabetes, Elsevier*; 2019, p. 91–114. <https://doi.org/10.1016/B978-0-12-816864-6.00007-9>.
- [53] Roglic G, World Health Organization, editors. *Global report on diabetes*. Geneva, Switzerland: World Health Organization; 2016.
- [54] Chatterjee S, Khunti K, Davies MJ. Type 2 diabetes. *The Lancet* 2017;389:2239–51. [https://doi.org/10.1016/S0140-6736\(17\)30058-2](https://doi.org/10.1016/S0140-6736(17)30058-2).
- [55] Tabák AG, Herder C, Rathmann W, Brunner EJ, Kivimäki M. Prediabetes: A high-risk state for developing diabetes. *Lancet* 2012;379:2279–90. [https://doi.org/10.1016/S0140-6736\(12\)60283-9](https://doi.org/10.1016/S0140-6736(12)60283-9).
- [56] Abid A, Ahmad S, Waheed A. Screening for Type II Diabetes Mellitus in the United States: The Present and the Future. *Clin Med Insights Endocrinol Diabetes* 2016;9:19–22. <https://doi.org/10.4137/CMED.S38247>.
- [57] Meigs JB, McAteer JB, Manning AK, D’Agostino RB. Genotype Score in Addition to Common Risk Factors for Prediction of Type 2 Diabetes. *N Engl J Med* 2008;12.
- [58] The InterAct Consortium. The link between family history and risk of type 2 diabetes is not explained by anthropometric, lifestyle or genetic risk factors: the EPIC-InterAct study. *Diabetologia* 2013;56:60–9. <https://doi.org/10.1007/s00125-012-2715-x>.
- [59] Arroyo-Johnson C, Mincey KD. Obesity epidemiology trends by race/ethnicity, gender, and education: National Health Interview Survey, 1997–2012. *Gastroenterol Clin North Am* 2016;45:571–9. <https://doi.org/10.1016/j.gtc.2016.07.012>.
- [60] Spanakis EK, Golden SH. Race/Ethnic Difference in Diabetes and Diabetic Complications. *Curr Diab Rep* 2013;13. <https://doi.org/10.1007/s11892-013-0421-9>.
- [61] IDF Diabetes Atlas 9th edition 2019 n.d. <https://diabetesatlas.org/en/> (accessed April 8, 2020).
- [62] Thrasher J. Pharmacologic Management of Type 2 Diabetes Mellitus: Available Therapies. *Am J Med* 2017;130:S4–17. <https://doi.org/10.1016/j.amjmed.2017.04.004>.
- [63] Foretz M, Guigas B, Viollet B. Understanding the glucoregulatory mechanisms of metformin in type 2 diabetes mellitus. *Nat Rev Endocrinol* 2019;15:569–89. <https://doi.org/10.1038/s41574-019-0242-2>.

- [64] Tahrani AA, Barnett AH, Bailey CJ. Pharmacology and therapeutic implications of current drugs for type 2 diabetes mellitus. *Nat Rev Endocrinol* 2016;12:566–92. <https://doi.org/10.1038/nrendo.2016.86>.
- [65] Buchwald H, Estok R, Fahrbach K, Banel D, Jensen MD, Pories WJ, et al. Weight and type 2 diabetes after bariatric surgery: systematic review and meta-analysis. *Am J Med* 2009;122:248–256.e5. <https://doi.org/10.1016/j.amjmed.2008.09.041>.
- [66] Garg A. Clinical review: Lipodystrophies: genetic and acquired body fat disorders. *J Clin Endocrinol Metab* 2011;96:3313–25. <https://doi.org/10.1210/jc.2011-1159>.
- [67] Krotkiewski M, Björntorp P, Sjöström L, Smith U. Impact of obesity on metabolism in men and women. Importance of regional adipose tissue distribution. *J Clin Invest* 1983;72:1150–62. <https://doi.org/10.1172/JCI111040>.
- [68] Jeffery E, Church CD, Holtrup B, Colman L, Rodeheffer MS. Rapid depot-specific activation of adipocyte precursor cells at the onset of obesity. *Nat Cell Biol* 2015;17:376–85. <https://doi.org/10.1038/ncb3122>.
- [69] Jeffery E, Wing A, Holtrup B, Sebo Z, Kaplan JL, Saavedra-Peña R, et al. The Adipose Tissue Microenvironment Regulates Depot-Specific Adipogenesis in Obesity. *Cell Metab* 2016;24:142–50. <https://doi.org/10.1016/j.cmet.2016.05.012>.
- [70] Fuente-Martín E, Argente-Arízón P, Ros P, Argente J, Chowen JA. Sex differences in adipose tissue: It is not only a question of quantity and distribution. *Adipocyte* 2013;2:128–34. <https://doi.org/10.4161/adip.24075>.
- [71] Fox CS, Massaro JM, Hoffmann U, Pou KM, Maurovich-Horvat P, Liu C-Y, et al. Abdominal visceral and subcutaneous adipose tissue compartments: association with metabolic risk factors in the Framingham Heart Study. *Circulation* 2007;116:39–48. <https://doi.org/10.1161/CIRCULATIONAHA.106.675355>.
- [72] Kwon H, Kim D, Kim JS. Body Fat Distribution and the Risk of Incident Metabolic Syndrome: A Longitudinal Cohort Study. *Sci Rep* 2017;7:1–8. <https://doi.org/10.1038/s41598-017-09723-y>.
- [73] Rosen ED, Spiegelman BM. What We Talk About When We Talk About Fat. *Cell* 2014;156:20–44. <https://doi.org/10.1016/j.cell.2013.12.012>.
- [74] Shao M, Vishvanath L, Busbuso NC, Hepler C, Shan B, Sharma AX, et al. De novo adipocyte differentiation from Pdgfr β + preadipocytes protects against pathologic visceral adipose expansion in obesity. *Nat Commun* 2018;9:1–16. <https://doi.org/10.1038/s41467-018-03196-x>.
- [75] Klötting N, Fasshauer M, Dietrich A, Kovacs P, Schön MR, Kern M, et al. Insulin-sensitive obesity. *Am J Physiol Endocrinol Metab* 2010;299:E506–515. <https://doi.org/10.1152/ajpendo.00586.2009>.
- [76] Meissburger B, Ukropec J, Roeder E, Beaton N, Geiger M, Teupser D, et al. Adipogenesis and insulin sensitivity in obesity are regulated by retinoid-related orphan receptor gamma. *EMBO Mol Med* 2011;3:637–51. <https://doi.org/10.1002/emmm.201100172>.
- [77] Halberg N, Khan T, Trujillo ME, Wernstedt-Asterholm I, Attie AD, Sherwani S, et al. Hypoxia-inducible factor 1 α induces fibrosis and insulin resistance in white adipose tissue. *Mol Cell Biol* 2009;29:4467–83. <https://doi.org/10.1128/MCB.00192-09>.

- [78] Sun K, Kusminski CM, Scherer PE. Adipose tissue remodeling and obesity. *J Clin Invest* 2011;121:2094–101. <https://doi.org/10.1172/JCI45887>.
- [79] Murano I, Barbatelli G, Parisani V, Latini C, Muzzonigro G, Castellucci M, et al. Dead adipocytes, detected as crown-like structures, are prevalent in visceral fat depots of genetically obese mice. *J Lipid Res* 2008;49:1562–8. <https://doi.org/10.1194/jlr.M800019-JLR200>.
- [80] Tilg H, Moschen AR. Inflammatory Mechanisms in the Regulation of Insulin Resistance. *Mol Med* 2008;14:222–31. <https://doi.org/10.2119/2007-00119.Tilg>.
- [81] Feingold KR, Doerrler W, Dinarello CA, Fiers W, Grunfeld C. Stimulation of lipolysis in cultured fat cells by tumor necrosis factor, interleukin-1, and the interferons is blocked by inhibition of prostaglandin synthesis. *Endocrinology* 1992;130:10–6. <https://doi.org/10.1210/endo.130.1.1370149>.
- [82] Guilherme A, Virbasius JV, Puri V, Czech MP. Adipocyte dysfunctions linking obesity to insulin resistance and type 2 diabetes. *Nat Rev Mol Cell Biol* 2008;9:367–77. <https://doi.org/10.1038/nrm2391>.
- [83] Lumeng CN, Bodzin JL, Saltiel AR. Obesity induces a phenotypic switch in adipose tissue macrophage polarization. *J Clin Invest* 2007;117:175–84. <https://doi.org/10.1172/JCI29881>.
- [84] Becerril S, Rodríguez A, Catalán V, Méndez-Giménez L, Ramírez B, Sáinz N, et al. Targeted disruption of the iNOS gene improves adipose tissue inflammation and fibrosis in leptin-deficient ob/ob mice: role of tenascin C. *Int J Obes* 2018;42:1458–70. <https://doi.org/10.1038/s41366-018-0005-5>.
- [85] Mathis D. Immunological Goings-on in Visceral Adipose Tissue. *Cell Metab* 2013;17:851–9. <https://doi.org/10.1016/j.cmet.2013.05.008>.
- [86] Zhang Y, Proenca R, Maffei M, Barone M, Leopold L, Friedman JM. Positional cloning of the mouse obese gene and its human homologue. *Nature* 1994;372:425–32. <https://doi.org/10.1038/372425a0>.
- [87] Scherer PE, Williams S, Fogliano M, Baldini G, Lodish HF. A novel serum protein similar to C1q, produced exclusively in adipocytes. *J Biol Chem* 1995;270:26746–9. <https://doi.org/10.1074/jbc.270.45.26746>.
- [88] Lehr S, Hartwig S, Sell H. Adipokines: A treasure trove for the discovery of biomarkers for metabolic disorders. *PROTEOMICS – Clin Appl* 2012;6:91–101. <https://doi.org/10.1002/prca.201100052>.
- [89] Lehr S, Hartwig S, Lamers D, Famulla S, Müller S, Hanisch F-G, et al. Identification and Validation of Novel Adipokines Released from Primary Human Adipocytes. *Mol Cell Proteomics* 2012;11. <https://doi.org/10.1074/mcp.M111.010504>.
- [90] Frederich RC, Hamann A, Anderson S, Löllmann B, Lowell BB, Flier JS. Leptin levels reflect body lipid content in mice: Evidence for diet-induced resistance to leptin action. *Nat Med* 1995;1:1311–4. <https://doi.org/10.1038/nm1295-1311>.
- [91] Montague CT, Farooqi IS, Whitehead JP, Soos MA, Rau H, Wareham NJ, et al. Congenital leptin deficiency is associated with severe early-onset obesity in humans. *Nature* 1997;387:903–8. <https://doi.org/10.1038/43185>.

- [92] Harrison L, Schriever SC, Feuchtinger A, Kyriakou E, Baumann P, Pfuhlmann K, et al. Fluorescent blood–brain barrier tracing shows intact leptin transport in obese mice. *Int J Obes* 2019;43:1305–18. <https://doi.org/10.1038/s41366-018-0221-z>.
- [93] William Jr. WN, Ceddia RB, Curi R. Leptin controls the fate of fatty acids in isolated rat white adipocytes. *J Endocrinol* 2002;175:735–44. <https://doi.org/10.1677/joe.0.1750735>.
- [94] Zeng W, Pirzgalska RM, Pereira MMA, Kubasova N, Barateiro A, Seixas E, et al. Sympathetic Neuro-adipose Connections Mediate Leptin-Driven Lipolysis. *Cell* 2015;163:84–94. <https://doi.org/10.1016/j.cell.2015.08.055>.
- [95] Kadowaki T, Yamauchi T, Kubota N, Hara K, Ueki K, Tobe K. Adiponectin and adiponectin receptors in insulin resistance, diabetes, and the metabolic syndrome. *J Clin Invest* 2006;116:1784–92. <https://doi.org/10.1172/JCI29126>.
- [96] Yamauchi T, Kamon J, Waki H, Terauchi Y, Kubota N, Hara K, et al. The fat-derived hormone adiponectin reverses insulin resistance associated with both lipoatrophy and obesity. *Nat Med* 2001;7:941–6. <https://doi.org/10.1038/90984>.
- [97] Kolak M, Yki-Järvinen H, Kannisto K, Tiikkainen M, Hamsten A, Eriksson P, et al. Effects of Chronic Rosiglitazone Therapy on Gene Expression in Human Adipose Tissue in Vivo in Patients with Type 2 Diabetes. *J Clin Endocrinol Metab* 2007;92:720–4. <https://doi.org/10.1210/jc.2006-1465>.
- [98] Fasshauer M, Blüher M. Adipokines in health and disease. *Trends Pharmacol Sci* 2015;36:461–70. <https://doi.org/10.1016/j.tips.2015.04.014>.
- [99] Hankir MK, Klingenspor M. Brown adipocyte glucose metabolism: a heated subject. *EMBO Rep* 2018;19. <https://doi.org/10.15252/embr.201846404>.
- [100] Chouchani ET, Kajimura S. Metabolic adaptation and maladaptation in adipose tissue. *Nat Metab* 2019;1:189–200. <https://doi.org/10.1038/s42255-018-0021-8>.
- [101] Saito M, Okamatsu-Ogura Y, Matsushita M, Watanabe K, Yoneshiro T, Nio-Kobayashi J, et al. High incidence of metabolically active brown adipose tissue in healthy adult humans: effects of cold exposure and adiposity. *Diabetes* 2009;58:1526–31. <https://doi.org/10.2337/db09-0530>.
- [102] Chondronikola M, Volpi E, Børsheim E, Porter C, Annamalai P, Enerbäck S, et al. Brown Adipose Tissue Improves Whole-Body Glucose Homeostasis and Insulin Sensitivity in Humans. *Diabetes* 2014;63:4089–99. <https://doi.org/10.2337/db14-0746>.
- [103] Chondronikola M, Volpi E, Børsheim E, Porter C, Saraf MK, Annamalai P, et al. Brown Adipose Tissue Activation Is Linked to Distinct Systemic Effects on Lipid Metabolism in Humans. *Cell Metab* 2016;23:1200–6. <https://doi.org/10.1016/j.cmet.2016.04.029>.
- [104] Cypess AM, Weiner LS, Roberts-Toler C, Elia EF, Kessler SH, Kahn PA, et al. Activation of Human Brown Adipose Tissue by a β ₃-Adrenergic Receptor Agonist. *Cell Metab* 2015;21:33–8. <https://doi.org/10.1016/j.cmet.2014.12.009>.
- [105] O'Mara AE, Johnson JW, Linderman JD, Brychta RJ, McGehee S, Fletcher LA, et al. Chronic mirabegron treatment increases human brown fat, HDL cholesterol, and insulin sensitivity. *J Clin Invest* 2020;130. <https://doi.org/10.1172/JCI131126>.
- [106] Scheele C, Wolfrum C. Brown Adipose Crosstalk in Tissue Plasticity and Human Metabolism. *Endocr Rev* 2020;41. <https://doi.org/10.1210/edrev/bnz007>.

- [107] Neff KJ, Olbers T, le Roux CW. Bariatric surgery: the challenges with candidate selection, individualizing treatment and clinical outcomes. *BMC Med* 2013;11:8. <https://doi.org/10.1186/1741-7015-11-8>.
- [108] O'Brien PE, Hindle A, Brennan L, Skinner S, Burton P, Smith A, et al. Long-Term Outcomes After Bariatric Surgery: a Systematic Review and Meta-analysis of Weight Loss at 10 or More Years for All Bariatric Procedures and a Single-Centre Review of 20-Year Outcomes After Adjustable Gastric Banding. *Obes Surg* 2019;29:3–14. <https://doi.org/10.1007/s11695-018-3525-0>.
- [109] Nguyen NT, Varela JE. Bariatric surgery for obesity and metabolic disorders: state of the art. *Nat Rev Gastroenterol Hepatol* 2017;14:160–9. <https://doi.org/10.1038/nrgastro.2016.170>.
- [110] Holst JJ, Madsbad S, Bojsen-Møller KN, Svane MS, Jørgensen NB, Dirksen C, et al. Mechanisms in bariatric surgery: Gut hormones, diabetes resolution, and weight loss. *Surg Obes Relat Dis* 2018;14:708–14. <https://doi.org/10.1016/j.soard.2018.03.003>.
- [111] Steven S, Hollingsworth KG, Small PK, Woodcock SA, Pucci A, Aribasala B, et al. Calorie restriction and not glucagon-like peptide-1 explains the acute improvement in glucose control after gastric bypass in Type 2 diabetes. *Diabet Med* 2016;33:1723–31. <https://doi.org/10.1111/dme.13257>.
- [112] Cornejo-Pareja I, Clemente-Postigo M, Tinahones FJ. Metabolic and Endocrine Consequences of Bariatric Surgery. *Front Endocrinol* 2019;10. <https://doi.org/10.3389/fendo.2019.00626>.
- [113] Mcintyre N, Holdsworth CD, Turner DS. NEW INTERPRETATION OF ORAL GLUCOSE TOLERANCE. *Lancet Lond Engl* 1964;2:20–1. [https://doi.org/10.1016/s0140-6736\(64\)90011-x](https://doi.org/10.1016/s0140-6736(64)90011-x).
- [114] Drucker DJ. The role of gut hormones in glucose homeostasis. *J Clin Invest* 2007;117:24–32. <https://doi.org/10.1172/JCI30076>.
- [115] Billing LJ, Smith CA, Larraufie P, Goldspink DA, Galvin S, Kay RG, et al. Co-storage and release of insulin-like peptide-5, glucagon-like peptide-1 and peptide YY from murine and human colonic enteroendocrine cells. *Mol Metab* 2018;16:65–75. <https://doi.org/10.1016/j.molmet.2018.07.011>.
- [116] Grosse J, Heffron H, Burling K, Akhter Hossain M, Habib AM, Rogers GJ, et al. Insulin-like peptide 5 is an orexigenic gastrointestinal hormone. *Proc Natl Acad Sci U S A* 2014;111:11133–8. <https://doi.org/10.1073/pnas.1411413111>.
- [117] Brandt SJ, Götz A, Tschöp MH, Müller TD. Gut hormone polyagonists for the treatment of type 2 diabetes. *Peptides* 2018;100:190–201. <https://doi.org/10.1016/j.peptides.2017.12.021>.
- [118] Drucker DJ. Mechanisms of Action and Therapeutic Application of Glucagon-like Peptide-1. *Cell Metab* 2018;27:740–56. <https://doi.org/10.1016/j.cmet.2018.03.001>.
- [119] Deacon CF, Lebovitz HE. Comparative review of dipeptidyl peptidase-4 inhibitors and sulphonylureas. *Diabetes Obes Metab* 2016;18:333–47. <https://doi.org/10.1111/dom.12610>.

- [120] Holst JJ, Rosenkilde MM. GIP as a Therapeutic Target in Diabetes and Obesity: Insight From Incretin Co-agonists. *J Clin Endocrinol Metab* 2020;105. <https://doi.org/10.1210/clinem/dgaa327>.
- [121] Frias JP, Nauck MA, Van J, Kutner ME, Cui X, Benson C, et al. Efficacy and safety of LY3298176, a novel dual GIP and GLP-1 receptor agonist, in patients with type 2 diabetes: a randomised, placebo-controlled and active comparator-controlled phase 2 trial. *Lancet Lond Engl* 2018;392:2180–93. [https://doi.org/10.1016/S0140-6736\(18\)32260-8](https://doi.org/10.1016/S0140-6736(18)32260-8).
- [122] Coskun T, Sloop KW, Loghin C, Alsina-Fernandez J, Urva S, Bokvist KB, et al. LY3298176, a novel dual GIP and GLP-1 receptor agonist for the treatment of type 2 diabetes mellitus: From discovery to clinical proof of concept. *Mol Metab* 2018;18:3–14. <https://doi.org/10.1016/j.molmet.2018.09.009>.
- [123] Pathak V, Flatt PR, Irwin N. Cholecystikinin (CCK) and related adjunct peptide therapies for the treatment of obesity and type 2 diabetes. *Peptides* 2018;100:229–35. <https://doi.org/10.1016/j.peptides.2017.09.007>.
- [124] Behary P, Tharakan G, Alexiadou K, Johnson N, Albrechtsen NJW, Kenkre J, et al. Combined GLP-1, Oxyntomodulin, and Peptide YY Improves Body Weight and Glycemia in Obesity and Prediabetes/Type 2 Diabetes: A Randomized, Single-Blinded, Placebo-Controlled Study. *Diabetes Care* 2019;42:1446–53. <https://doi.org/10.2337/dc19-0449>.
- [125] Sinclair P, Brennan DJ, le Roux CW. Gut adaptation after metabolic surgery and its influences on the brain, liver and cancer. *Nat Rev Gastroenterol Hepatol* 2018;15:606–24. <https://doi.org/10.1038/s41575-018-0057-y>.
- [126] Clemmensen C, Müller TD, Woods SC, Berthoud H-R, Seeley RJ, Tschöp MH. Gut-Brain Cross-Talk in Metabolic Control. *Cell* 2017;168:758–74. <https://doi.org/10.1016/j.cell.2017.01.025>.
- [127] Bäckhed F, Ding H, Wang T, Hooper LV, Koh GY, Nagy A, et al. The gut microbiota as an environmental factor that regulates fat storage. *Proc Natl Acad Sci U S A* 2004;101:15718–23. <https://doi.org/10.1073/pnas.0407076101>.
- [128] Tremaroli V, Karlsson F, Werling M, Ståhlman M, Kovatcheva-Datchary P, Olbers T, et al. Roux-en-Y Gastric Bypass and Vertical Banded Gastroplasty Induce Long-Term Changes on the Human Gut Microbiome Contributing to Fat Mass Regulation. *Cell Metab* 2015;22:228–38. <https://doi.org/10.1016/j.cmet.2015.07.009>.
- [129] Liou AP, Paziuk M, Luevano J-M, Machineni S, Turnbaugh PJ, Kaplan LM. Conserved Shifts in the Gut Microbiota Due to Gastric Bypass Reduce Host Weight and Adiposity. *Sci Transl Med* 2013;5:178ra41-178ra41. <https://doi.org/10.1126/scitranslmed.3005687>.
- [130] Turnbaugh PJ, Hamady M, Yatsunencko T, Cantarel BL, Duncan A, Ley RE, et al. A core gut microbiome in obese and lean twins. *Nature* 2009;457:480–4. <https://doi.org/10.1038/nature07540>.
- [131] Al-Assal K, Martinez AC, Torrinhas RS, Cardinelli C, Waitzberg D. Gut microbiota and obesity. *Clin Nutr Exp* 2018;20:60–4. <https://doi.org/10.1016/j.yclnex.2018.03.001>.
- [132] Hooper LV, Wong MH, Thelin A, Hansson L, Falk PG, Gordon JI. Molecular analysis of commensal host-microbial relationships in the intestine. *Science* 2001;291:881–4. <https://doi.org/10.1126/science.291.5505.881>.

- [133] Winer DA, Luck H, Tsai S, Winer S. The Intestinal Immune System in Obesity and Insulin Resistance. *Cell Metab* 2016;23:413–26. <https://doi.org/10.1016/j.cmet.2016.01.003>.
- [134] Moulin K, Truel N, Andre M, Arnauld E, Nibbelink M, Cousin B, et al. Emergence during development of the white-adipocyte cell phenotype is independent of the brown-adipocyte cell phenotype. *Biochem J* 2001;356:659–64. <https://doi.org/10.1042/0264-6021:3560659>.
- [135] Petrovic N, Walden TB, Shabalina IG, Timmons JA, Cannon B, Nedergaard J. Chronic peroxisome proliferator-activated receptor gamma (PPARgamma) activation of epididymally derived white adipocyte cultures reveals a population of thermogenically competent, UCP1-containing adipocytes molecularly distinct from classic brown adipocytes. *J Biol Chem* 2010;285:7153–64. <https://doi.org/10.1074/jbc.M109.053942>.
- [136] Wu J, Bostrom P, Sparks LM, Ye L, Choi JH, Giang AH, et al. Beige adipocytes are a distinct type of thermogenic fat cell in mouse and human. *Cell* 2012;150:366–76. <https://doi.org/10.1016/j.cell.2012.05.016>.
- [137] Vitali A, Murano I, Zingaretti MC, Frontini A, Ricquier D, Cinti S. The adipose organ of obesity-prone C57BL/6J mice is composed of mixed white and brown adipocytes. *J Lipid Res* 2012;53:619–29. <https://doi.org/10.1194/jlr.M018846>.
- [138] Zhang F, Hao G, Shao M, Nham K, An Y, Wang Q, et al. An Adipose Tissue Atlas: An Image-Guided Identification of Human-like BAT and Beige Depots in Rodents. *Cell Metab* 2018;27:252–262.e3. <https://doi.org/10.1016/j.cmet.2017.12.004>.
- [139] Cousin B, Bascands-Viguerie N, Kassis N, Nibbelink M, Ambid L, Casteilla L, et al. Cellular changes during cold acclimatation in adipose tissues. *J Cell Physiol* 1996;167:285–9. [https://doi.org/10.1002/\(sici\)1097-4652\(199605\)167:2<285::Aid-jcp12>3.0.Co;2-7](https://doi.org/10.1002/(sici)1097-4652(199605)167:2<285::Aid-jcp12>3.0.Co;2-7).
- [140] Rehnmark S, Nedergaard J. DNA synthesis in mouse brown adipose tissue is under beta-adrenergic control. *Exp Cell Res* 1989;180:574–9. [https://doi.org/10.1016/0014-4827\(89\)90086-4](https://doi.org/10.1016/0014-4827(89)90086-4).
- [141] Geloan A, Collet AJ, Bukowiecki LJ. Role of sympathetic innervation in brown adipocyte proliferation. *Am J Physiol* 1992;263:R1176–81. <https://doi.org/10.1152/ajpregu.1992.263.6.R1176>.
- [142] Long JZ, Svensson KJ, Tsai L, Zeng X, Roh HC, Kong X, et al. A smooth muscle-like origin for beige adipocytes. *Cell Metab* 2014;19:810–20. <https://doi.org/10.1016/j.cmet.2014.03.025>.
- [143] Shao M, Wang QA, Song A, Vishvanath L, Busbuso NC, Scherer PE, et al. Cellular Origins of Beige Fat Cells Revisited. *Diabetes* 2019;68:1874–85. <https://doi.org/10.2337/db19-0308>.
- [144] de Jong JMA, Sun W, Pires ND, Frontini A, Balaz M, Jespersen NZ, et al. Human brown adipose tissue is phenocopied by classical brown adipose tissue in physiologically humanized mice. *Nat Metab* 2019;1:830–43. <https://doi.org/10.1038/s42255-019-0101-4>.
- [145] Roh HC, Tsai LTY, Shao M, Tenen D, Shen Y, Kumari M, et al. Warming Induces Significant Reprogramming of Beige, but Not Brown, Adipocyte Cellular Identity. *Cell Metab* 2018;27:1121–1137 e5. <https://doi.org/10.1016/j.cmet.2018.03.005>.
- [146] Gomez-Serrano M, Camafeita E, Garcia-Santos E, Lopez JA, Rubio MA, Sanchez-Pernaute A, et al. Proteome-wide alterations on adipose tissue from obese patients as age-,

- diabetes- and gender-specific hallmarks. *Sci Rep* 2016;6:25756. <https://doi.org/10.1038/srep25756>.
- [147] Nedergaard J, Cannon B. The browning of white adipose tissue: some burning issues. *Cell Metab* 2014;20:396–407. <https://doi.org/10.1016/j.cmet.2014.07.005>.
- [148] Cui X, Nguyen NL, Zarebidaki E, Cao Q, Li F, Zha L, et al. Thermoneutrality decreases thermogenic program and promotes adiposity in high-fat diet-fed mice. *Physiol Rep* 2016;4. <https://doi.org/10.14814/phy2.12799>.
- [149] Kalinovich AV, de Jong JM, Cannon B, Nedergaard J. UCP1 in adipose tissues: two steps to full browning. *Biochimie* 2017;134:127–37. <https://doi.org/10.1016/j.biochi.2017.01.007>.
- [150] Bukowiecki LJ, Geloën A, Collet AJ. Proliferation and differentiation of brown adipocytes from interstitial cells during cold acclimation. *Am J Physiol* 1986;250:C880–7. <https://doi.org/10.1152/ajpcell.1986.250.6.C880>.
- [151] Walden TB, Hansen IR, Timmons JA, Cannon B, Nedergaard J. Recruited vs. nonrecruited molecular signatures of brown, “brite,” and white adipose tissues. *Am J Physiol Endocrinol Metab* 2012;302:E19–31. <https://doi.org/10.1152/ajpendo.00249.2011>.
- [152] Scherer PE. The many secret lives of adipocytes: implications for diabetes. *Diabetologia* 2019;62:223–32. <https://doi.org/10.1007/s00125-018-4777-x>.
- [153] Roh HC, Tsai LT-Y, Lyubetskaya A, Tenen D, Kumari M, Rosen ED. Simultaneous Transcriptional and Epigenomic Profiling from Specific Cell Types within Heterogeneous Tissues In Vivo. *Cell Rep* 2017;18:1048–61. <https://doi.org/10.1016/j.celrep.2016.12.087>.
- [154] Sun W, Dong H, Balaz M, Slyper M, Drokhyansky E, Colleluori G, et al. snRNA-seq reveals a subpopulation of adipocytes that regulates thermogenesis. *Nature* 2020;587:98–102. <https://doi.org/10.1038/s41586-020-2856-x>.
- [155] Xue Y, Petrovic N, Cao R, Larsson O, Lim S, Chen S, et al. Hypoxia-independent angiogenesis in adipose tissues during cold acclimation. *Cell Metab* 2009;9:99–109. <https://doi.org/10.1016/j.cmet.2008.11.009>.
- [156] Fischer AW, Shabalina IG, Mattsson CL, Abreu-Vieira G, Cannon B, Nedergaard J, et al. UCP1 inhibition in Cidea-overexpressing mice is physiologically counteracted by brown adipose tissue hyperrecruitment. *Am J Physiol Endocrinol Metab* 2017;312:E72–87. <https://doi.org/10.1152/ajpendo.00284.2016>.
- [157] Barbatelli G, Murano I, Madsen L, Hao Q, Jimenez M, Kristiansen K, et al. The emergence of cold-induced brown adipocytes in mouse white fat depots is determined predominantly by white to brown adipocyte transdifferentiation. *Am J Physiol Endocrinol Metab* 2010;298:E1244–1253. <https://doi.org/10.1152/ajpendo.00600.2009>.
- [158] Murano I, Zingaretti CM, Cinti S. The adipose organ of Sv129 mice contains a prevalence of brown adipocytes and shows plasticity after cold exposure. *Adipocytes* 2005;1:121–30.
- [159] Schulz TJ, Huang P, Huang TL, Xue R, McDougall LE, Townsend KL, et al. Brown-fat paucity due to impaired BMP signalling induces compensatory browning of white fat. *Nature* 2013;495:379–83. <https://doi.org/10.1038/nature11943>.
- [160] Cannon B, Nedergaard J. Brown adipose tissue: function and physiological significance. *Physiol Rev* 2004;84:277–359. <https://doi.org/10.1152/physrev.00015.2003>.

- [161] Barnett SA. The skin and hair of mice living at a low environmental temperature. *Q J Exp Physiol Cogn Med Sci* 1959;44:35–42.
- [162] Gordon CJ. The mouse thermoregulatory system: Its impact on translating biomedical data to humans. *Physiol Behav* 2017;179:55–66. <https://doi.org/10.1016/j.physbeh.2017.05.026>.
- [163] Keipert S, Kutschke M, Ost M, Schwarzmayr T, van Schothorst EM, Lamp D, et al. Long-Term Cold Adaptation Does Not Require FGF21 or UCP1. *Cell Metab* 2017;26:437–446.e5. <https://doi.org/10.1016/j.cmet.2017.07.016>.
- [164] Ukropec J, Anunciado RP, Ravussin Y, Hulver MW, Kozak LP. UCP1-independent thermogenesis in white adipose tissue of cold-acclimated Ucp1^{-/-} mice. *J Biol Chem* 2006;281:31894–908. <https://doi.org/10.1074/jbc.M606114200>.
- [165] Kazak L, Chouchani ET, Jedrychowski MP, Erickson BK, Shinoda K, Cohen P, et al. A creatine-driven substrate cycle enhances energy expenditure and thermogenesis in beige fat. *Cell* 2015;163:643–55. <https://doi.org/10.1016/j.cell.2015.09.035>.
- [166] Golozoubova V, Hohtola E, Matthias A, Jacobsson A, Cannon B, Nedergaard J. Only UCP1 can mediate adaptive nonshivering thermogenesis in the cold. *FASEB J Off Publ Fed Am Soc Exp Biol* 2001;15:2048–50. <https://doi.org/10.1096/fj.00-0536fje>.
- [167] Long JZ, Svensson KJ, Bateman LA, Lin H, Kamenecka T, Lokurkar IA, et al. The Secreted Enzyme PM20D1 Regulates Lipidated Amino Acid Uncouplers of Mitochondria. *Cell* 2016;166:424–35. <https://doi.org/10.1016/j.cell.2016.05.071>.
- [168] Pajvani UB, Trujillo ME, Combs TP, Iyengar P, Jelicks L, Roth KA, et al. Fat apoptosis through targeted activation of caspase 8: a new mouse model of inducible and reversible lipodystrophy. *Nat Med* 2005;11:797–803. <https://doi.org/10.1038/nm1262>.
- [169] Sakaguchi M, Fujisaka S, Cai W, Winnay JN, Konishi M, O’Neill BT, et al. Adipocyte Dynamics and Reversible Metabolic Syndrome in Mice with an Inducible Adipocyte-Specific Deletion of the Insulin Receptor. *Cell Metab* 2017;25:448–62. <https://doi.org/10.1016/j.cmet.2016.12.008>.
- [170] Song A, Dai W, Jang MJ, Medrano L, Li Z, Zhao H, et al. Low- and high-thermogenic brown adipocyte subpopulations coexist in murine adipose tissue. *J Clin Invest* 2019. <https://doi.org/10.1172/jci129167>.
- [171] Schwalie PC, Dong H, Zachara M, Russeil J, Alpern D, Akchiche N, et al. A stromal cell population that inhibits adipogenesis in mammalian fat depots. *Nature* 2018;559:103–8. <https://doi.org/10.1038/s41586-018-0226-8>.
- [172] Merrick D, Sakers A, Irgebay Z, Okada C, Calvert C, Morley MP, et al. Identification of a mesenchymal progenitor cell hierarchy in adipose tissue. *Science* 2019;364. <https://doi.org/10.1126/science.aav2501>.
- [173] Luche H, Weber O, Nageswara Rao T, Blum C, Fehling HJ. Faithful activation of an extra-bright red fluorescent protein in “knock-in” Cre-reporter mice ideally suited for lineage tracing studies. *Eur J Immunol* 2007;37:43–53. <https://doi.org/10.1002/eji.200636745>.
- [174] Challa TD, Dapito DH, Kulenkampff E, Kiehlmann E, Moser C, Straub L, et al. A Genetic Model to Study the Contribution of Brown and Brite Adipocytes to Metabolism. *Cell Rep* 2020;30:3424–3433.e4. <https://doi.org/10.1016/j.celrep.2020.02.055>.

- [175] Johansson T, Broll I, Frenz T, Hemmers S, Becher B, Zeilhofer HU, et al. Building a zoo of mice for genetic analyses: a comprehensive protocol for the rapid generation of BAC transgenic mice. *Genesis* 2010;48:264–80. <https://doi.org/10.1002/dvg.20612>.
- [176] Rulicke T. Pronuclear microinjection of mouse zygotes. *Methods Mol Biol* 2004;254:165–94. <https://doi.org/10.1385/1-59259-741-6:165>.
- [177] Kulenkampff E, Wolfrum C. Proliferation of nutrition sensing preadipocytes upon short term HFD feeding. *Adipocyte* 2019;8:16–25. <https://doi.org/10.1080/21623945.2018.1521229>.
- [178] Ye R, Wang QA, Tao C, Vishvanath L, Shao M, McDonald JG, et al. Impact of tamoxifen on adipocyte lineage tracing: Inducer of adipogenesis and prolonged nuclear translocation of Cre recombinase. *Mol Metab* 2015;4:771–8. <https://doi.org/10.1016/j.molmet.2015.08.004>.
- [179] Hesselbarth N, Pettinelli C, Gericke M, Berger C, Kunath A, Stumvoll M, et al. Tamoxifen affects glucose and lipid metabolism parameters, causes browning of subcutaneous adipose tissue and transient body composition changes in C57BL/6NTac mice. *Biochem Biophys Res Commun* 2015;464:724–9. <https://doi.org/10.1016/j.bbrc.2015.07.015>.
- [180] Zheng Y, Ley SH, Hu FB. Global aetiology and epidemiology of type 2 diabetes mellitus and its complications. *Nat Rev Endocrinol* 2018;14:88–98. <https://doi.org/10.1038/nrendo.2017.151>.
- [181] Tahrani AA, Barnett AH, Bailey CJ. Pharmacology and therapeutic implications of current drugs for type 2 diabetes mellitus. *Nat Rev Endocrinol* 2016;12:566–92. <https://doi.org/10.1038/nrendo.2016.86>.
- [182] Zhang X, Yang W, Wang J, Meng Y, Guan Y, Yang J. FAM3 gene family: A promising therapeutical target for NAFLD and type 2 diabetes. *Metabolism* 2018;81:71–82. <https://doi.org/10.1016/j.metabol.2017.12.001>.
- [183] Wang C, Chi Y, Li J, Miao Y, Li S, Su W, et al. FAM3A activates PI3K p110 α /Akt signaling to ameliorate hepatic gluconeogenesis and lipogenesis. *Hepatology* 2014;59:1779–90. <https://doi.org/10.1002/hep.26945>.
- [184] Chen Z, Ding L, Yang W, Wang J, Chen L, Chang Y, et al. Hepatic Activation of the FAM3C-HSF1-CaM Pathway Attenuates Hyperglycemia of Obese Diabetic Mice. *Diabetes* 2017;66:1185–97. <https://doi.org/10.2337/db16-0993>.
- [185] Cao X, Gao Z, Robert CE, Greene S, Xu G, Xu W, et al. Pancreatic-derived factor (FAM3B), a novel islet cytokine, induces apoptosis of insulin-secreting beta-cells. *Diabetes* 2003;52:2296–303. <https://doi.org/10.2337/diabetes.52.9.2296>.
- [186] Liang W, Peng X, Li Q, Wang P, Lv P, Song Q, et al. FAM3D is essential for colon homeostasis and host defense against inflammation associated carcinogenesis. *Nat Commun* 2020;11:5912. <https://doi.org/10.1038/s41467-020-19691-z>.
- [187] de Wit NJ, I. Jssennagger N, Oosterink E, Keshtkar S, Hooiveld GJ, Mensink RP, et al. Oit1/Fam3D, a gut-secreted protein displaying nutritional status-dependent regulation. *J Nutr Biochem* 2012;23:1425–33. <https://doi.org/10.1016/j.jnutbio.2011.09.003>.
- [188] Peng X, Xu E, Liang W, Pei X, Chen D, Zheng D, et al. Identification of FAM3D as a new endogenous chemotaxis agonist for the formyl peptide receptors. *J Cell Sci* 2016;129:1831–42. <https://doi.org/10.1242/jcs.183053>.

- [189] Rollins KA, Opitz L, Arnold M, Simon E, Neubauer H, Wolfrum S. The L cell transcriptome is unaffected by vertical sleeve gastrectomy but highly dependent upon position within the gastrointestinal tract. *Peptides* 2019;113:22–34. <https://doi.org/10.1016/j.peptides.2019.01.001>.
- [190] Nguyen KT, Korner J. The sum of many parts: potential mechanisms for improvement in glucose homeostasis after bariatric surgery. *Curr Diab Rep* 2014;14:481. <https://doi.org/10.1007/s11892-014-0481-5>.
- [191] Ayala JE, Bracy DP, Malabanan C, James FD, Ansari T, Fueger PT, et al. Hyperinsulinemic-euglycemic clamps in conscious, unrestrained mice. *J Vis Exp* 2011. <https://doi.org/10.3791/3188>.
- [192] Kim JK. Hyperinsulinemic-euglycemic clamp to assess insulin sensitivity in vivo. *Methods Mol Biol* 2009;560:221–38. https://doi.org/10.1007/978-1-59745-448-3_15.
- [193] InterProScan Search Result (iprscan5-R20210308-121416-0818-29031159-p1m) - protein - InterPro n.d. <https://www.ebi.ac.uk/interpro/result/InterProScan/iprscan5-R20210308-121416-0818-29031159-p1m/> (accessed March 8, 2021).
- [194] Lemmon MA, Schlessinger J. Cell signaling by receptor-tyrosine kinases. *Cell* 2010;141:1117–34. <https://doi.org/10.1016/j.cell.2010.06.011>.
- [195] Lapenna S, Giordano A. Cell cycle kinases as therapeutic targets for cancer. *Nat Rev Drug Discov* 2009;8:547–66. <https://doi.org/10.1038/nrd2907>.
- [196] Mackay HJ, Twelves CJ. Targeting the protein kinase C family: are we there yet? *Nat Rev Cancer* 2007;7:554–62. <https://doi.org/10.1038/nrc2168>.
- [197] Höpfner M, Schuppan D, Scherübl H. Growth factor receptors and related signalling pathways as targets for novel treatment strategies of hepatocellular cancer. *World J Gastroenterol WJG* 2008;14:1–14. <https://doi.org/10.3748/wjg.14.1>.
- [198] Katz M, Amit I, Yarden Y. Regulation of MAPKs by growth factors and receptor tyrosine kinases. *Biochim Biophys Acta* 2007;1773:1161–76. <https://doi.org/10.1016/j.bbamcr.2007.01.002>.
- [199] Saxton RA, Sabatini DM. mTOR Signaling in Growth, Metabolism, and Disease. *Cell* 2017;169:361–71. <https://doi.org/10.1016/j.cell.2017.03.035>.
- [200] Padhi S, Nayak AK, Behera A. Type II diabetes mellitus: a review on recent drug based therapeutics. *Biomed Pharmacother Biomedecine Pharmacother* 2020;131:110708. <https://doi.org/10.1016/j.biopha.2020.110708>.
- [201] Hayashi Y, Yamamoto M, Mizoguchi H, Watanabe C, Ito R, Yamamoto S, et al. Mice deficient for glucagon gene-derived peptides display normoglycemia and hyperplasia of islet {alpha}-cells but not of intestinal L-cells. *Mol Endocrinol Baltim Md* 2009;23:1990–9. <https://doi.org/10.1210/me.2009-0296>.
- [202] Nasteska D, Harada N, Suzuki K, Yamane S, Hamasaki A, Joo E, et al. Chronic reduction of GIP secretion alleviates obesity and insulin resistance under high-fat diet conditions. *Diabetes* 2014;63:2332–43. <https://doi.org/10.2337/db13-1563>.
- [203] Takagi Y, Kinoshita K, Ozaki N, Seino Y, Murata Y, Oshida Y, et al. Mice Deficient in Proglucagon-Derived Peptides Exhibit Glucose Intolerance on a High-Fat Diet but Are

- Resistant to Obesity. *PloS One* 2015;10:e0138322. <https://doi.org/10.1371/journal.pone.0138322>.
- [204] Roberts GP, Larraufie P, Richards P, Kay RG, Galvin SG, Miedzybrodzka EL, et al. Comparison of Human and Murine Enteroendocrine Cells by Transcriptomic and Peptidomic Profiling. *Diabetes* 2019;68:1062–72. <https://doi.org/10.2337/db18-0883>.
- [205] Hansotia T, Drucker DJ. GIP and GLP-1 as incretin hormones: lessons from single and double incretin receptor knockout mice. *Regul Pept* 2005;128:125–34. <https://doi.org/10.1016/j.regpep.2004.07.019>.
- [206] Wellen KE, Hotamisligil GS. Inflammation, stress, and diabetes. *J Clin Invest* 2005;115:1111–9. <https://doi.org/10.1172/JCI25102>.
- [207] P B-J, T H. Oncogenic kinase signalling. *Nature* 2001. <https://doi.org/10.1038/35077225>.
- [208] Goh LK, Sorkin A. Endocytosis of receptor tyrosine kinases. *Cold Spring Harb Perspect Biol* 2013;5:a017459. <https://doi.org/10.1101/cshperspect.a017459>.
- [209] Fountas A, Diamantopoulos L-N, Tsatsoulis A. Tyrosine Kinase Inhibitors and Diabetes: A Novel Treatment Paradigm? *Trends Endocrinol Metab TEM* 2015;26:643–56. <https://doi.org/10.1016/j.tem.2015.09.003>.
- [210] Prada PO, Saad MJ. Tyrosine kinase inhibitors as novel drugs for the treatment of diabetes. *Expert Opin Investig Drugs* 2013;22:751–63. <https://doi.org/10.1517/13543784.2013.802768>.
- [211] Mokhtari D, Welsh N. Potential utility of small tyrosine kinase inhibitors in the treatment of diabetes. *Clin Sci Lond Engl* 1979 2009;118:241–7. <https://doi.org/10.1042/CS20090348>.
- [212] Fitter S, Vandyke K, Schultz CG, White D, Hughes TP, Zannettino ACW. Plasma adiponectin levels are markedly elevated in imatinib-treated chronic myeloid leukemia (CML) patients: a mechanism for improved insulin sensitivity in type 2 diabetic CML patients? *J Clin Endocrinol Metab* 2010;95:3763–7. <https://doi.org/10.1210/jc.2010-0086>.
- [213] Yilmaz M, Hotamisligil GS. Damned if you do, damned if you don't: the conundrum of adipose tissue vascularization. *Cell Metab* 2013;17:7–9. <https://doi.org/10.1016/j.cmet.2012.12.014>.
- [214] Ozaki K-I, Awazu M, Tamiya M, Iwasaki Y, Harada A, Kugisaki S, et al. Targeting the ERK signaling pathway as a potential treatment for insulin resistance and type 2 diabetes. *Am J Physiol Endocrinol Metab* 2016;310:E643–51. <https://doi.org/10.1152/ajpendo.00445.2015>.
- [215] Banks AS, McAllister FE, Camporez JPG, Zushin P-JH, Jurczak MJ, Laznik-Bogoslavski D, et al. An ERK/Cdk5 axis controls the diabetogenic actions of PPAR γ . *Nature* 2015;517:391–5. <https://doi.org/10.1038/nature13887>.
- [216] Choi E, Kikuchi S, Gao H, Brodzik K, Nassour I, Yopp A, et al. Mitotic regulators and the SHP2-MAPK pathway promote IR endocytosis and feedback regulation of insulin signaling. *Nat Commun* 2019;10:1473. <https://doi.org/10.1038/s41467-019-09318-3>.
- [217] Hong S, Song W, Zushin P-JH, Liu B, Jedrychowski MP, Mina AI, et al. Phosphorylation of Beta-3 adrenergic receptor at serine 247 by ERK MAP kinase drives lipolysis in obese adipocytes. *Mol Metab* 2018;12:25–38. <https://doi.org/10.1016/j.molmet.2018.03.012>.

- [218] Heinemann F, Birk G, Stierstorfer B. Deep learning enables pathologist-like scoring of NASH models. *Sci Rep* 2019;9:18454. <https://doi.org/10.1038/s41598-019-54904-6>.
- [219] Strobel B, Zuckschwerdt K, Zimmermann G, Mayer C, Eytner R, Rechtsteiner P, et al. Standardized, Scalable, and Timely Flexible Adeno-Associated Virus Vector Production Using Frozen High-Density HEK-293 Cell Stocks and CELLdiscs. *Hum Gene Ther Methods* 2019;30:23–33. <https://doi.org/10.1089/hgtb.2018.228>.
- [220] de Jong JMA, Cannon B, Nedergaard J, Wolfrum C, Petrovic N. Reply to “Confounding issues in the ‘humanized’ brown fat of mice.” *Nat Metab* 2020;2:305–6. <https://doi.org/10.1038/s42255-020-0193-x>.
- [221] Keijer J, Li M, Speakman JR. What is the best housing temperature to translate mouse experiments to humans? *Mol Metab* 2019;25:168–76. <https://doi.org/10.1016/j.molmet.2019.04.001>.
- [222] Fischer AW, Cannon B, Nedergaard J. The answer to the question “What is the best housing temperature to translate mouse experiments to humans?” is: thermoneutrality. *Mol Metab* 2019;26:1–3. <https://doi.org/10.1016/j.molmet.2019.05.006>.
- [223] Fischer AW, Cannon B, Nedergaard J. Optimal housing temperatures for mice to mimic the thermal environment of humans: An experimental study. *Mol Metab* 2018;7:161–70. <https://doi.org/10.1016/j.molmet.2017.10.009>.
- [224] Fischer AW, de Jong JMA, Sass F, Schlein C, Heeren J, Petrovic N. Thermoneutrality-Induced Macrophage Accumulation in Brown Adipose Tissue Does Not Impair the Tissue’s Competence for Cold-Induced Thermogenic Recruitment. *Front Endocrinol* 2020;11:568682. <https://doi.org/10.3389/fendo.2020.568682>.
- [225] Schlein C, Fischer AW, Sass F, Worthmann A, Tödter K, Jaekstein MY, et al. Endogenous Fatty Acid Synthesis Drives Brown Adipose Tissue Involution. *Cell Rep* 2021;34:108624. <https://doi.org/10.1016/j.celrep.2020.108624>.
- [226] Altshuler-Keylin S, Shinoda K, Hasegawa Y, Ikeda K, Hong H, Kang Q, et al. Beige Adipocyte Maintenance Is Regulated by Autophagy-Induced Mitochondrial Clearance. *Cell Metab* 2016;24:402–19. <https://doi.org/10.1016/j.cmet.2016.08.002>.
- [227] Sass F, Schlein C, Jaekstein MY, Pertzborn P, Schweizer M, Schinke T, et al. TFEB-deficiency attenuates mitochondrial degradation upon brown adipose tissue whitening at thermoneutrality. *Mol Metab* 2021:101173. <https://doi.org/10.1016/j.molmet.2021.101173>.
- [228] Roh HC, Tsai LT, Lyubetskaya A, Tenen D, Kumari M, Rosen ED. Simultaneous Transcriptional and Epigenomic Profiling from Specific Cell Types within Heterogeneous Tissues In Vivo. *Cell Rep* 2017;18:1048–61. <https://doi.org/10.1016/j.celrep.2016.12.087>.
- [229] Sharp LZ, Shinoda K, Ohno H, Scheel DW, Tomoda E, Ruiz L, et al. Human BAT possesses molecular signatures that resemble beige/brite cells. *PLoS One* 2012;7:e49452. <https://doi.org/10.1371/journal.pone.0049452>.
- [230] Cypess AM, White AP, Vernochet C, Schulz TJ, Xue R, Sass CA, et al. Anatomical localization, gene expression profiling and functional characterization of adult human neck brown fat. *Nat Med* 2013;19:635–9. <https://doi.org/10.1038/nm.3112>.
- [231] Jespersen NZ, Larsen TJ, Peijs L, Daugaard S, Homøe P, Loft A, et al. A classical brown adipose tissue mRNA signature partly overlaps with brite in the supraclavicular region of adult humans. *Cell Metab* 2013;17:798–805. <https://doi.org/10.1016/j.cmet.2013.04.011>.

- [232] Cannon B, de Jong JMA, Fischer AW, Nedergaard J, Petrovic N. Human brown adipose tissue: Classical brown rather than brite/beige? *Exp Physiol* 2020;105:1191–200. <https://doi.org/10.1113/EP087875>.
- [233] Perdikari A, Leparac GG, Balaz M, Pires ND, Lidell ME, Sun W, et al. BATLAS: Deconvoluting Brown Adipose Tissue. *Cell Rep* 2018;25:784–797.e4. <https://doi.org/10.1016/j.celrep.2018.09.044>.
- [234] Nedergaard J, Wang Y, Cannon B. Cell proliferation and apoptosis inhibition: essential processes for recruitment of the full thermogenic capacity of brown adipose tissue. *Biochim Biophys Acta Mol Cell Biol Lipids* 2019;1864:51–8. <https://doi.org/10.1016/j.bbalip.2018.06.013>.
- [235] Gesta S, Tseng Y-H, Kahn CR. Developmental Origin of Fat: Tracking Obesity to Its Source. *Cell* 2007;131:242–56. <https://doi.org/10.1016/j.cell.2007.10.004>.
- [236] Seale P, Kajimura S, Yang W, Chin S, Rohas LM, Uldry M, et al. Transcriptional control of brown fat determination by PRDM16. *Cell Metab* 2007;6:38–54. <https://doi.org/10.1016/j.cmet.2007.06.001>.
- [237] Seale P, Bjork B, Yang W, Kajimura S, Chin S, Kuang S, et al. PRDM16 controls a brown fat/skeletal muscle switch. *Nature* 2008;454:961–7. <https://doi.org/10.1038/nature07182>.
- [238] Puigserver P, Wu Z, Park CW, Graves R, Wright M, Spiegelman BM. A cold-inducible coactivator of nuclear receptors linked to adaptive thermogenesis. *Cell* 1998;92:829–39. [https://doi.org/10.1016/s0092-8674\(00\)81410-5](https://doi.org/10.1016/s0092-8674(00)81410-5).
- [239] Uldry M, Yang W, St-Pierre J, Lin J, Seale P, Spiegelman BM. Complementary action of the PGC-1 coactivators in mitochondrial biogenesis and brown fat differentiation. *Cell Metab* 2006;3:333–41. <https://doi.org/10.1016/j.cmet.2006.04.002>.
- [240] Sanchez-Gurmaches J, Guertin DA. Adipocyte lineages: tracing back the origins of fat. *Biochim Biophys Acta* 2014;1842:340–51. <https://doi.org/10.1016/j.bbadis.2013.05.027>.
- [241] Sebo ZL, Rodeheffer MS. Assembling the adipose organ: adipocyte lineage segregation and adipogenesis in vivo. *Dev Camb Engl* 2019;146. <https://doi.org/10.1242/dev.172098>.
- [242] Jung SM, Sanchez-Gurmaches J, Guertin DA. Brown Adipose Tissue Development and Metabolism. *Handb Exp Pharmacol* 2019;251:3–36. https://doi.org/10.1007/164_2018_168.
- [243] Carobbio S, Guenantin A-C, Bahri M, Rodriguez-Fdez S, Honig F, Kamzolas I, et al. Unraveling the Developmental Roadmap toward Human Brown Adipose Tissue. *Stem Cell Rep* 2021;16:641–55. <https://doi.org/10.1016/j.stemcr.2021.01.013>.
- [244] Cannon B, Nedergaard J. Brown Adipose Tissue: Function and Physiological Significance. *Physiol Rev* 2004;84:277–359. <https://doi.org/10.1152/physrev.00015.2003>.
- [245] Sambeat A, Gulyaeva O, Dempersmier J, Sul HS. Epigenetic Regulation of the Thermogenic Adipose Program. *Trends Endocrinol Metab TEM* 2017;28:19–31. <https://doi.org/10.1016/j.tem.2016.09.003>.
- [246] Rando OJ, Verstrepen KJ. Timescales of genetic and epigenetic inheritance. *Cell* 2007;128:655–68. <https://doi.org/10.1016/j.cell.2007.01.023>.
- [247] Wang L, Xu S, Lee J-E, Baldridge A, Grullon S, Peng W, et al. Histone H3K9 methyltransferase G9a represses PPAR γ expression and adipogenesis. *EMBO J* 2013;32:45–59. <https://doi.org/10.1038/emboj.2012.306>.

- [248] Yoo EJ, Chung J-J, Choe SS, Kim KH, Kim JB. Down-regulation of histone deacetylases stimulates adipocyte differentiation. *J Biol Chem* 2006;281:6608–15. <https://doi.org/10.1074/jbc.M508982200>.
- [249] Sequential changes in genome-wide DNA methylation status during adipocyte differentiation - PubMed n.d. <https://pubmed.ncbi.nlm.nih.gov/18062916/> (accessed February 19, 2021).
- [250] Shore A, Karamitri A, Kemp P, Speakman JR, Lomax MA. Role of Ucp1 enhancer methylation and chromatin remodelling in the control of Ucp1 expression in murine adipose tissue. *Diabetologia* 2010;53:1164–73. <https://doi.org/10.1007/s00125-010-1701-4>.
- [251] Shao M, Wang QA, Song A, Vishvanath L, Busbuso NC, Scherer PE, et al. Cellular Origins of Beige Fat Cells Revisited. *Diabetes* 2019;68:1874–85. <https://doi.org/10.2337/db19-0308>.
- [252] Blondin DP, Nielsen S, Kuipers EN, Severinsen MC, Jensen VH, Miard S, et al. Human Brown Adipocyte Thermogenesis Is Driven by β 2-AR Stimulation. *Cell Metab* 2020;32:287–300.e7. <https://doi.org/10.1016/j.cmet.2020.07.005>.
- [253] Payab M, Abedi M, Foroughi Heravani N, Hadavandkhani M, Arabi M, Tayanloo-Beik A, et al. Brown adipose tissue transplantation as a novel alternative to obesity treatment: a systematic review. *Int J Obes* 2021;45:109–21. <https://doi.org/10.1038/s41366-020-0616-5>.
- [254] Soler-Vázquez MC, Mera P, Zagmutt S, Serra D, Herrero L. New approaches targeting brown adipose tissue transplantation as a therapy in obesity. *Biochem Pharmacol* 2018;155:346–55. <https://doi.org/10.1016/j.bcp.2018.07.022>.
- [255] Frei AP, Jeon O-Y, Kilcher S, Moest H, Henning LM, Jost C, et al. Direct identification of ligand-receptor interactions on living cells and tissues. *Nat Biotechnol* 2012;30:997–1001. <https://doi.org/10.1038/nbt.2354>.
- [256] Frei AP, Moest H, Novy K, Wollscheid B. Ligand-based receptor identification on living cells and tissues using TRICEPS. *Nat Protoc* 2013;8:1321–36. <https://doi.org/10.1038/nprot.2013.072>.
- [257] Lopez-Garcia LA, Demiray L, Ruch-Marder S, Hopp A-K, Hottiger MO, Helbling PM, et al. Validation of extracellular ligand-receptor interactions by Flow-TriCEPS. *BMC Res Notes* 2018;11:863. <https://doi.org/10.1186/s13104-018-3974-5>.
- [258] Lam SS, Martell JD, Kamer KJ, Deerinck TJ, Ellisman MH, Mootha VK, et al. Directed evolution of APEX2 for electron microscopy and proximity labeling. *Nat Methods* 2015;12:51–4. <https://doi.org/10.1038/nmeth.3179>.
- [259] Hung V, Udeshi ND, Lam SS, Loh KH, Cox KJ, Pedram K, et al. Spatially resolved proteomic mapping in living cells with the engineered peroxidase APEX2. *Nat Protoc* 2016;11:456–75. <https://doi.org/10.1038/nprot.2016.018>.
- [260] Zhen Y, Haugsten EM, Singh SK, Wesche J. Proximity Labeling by a Recombinant APEX2-FGF1 Fusion Protein Reveals Interaction of FGF1 with the Proteoglycans CD44 and CSPG4. *Biochemistry* 2018;57:3807–16. <https://doi.org/10.1021/acs.biochem.8b00120>.
- [261] Tan B, Peng S, Yatim SMJM, Gunaratne J, Hunziker W, Ludwig A. An Optimized Protocol for Proximity Biotinylation in Confluent Epithelial Cell Cultures Using the Peroxidase APEX2. *STAR Protoc* 2020;1:100074. <https://doi.org/10.1016/j.xpro.2020.100074>.

- [262] Emanuelli B, Vienberg SG, Smyth G, Cheng C, Stanford KI, Arumugam M, et al. Interplay between FGF21 and insulin action in the liver regulates metabolism. *J Clin Invest* 2015;125:458. <https://doi.org/10.1172/JCI80223>.
- [263] Capozza R, Eckenhoff B, Yum SI. Design and performance of the implantable osmotic minipump. *J Med Eng Technol* 1977;1:281–3. <https://doi.org/10.3109/03091907709162196>.
- [264] Struyker-Boudier HA, Smits JF. The osmotic minipump: a new tool in the study of steady-state kinetics of drug distribution and metabolism. *J Pharm Pharmacol* 1978;30:576–8. <https://doi.org/10.1111/j.2042-7158.1978.tb13327.x>.
- [265] Unniappan S, McIntosh CHS, Demuth H-U, Heiser U, Wolf R, Kieffer TJ. Effects of dipeptidyl peptidase IV on the satiety actions of peptide YY. *Diabetologia* 2006;49:1915–23. <https://doi.org/10.1007/s00125-006-0310-8>.
- [266] Bertsch T, McKeirnan K. ITCA 650. *Clin Diabetes Publ Am Diabetes Assoc* 2018;36:265–7. <https://doi.org/10.2337/cd18-0039>.
- [267] Ritzel R, Orskov C, Holst JJ, Nauck MA. Pharmacokinetic, insulinotropic, and glucagonostatic properties of GLP-1 [7-36 amide] after subcutaneous injection in healthy volunteers. Dose-response-relationships. *Diabetologia* 1995;38:720–5. <https://doi.org/10.1007/BF00401846>.
- [268] Drucker DJ, Habener JF, Holst JJ. Discovery, characterization, and clinical development of the glucagon-like peptides. *J Clin Invest* 2017;127:4217–27. <https://doi.org/10.1172/JCI97233>.
- [269] Yki-Järvinen H. Non-alcoholic fatty liver disease as a cause and a consequence of metabolic syndrome. *Lancet Diabetes Endocrinol* 2014;2:901–10. [https://doi.org/10.1016/S2213-8587\(14\)70032-4](https://doi.org/10.1016/S2213-8587(14)70032-4).
- [270] Chen Z, Yu R, Xiong Y, Du F, Zhu S. A vicious circle between insulin resistance and inflammation in nonalcoholic fatty liver disease. *Lipids Health Dis* 2017;16:203. <https://doi.org/10.1186/s12944-017-0572-9>.
- [271] Saponaro C, Gaggini M, Carli F, Gastaldelli A. The Subtle Balance between Lipolysis and Lipogenesis: A Critical Point in Metabolic Homeostasis. *Nutrients* 2015;7:9453–74. <https://doi.org/10.3390/nu7115475>.
- [272] Adolph TE, Grander C, Grabherr F, Tilg H. Adipokines and Non-Alcoholic Fatty Liver Disease: Multiple Interactions. *Int J Mol Sci* 2017;18. <https://doi.org/10.3390/ijms18081649>.
- [273] Titchenell PM, Lazar MA, Birnbaum MJ. Unraveling the Regulation of Hepatic Metabolism by Insulin. *Trends Endocrinol Metab TEM* 2017;28:497–505. <https://doi.org/10.1016/j.tem.2017.03.003>.
- [274] Lv X, Dong Y, Hu L, Lu F, Zhou C, Qin S. Glucagon-like peptide-1 receptor agonists (GLP-1 RAs) for the management of nonalcoholic fatty liver disease (NAFLD): A systematic review. *Endocrinol Diabetes Metab* 2020;3:e00163. <https://doi.org/10.1002/edm2.163>.
- [275] Seghieri M, Christensen AS, Andersen A, Solini A, Knop FK, Vilsbøll T. Future Perspectives on GLP-1 Receptor Agonists and GLP-1/glucagon Receptor Co-agonists in the Treatment of NAFLD. *Front Endocrinol* 2018;9. <https://doi.org/10.3389/fendo.2018.00649>.

- [276] Blazina I, Selph S. Diabetes drugs for nonalcoholic fatty liver disease: a systematic review. *Syst Rev* 2019;8:295. <https://doi.org/10.1186/s13643-019-1200-8>.
- [277] Scheen AJ. Beneficial effects of SGLT2 inhibitors on fatty liver in type 2 diabetes: A common comorbidity associated with severe complications. *Diabetes Metab* 2019;45:213–23. <https://doi.org/10.1016/j.diabet.2019.01.008>.
- [278] Leiter LA, Forst T, Polidori D, Balis DA, Xie J, Sha S. Effect of canagliflozin on liver function tests in patients with type 2 diabetes. *Diabetes Metab* 2016;42:25–32. <https://doi.org/10.1016/j.diabet.2015.10.003>.
- [279] Cusi K, Orsak B, Bril F, Lomonaco R, Hecht J, Ortiz-Lopez C, et al. Long-Term Pioglitazone Treatment for Patients With Nonalcoholic Steatohepatitis and Prediabetes or Type 2 Diabetes Mellitus: A Randomized Trial. *Ann Intern Med* 2016;165:305–15. <https://doi.org/10.7326/M15-1774>.
- [280] Green CJ, Marjot T, Tomlinson JW, Hodson L. Of mice and men: Is there a future for metformin in the treatment of hepatic steatosis? *Diabetes Obes Metab* 2019;21:749–60. <https://doi.org/10.1111/dom.13592>.

Curriculum Vitae

Name Caroline Moser
Date of Birth 08.11.1990
Address Winterthurerstrasse 460
8051 Zürich
Nationality German

Education

02/2017 – present **Swiss Federal Institute of Technology, Zurich**
PhD ETH
Title Doctoral Thesis : "Different Perspectives of Metabolism: Gut Feelings and Love Handles"

09/2016 – 07/2019 **Swiss Federal Institute of Technology, Zurich**
Teaching Certificate HST

09/2014 – 02/2017 **Swiss Federal Institute of Technology, Zurich**
MSc ETH HST
Focus: Molecular Health Science
Title Master Thesis : "Directing osteogenic differentiation of mesenchymal stromal cells *in vitro*"

09/2011 – 09/2014 **Swiss Federal Institute of Technology, Zurich**
BSc ETH HST

Practical Experience

02/2017 – present **Swiss Federal Institute of Technology, Zurich**
Laboratory for Translational Nutritional Biology
Research Assistant

03/2019 – 06/2019 **Careum Educational Center, Zurich**
Internship

08/2015 - 08/2016 **AO Foundation Research Institute, Davos**
Regenerative Orthopedics, Bone Biology
Internship

09/2014 – 12/2014 **Swiss Federal Institute of Technology, Zurich**
Laboratory for Translational Nutritional Biology
Internship

02/2014 – 07/2014 **Swiss Federal Institute of Technology, Zurich**
Laboratory for Translational Nutritional Biology
Student Assistant

12/2010 – 08/2011 **Coperion GmbH, Weingarten**
Internship

Skills

Languages	German (native), English (fluent)
Prices and Fellowships	Will-Studer Prize 2017, ETH Zürich ETH Medal 2017, ETH Zürich AO Foundation Fellowship 2016

Conferences

2016	eCM Conference Davos Poster Presentation
2021	Virtual Keystone Conference: Diabetes: Many Faces of the Disease & Obesity: From Cell to Patient Poster Presentation

List of Publications

A Genetic Model to Study the Contribution of Brown and Brite Adipocytes to Metabolism	2020 <i>Cell Reports</i>
T. Challa, D. Dapito, E. Kulenkampff, E. Kiehlmann, <u>C. Moser</u> , L. Straub, W. Sun, C. Wolfrum	
Antioxidants protect against diabetes by improving glucose homeostasis in mouse models of inducible insulin resistance and obesity	2019 <i>Diabetologia</i>
L. Straub, V. Efthymiou, G. Grandl, M. Balaz, T. Challa, L. Truscillo, C. Horvath, <u>C. Moser</u> , Y. Rachamin, M. Arnold, W. Sun, S. Modica, C. Wolfrum	
Inhibition of mevalonate pathway prevents adipocyte browning in mice and men by affecting protein prenylation	2019 <i>Cell Metabolism</i>
M. Balaz, A. Becker, L. Balazova, L. Straub, J. Müller, G. Gashi, C. Maushart, W. Sun, H. Dong, <u>C. Moser</u> , (...) C. Wolfrum	
A Perfusion Culture System for Assessing Bone Marrow Stromal Cell Differentiation on PLGA Scaffolds for Bone Repair	2018 <i>Frontiers in Bioengineering and Biotechnology</i>
<u>C. Moser</u> , K. Bardsley, A. El Haj, M. Alini, M. Stoddart, J. Bara	
Depot specific differences in the adipogenic potential of precursors are mediated by collagenous extracellular matrix and Flotillin 2 dependent signaling	2016 <i>Molecular Metabolism</i>
G. Grandl, S. Müller, H. Moest, <u>C. Moser</u> , B. Wollscheid, C. Wolfrum	

